Exploring the role of biota and biogenic components for the formation and function of (micro-)aggregates in soil

Dissertation

(kumulativ)

zur Erlangung des akademischen Grades doctor rerum naturalium

(Dr. rer. nat.)

FRIEDRICH-SCHILLER-
UNIVERSITÄT
JENA

vorgelegt dem Rat der Chemisch-Geowissenschaftlichen Fakultät der

Friedrich-Schiller-Universität Jena

von M.Sc. Tom Guhra

Geboren am 28.05.1990 in Cottbus

Gutachter:

1. Prof. Dr. Kai Uwe Totsche, Friedrich-Schiller-Universität Jena

2. Prof. Dr. Juraj Majzlan, Friedrich-Schiller-Universität Jena

Tag der Verteidigung: 29.06.2022

Contents

Danksagung

Warnung: Die folgenden Zeilen spiegeln nicht einmal ansatzweise wider, wie dankbar ich für die großartigen Menschen (Familie, Freunde und Kollegen) bin, die mich die letzten Jahre durch eine sehr bewegte Zeit begleitet haben. Etwaige Beschwerden werden durch meine Person entgegengenommen.

Einleitend möchte ich mich bei Prof. Dr. Totsche bedanken. Einerseits für die Möglichkeit, eine Promotionsarbeit unter seiner Supervision schreiben zu dürfen und anderseits dafür, dass sein Vertrauen in meine Person über die obligatorischen drei Jahre hinaus gereicht hat. In dieser Zeit ermöglichte er mir, vor allem durch progressive Denkansätze, vielfältige Arbeitsfelder und anspruchsvolle Aufgabenstellungen, meinen Horizont zu erweitern und gemeinsam mit großartigen Kolleg*innen einen Beitrag zu der aktuellen Forschung zu leisten. Trotz einiger Igel, die während der Promotionszeit zu bürsten waren, konnte ich mich insbesondere in extremen Situationen immer auf die Zuwendung und Unterstützung meines Doktorvaters verlassen.

Für die Übernahme des Zweitgutachtens danke ich Prof. Dr. Majzlan, der diese Arbeit im Rahmen von studentischen Projektmodulen und Abschlussarbeiten mit seiner Expertise und dem Zugriff auf technische Ressourcen immer wohlwollend unterstützt hat.

Ein großer Dank und meine Anerkennung gelten Dr. Thomas Ritschel. Die von ihm gewährleistete fachliche als auch emotionale Unterstützung/Beratung/Betreuung hat mich durch einige tiefe Täler geführt und mir geholfen, nicht den Boden unter den Füßen zu verlieren. Die gemeinsame Arbeit war/ist für mich sehr lehrreich (und für ihn sicher sehr anstrengend).

Des Weiteren möchte ich meine Kommilitonin, Arbeitsehefrau und gute Freundin Katharina Stolze mit Dank bewerfen. Für ihre Geduld bei unzähligen Nachfragen „Kannst du da bitte nochmal schnell drüber lesen?“ und das gemeinsame Leiden, Lernen und Lachen während der Promotion.

Weitere Dankesbekundungen entfallen auf die gesamte Arbeitsgruppe des Lehrstuhls für Hydrogeologie, in der es auf jede Frage eine Antwort gibt. Die beharrliche Unterstützung bei Labor- und Feldarbeiten wie auch die fachspezifische Beratung rund um die bunte Welt der Naturwissenschaften sucht seinesgleichen.

Ich möchte mich auch bei den Studierenden bedanken, welche ich während meiner Promotion bei ihren Abschlussarbeiten betreuen durfte. Deren Interesse an den ihnen angebotenen Themen haben es ermöglicht, wissenschaftliche Leidenschaften zu bearbeiten, denen ich allein in dem vorgegebenen Zeitrahmen nicht hätte nachgehen können.

Auch der DFG und dem MADsoil Konsortium (DFG RU 2179) möchte ich für die Möglichkeiten danken, dass ich tief in die Welt unserer Böden eintauchen durfte. Vor allem für die Kooperationen mit den Teilprojekten PC (Project coordination), PM (Mechanistic modelling of the formation and consolidation of soil microaggregates), SP4 (Spatiotemporal interactions of aggregate-forming agents within soil microaggregates: Consequences for aggregate structure and stability) und SP3 (Formation and composition of soil microaggregates as explored by their elemental and isotopic label composition) im Rahmen der gemeinschaftlichen Forschungsarbeit und den Manuskripten möchte ich meinen Dank aussprechen.

Auch meinen lieben Freunden möchte ich danken, dass sie regelmäßig für Ablenkung und Unterhaltung gesorgt haben. Dabei ist Lisa Pfülb für ihren mutigen Einsatz als Rechtschreibkorrektorin gesondert zu erwähnen.

Ein besonderer Dank gilt meiner lieben Familie, die mich schon so lange auf meiner Reise begleitet und auf deren Unterstützung sowie Inspiration ich mich immer verlassen kann - meinem lieben Vater Hans-Jürgen, meiner lieben Mutter Iris und meinem großartigen Bruder Peter, welche mir den Weg geebnet haben, immer für mich da sind und mir als Vorbilder dienen. Ich danke auch meiner lieben Valentina, meinen beiden Schwestern Josephin und Carolin als auch meiner Nichte Leni und meinem Neffen Luca, die noch etwas mehr Farbe und Freude in mein Leben gebracht haben.

Zu guter Letzt möchte ich meiner Frau Stefanie danken, dass sie die unzähligen Herausforderungen des Lebens mit mir bewältigt und mich auffängt, wenn wieder ein neuer Igel zu bürsten ist. Besonders auch dafür, dass sie mir meinen kleinen Sonnenschein Helena geschenkt hat, welche sich ab ihrer Geburt darauf verstand, Igel zu verscheuchen, bevor sie gebürstet werden müssen.

Nun genug der Igel-Metaphern! DANKE!

Lebenslauf

Selbstständigkeitserklärung

Ich erkläre, dass ich die vorliegende Arbeit selbstständig und unter Verwendung der angegebenen Hilfsmittel, persönlichen Mitteilungen und Quellen angefertigt habe.

Tom Guhra Jena, den

Erklärung zur Urheberschaft/Declaration of authorship

Erklärung zu den Eigenanteilen der Promovendin/des Promovenden sowie der weiteren Doktorandinnen/Doktoranden als Co-Autorinnen/-Autoren an den Publikationen und Zweitpublikationsrechten bei einer kumulativen Dissertation

Für alle in dieser kumulativen Dissertation verwendeten Manuskripte liegen die notwendigen Genehmigungen der Verlage („Reprint permissions“) für die Zweitpublikation vor.

Die Co-Autorinnen/-Autoren der in dieser kumulativen Dissertation verwendeten Manuskripte sind sowohl über die Nutzung, als auch über die angegebenen Eigenanteile der weiteren Doktorandinnen/Doktoranden als Co-Autorinnen/-Autoren an den Publikationen und Zweitpublikationsrechten bei einer kumulativen Dissertation informiert und stimmen dem zu.

Die Anteile der Promovendin/des Promovenden sowie der weiteren Doktorandinnen/Doktoranden als Co-Autorinnen/Co-Autoren an den Publikationen und Zweitpublikationsrechten bei einer kumulativen Dissertation sind in der Anlage aufgeführt.

M.Sc. Tom Guhra Jena, den

Ich bin mit der Abfassung der Dissertation als publikationsbasierte Dissertation, d.h. kumulativ, einverstanden und bestätige die vorstehenden Angaben.

Prof. Dr. Kai Uwe Totsche Jena, den

Abbreviations

AFM	atomic force microscopy
B	Born repulsion
CAM	cellular automaton method
CBU	composite building units
DFG	Deutsche Forschungsgemeinschaft
DLVO	Derjaguin–Landau–Verwey–Overbeek (Theory)
EPS	extracellular polymeric substances
EW	earthworm
FTIR	Fourier-transform infrared spectroscopy
IEP	isoelectric point
MFM	microaggregate forming materials
NMR	^{13}C-nuclear magnetic resonance spectroscopy
OC	organic carbon
OM	organic matter
P_I	publication 1: Pathways of biogenically excreted organic matter into soil aggregates
P_{II}	publication 2: Earthworm mucus contributes to the formation of organo-mineral associations in soil
P_{III}	publication 3: Formation of mineral–mineral and organo–mineral composite building units from microaggregate-forming materials including microbially produced extracellular polymeric substances
P_{IV}	publication 4: Application of a Cellular Automaton Method to Model the Structure Formation in Soils Under Saturated Conditions: A Mechanistic Approach
P_V	publication 5: The mechanisms of gravity-constrained aggregation in natural colloidal suspensions
PZC	point of zero charge
SEM-EDX	scanning electron microscopy with energy-dispersive X-ray spectroscopy
V_A	attractive energies
V_R	repulsive energies
V_T	total energy profile

List of figures

Zusammenfassung

Das Thema der kumulativen Dissertation ist die initiale Aggregatbildung im Boden. Die Bedeutsamkeit der (Mikro-)Aggregate im Boden liegt darin, dass diese die kleinste den Boden in seinen Funktionen repräsentierende Einheit bilden. Daher wird der Umfang der Aggregatbildung und deren Stabilität oft als Analogon für die Bodenqualität betrachtet. Somit ist das Aggregat, welches als dreidimensionale, in sich poröse Struktur aus organischen als auch anorganischen Komponenten aufgebaut ist, der Schlüssel zu den meisten Bodenfunktionen. Jedoch sind die Bildungswege der Aggregate im Boden mannigfaltig und durch die bodenbildenden Faktoren wie z.B. Ausgangsgestein und Biota kontrolliert. In dieser Arbeit habe ich mich vor allem auf die durch Bodenorganismen induzierten Aggregatbildungsprozesse und die initiale Aggregierung innerhalb der wässrigen Phase konzentriert. Der Focus der kumulierten Veröffentlichungen lag darauf, die Aggregation *in vitro* nachzuempfinden und die zugrundeliegenden Modellannahmen *in silico* zu rekonstruieren und zu evaluieren. Um möglichst einfache, aber repräsentative Systeme zu beschreiben, basierten alle Studien auf drei Prototypen für Bodenminerale. Diese umfassen die Sekundärminerale Goethit und Illit, sowie Quarz als gegen Verwitterungsprozesse persistentes Primärmineral. Der Einfluss der Bodenorganismen und des biogen gebildeten organischen Materials (OM) wurde anhand des von Regenwürmern sekretierten kutanen Mucus und mikrobiellen extrazellulären polymeren Substanzen (EPS) untersucht. Die Wechselwirkungen zwischen biogenem OM und den Mineralphasen ist ein komplexes Wechselspiel aus verschiedenen Subprozessen, welche von der Bereitstellung des biogenen OM durch den Organismus über die Bildung von organo-mineralischen Assoziationen zu deren Einbindung in Aggregate reicht. Des Weiteren gestalten Verlagerungsprozesse und Transport von Partikeln, Assoziationen und Aggregaten in der Bodenlösung die Strukturierung des Bodens ebenso wie Bioturbation, Austrocknung, Befeuchtung, Quellen und Schrumpfen. Eine der größten Herausforderungen ist es, dass alle diese Faktoren und Prozesse gleichzeitig ihren Einfluss auf die Aggregation nehmen und sich gegenseitig beeinflussen. Somit haben wir uns sukzessiv folgenden Kernfragenstellungen gewidmet:

Wie gelangt biogenes organisches Material in Bodenaggregate? (Guhra et al., 2022: **P_I**)

Das erste hier vorgestellte Manuskript ist ein Review rund um biogen induzierte Aggregation und bildet die inhaltliche Basis dieser Dissertation. Dabei lag der Schwerpunkt im Besonderen auf dem Einfluss von durch Bodenorganismen sekretiertem biogenem OM wie z.B. Wurzelexsudate, Regenwurmmucus und mikrobieller EPS. Die OM-Exkretion erfolgt dabei zum Teil in Kombination mit Bioturbation, Kompaktierung und anschließender Alteration, was zu der Bildung von wasserstabilen Aggregaten führt. Die dabei entstehenden biogenen Aggregate sind strukturgebend, an der Speicherung von Nährstoffen beteiligt und bieten ein Habitat für Mikroorganismen. Die Aggregatbildung durch Organismen und deren Ausscheidungen basiert dabei auf einer Kaskade von zumeist separat betrachteten Teilprozessen wie z.B. OM-Freisetzung, Bildung organo-mineralischer Assoziationen und deren (Im-)Mobilisierung. Letztendlich zeigen die durch Organismen beeinflussten Aggregate charakteristische Merkmale wie OM-Ummantelungen, Verklebungen und Vernetzungen, die einzelne Bodenpartikel zusammenhalten. Trotz dessen unterliegt die Rolle von biogenem OM bei der Aggregierung einer kontroversen Diskussion, da biogenes OM in der Literatur sowohl als aggregationsfördernd als auch -hemmend beschrieben wird. Ein Teilaspekt dabei ist das Assoziieren bzw.

Adsorbieren des biogenen OM mit den Bodenpartikeln, welches eine OM-Ummantelung von Bodenpartikeln bzw. Mineralen zur Folge hat und somit Einfluss auf die Oberflächeneigenschaften nimmt. Gegensätzliche Effekte wie die Promotion und Hemmung einer Aggregation sind auf das komplexe Zusammenspiel von Milieu-Parametern und den physikochemischen Eigenschaften von biogenem OM während einer potenziellen Aggregation zurückzuführen. Dementsprechend kann biogenes OM je nach Herkunft und vorherrschenden Umweltbedingungen drei verschiedene Aufgaben bei der Aggregierung einnehmen: (I) als Überbrückungsmittel, welches die Aggregation aufgrund von Oberflächenmodifikationen und attraktiven Wechselwirkungen ermöglicht, (II) als Separationsmittel, welches die Bildung von organo-mineralischen Assoziationen, deren Mobilität und Transport begünstigt, jedoch deren weitere Beteiligung an der Aggregation hemmt und (III) als Klebemittel, welches eine Aggregierung vermittelt, nachdem äußere Einflüsse (z.B. Wassermenisken) zu einer Annäherung von Bodenpartikeln geführt haben. Es liegt auf der Hand, dass diese Prozesse in belebten natürlichen Systemen simultan und sowohl zeitlich als auch räumlich skalenübergreifend stattfinden. Dabei ist die Beteiligung und Wechselwirkung verschiedener Bodenorganismen im Zuge der biogenen Aggregierung hervorzuheben, denn die verschiedenen taxonomischen Gruppen sind über Nahrungsketten, Abbauprozesse, Prädation und mutualistische Verhältnisse eng miteinander verknüpft. Die standort-spezifische Biodiversität trägt daher deutlicher zu einer effektiven Aggregierung bei als ein spezifischer Organismus.

Wie alteriert biogenes OM die Oberflächen von Mineralen? (Guhra et al., 2020b: **P_{II}**)

Die Bildung von organo-mineralischen Assoziationen wurde in **P_I** als essenzielle Zwischenstation der Aggregierung identifiziert, da das Maskieren der Oberflächeneigenschaften von Bodenpartikeln wie Mineralen über die anschließende Einbindung in Aggregatstrukturen oder eine Verlagerung im Boden entscheiden kann. Dabei lag der Fokus auf den kaum erforschten Wechselwirkungen zwischen kutanem Regenwurmmucus und typischen Sekundärmineralen des Bodens. Als Referenz dienten die umfangreichen Erkenntnisse zu dem Wechselwirken von bakteriellem EPS mit Bodenmineralen. Die Studie bezog sich im Besonderen auf anektische und endogäische Regenwurmarten. Während des Prozessierens des Bodens scheiden sie nährstoffreichen kutanen Mucus aus. Auf diese Weise beeinflussen Regenwürmer nicht nur die Bodenstruktur, sondern auch das chemische Milieu der Drilosphäre, in welcher der Mucus einen überwiegenden Anteil des OM ausmacht. Trotz der offensichtlich bedeutenden Rolle von Regenwürmern als Ökosystemingenieur existierten, im Vergleich zu mikrobiellen EPS, keine mechanistischen Studien über die Wechselwirkung von Regenwurmmucus mit Bodenmineralen. Mit unserer Studie trugen wir dazu bei, diese Wissenslücke zu schließen, indem wir das Adsorptionsverhalten von Mucus an die Sekundärminerale Goethit und Illit mittels Batch-Reaktorexperimenten untersuchten. Wir konzentrierten uns auf Mucus von anektischen *Lumbricus terrestris* L. und endogäischen *Aporrectodea caliginosa* Sav., welcher hauptsächlich aus Proteinen, Polysacchariden und Kohlenhydraten bestand. Der Vergleich zu mikrobieller EPS zeigte deutliche Unterschiede zu EPS der späten stationären Wachstumsphase. Die EPS der frühen stationären Wachstumsphase hingegen zeigt eine sehr ähnliche Zusammensetzung. Während der Batch-Experimente beobachteten wir für beide Mucus-Typen eine deutliche Adsorption an Goethit und Illit. Im Besonderen wurde eine Fraktionierung der Mucus-Komponenten zwischen der festen (Minerale) und der flüssigen (Überstände) Phase festgestellt. Vor allem für Goethit zeigte sich eine bevorzugte Adsorption von

phosphorhaltigen Mucus-Bestandteilen und die Adsorption zu Illit war auf hydrophobe Makromoleküle wie Proteine zurückzuführen. Diese spezifischen Adsorptionen führten zu der Bildung von wasserstabilen Organo-Mineral-Assoziationen, welche potenziell als persistenter Baustein für (Mikro-)Aggregate dienen. Dabei verändert die Ummantelung der Minerale mit Mucus den isoelektrischen Punkt (IEP) der Assoziationen im Vergleich zu den OM-freien Referenzen. Der IEP der Mucus-Goethit-Assoziationen nahm ab, während der der Mucus-Illit-Assoziationen im Vergleich zu den Referenzen zunahm. Somit weist die Adsorption von OM und die spezifische Anreicherung von Phosphor an Goethit bzw. die deutliche Adsorption von proteinreichem Mucus an Illit auf die Bedeutung von Regenwurm-beeinflussten wasserstabilen Organo-Mineral-Assoziationen für die Nährstoffkreisläufe hin. Darüber hinaus könnten die spezifischen Oberflächeneigenschaften dieser organo-mineralischen Assoziationen ihre Wege und ihre Translokation im Boden im Hinblick auf präferenzielles Fließen innerhalb der von Regenwürmern gebildeten Bioporen massiv beeinflussen.

Wie beeinflussen biogenes OM die initiale Aggregatbildung? (Guhra et al., 2019: $\mathbf{P_{III}}$)

Am Beispiel von mikrobieller EPS haben wir uns detailliert die Einflussnahme von biogenem OM auf die Aggregierung und das Wechselwirken zwischen drei unterschiedlichen Bodenmineraltypen untersucht. Die in $\mathbf{P_I}$ suggerierten Rollen von biogenem OM als Separations- und Klebe-Mittel zeigten sich dabei deutlich im Verlauf der Experimente. Die Bildung von organo-mineralischen Assoziationen stand dabei als aggregationskontrollierender Zwischenschritt im Fokus des Manuskripts. Wir untersuchten mittels Batch-Reaktorexperimenten die Aggregierung von Bodenmineralien verschiedener Größe, Oberflächenladung und Form in Gegenwart von EPS der späten stationären Wachstumsphase von *Bacillus subtilis* als Prototyp für biogenes OM. Dabei fokussierten wir uns auf die Interaktionen innerhalb eines Multikomponentensystems, welches gleichzeitig Quarz, Goethit und Illit beinhaltete. Während der Experimente zeigten sich in Abhängigkeit der Gegenwart oder Abwesenheit von EPS deutlich unterschiedliche Wechselwirkungen zwischen den drei mineralischen Komponenten. EPS-freie Ansätze zeigten eine homogene Verteilung der Mineralphasen, die Bildung von Mineral-Mineral-Assoziationen und eine rapide Aggregation auf, die einer gravitativen Sedimentation der gebildeten Strukturen folgte. Die Bildung der Mineral-Mineral-Assoziationen erfolgte dabei über Goethit als Überbrückungsmittel, welches im Vergleich zu Illit und Quarz unter den experimentellen Bedingungen eine positive Nettoladung besaß. Im Gegensatz dazu zeigten EPS-haltige Ansätze eine deutliche heterogene Verteilung der Mineralphasen. Man konnte eine deutliche Fraktionierung der Mineralphasen erkennen, wobei beispielsweise Quarz subsequent sedimentierte und Goethit dispers im Überstand zurückblieb. Diese spezifischen räumlichen Anordnungen waren nach einem Trocknungsschritt auf der Mikrometer-Skala mittels energiedispersiver Röntgenspektroskopie weiterhin nachweisbar. Den Mineralen zugeordnete Element-Kombinationen traten dabei in EPS-freien Ansätzen in unmittelbarer Nähe zueinander auf, wohingegen in EPS-haltigen Ansätzen eine deutliche Separierung der Minerale vorlag. Im Vergleich zu den nicht EPS-assoziierten Mineralien wurde vor allem für Goethit eine Umkehrung bzw. eine Anpassung der Oberflächenladung aufgrund eines EPS-Oberflächenscreenings beobachtet. Folglich lagen unter den experimentellen Bedingungen ausschließlich negative Oberflächenladungen in dem beobachteten wässrigen System vor, die eine weitere Aggregierung der organo-mineralischen Assoziationen über elektrostatische Wechselwirkungen hemmte. Wir schließen

daraus, dass die initiale Bildung der Assoziationen und Aggregate sowie deren räumliche Anordnung durch die elektrostatischen Wechselwirkungen gesteuert wurden. Trotz dieser Beobachtung konnte die verwendete EPS nicht ausschließlich als Separationsmittel identifiziert werden. Laserlichtbeugungsmessungen ergaben eine Zunahme der Partikelgröße mit Erhöhung der Konzentration des Hintergrundelektrolyten und vor allem wenn die EPS-haltigen Ansätze einen Trocknungsschritt erfahren haben. An dieser Stelle übernahm die EPS die Rolle eines Klebemittels. Anhand der in dieser Arbeit gewonnenen Erkenntnisse zeigte sich deutlich, dass vor allem die initialen Schritte einer Aggregation in der wässrigen Phase von den weitreichenden elektrostatischen Wechselwirkungen gestaltet werden und damit massiven Einfluss auf den Transport bzw. die Involvierung der beteiligten Komponenten in eine übergeordnete 3D-Aggregatstruktur nehmen.

Welche Randbedingungen kontrollieren die Aggregation durch ladungsbedingte Wechselwirkungen? (Rupp et al., 2019: **P_{IV}**)

In dieser *in silico* Studie arbeiteten wir in Kooperation mit dem Teilprojekt Modellierung des DFG Forschungsbereiches MADsoil um anhand simpler ladungsorientierter Aggregationsregeln die Selbstorganisation von Mineralprototypen zu untersuchen. Für die hier vorgestellte numerische Untersuchung verwendeten wir ebenfalls ein Multikomponentensystem, welches drei verschiedene, in Größe, Form und Ladung variierende, Mineralprototypen beinhaltete. Mittels eines zellulären Automatenmodells (Rupp et al., 2018) untersuchten wir das Zusammenspiel zwischen den drei bereits vorgestellten Mineralprototypen, in Bezug auf attraktive und abstoßende Wechselwirkungen. Dabei wurde der dem Illit nachempfundene Prototyp szenarienspezifisch in seiner Ladung angepasst, um einerseits den Einfluss von variablen Oberflächenladungen oder die Oberflächenmodifikation durch dünne organische bzw. mineralische Beschichtungen zu simulieren. Mittels repräsentativ gewählter Szenarien wurden die Randbedingungen wie Partikelverhältnisse, Größe, Ladung und Anzahl innerhalb der Simulationen modifiziert. Anhand der Szenarien zeigte sich, dass die umfangreichsten Aggregationen nahe einer Systemnettoladung von Null auftraten. Hier führte die ausgeglichene Verfügbarkeit von positiv und negativ geladenen Oberflächen dazu, dass die Aggregation nicht durch die begrenzte Verfügbarkeit von Aggregationspartnern limitiert wurde. Im Kontrast dazu zeigten Szenarien, in welchen ein deutlicher Überschuss an positiven oder negativen Ladungen vorlag, einen Mangel bzw. einen Überschuss an aggregationsvermittelnden Partikeln. Vor allem der Überschuss kleiner Partikel führte zu einer Belegung größerer revers geladener Partikel, welches eine Neutralisation der Oberflächenladungen zufolge hatte und somit ein weiteres Aggregatwachstum inhibierte. Somit zeigte sich deutlich, dass die Anteile sowie die Größe der wechselwirkenden, gegensätzlich geladenen Bestandteile die Größe, Form und Menge, der sich bildenden Aggregate bestimmen. Liegen jedoch konstante Anteile zwischen den wechselwirkenden Mineralprototypen vor, aber ein variables Fest-Flüssig-Verhältnis, lässt sich eine beschleunigte Aggregation bei Systemen mit hoher Partikelanzahl nachweisen. In diesen Szenarien ergaben sich kurze Interaktionsschrittweiten, bis der nächste potenzielle Interaktionspartner gefunden werden konnte. Darüber hinaus ermöglichte die Untersuchung einen Einblick in die zeitliche und hierarchische Entwicklung der Aggregatentstehung anhand der sukzessiven Bildung von Partikeldimeren in frühen Stadien im Vergleich zu komplexen fraktalen Aggregaten in späteren Stadien. Mit Hilfe dieser Studie zeigten wir den Einfluss von

Partikelzusammensetzung, Ladungen, Größenverhältnissen, Partikelkonzentrationen und der Zeit auf die Bildung von Mikroaggregaten. Dies ermöglicht Vorhersagen für die dynamischen Wechselwirkungen des Aggregationsverhaltens in der Bodenlösung, vor allem falls *in situ* Monitoring oder mechanistische Laborstudien einen immensen experimentellen Aufwand erfordern würden.

Welchen Einfluss hat die Schwerkraft auf die durch elektrostatische Wechselwirkungen induzierte Aggregation? (Guhra et al., 2021: **P_V**)

Die letzte Veröffentlichung erweitert die in **P_{IV}** behandelte Fragestellungen um den Einfluss der Schwerkraft. Dafür wurde das von Ritschel and Totsche (2019) entwickelte, physikalisch rigorose und auf der DLVO-Theorie basierende, Aggregationsmodell zu einem 3D-Visualisierungstool weiterentwickelt. Ein derartiges Modellierungswerkzeug erlaubt es die Entwicklung einer subsequent aggregierenden dreidimensionalen Struktur aufgrund von Diffusion, Oberflächenwechselwirkungen und Schwerkraft in Vergleich zu einer von Schwerkraft unbeeinflussten Referenz zu simulieren. Dabei lag der Schwerpunkt auf dem Übergangsbereich zwischen dem durch Schwerkraft (orthokinetisch) kontrollierten und durch Diffusion (perikinetisch) kontrollierten Aggregation. Im Zuge dieser Studie führten wir repräsentative Modellierungen durch, um systematisch den Einfluss der Partikelgröße und des pH-Werts auf die schwerkraftgesteuerte Aggregierung zu untersuchen. Mit Hilfe des Modellierungswerkzeuges identifizierten wir drei, in Abhängigkeit der Partikelgröße und Oberflächenladung wirkende Mechanismen. In den von Schwerkraft dominierten Systemen mit den initial größten Partikeln, identifizierten wir eine indirekte Förderung der Aggregation durch die kontinuierliche Abnahme des maximalen Partikelabstandes während der schnellen Sedimentation großer Partikel (Mechanismus I). Eine direkte aggregationsfördernde Wirkung der Schwerkraft fanden wir in dem Übergangsszenario von perikinetischer zu orthokinetischer Aggregation, wobei schneller sedimentierende Partikel, während der Sedimentation mit kleineren Partikeln kollidieren und aggregieren (Mechanismus II). Eine Hemmung der Aggregation zeigte sich am deutlichsten in Szenarien, welche unter ausschließlich diffusiven Bedingungen starteten. Hier beobachteten wir eine räumliche Fraktionierung zwischen einem diffusions- und sedimentationsgesteuerten Bereich innerhalb des beobachteten Systems (Mechanismus III). Des Weiteren führte die Abwesenheit von Energiebarrieren zwischen den Mineralprototypen bei niedrigen pH-Werten zu der schnellsten Interpartikel-Aggregation, da die Aggregation nicht über ein Überbrückungsmittel vermittelt werden musste. Im Kontrast dazu stand die Erhöhung der Energiebarriere zum Überbrückungsmittel, was zu einer deutlichen Limitierung potenzieller Aggregationsplätze führte. Somit zeigte sich das neben der Schwerkraft, die Eigenschaften und die Verfügbarkeit des Überbrückungsmittels die Aggregation beeinflusste. Die Live-Verfolgung der Aggregatbildung zeigte dabei deutlich die sukzessive Bildung von zunehmend komplexer werdenden Strukturen, welche in ihrer Ausdehnung in der Z-Achse aufgrund des Wirkens der Schwerkraft begrenzt wurden. Des Weiteren zeigten diese, im Vergleich zu der von Schwerkraft unbeeinflussten Referenz, mit zunehmender Partikelgröße die Ansammlung großer Initialpartikel im unteren Bereich der Aggregatstruktur und bildeten somit deutlich anisotrope Strukturen.

Summary

The superordinated theme of the cumulative dissertation and the related publications is the initial aggregate formation in soil. The meaning of (micro-)aggregates in soil is attributed to the fact that they form the smallest unit in soil which represents soil in their functions. Therefore, the extent of aggregation and the aggregate stability is frequently considered as an analogue for soil quality. Thus, the aggregate as key to most soil functions is a three-dimensional and porous structure, composed of both organic and inorganic components. However, the formation pathways of aggregates in soil are manifold and controlled by the soil-forming factors of climate, relief, parent rock, time, and organisms. In this work, I focused primarily on aggregate formation processes induced by soil organisms and the initial aggregation within an aqueous phase. In the course of the publications presented here, we aim to follow the aggregation stepwise *in vitro* and then subsequently reconstruct and evaluate the basic model assumptions *in silico*. For this, we utilize simple but representative model systems based on three prototypes of soil minerals. These include the secondary minerals goethite and illite as typical iron oxide and clay minerals in temperate latitudes as well as quartz as a weathering persistent primary mineral. The influence of soil organisms and biogenic organic matter (OM) was investigated using earthworm excreted cutaneous mucus and microbial produced extracellular polymeric substances (EPS). The interaction between biogenic OM and soil mineral phases is a complex interplay of diverse hierarchical sub-processes, ranging from the biogenic OM provision by the soil biota, to the formation of organo-mineral associations and their incorporation into aggregates. Furthermore, translocation and transport of particles, associations, and aggregates in the liquid phase of the soil shape the structuring of the soil as well as impact of bioturbation, desiccation, wetting, swelling, and shrinking. One of the main challenges is that all these factors and processes simultaneously influence aggregation and affect each other. Thus, following key questions arise:

How does biogenic organic material get into soil aggregates? (Guhra et al., 2022: **P_I**)

The first manuscript comprises a critical literature review around biogenically induced aggregation and forms the fundament of this dissertation. In particular, the focus was on biogenic OM excreted by soil organisms. Root exudates, earthworm mucus, and microbial EPS contribute to the formation of organo-mineral associations and aggregates in soil. The excretion of biogenic OM partially occurs in combination with bioturbation, compaction, and subsequent alteration, which lead to the formation of water-stable aggregates. The resulting biogenic aggregates are involved in soil structuring, nutrient storage, and habitat provision for microorganisms. The aggregate formation induced by the activity and excretions of soil organisms is based on a cascade of mostly separately thematized sub-processes such as OM release, formation of organo-mineral associations, their transport and (im-)mobilization. Specifically, soil biota impacted aggregates exhibit characteristic features such as OM-screenings/coatings, agglutination, and enmeshment which hold individual soil particles together. Despite this, the role of biogenic OM in aggregation is subject to controversy, as biogenic OM is described in the literature as both promoting and inhibiting aggregation. An essential aspect of this is the association or adsorption of biogenic OM with soil particles, which results in OM-coatings of the soil particles or minerals and consequently influences their surface properties. The opposing effects, promotion and inhibition of aggregation is due to the complex interaction of environmental parameters and the physicochemical properties of biogenic OM during

potential aggregate formation. In accordance with this, biogenic OM can play three different roles in aggregation, depending on its origin and prevailing environmental conditions:
(I) Biogenic OM can serve as a bridging agent that enables aggregation due to surface modifications and attractive interactions, (II) as a separating agent that favors the formation of organo-mineral associations, their mobility and transport, but inhibits their further incorporation into aggregates, and (III) as a gluing agent that mediates aggregation after external force (e.g., water menisci) led to the convergence of soil particles. In soil as natural and enlivened systems these processes occur simultaneously and across temporal and spatial scales. Furthermore, biogenic aggregation is driven by the activity of and the interactions between various soil organisms, because the different taxonomic groups are closely inter-linked via food chains, decomposition processes, predation, and mutualistic relationships. The site-specific biodiversity therefore contributes more to effective aggregation than the intervention of a specific organism.

How does biogenic OM alter the surfaces of minerals? (Guhra et al., 2020b: **P_{II}**)
In **P_I** the formation of organo-mineral associations was identified as an essential intermediate step in aggregation, as the screening the surface properties of soil particles such as minerals can be a determinant for the subsequent incorporation into an aggregate structure or the mobilization and translocation within the soil. In this study we focus on the poorly studied interactions between cutaneous earthworm mucus and typical secondary soil minerals such as goethite and illite. The extensive knowledge on the interaction of bacterial EPS with soil minerals served as a reference. The study was specifically related to anecic and endogeic earthworm species which excrete nutrient-rich cutaneous mucus during active soil processing. In this way, earthworms influence not only soil structure, but also the milieu of the drilosphere, in which mucus represents a predominant portion fraction of OM.
Despite the important role of earthworms as ecosystem engineers, no mechanistic studies on the interaction of earthworm mucus with soil minerals existed in comparison to microbial EPS. With the utilization of completely mixed batch reactor experiments, we contributed to fill this knowledge gap by investigating the adsorption behavior of mucus to the secondary mineral phase goethite and illite. We focused on mucus from anecic *Lumbricus terrestris* L. and endogeic *Aporrectodea caliginosa* Sav. Which is predominantly composed of proteins, polysaccharides, and carbohydrates. The comparison of mucus to microbial EPS of the late stationary growth phase showed significant compositional differences. In contrast, EPS of the early stationary growth phase was found to be of similar composition. However, different protein types could be identified, based on shift of bands attributed to proteins by infrared spectrometric measurements. During the batch experiments, we observed an adsorption to goethite and illite for both types of mucus. Specifically, we detected a fractionation of the mucus components between the solid (minerals) and liquid (supernatant) phases. In particular, goethite showed preferential adsorption of phosphorus-containing mucus components and the adsorption to illite was facilitated due to hydrophobic macromolecules such as proteins. These specific adsorptions led to the formation of water-stable organo-mineral associations, which potentially serve as persistent building units of (micro-)aggregates. Particularly, the coating of the minerals with mucus alters the isoelectric point (IEP) of the resulting associations in comparison to the corresponding pure mineral phases. The IEP of the mucus-goethite associations decreased, while that of the mucus-illite associations increased compared to the bare minerals. Thus, the

adsorption of organic carbon and the specific enrichment of phosphorus on goethite and the adsorption of protein-rich mucus on illite indicate the importance of earthworm-influenced water-stable organo-mineral associations for nutrient cycling. In respect of the preferential flow within the biopores formed by earthworms, the specific surface properties of these organo-mineral associations could massively influence their pathways and translocation in the soil.

How biogenic OM affect initial aggregate formation? (Guhra et al., 2019: **P_{III}**)

We investigate the influence of microbial EPS as biogenic OM on the aggregation and interaction between three fundamentally different soil mineral types. During this experimental approach, the in **P_I** suggested roles of biogenic OM as a separation agent and gluing agent were revealed. The focus of the manuscript was the formation of organo-mineral associations as intermediate step of aggregation. By using completely mixed batch reactor experiments, we investigated the aggregation of soil minerals of different size, surface charge, and shape in the presence of EPS of the late stationary growth phase of *Bacillus subtili*s as a representative for biogenic OM. We focused on the interactions within a multicomponent system that simultaneously included quartz, goethite, and illite. Depending on the presence or absence of EPS, significantly different interactions between the three mineral components were apparent. EPS-free treatments revealed a homogeneous distribution of mineral phases, the formation of mineral-mineral associations, and rapid aggregation which was followed by a gravitational sedimentation of the formed aggregates. Under these experimental conditions, the formation of mineral-mineral associations occurred via goethite as a bridging agent, which possessed a net positive charge compared to illite and quartz. In contrast, EPS-containing treatments showed a heterogeneous distribution of mineral phases. A clear fractionation of the mineral phases could be seen by quartz sedimenting subsequently and goethite remaining dispersed in the supernatant. These specific spatial arrangements were still detectable on the micrometer scale after a drying step was conducted by energy dispersive X-ray spectroscopy. In EPS-free treatments, the different mineral types representing elemental combinations occurred in close proximity to each other, whereas in EPS-containing treatments a clear separation of the minerals was identified. Especially for goethite, a reversal/adjustment of the surface charge due to EPS surface screening was observed, in comparison to the bare mineral. Consequently, under the experimental conditions, only negative surface charges were present, which inhibited further aggregation of the organo-mineral associations via electrostatic interactions. We concluded that the initial formation of the associations and aggregates as well as their spatial arrangement were controlled by the electrostatic interactions. Despite this observation, the EPS could not exclusively identify as a separating agent. Laser light diffraction measurements revealed an increase in particle size with increasing concentration of the background electrolyte and especially when the EPS-containing treatments were previously dried. At this point, the EPS took on the role of a gluing-agent. Consequently, it became clear that especially the initial steps of an aggregation in the aqueous phase are shaped by the long-range electrostatic interactions and thus have a massive influence on the transport or the involvement of the involved component in a superordinate 3D aggregate structure.

Which boundary conditions control charge-induced aggregation? (Rupp et al., 2019: **P_{IV}**)

In this *in silico* study, we worked in cooperation with the modeling subproject of the DFG research unit MADsoil to investigate the self-assembly of mineral prototypes based on simple charge-driven aggregation rules. For the numerical investigation presented here, we also used a multicomponent system containing three different mineral prototypes varying in size, shape, and charge. By applying a cellular automata model (Rupp et al., 2018), we investigated the interplay between the three already introduced mineral prototypes, in terms of attractive and repulsive interactions. The charge of the illite inspired prototype, was scenario-specifically adapted to simulate the influence of variable surface charges or the surface modification by thin organic or mineral coatings. With the help of representative scenarios, the boundary conditions such as particle ratios, size, charge, and number were modified within the simulations. Based on these scenarios, it was found that the most extensive aggregations occurred near a net system charge of zero. Here, the balanced availability of positively and negatively charged surfaces led to an aggregation which was not inhibited by the limited availability of aggregation partners. In contrast, scenarios which were characterized by an excess of positive or negative charges corresponded to a lack or excess of aggregation-mediating particles (bridging agents), respectively. In particular, the excess of small particles led to an occupation of larger reversely charged particles, which resulted in a neutralization of their surface charges. Such shielding inhibited further aggregate growth.

Thus, it was clearly shown that the proportions as well as the size of the interacting, oppositely charged components determine the size, shape and quantity of the resulting aggregates. However, if there are constant proportions between the interacting mineral prototypes, but a variable solid-liquid ratio, an accelerated aggregation can be demonstrated in systems with high particle numbers. In these scenarios, short interaction step sizes (e.g., diffusion lengths) led to fast aggregate formation if the next potential interaction partner is in close vicinity. Furthermore, the study provided insight into the temporal and hierarchical evolution of aggregate formation based on the successive formation of particle dimers at early stages compared to complex fractal aggregates at later stages.

Using this mechanistic *in silico* study, we showed the influence of particle composition, charges, size ratios, particle concentrations, and time on the formation of microaggregates. This allows predictions for the dynamic interactions of aggregation behavior in soil and in soil solution, especially if *in situ* monitoring or mechanistic laboratory studies would require immense experimental efforts.

What is the influence of gravity on aggregation induced by electrostatic interactions? (Guhra et al., 2021: **P_{V}**)

The last publication addressed in the cumulative dissertation extends the issues addressed in **P_{IV}** by including the influence of gravity. For this purpose, the physically rigorous aggregation model developed by Ritschel and Totsche (2019) based on DLVO theory was further developed into a 3D visualization tool. Modeling tools like this allow to simulate the *in silico* evolution of a subsequent aggregating three-dimensional structure due to diffusion, surface interactions and gravity in comparison to a gravity-unaffected reference. The focus was on the transition between gravity (orthokinetic) controlled and diffusion (perikinetic) controlled aggregation. In the course of this study, representative simulations were performed to systematically investigate the influence of particle size and pH on gravity-controlled

aggregation. Using the modeling tool, we identified three mechanisms acting in response to particle size and surface charge. In the gravity-dominated systems with the initially largest particles, we identified an indirect promotion of aggregation due to the continuous spatial confinement during rapid sedimentation of large particles (mechanism I). In the transition scenarios from perikinetic to orthokinetic aggregation, a direct aggregation-promoting effect of gravity was identified, where faster-sedimenting particles collide with smaller particles and aggregate during ongoing sedimentation (mechanism II). The inhibition of aggregation was evident in a scenario which started under diffusive conditions. Here, we observed spatial fractionation between a diffusion- and sedimentation-driven domain within the observed system (mechanism III). Furthermore, the absence of energy barriers between mineral prototypes at low pH resulted in the fastest interparticle aggregation since aggregation did not need to be mediated by a dedicated bridging agent. In comparison, the increase in the energy barrier to the bridging agent resulted in a significant limitation of potential aggregation sites. Thus, in addition to gravity, the properties and availability of the bridging agent were shown to influence aggregation. The live tracking of the aggregate formation clearly showed successive and hierarchical formation of increasingly complex structures, which were limited in their Z-axis extension due to the effect of gravity. Furthermore, with increasing initial particle size, the aggregates showed the accumulation of large initial particles in the lower part of the fractal structures, thus forming clearly anisotropic structures in comparison to the reference unaffected by gravity.

1. Introduction

The pedosphere is the highly dynamic, enlivened, and altered interface between atmosphere and lithosphere and serves as one of the most important resources for human life by providing diverse essential soil functions. A few examples are soils acting as carbon sink, pollutant filter, nutrient reservoir and habitat for fauna and flora (Blume et al., 2010). Soil is characterized as natural porous media with a complex and heterogeneous composition. It consists of a liquid, solid and gaseous phase (Evangelou, 1998). This multi-phase system is driven by the interplay of biogeochemical processes and hence controls nutrient as well as pollutant transport and fixation (Totsche et al., 2010). Major inorganic ingredients of the solid phase are secondary soil minerals (e.g., metal oxides and clay minerals) and persistent primary minerals (e.g., quartz) (e.g., Edwards and Bremner, 1967; Tisdall and Oades, 1982; Nwadialo and Mbagwu, 1991; Six et al., 2004). The amount of organic matter (OM) in soil results from microbial biomass and the decomposition of plant litter, faunal tissues (Brown et al., 2000; Landeweert et al., 2001; McMaster, 2012; Lavelle et al., 2016). These components formed and/or altered during pedogenesis, build the basis for aggregates arranged in a three-dimensional system (Oades, 1984; Totsche et al., 2010; Menon et al., 2020) and can be classified as microaggregate forming materials (MFMs) (Totsche et al., 2018). The definition by Totsche et al. (2018) contains all mineral, organic and biotic components which are involved in the formation and stabilization of aggregates (Nichols and Halvorson, 2013) e.g. serving as bridging, gluing, or cementing agents. If more than one MFM is bound together, composite building units (CBUs) are formed (Totsche et al., 2018) which can be characterized as mineral-mineral and organo-mineral associations. The inorganic clay to silt sized MFMs (Nwadialo and Mbagwu, 1991), form aggregates via rearrangement, flocculation, and cementation in the presence of organic and inorganic binding agents (Six et al., 2004; Kögel-Knabner et al., 2008). Organic binding agents are classically distinguished in temporary (roots and hyphae which can be decomposed), transient (e.g., polysaccharides which are fast degraded by organisms) and persistent (dissolved OM which is strongly bound and protected by minerals) binding agents (Tisdall and Oades, 1982; Oades, 1984). Thus, aggregation agents stabilize aggregates against external stress (Nichols and Halvorson, 2013) and the resulting resistance against external forces like wetting and hydraulic stress depending on organic and inorganic composition (Felde et al., 2021).

In general, the process of aggregation is driven by complex interactions between the five major aggregation factors summarized by Six et al. (2004) as microorganisms, roots, soil fauna, environmental variables, and the inorganic binding/aggregation agents. The dissertation focuses on biogenic and biogenically influenced aggregation factors and how they shape aggregation at the mechanistic level, because the importance of these aggregation factors is frequently underrepresented and underestimated in literature (e.g., Bottinelli et al., 2015; Lavelle et al., 2020). Soil biota like bacteria, earthworms, fungi and roots are able to actively release complexly composed molecule mixtures (e.g.,

root mucilage, earthworm mucus and microbial EPS) which harbor the potential to alter the circumjacent environmental conditions (e.g., pH, electric conductivity and the availability of nutrients) (Brown et al., 2000; Landeweert et al., 2001; Blume et al., 2010; McMaster, 2012). The surface interactions between organisms, OM and minerals are presumed as crucial in regulating the formation of organo-mineral associations (Christensen, 2001) and lead to a screening of surface properties due to an adsorption to inorganic soil constituents (Omoike and Chorover, 2004; Tombácz et al., 2004; Kleber et al., 2015). In addition, OM inside organo-mineral associations is reported to be protected from being decomposed by soil fauna or flora (Oades, 1984; Jastrow and Miller, 1998; Baldock, 2002). Therefore, adsorption and precipitation of soil OM inside CBUs and aggregates are protecting processes (Eusterhues et al., 2014). Furthermore, many of the essential soil functions (e.g., habitat, nutrient storage, and water retention) can be retraced to the presence and arrangement of organo-mineral associations and aggregates in soil (Totsche et al., 2018) which are substantially controlled, formed and altered by soil flora and fauna (Lavelle et al., 2020).

1.1. The theory of aggregation

The ongoing development of aggregation theories is a broad field which reconciles diverse approaches, techniques and disciplines and is frequently discussed critically (e.g., Baveye, 2021). However, Yudina and Kuzyakov (2019) highlighted the concept of (micro-)aggregates as essential building blocks of soil and deduce the critical discussion around aggregates and their role in soil to the missing clear or blurred definition of the terminus aggregates and related methods for their extraction. Menon et al. (2020) discusses aggregates as the leading structural units of soil and their stability against external stress as one major parameter for soil quality. The stability of aggregates against external forces based on their intra-aggregate bonding caused by the adherent effect of organic and inorganic binding/aggregation agents (Nichols and Halvorson, 2013). Exemplarily, Felde et al. (2021) showed the variance in aggregate stability in relation to clay content, OC contents and microbial community composition due to extraction by wet sieving (hydraulic pressures) or dry-crushing (mechanical stresses). Specifically, OM can serve as gluing agent after an external force provokes a close approach of particles and enables their agglutination (Pen et al., 2015; Carminati et al., 2016; Krause et al., 2019). In contrast, primary inorganic compounds like carbonates and metal-oxides are able to serve as cementing agents via (co-)precipitation with and between further soil particles (Tisdall and Oades, 1982; Chartres et al., 1990; Buettner et al., 2014). Furthermore, the aggregation can be shaped by the surface alteration due to inorganic and organic bridging and separation agents. For example, Goldberg and Glaubig (1987) demonstrate a flocculation of clay minerals facilitated by metal oxides. Vice versa if metal oxides are available in excess, a shielding of the surface occurs and inhibits a subsequent aggregation (Ohtsubo et al., 1991). Similar observations are reported for OM which can alter the solution conditions (e.g., pH

and electrical conductivity) and screening/coating mineral surfaces which control the aggregation of particles (e.g., Tombácz et al., 2004; Flynn et al., 2012; Freitas et al., 2015; Sheng et al., 2016; Narvekar et al., 2017).

A conceptual model that explains in which order aggregates evolve as function of the interplaying binding/aggregation agents is given by the hierarchy theory developed by Tisdall and Oades in the early 1980s (Tisdall and Oades, 1982). They assumed that clay and silt sized particles are bound to microaggregates with a size smaller than 250 µm by persistent binding agents. These microaggregates are associated into macroaggregates with a size greater than 250 µm by temporary and transient binding agents. A few years later Oades disproved this theory and proposed that microaggregates are formed inside macroaggregates with roots and hyphae as temporary binding agents, which are later decomposed in fragments (Oades, 1984). This organic debris serves as nutrient source for soil (micro-)organisms, which produce organic binding/aggregation agents such as extracellular polymeric substances (EPS) that cause an aggregation of silt to clay sized mineral constituents. Further investigations could show that microaggregates can be distinguished into large and small microaggregates, which are more stable against mechanical treatments like tillage (Golchin et al., 1997; Christensen, 2001). The smallest and most stable building unit with a size smaller than 2 µm is described by Chenu and Plante (2006) as OM incrusted by minerals or OM coated minerals, typically referred to as organo-mineral associations (Kleber et al., 2015) and CBUs (Totsche et al., 2018). Thus, the stability of aggregates is mainly impacted by the type of aggregation agent permitting the association of MFMs and the aggregation agent present is related to the potential size of the aggregates (Oades, 1984; Christensen, 2001). A comprehensive approach bringing all these size specific classifications together is given in Totsche et al. (2018). They classified composite building units (CBUs) smaller than 2 µm, small microaggregates with a size between 2 and 20 µm and large microaggregates greater than 20 µm up to 250 µm. In addition, the study of Semenov et al. (2020) where they investigated the aggregate size specific decomposition rate of plant residues includes also mega-aggregates (2 to 10 mm). The aggregation theory of Lavelle et al. (2020) is more “biocentric”. They recommended a conceptual model based on three assumptions. The first assumption is an origin-based (e.g., biogenic or physicogenic) classification of aggregate fractions. Secondly, microaggregates are mainly formed inside macroaggregates as more stable fraction. The last assumption states that aggregate and OM dynamics are closely linked together, especially in terms of biologically triggered processes. Despite the increasing awareness that organisms and their biogenic excretions have a non-negligible role in the soil structuring and aggregate formation, the mechanistic understanding of small-scale processes which contribute to particle association are only described diffusely and fragmentarily in literature.

The formation of (micro-)aggregates and their smaller building units is scarcely illuminated especially in terms of biogenic aggregation factors (Lavelle et al., 2020) and in most cases based on observations from larger macroaggregate scale and aggregation theories (Totsche et al., 2018). Reviews like Six et al. (2004), Totsche et al. (2018), and Lavelle et al. (2020) started to entangle and reveal the range of potential formation pathways of soil (micro-)aggregates and their CBUs. They consider the impact of interplaying soil fauna, flora, inorganic and organic binding agents, wetting and drying and the role of surface properties on initial aggregation of soil (micro-)aggregates on a mechanistic level. For example, they showed that small scale interactions like interparticle forces were badly examined for the soil system for a long time and were rather separately discussed as a part of colloidal and flocculation studies. Yudina and Kuzyakov (2019) outline the pore space and the interface between the solid and liquid phase as hotspot of aggregate forming processes. Exemplary, major pedogenic processes as result of eluviation and illuviation, including particle (i.e. organo-mineral associations and soil aggregates) transport, relocation, and immobilization inside pore space (Lehmann et al., 2021) lead to the formation of diagnostic soil horizons(Bronick and Lal, 2005) Additionally, external physical forces, induced for example by drying of soil, are known to have a positive effect on aggregation. For instance, aggregate stability increases with decreasing water content through the occurrence of water menisci between greater mineral particles or aggregates which pull small clay sized MFMs together(Horn and Dexter, 1989; Semmel et al., 1990; Horn et al., 1994; Denef et al., 2002). Furthermore, the pure presence of organic matter in soil often is not a sufficient trigger for aggregation, because the activity and soil processing of organisms as part of nutrient and carbon cycling is needed to form aggregates in soil (Lavelle et al., 2006). The resulting biogenic aggregates and organo-mineral associations are able to outlive the creating organism (Lavelle, 2002) and thus the accumulation of nutrients and carbon in soil can be persistent (Le Mer et al., 2020). Additionally, the bioturbation in the upper soil horizons shapes the soil structure and the formation of aggregates due to carbon turnover and preferential pathway formation (biopores) for fluid flow and matter transport, including organic, biotic and inorganic colloids as potential MFMs and CBUs (Lee and Foster, 1991; Brown et al., 2000; Six et al., 2004; Bottinelli et al., 2015; Franco et al., 2020) (Figure 1).

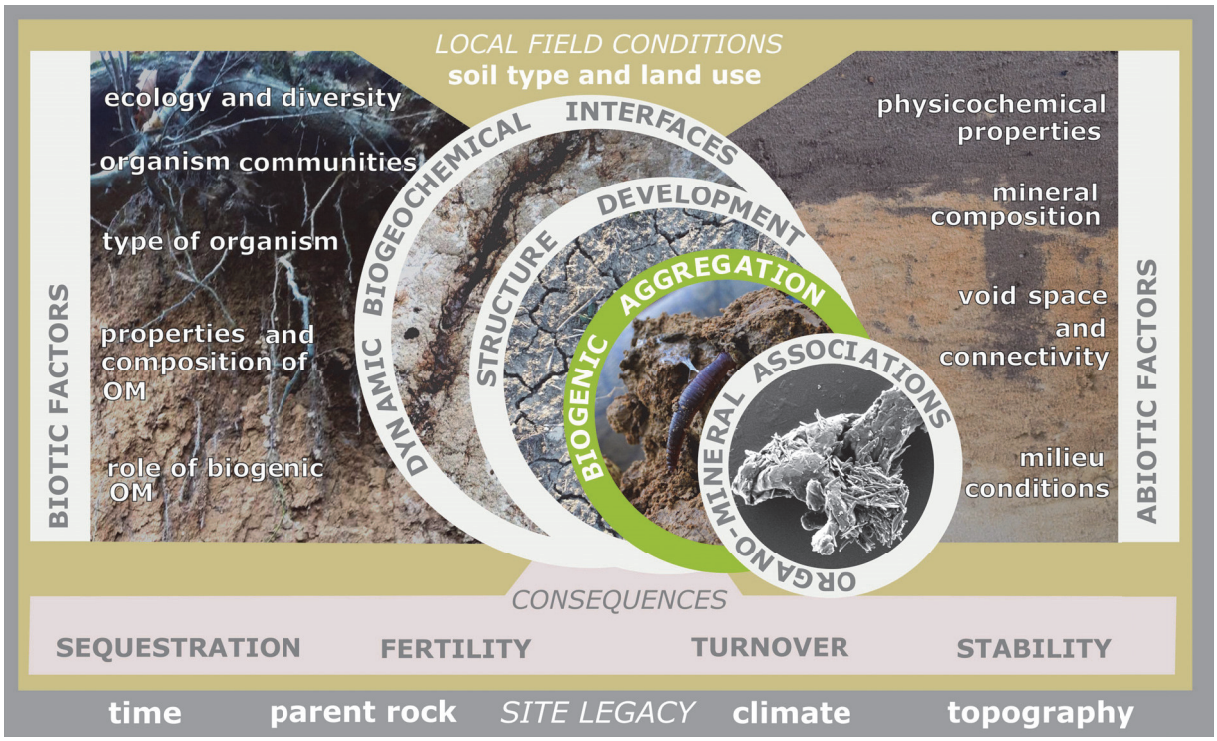

Figure 1: Nested hierarchy of biogenic aggregation impacting factors. The site legacy (grey level) including the superordinated soil formation factors which determine the expression of local field conditions (beige level). The site-specific soil type and land use predefine the prevailing biotic and abiotic aggregation impacting factors. Biotic factors include the ecology identified by the structural and functional biodiversity in soil. The resulting organism communities and their interactions are based on food webs and mutualistic relationships and feedbacks. The type of soil biota specifies which composition and properties of biogenically excreted OM to be expected, and, consequently, which functional role biogenically excreted OM may take in soil. The abiotic factors comprise the physicochemical properties of the immediate environment which determine the milieu conditions of the soil fluids (liquid and gas phases). Included therein is the mineral composition which conditions the reactive surfaces of soil. These are located within the pore space network characterized by their topology. Along the dynamic biogeochemical interfaces, i.e., zones of interaction between biotic and abiotic factors (e.g., rhizosphere, drilosphere, and detritussphere) soil structure development, especially biogenic aggregation occurs (highlighted in green). Depending on the functional role of the involved biogenically excreted OM, organo-mineral-associations with different fates (i.e., transport and (im-)mobilization) develop. As consequence (rose level), the soil structure is altered in terms of aggregate stability. Furthermore, the formation of biogenic aggregates affects the nutrient cycle by turnover and sequestration processes and thus soil fertility and health (promotional image for P_I according to Guhra et al., 2022).

1.2. Biogenic aggregation and aggregation agents

Holistic insights in biogenic aggregate formation induced by soil biota requires interdisciplinary knowledge obtained from various scientific disciplines e.g., ecology, microbiology, biogeochemistry, soil and colloid science since it can be seen as cascade of biotic and abiotic sub-processes. In particular, the outstanding role of the soil biota community in terms of aggregate formation (Lehmann et al., 2017) was elaborated, if producers and decomposers of OM are strongly interconnected via food chains and mutualistic relationships (Barrios, 2007) (Figure 2). As consequence review paper entitled “Why is the influence of soil macrofauna on soil structure only considered by soil ecologists?” (Bottinelli et al., 2015) occur from time to time. To address this fragmentarily illuminated field, we condensed the knowledge given in literature in respect of the scientific progress of our working group and the DFG funded research unit 2179 (MADsoil) with a review article. With “Pathways of biogenically excreted

organic matter into soil aggregates" (**P_I**) we provide a review article that combines different scales and disciplines, thematizing biogenic formation pathway of soil aggregates. We start with the biogenic OM (e.g., root exudates, mucus, and extracellular polymeric substances), their composition (organism specify portions of biopolymers like proteins and polysaccharides), supplying organisms (plants, earthworms, and microorganisms) and their role in aggregation and soil structuring (e.g., compaction, gluing, enmeshing, and coating). In the following we discussed the adsorption of biogenic OM to soil particles (predominantly minerals) as initial and important step in organo-mineral association and aggregate formation. In respect of the surrounding conditions/milieu (e.g., ionic strength, temperature, pH, and redox-potential), the formation of these organo-mineral associations (as important CBUs), their subsequent fate in soil (e.g., (im-)mobilization and translocation) and their path into soil aggregates is strongly influenced by their surface alterations and screenings in comparison to the initial bare soil particles. Biogenic OM is controversially discussed as **binding/aggregation agent,** as they may promote as well as inhibit aggregation at the same time as function milieu conditions and biogenic OM inherent physicochemical properties OM (e.g., composition, concentration, protein-to-polysaccharide-ratio, molecular weight of biopolymers, functional groups, and biopolymer structure). Based on the current state of knowledge we introduce biogenic OM according to their three different roles in aggregation: as **bridging agent** which permits the aggregation due to attraction and surface modifications, as **separation agent** which favors the formation, mobility and transport of organo-mineral associations and inhibits their further involvement into aggregates, and as **gluing agent** which mediates aggregate stability, after an external force (pressure supply, menisci forces and/or gravitative sedimentation) provokes a close approach of soil particles.

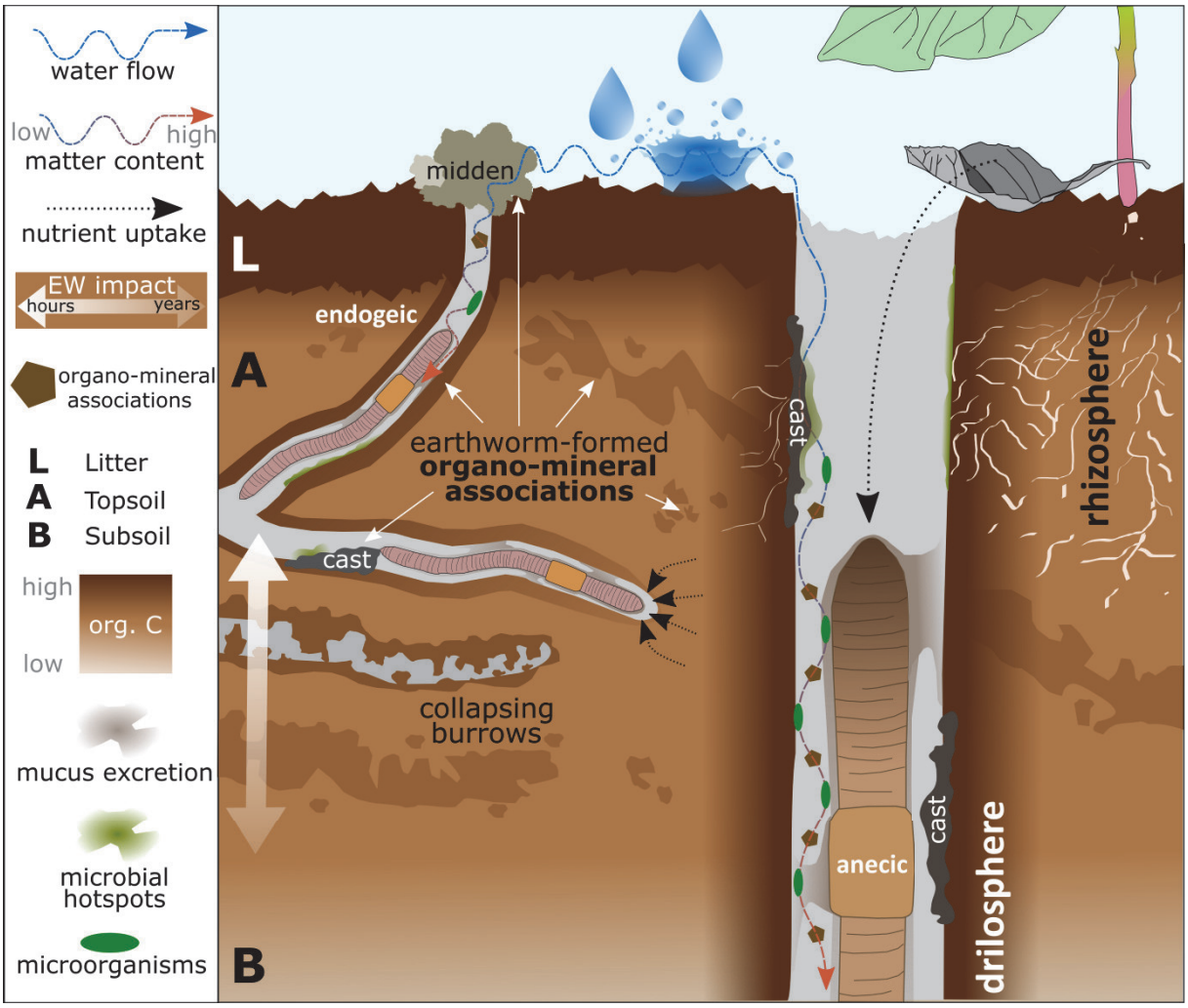

Figure 2: Scheme of the evolution of earthworm-formed (EW) organo-mineral associations and aggregates due to the activity and mucus excretion of anecic and endogeic earthworms in soil. Earthworm formed burrows and aggregates (casts, middens, and burrow linings) are enriched in nutrients and form habitats for microorganisms and paths of preferential root growth. Especially, in the upper soil horizons, the transition zones between organisms and soil material like the drilosphere, rhizosphere and detritussphere occur in direct vicinity and influences each other (according to Guhra et al., 2020a).

1.3. Aggregate formation from the scratch

Humans need models and simplification trying to understand their environment. Thus, in the applied soil science simpleminded reference systems like artificial porous media (e.g., Narvekar et al., 2017; Lehmann et al., 2018; Ritschel et al., 2021) and well-defined colloidal systems containing a defined amount of interacting constituents (e.g., Ali and Bandyopadhyay, 2016; Syngouna and Chrysikopoulos, 2016; Yang et al., 2016; Tiraferri et al., 2017; Upendar et al., 2018) are used to conduct mechanistic studies of specific processes as small part of highly dynamic systems like pedogenesis and soil aggregate formation. Furthermore, mathematic models are shown as helpful to relate basic assumptions to experimental results and to get an insight in small scale processes which are not or hardly traceable with actual measurements (e.g., Szilagyi et al., 2014a; Rupp et al., 2018; Ritschel and Totsche, 2019).

In our experimental ($\mathbf{P_{II}}$ and $\mathbf{P_{III}}$) and numerical studies ($\mathbf{P_{IV}}$ and $\mathbf{P_{V}}$) we focus on aggregation processes

occurring potentially in soils of the humid latitudes. Consequently, we worked with the well-defined secondary soil minerals goethite and illite, quartz as primary soil mineral and biogenically excreted OM provided by earthworms and bacteria (e.g., mucus and microbial EPS) as surrogates for typical inorganic and organic constituents and potentially aggregate forming materials found in soil. The following sections shortly outline the basic assumptions and concepts in terms of interparticle interactions and impact of environmental conditions on the formation of organo-mineral association and aggregates from the presented model components (Figure 3).

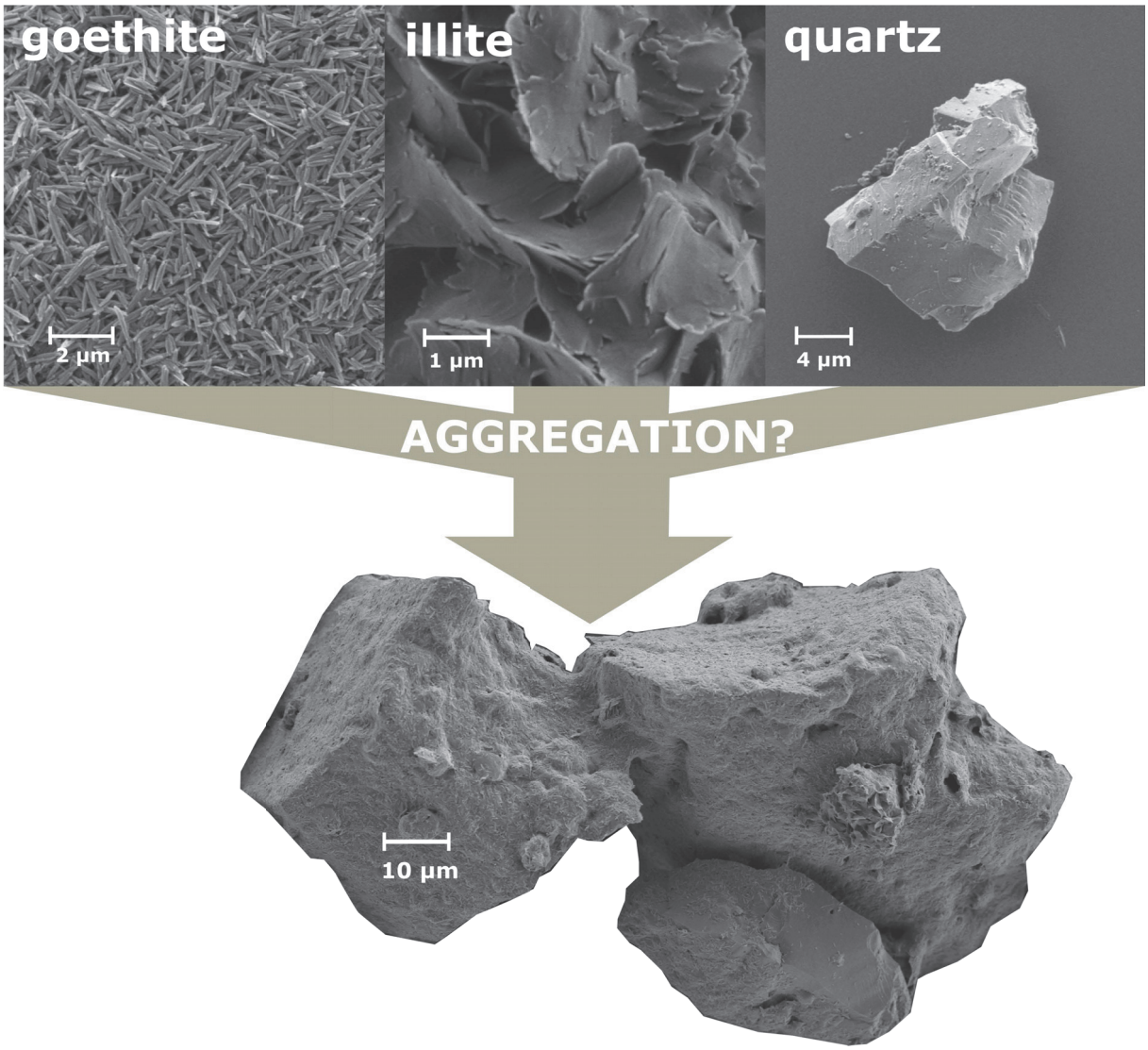

Figure 3: What impacts aggregation? *In vitro* aggregate formation from three mineral prototypes serving as potential microaggregate forming materials (MFMs) resulting in aggregate composed of large quartz particles screened and bridged by a coating composed of illite and goethite.

1.3.1. Morphological properties of solids

Beside the prevalent environmental conditions the MFM inherent morphological properties like shape, roughness and size (Figure 4)are known as aggregation influencing factors and are reported to shaping aggregate structure, stability as well as OM adsorption (Buffle and Leppard, 1995; Philippe and Schaumann, 2014; Harrison et al., 2015; Lazzari et al., 2016). For example, changed homo-aggregation kinetics and adsorption properties for OM can be found for ZnO nanoparticles with different morphologies and specific surface area (Zhou and Keller, 2010). Furthermore, experimental studies show that the adhesion between particles increases with increasing contact area (Katainen et al., 2006; Hotze et al., 2010; Ramakrishna et al., 2011). The prominent example is the adhesion between two sheets which is stronger than between two spheres (Lagaly et al., 1997). If the surface roughness of a particle is increased, the effective contact points to another smooth surface can be reduced, but if the surface roughness of both surfaces is increased (on the same size scale) the surface irregularities can lock in each other and the contact area between the two particles is increased (Zou et al., 2015). Therefore, the shape and relative size of a particle in relation to the interacting surface irregularities and features where the association takes place is reported as important for interparticle bonding (Katainen et al., 2006).

A change in inter-particle aggregation can be achieved by surface modifications like coatings. For instance, an OM coating reduces the surface roughness and consequently the specific surface area by covering the surface irregularities and fill inter- and intra-particle pores (Wagai et al., 2009), but can also increase the interparticle bonds by gluing surfaces together or enmesh particles (Costa et al., 2018). Also, mineral coatings can be found in soil resulting from coprecipitation or surface attachment (e.g., Tisdall and Oades, 1982; Fritzsche et al., 2015; Totsche et al., 2018). Larrahondo et al. (2011) modified silica surfaces by iron oxide coatings which lead to an increased specific surface area and enhanced number of interparticle contacts between the modified particles. Scheidegger et al. (1993) summarized that the mineral coatings can modify the adsorption and cation exchange capacities and can provoke flocculation and particle association which potentially alter hydraulic properties and transport in soil.

Besides, the size relation between surface features and interacting particles (Katainen et al., 2006) the size ratio between interacting particles was also reported to affect aggregation. For instance, high size discrepancies between interacting particles result in an effective bridging between large particles, until the number of small particles becomes large enough to totally occupy the surface of large particles (Yates et al., 2005). The resulting aggregates from aqueous systems with a large size difference are described as more dense and containing a lower inter-aggregate pore volume in comparison to the more fractal structures resulting from systems with lower size differences (Cerbelaud et al., 2010; Cerbelaud et al., 2017). Nonetheless, the aggregation of heterogeneous colloids is a function of the

size as well as the number of interacting particles and depending on this can lead to different aggregate structures (Olsen et al., 2005; Yates et al., 2008).

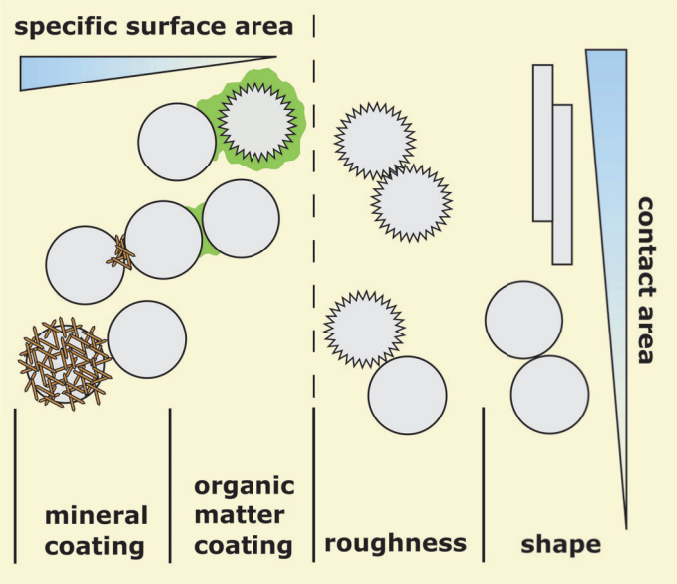

Figure 4: Effect of different shapes and surface roughness for the aggregation between particles. Mineral (brown rods) and organic matter coatings (green screenings) potentially change the contact area and specific surface area of particles which alters attachment properties.

Furthermore, under the influence of gravity the particle aggregation and deposition (Dukhin et al., 2007) is impacted by particle specific size and density (Dokou et al., 2001; Wu et al., 2003). In consequence, a fractionation between small/low density colloids and large/high density colloids/aggregates is induced, which could result in the formation of layered sediments (e.g., de las Heras et al., 2016; González, 2016). Hence, the sedimentation velocity of aggregates is controlled and increased by the ongoing particle aggregation (Yang et al., 2016). However, during aggregation and sedimentation mechanical forces lead to the breaking apart of fractal aggregates and a subsequent restructuring of these, which result in higher fractal dimensions in comparison to aggregates which are formed under predominantly diffusive conditions (Allain et al., 1996). The higher fractal dimensions are explained by the occlusion of small aggregates and particles into the cavities of larger sedimenting clusters which lead to compact structures (González, 2016). Furthermore, the structure formation depends on the initial volume fraction of interacting particles which result in the formation of gelled (high particle amounts) or clustered (low amounts of particles) deposits (Allain et al., 1995).

1.3.2. Physicochemical conditions of the aqueous phase

The physicochemical conditions of the aqueous phase (e.g., temperature, pH, and electric conductivity) are major factors controlling the interactions (e.g., electrostatics) between charged particles as well as OM with protonatable functional groups, in terms of adsorption mechanisms and aggregate formation (e.g., Mosley et al., 2003; Tombácz et al., 2004; Philippe and Schaumann, 2014; Lin et al., 2016). In this section the potential physicochemical interactions between the previously mentioned model components as base of our experimental and numerical models are shortly stated (Figure 5).

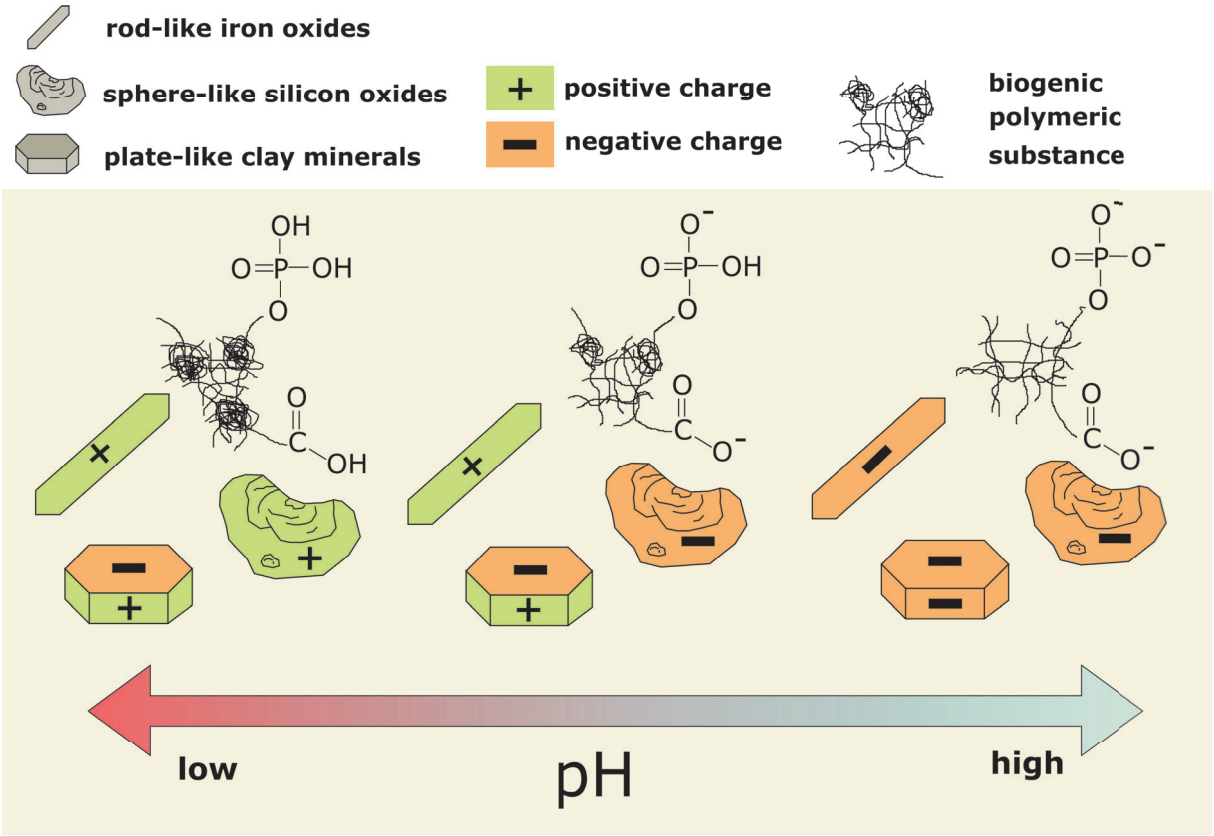

Figure 5: Change of the surface charge (orange: negative / green: positive) of the model MFMs illite (platy), goethite (rod-like), quartz (grained) and EPS (polymer chain network) (according to: Tombácz and Szekeres, 2004; Dogsa et al., 2005; Wang et al., 2012).

Surface charges

Goethite potentially provides positive surface charges in soil and is characterized by a variable surface charge (Cornell and Schwertmann, 2003). As reference for the prevalent surface charge conditions of mineral phases serves the point of zero charge (PZC: measured by acid-base titration) or the isoelectric point (measured by electro-kinetic methods) representing the specific pH were the net zero charge of a surface resulting from an equivalent amount of positive and negative charged surface groups (Kosmulski, 2016). The most natural and synthesized goethite phases are characterized by high IEP/PZC

ranking from 6.4 to 9.7, with a positive charge at lower pH values and a negative charge at higher values (Kosmulski, 2016, 2020). In comparison to goethite, quartz also possesses variably charged surfaces, but the IEP is clearly lower and reaching from ≤1 to 4 for quartz-phases (Kosmulski, 2016). Platy shaped clay minerals like illite providing aluminol- and silanol-groups on the edges and have negatively charged basal planes over the whole pH range (e.g., Sondi et al., 1996; Liu et al., 1999; Kosmulski and Dahlsten, 2006; Tombácz and Szekeres, 2006; Kosmulski, 2011; Hong et al., 2013; Yu et al., 2013). In respect of the heterogeneous charge types provided by the specific shape of clay minerals, these tend to homo-aggregate via edge-to-face coagulation at low pH values (Tombácz and Szekeres, 2004). Under this condition the edges are positively charged and can attract to the basal planes with the continuous negative charges (Dultz et al., 2019).

In binary and ternary composed systems containing different mineral phases electrostatic attraction is a main driver for mineral-mineral associations and aggregate formation. For example, positively charged iron oxides are reported to permit the flocculation of net negative charged clay minerals (Ohtsubo, 1989). Vice versa, an availability of iron oxides in excess led to the neutralization of clay mineral surface charges and a shielding which inhibit an ongoing aggregation (Ohtsubo et al., 1991). In general, a balanced availability of positive and negative charges in a multi component system is reported to promote the formation of large aggregate structures (Bansal et al., 2017; Cerbelaud et al., 2017).

Beside mineral constituents, OM in soil provide variable surface charges and is known to alter the surface charges of the soil mineral phase by screenings and coatings (e.g., Zhuang and Yu, 2002; Tombácz et al., 2004; Kleber et al., 2007; Kleber et al., 2015). For example, the biogenic organic matter we focused on is composed of various biopolymers like proteins and polysaccharides (Walker et al., 2003; Pan et al., 2010; Mahapatra and Banerjee, 2013; Frey, 2019) which provide a high diversity of functional groups with a broad range of pK_a-values (Wang et al., 2012; Zhao et al., 2015). Thus, functional groups enable the electrostatic interaction between biogenic OM and mineral surfaces controlled by pH and electric conductivity (e.g., Omoike and Chorover, 2004; Labille et al., 2005; Omoike and Chorover, 2006; Fang et al., 2010; Cao et al., 2011; Fang et al., 2012; Lin et al., 2016) as well as interaction between the functional groups of biopolymer mixtures which led to changes in their internal structure resulting in swelling, shrinking, folding and unfolding (e.g., Dogsa et al., 2005; Becker et al., 2011; Wang et al., 2012; Pen et al., 2015; Kubiak-Ossowska et al., 2016; for more details see PI).

Together with the prominently discussed electrostatics, Van der Waals interactions, hydrophobic interactions, ligand exchange, cation bridging and H-bonding contribute to OM adsorption and aggregation (e.g., Six et al., 2004; Nichols and Halvorson, 2013; Philippe and Schaumann, 2014) of the here discussed MFMs. For example, inter particle force measurements (with atomic force microscopy: AFM) between a SiO_2 sphere (PZC: ~2) and a goethite surface (PZC: 6.5-7.4) showed repulsive forces

between both components at a pH value of 9 (Assemi et al., 2004). In comparison, at a pH value of 6 where both components are oppositely charged an attraction was measured. The addition of fulvic acid as surrogate for OM to the system, leads to the surface screening of goethite and thus to the measurement of repulsive forces between goethite and the SiO_2-sphere during similar pH values (pH 5.6) (Assemi et al., 2004). Furthermore, stable associations and aggregates are reported as result of adsorption mechanisms like complex formation. A prominent example is the functionalization of SiO_2-surfaces due to a goethite coating under the formation of inner-sphere complexes (Xu and Axe, 2005). Hence, a high stability of these iron oxide coatings against strong acids (1 M HNO_3) and strong bases (10 M NaOH) could be reported by Scheidegger et al. (1993). Furthermore, the adsorption of EPS to goethite during unfavorable electrostatic conditions are reported by the detection of high adsorption enthalpies between goethite and EPS (Lin et al., 2016) due to the formation of monodentate inner-sphere complexes at low pH and bidentate inner-sphere complexes at high pH (Fang et al., 2012). Additionally, high molecular weight proteins are reported to adsorb to silica surfaces under electrostatically unfavorable conditions by hydrophobic surface interaction (Kubiak-Ossowska et al., 2017). For more details in terms of OM induced adsorption and aggregation mechanisms please see **P_I**.

Electrolytes

Besides biopolymers, polyvalent cations (Ca^{2+} and Mg^{2+}) are known to bridge between organic and inorganic soil constituents and permit flocculation and the formation of organo-mineral associations, i.e. via cation bridging (e.g., Shipitalo and Protz, 1989; Ramos and McBride, 1996; Lagaly et al., 1997; Long et al., 2006; Szilagyi et al., 2014a). Thus, studies performed at various ionic strengths exhibit an increased adsorption of microbial EPS to mineral surfaces with increasing electrolyte concentration (Cao et al., 2011). Vice versa, the homo- and hetero-aggregation of colloids are promoted with increasing background electrolyte concentrations until the critical coagulation concentration (CCC) is reached (He et al., 2008; Narvekar et al., 2017; Trefalt et al., 2020). The promoted aggregation with increased electrolyte concentration, result from the fact that the ionic strength of a solution governs the spread of the electric double layer around a charged particle which shrinking with increasing number of counter ions (decrease range of potentially repulsive electrostatics)(Lagaly et al., 1997; McBride and Baveye, 2002; Lauth and Kowalczyk, 2016). A representative example is given by Tombácz and Szekeres (2006) considering the electric double layer around clay minerals. In this special case the basal planes show a constant negative charge in comparison to the variably charged edges at a pH under the IEP/PZC of the edges. At low electrolyte concentrations the electric double layer around the basal planes of the clay mineral is extensive and covers the oppositely charged edges. If the electrolyte concentration is increased the layer shrinks as function of available counterions and the edges are no longer covered and now available for electrostatic attraction (Tombácz et al., 2001; Jiang et al., 2012). In general, high electrolyte concentrations lead to a massive decrease of the electric double layer,

which can compensate electrostatic repulsive condition between two similarly charged surfaces, if the electric double layer becomes small enough that attractive Van der Waals forces can become apparent (Jiang et al., 2013).

Interplay between attraction and repulsion

The relationship between the short-range Van der Waals attraction and the long-range electrostatics is the basis of the DLVO (Derjaguin–Landau–Verwey–Overbeek) theory developed in the middle of the 20th century (Grasso et al., 2002). During the interaction of two colloidal particles an energy profile as function of the separation distance (V_T) evolves, which is the sum of repulsive (V_R) and attractive (V_A) energies, until two particles collide, and a further approach is impossible due to Born repulsion (B) (Figure 6I) (Ruckenstein and Prieve, 1976; Lagaly et al., 1997; Lauth and Kowalczyk, 2016). The attractive energies originate from the Van der Waals attraction and potentially electrostatic attractions which occur during the hetero-aggregation of two unequally charged MFMs (e.g., Wang et al., 2015; Cao et al., 2020) or during the homo-aggregation of MFMs at the IEP where positively and negatively charged functional groups are equivalently available (e.g., Alvarez-Silva et al., 2010; Ilina et al., 2017). Such systems tend to aggregate fast if no energy barrier inhibits a subsequent aggregate development (Figure 6II). A different behavior occurs if the system is dominated by electrostatic repulsion between two equally charged MFMs (e.g., Tawari et al., 2001; Trefalt et al., 2014). In such systems the Van der Waals interactions are not always able to compensate the electrostatic repulsion. Thus, an energy barrier between the MFMs occurs and inhibits aggregation (Figure 6III). As mentioned before, the range of electrostatic interaction is controlled by the electric double layer thus their impact can be massively reduced with increasing electrolyte concentration (e.g., Burns et al., 1997; Shih et al., 2012; Zhu et al., 2014; Diao and Espinosa-Marzal, 2016). Furthermore, the size of interacting particles controls their surface potentials and thus the strength of repulsive and attractive interactions (Hsu and Liu, 1998; Strubbe et al., 2007; He et al., 2008).

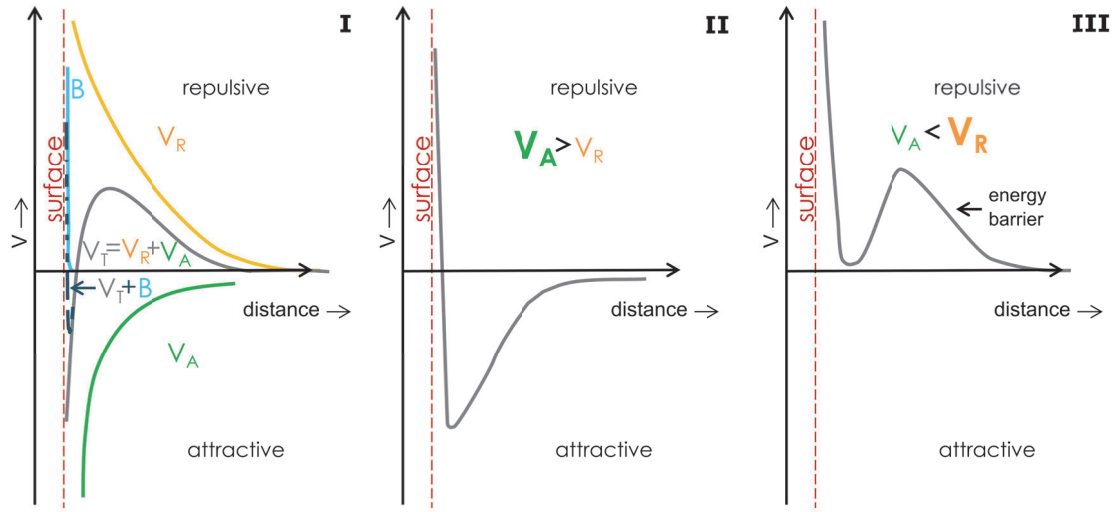

Figure 6: Energy profile (V_T) between two equally charged surfaces, as the summation (I) of repulsive (V_R) and attractive energies (V_A) (according to Lagaly et al., 1997). A further approach of particles is limited by the Born repulsion (B) of the surface. For example, if oppositely charged MFMs interact with each other, and V_A is greater than V_R aggregation can occur (II). In comparison for equally charged MFMs, aggregation can be inhibited by an energy barrier if V_R overreach V_A (III).

1.4. *In silico* aggregation

Mathematic models are powerful tools to validate concepts in terms of colloidal systems and aggregate formation. The via numerical models simulated formation of aggregate structures (*in silico* aggregation) enables to test concepts attributed to the summarized aggregation factors like the impact of particle size/number mismatch, environmental conditions (e.g., pH and electric conductivity), external fields (e.g., magnetic and gravitative), flow and particle transport. This harbors the potential to reduce enormous experimental effort to find optimal conditions for conducting aggregation experiments. Additionally, the *in silico* formed aggregates are 2D or 3D structures which can be further investigated with respect to their structure-based functions (e.g., water retention, intra-aggregate nutrient diffusion, and habitat function) without artefact biased and cumbersome aggregate preparations and expensive visualization techniques. However, based on the complexity and scale overlapping character of aggregation concepts the most scientific efforts in terms *of in silico* aggregation and structure formation concentrate on very specific issues and sub-processes. In consequence, models are mostly limited to a specific scale like microsite, ecosystem level or global level (for soil OM dynamics: Campbell and Paustian, 2015). For example, diverse multi pool models (e.g., KEYLINK and MEMS) are used to investigate the feedbacks between OM-input/-output and soil structure (Sollins and Gregg, 2017; Robertson et al., 2019; Deckmyn et al., 2020; Meurer et al., 2020; Flores et al., 2021). Davis et al. (2021) address how the structural heterogeneity of the soil pore network impacts soil biodiversity. Furthermore, some numerical studies concentrate on the feedback between microbial activity and soil

architecture via pore scale models (Pot et al., 2021). Exemplary, Crawford et al. (2012) provide a model dealing with the self-organization of microorganisms and soil particles, including micro-structural changes as function of microbial biomass. The physicochemical aspects of particle aggregation can be frequently found as part of model approaches develop in the scope of colloidal science. The aggregation as well as the breakage of fractal structures is discussed as shaped by the type of interparticle forces, particle morphology, size, concentration, and the impact of an external field (Lazzari et al., 2016).Furthermore, at the molecular scale, molecular modelling is used to investigate surface group specific adsorption mechanisms between OM and mineral surrogate surfaces (Kwon et al., 2006; Tunega et al., 2009).

For soil (micro-)aggregate formation and functions the structure development of aggregates is of particular importance. For instance, “Cellular Automaton Method” (CAM) based models, considering aggregate formation as catalog of particle interaction rules, oriented on physically plausible processes (Ray et al., 2017). In the CAM approach of Rupp et al. (2018) 2D-structures are formed due to the interaction of charged particles and their interplay with ions in solution inside three-phase system (liquid, solid and aqueous phase). In the work of Zech et al. (2020) the CAM model was used to simulate satisfying the aggregation behavior observed in lab scale aggregation experiments, which demonstrate the applicability of a simplified and abstract model which lacks the third dimension and a rigorous physical background like the DLVO theory. The reviews of Dukhin et al. (2007) and González (2016) thematize the extended complexity of DLVO based aggregation models in presence of gravity. Further models consider the stability of aggregate and show their impact on aggregate structure controlled by the balance between aggregate breakage and re-aggregation (Jeldres et al., 2018). Beside the fundamental chemical and physical mechanisms of aggregate formation, recent work of Ritschel and Totsche (2020) investigates the properties and characteristics of the resulting three-dimensional *in silico* aggregate like the water retention capacity and intra-aggregate pore system to provide a link between aggregate formation, structure, and function.

1.5. Motivation

This dissertation is motivated in the framework of “MAD Soil - Microaggregates: Formation and turnover of the structural building blocks of soils” (DFG research unit 2179). The purpose of the project was to elucidate the formation and turnover of soil microaggregates by identifying microaggregate forming processes as well as the role and function of microaggregates in soil (Totsche et al., 2018). The release and translocation of organic and inorganic microaggregate forming materials (MFMs) and composite building units (CBUs) of aggregates during transient environmental conditions in the dynamic soil system is an important part of pedogenesis and additionally affected by bioturbation as well as biogenically induced formation and destabilization of soil structures. To elucidate aggregation

relevant processes from the scratch we focused on *in vitro* and *in silico* aggregation inside multi-component aqueous systems (considering MFMs of different biotic and abiotic origin) to illuminate the formation of organo-mineral and mineral-mineral associations as essential CBUs of (micro-)aggregates. Because most lab scale studies consider binary systems (composed of two MFMs), we investigated systems with increasing complexity containing up to four potently microaggregate forming materials simultaneously and aimed to identify their specific roles during aggregation. Particularly, the role of biogenically produced OM in aggregation was in focus of efforts to clarify its critical and ambivalent impact in aggregate formation. In addition, a conceptual proof of boundary conditions relevant for aggregation inside aqueous ternary suspensions was aimed at identifying further hidden (experimentally hardly traceable) mechanisms and factors shaping aggregation. Therefore, we examined the following questions:

How does biogenic organic material get into soil aggregates? (Guhra et al., 2022: **P_I**)

The processing of soil by bioturbation and the active release of organism-specific excretions as earthworm mucus, root exudates and microbial extracellular polymeric substances result in the formation of organo-mineral associations and aggregates. The biogenic formation pathways of soil aggregates are a challenging topic, if they reflect a cascade of small-scale sub-processes (e.g., OM supply, OM adsorption, organo-mineral association formation, their transport, (im-)mobilization, and involvement into aggregate structure) which are often only portrayed in literature solitarily (e.g., Nichols and Halvorson, 2013; Bottinelli et al., 2015; Lavelle et al., 2020). With respect to this multitude of processes, the role of complexly composed biogenic OM as bridging/aggregation agent is controversially discussed in literature, as they may promote (e.g., Freitas et al., 2015; Sheng et al., 2016) as well as inhibit (e.g., Tombácz et al., 2004; Flynn et al., 2012; Pen et al., 2015) aggregation at the same time.

Thus, we provide a comprehensive framework that consistently describes the synergies and dependencies of these sub-processes. Furthermore, we critically discuss biogenically excreted OM in terms of its three different roles during aggregation: as bridging, separation, and gluing agent. Thus, we are reviewing the recent state of knowledge and discuss aggregation induced by biogenic OM on a mechanistic level from the nanometer scale to the field scale (**P_I**).

How does biogenic OM alter the surfaces of minerals? (Guhra et al., 2020b: **P_{II}**)

Earthworms are ecosystem engineers by altering the physicochemical conditions of soil in the drilosphere due to mucus secretion, actively transporting and releasing microorganisms, forming microbial hotspots, forming biopores (preferential flow pathways), destroying and forming soil aggregates (e.g., Brown et al., 2000). Up to several hundred earthworms live per square meter and

actively spread nutrient rich mucus throughout the whole soil profile (e.g., Lee and Foster, 1991; Scheu, 1991; Schrader, 1994). A vast variety of literature suggest earthworms as organisms which increase the aggregation and nutrient content in soil, for instance by comparing earthworm free and earthworm treated study sides (e.g., Six et al., 2004; Lavelle et al., 2006; Lavelle et al., 2016; Le Mer et al., 2020). In consequence, in the last decades the spotlight was focused on the effect of earthworm activity on nutrient cycles and number of soil aggregates. However, the mechanisms how earthworm provided OM (cutaneous and intestinal mucus) interacting with soil and altering properties of soil minerals was nearly ignored. In comparison, the interactions between soil minerals and microbially formed EPS are extensively investigated (e.g., Omoike and Chorover, 2004; Cao et al., 2011; Mikutta et al., 2011; Lin et al., 2016), even though earthworms process the soil more actively and are involved in the habitat formation and spreading of microorganisms in soil (e.g., Brown et al., 2000; Aira et al., 2009; Stromberger et al., 2012).

Thus, we provide comparative research based on mechanistic lab scale experiments including the compositional investigation of bacterial EPS and earthworm mucus and their adsorption behavior to typical soil mineral (e.g., illite and goethite). As earthworm cutaneous mucus serve as lubricant, we expected that mucus of *L. terrestris* and *A. caliginosa* are similar in their chemical composition, adsorption behavior and ability to form organo-mineral associations and further compare mucus to microbial EPS as well investigated type of soil OM. We are interested in the comparability of the soil mineral specific adsorption mechanisms between microbial EPS and earthworm mucus, that determine which fraction of biogenic OM becomes associated and contributes to nutrient element enrichment in soil or is prone to become decomposed or translocated.

How biogenic OM affects initial aggregate formation? (Guhra et al., 2019: $\mathbf{P_{III}}$)

After the adsorption of OM to soil minerals, the formation of (micro-)aggregates and CBUs from MFMs, is controlled by various factors for example pH, electric conductivity, alternating water content. Thus, the screening of surface properties (e.g., charge or hydrophobicity) due to OM coatings is often reported to alter inter-particle interactions in comparison to OM free systems (e.g., Philippe and Schaumann, 2014). The role of biogenic OM in MFM aggregation is reported from aggregation supporting towards aggregation inhibiting as result of OM surface coatings around minerals and the resulting screening of the initials surface charges (e.g., Tombácz et al., 2004; Pen et al., 2015; Narvekar et al., 2017). Thus, the role of biogenic OM is contrarily discussed in literature which requires more mechanistic studies of the small-scale processes between potential MFMs in soil and the soil liquid phase. Specific environmental conditions like high electrolyte concentrations or drought are expected to force aggregation. The electric conductivity controls the extension of the electric double layer around charged MFMs and therefore also the range of electrostatic forces which can compete (in

respect of charge equality between MFMs) the attractive short-range Van der Waals forces (e.g., Grasso et al., 2002; Szilagyi et al., 2014b). Furthermore, drying is an external force which provokes a near approach of potential MFMs by continuously contracting menisci during decreasing water content (e.g., Horn and Dexter, 1989; Seiphoori et al., 2020).

Therefore, in our studies, we use bacterial EPS as biogenic OM analog in multi component aggregation experiments, to obtain specific aggregation behavior between mineral MFMs (goethite, illite and quartz) in absence and presence of bacterial EPS. We consider more than three interacting MFMs in the aggregation experiments to examine the specific role of MFMs during aggregation, determining agents of aggregation and compositional features of resulting structures. We also consider different electrolyte concentrations and a drying step as relevant because variable electrolyte concentrations and water contents are typical factors which fluctuate in the soil system and are considered to modify the ability of MFMs to aggregate (**P_{III}**).

Which boundary conditions control charge-induced aggregation? (Rupp et al., 2019: **P_{IV}**)

The temporal evolution of aggregates is a highly dynamic and hierarchical process. The capturing of aggregation dynamics inside aqueous systems containing more than two mineral prototypes, different in size, shape, and charge, is a challenging task. The initial boundary conditions like particle density, number of particles, relations between particle types and size discrepancies are predictors for the size and type of subsequent format aggregates (e.g., Olsen et al., 2005; Cerbelaud et al., 2010; Metin et al., 2014; Praetorius et al., 2014; Cerbelaud et al., 2017; Liang et al., 2017; Laganapan et al., 2018; Clavier et al., 2019). The evaluation of optimal conditions for an extensive and effective aggregation in the laboratory means an enormous experimental effort which can be potentially reduced by the utilization of numerical experiments.

In cooperation with the modelling unit of the MADsoil project, we apply the CAM model (Rupp et al., 2018) to test specific boundary conditions which we classified as aggregation controlling. In the course of our studies, the net charge of the whole system was addressed as promising indicator to identify an optimum of aggregation. Furthermore, the amount, the composition/portions of the three mineral prototypes as well as the size mismatch of the interacting mineral prototypes were investigated in their aggregation regulating function. However, we validate the CAM model as tool for pre-experimental assessment of an optimal lab experiment design (**P_{IV}**).

What is the influence of gravity on aggregation induced by electrostatic interactions? (Guhra et al., 2021: **P$_V$**)

The impact of gravity is ubiquitous and shapes almost all natural processes on earth. Especially in soils, gravity driven illuviation and eluviation processes contribute to the formation of diagnostic soil horizons (e.g., Bronick and Lal, 2005; Kögel-Knabner and Amelung, 2021). Furthermore, gravity drives translocation and transport processes of microorganisms, nutrient and toxic elements through the pedosphere and alters the quality of subjacent aquifers (e.g., Ranville et al., 2005; Lehmann et al., 2021). Furthermore, the interactions of solvates, soil particles and aggregates with the immobile phase as well as between each other are expected as regulating transport via retardation on the immobile phase or the formation of larger aggregates with increased sedimentation velocities (e.g., Dukhin et al., 2007; González, 2016). Observation of particles size specific layered sediments (e.g., de las Heras et al., 2016) contrasting homogeneous flocculated "fluffy" sediments (e.g., Hütter, 2000) in batch experiments and *in silico* simulations, regulated via Van der Walls, repulsive and attractive electrostatic interactions (exemplary found in **P$_{II}$**).

A physically rigorous DLVO based framework of aggregate formation was provided by Ritschel and Totsche (2019). In the last presented publication as part of this cumulative dissertation a version of this model extended by the impact of gravity was applied. In focus were the interactions between three differently shaped, sized, and charged prototypes of soil particles. By regulating the particle size und the surface charge, the self-assembly of gravity constrained aggregates and the comparison to a gravity unaffected reference was investigated. This comparison was done because a gravity unconstrained interaction between particles is widely but erroneously used as basic assumption in terms of particle aggregation. Hence, aggregation dynamics and aggregate structure shaping mechanisms of gravity are widely neglected. The real-time visualization and exploration tools programmed by Thomas Ritschel were applied to simulate representative charge and size dependent scenarios with the aim to identify how and when gravity promotes or inhibits aggregation in the aqueous phase.

2. Publications

2.1. Publication 1 (P_I): Pathways of biogenically excreted organic matter into soil aggregates

Citation: Guhra, T., Stolze, K. and Totsche, K.U. 2022. Pathways of biogenically excreted organic matter into soil aggregates. *Soil Biology and Biochemistry*, 164, 108483.

DOI: 10.1016/j.soilbio.2021.108483

Rights and licensing: All (co-)authors agree that this article is permitted to be used in the dissertation presented here. This article is published under the terms of the creative commons CC-BY license, thus no permission to reuse the article is required. The journal as the original source of the article is referenced above.

Authors: Tom Guhra[1], Katharina Stolze[2] and Kai Uwe Totsche[3]

P_I			
involved in:	**Author**		
	1	**2**	**3**
conception of research design	X		X
planning of research activities	X		X
data acquisition	X	X	
data analyses and interpretation	X	X	X
manuscript writing	X	X	X
suggested publication equivalence value	**1.0**	1.0	

Soil Biology and Biochemistry 164 (2022) 108483

Contents lists available at ScienceDirect

Soil Biology and Biochemistry

journal homepage: www.elsevier.com/locate/soilbio

Pathways of biogenically excreted organic matter into soil aggregates

Tom Guhra, Katharina Stolze, Kai Uwe Totsche *

Department of Hydrogeology, Institute of Geosciences, Friedrich Schiller University Jena, 07749, Germany

ARTICLE INFO

Keywords:
Earthworms
Mucus
Roots
Mucilage
Bacteria
Fungi
Extracellular polymeric substances
Gluing agent
Bridging agent
Separation agent

ABSTRACT

Soil organisms are recognized as ecosystem engineers and key for aggregation in soil due to bioturbation, organic matter (OM) decomposition, and excretion of biogenic OM. The activity of soil organisms is beneficial for soil quality, functions, and nutrient cycling. These attributions are based on field-scale observations that link the presence and activity of organisms to spatiotemporal changes in soil properties and can be traced back to the formation of biogenic aggregates. This biogenic formation pathway encompasses a cascade of processes so far not discussed comprehensively. A more general approach needs to consider the activity and feedback loops between soil biota, the active release of biogenic OM by excretion, the interaction of biogenic OM with soil constituents, the formation of organo-mineral associations, and how these become incorporated in aggregated structures. Especially the function of biogenically excreted OM, which is quite complex in composition, is controversial as it permits or inhibits aggregation. This review analyzes the various roles of biogenically excreted OM may take as an **aggregation agent.** We will show that its function depends on the interplay of numerous factors, including environmental conditions, variety of OM producers, composition and availability of biogenically excreted OM, and type of interacting mineral phase. We consider biogenically excreted OM to affect aggregate formation in three different ways: (I) as a **bridging agent** which promotes the aggregation due to surface modifications and attraction, (II) as a **separation agent** which favors the formation, mobility, and transport of organo-mineral associations and inhibits their further inclusion into aggregates, and (III) as a **gluing agent** which mediates aggregate stability, after an external force provokes a close approach of soil particles. We conclude that biogenically excreted OM takes these functional roles simultaneously and to a varying extent across spatiotemporal scales. Hence, biogenically excreted OM is involved in the surface modification of soil particles, in the enmeshment and gluing of particles into soil aggregates, in the (im-)mobilization, and in facilitating the transport of particles. All that depends on the interplay of a hierarchy of factors comprising the local soil community's composition, the properties of biogenically excreted OM, and the conditions of the immediate environment.

1. Introduction

During pedogenesis, organo-mineral associations evolve as the fundamental building units of (micro-) aggregates in soil (Totsche et al., 2018). These organo-mineral associations are presumed key for nutrient provision, preservation, and carbon storage (Kleber et al., 2015). They are composed of soil minerals and organic matter (OM) of various origins (e.g., Kögel-Knabner et al., 2008). Major inorganic constituents in aggregates are secondary soil minerals (e.g., metal (hydr-)oxides, clay minerals) and persistent primary minerals (e.g., quartz) (Edwards and Bremner, 1967a, b; Nwadialo and Mbagwu, 1991). The OM in soil results from microbial and root bio- and necromass, biogenic excretion, and the decomposition of plant and faunal tissues and debris (Tisdall and Oades, 1982; Oades, 1984; Jastrow and Miller, 1998; Golchin et al., 1998; Lützow et al., 2006; Amelung et al., 2008). Surface interactions between minerals and OM are presumed to control the formation of organo-mineral associations (Christensen, 2001) and aggregates. If at least two of these (micro-)aggregate forming materials are combined, composite building units emerge, representing the smallest size class of microaggregates (Totsche et al., 2018). Consequently, OM incrusted by minerals or OM-coated minerals form as the smallest (size <2 μm) and most stable building units of aggregates (Chenu and Plante, 2006). The stability of aggregates against external forces (e.g., wetting and osmotic stress) is related to their intra-aggregate bonding (Nichols and Halvorson, 2013). These bondings are mediated by organic and inorganic aggregation/binding agents, enabling aggregation by their attractive surface properties, agglutinating, and cementing characteristics (Totsche et al., 2018). Consequently, the stability of aggregates against

* Corresponding author. Department of Hydrogeology, Institute of Geosciences, Friedrich Schiller University Jena, Burgweg 11, 07749, Jena, Germany.
E-mail address: kai.totsche@uni-jena.de (K.U. Totsche).

https://doi.org/10.1016/j.soilbio.2021.108483
Received 11 April 2021; Received in revised form 25 October 2021; Accepted 2 November 2021
Available online 5 November 2021
This is an open access article under the CC BY license (http://creativecommons.org/licenses/by/4.0/).

external forces differs, e.g., with OC and clay content (Felde et al., 2020). Furthermore, adsorption of OM on and co-precipitation of OM with soil minerals protect OM (Eusterhues et al., 2014; Machmuller et al., 2015; Wagai et al., 2020) against decomposition (Baldock et al., 2002; Kögel-Knabner et al., 2008). Many of the essential soil functions (e.g., habitat provision, nutrient storage, and water retention) are linked to the presence and arrangement of these organo-mineral associations in a superordinated three-dimensional aggregate structure (Six et al., 2004; Asano et al., 2018; Menon et al., 2020; Yudina and Kuzyakov, 2019).

Lavelle et al. (2020) emphasized the critical role of soil organisms in soil structuring but indicated a lack of awareness of their function to form aggregates. Bacteria, fungi, and in particular, earthworms and roots shape the soil structure. Additionally, they actively release organic exudates, including root mucilage, earthworm mucus, and microbial extracellular polymeric substances, in the circumjacent soil (Brown et al., 2000; Landeweert et al., 2001; McMaster, 2012; Lavelle et al., 2016). Hence, soil biota alters the environmental conditions and physicochemical properties (e.g., pH, redox-potential, electric conductivity, density, microstructure, availability of nutrients) by soil processing, growth, and metabolization (Schrader, 1994; Walker et al., 2003; Haq et al., 2014; Bottinelli et al., 2015). These activities result in a close linkage of aggregate and OM dynamics, especially in biological processes such as bioturbation (Lavelle et al., 2020). The resulting biogenic structures and aggregates show altered color, composition, increased water stability, hydrophobicity, and carbon content compared to the bulk soil (Chenu and Cosentino, 2011; Lavelle et al., 2016). Consequently, biogenic aggregates can be physically and chemically distinct from physicogenic aggregates and are defined as formed under the influence of organic matter, roots, and microbial exudates, in addition to the mechanical (compressive) stress of roots and hyphae, and soil fauna activity (de Melo et al., 2019). However, physical, chemical, and biogenic aggregation processes do not run isolated within distinct spatial and functional domains in soil. Instead, interdependencies between these mechanisms establish dynamic equilibria (Nichols and Halvorson, 2013; Lavelle et al., 2020). Thus, "biogenic aggregation" is defined as the sum of all processes exerted or mediated by soil biota which trigger or alter physical (e.g., compaction by mechanical stress due to growing roots) and chemical aggregation processes (e.g., by excretion of OM that acts as coating or aggregation agent) (Fig. 1).

In this paper, we review the current understanding of the formation of biogenic aggregates by surveying the role of plants, earthworms, and microorganisms as critical producers of biogenically excreted OM (OM_{BE}). OM_{BE} can be considered as a mixture of biopolymers released after death or actively by soil biota to preserve their functionality and survival in soil. We highlight the adsorption to and agglutination of OM_{BE} with mineral surfaces (Morel et al., 1987; Omoike and Chorover, 2004) as one initial step for the formation of organo-mineral associations. In particular, the alteration of the surface properties controls the fate of organo-mineral associations inside porous media and their incorporation into aggregates (Flynn et al., 2012; Narvekar et al., 2017; Dultz et al., 2019; Krause et al., 2019; Guhra et al., 2019). Notably, the role of OM_{BE} as binding/aggregation agent (Nichols and Halvorson, 2013; Totsche et al., 2018) is critically discussed in literature since OM_{BE} has been likewise reported as facilitating (e.g., Freitas et al., 2015; Sheng et al., 2016) and inhibiting (e.g., Tombácz et al., 2004; Flynn et al., 2012; Pen et al., 2015) the aggregation. Thus, we discuss the

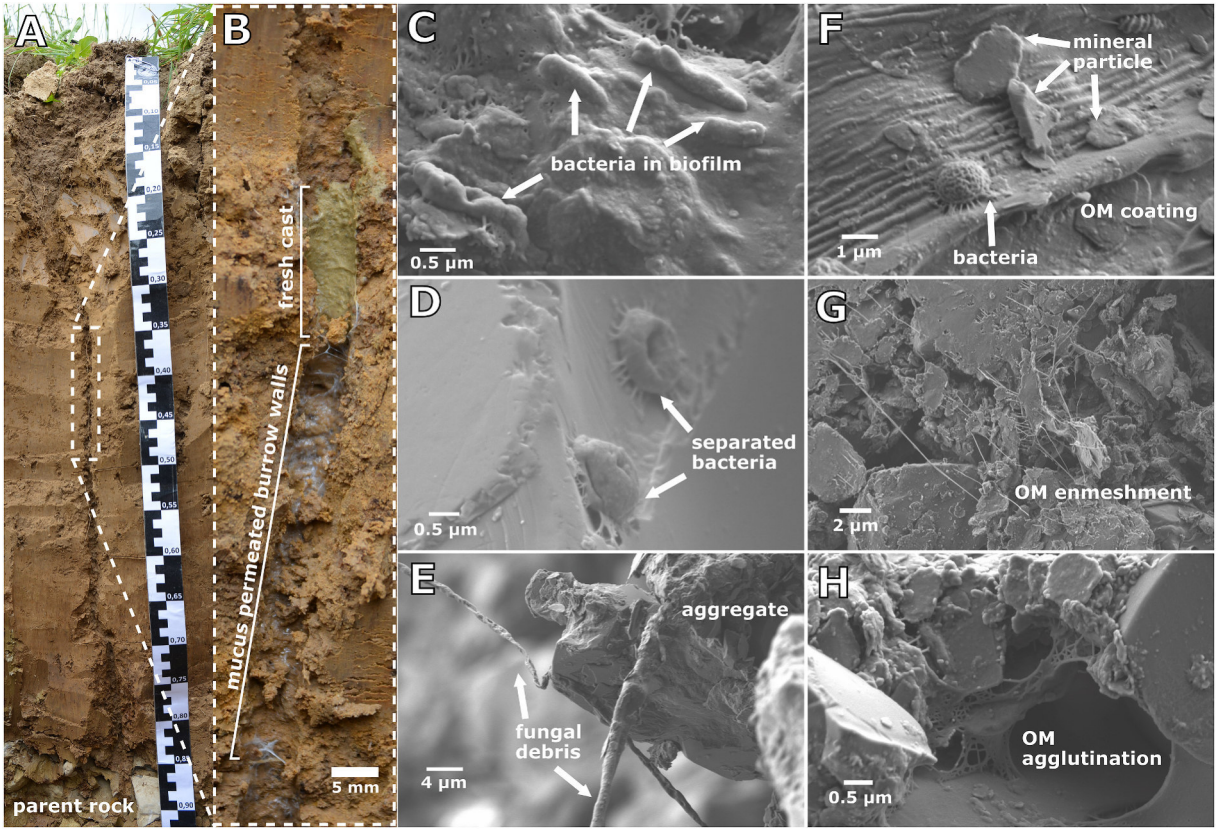

Fig. 1. Earthworm burrows are favorable locations of organo-mineral associations and biogenic aggregate formation in soil. Biopores of *Lumbricus terrestris* L. can reach down to the parent rock and bypass water flow and matter transport (A). A heterogeneous covering with nutrient-rich cutaneous mucus and casts characterizes the burrow walls (B). The so formed drilosphere provides habitats for microorganisms that stabilize soil aggregates with extracellular polymeric substances (EPS) (in biofilms: C and separated: D) and fungal hyphae (E) in addition to the earthworm mucus. The biogenically formed OM stabilizes aggregates by coatings which additionally serve as a new interface for microbial or mineral attachment (F), the enmeshment of soil particles (G), and as an adhesive between soil particles and aggregates (H).

ambivalently portrayed role of OM_{BE} in aggregate formation for the underlying mechanisms.

2. Origin of biogenically excreted organic matter in soil: producers, products, and properties

Biogenic organic matter (OM) originates from diverse sources. It ranges from plant debris and faunal tissues (Tisdall and Oades, 1982) to exudates released by plants, fungi, bacteria, and earthworms (Brown et al., 2000; Walker et al., 2003; Haq et al., 2014; Flemming et al., 2016). Additionally, the microbial necromass (Liang et al., 2020) and plant detritus (Hooker and Stark, 2012) contribute to soil organic matter (SOM) and nutrient cycles. Recent publications showed that microbial necromass could represent up to 50% of the SOM (Liang et al., 2019). Virus-induced cell lysis can lead to increased availability of labile C in soil (Williamson et al., 2017). Thereby, typical biofilm components such as proteins and DNA are released, but particularly adenosine triphosphate can be considered as an indicator for cell lysis (Redmile-Gordon et al., 2014). In general, OM_{BE} is a mixture of diverse biopolymers encompassing lipids, proteins, polysaccharides, and carbohydrates (Cortez and Bouché, 1987; Walker et al., 2003; Pan et al., 2010; Mahapatra and Banerjee, 2013; Frey, 2019). Specific compositions of OM_{BE} reflect the variety of its functions and producers in soil. Earthworms excrete cutaneous mucus as a lubricant to allow their movement through the soil (Zhang et al., 2016). The intestinal mucus serves as a carrier for symbiotic microorganisms and enables the passage of incorporated soil material through the earthworm gut (Brown et al., 2000). In contrast, microbial EPS supports various functions, like cell adhesion, adsorption of inorganic and organic nutrients, aggregation of bacterial cells, water retention, protective barrier formation, and information exchange (More et al., 2014; Flemming et al., 2016). Fungal secretions are involved in signal transmission, which can lead to the inhibition or stimulation of bacterial and fungal growth, the alteration of bacterial EPS composition, and the release of nutrient elements like N, P, S, or K, by facilitating the dissolution of soil minerals (Landeweert et al., 2001; Frey, 2019). Root exudates (containing mucilage and organic acids) regulate the selective storage and uptake of nutrient elements (e.g., released from the soil), serve as messenger molecules in the rhizosphere, and act as a lubricant facilitating the propagation of root tips. Moreover, exudates prevent roots from dehydration and mediate and maintain the contact between roots and soil (Walker et al., 2003). Given the soil biota-specific range of action, the impact of OM_{BE} is assumed to be locally restricted to specific regions in the soil, e.g., the drilosphere (Brown et al., 2000), mineralosphere (microorganisms-colonized mineral surfaces: Kandeler et al., 2019), mycosphere (zone influenced by fungal hyphae), rhizosphere (zone influenced by roots), mycorrhizosphere (zone affected by mycorrhized roots; Haq et al., 2014), and the detritusphere (zone next to decaying OM; Marschner et al., 2012; Kramer et al., 2016). Biogenic exudates of fungi, roots, earthworms, and bacteria influence the water repellency, transport, and retention within preferential flow paths (Morales et al., 2010). For example, earthworms produce hydrophobic and OM-enriched surface patches. These patches are heterogeneously spread over the burrow walls (Lipiec et al., 2015) and serve as microbial habitats (Aira et al., 2009; Stromberger et al., 2012). Furthermore, mucus secretion in the drilosphere buffers the pH towards circumneutral values (Schrader et al., 1994).

Interactions and relationships between organisms govern the fate of OM_{BE} in the soil in the form of competition of roots of neighboring plants, bacteria, fungi, and invertebrates for water, space, and (in-) organic nutrients (Walker et al., 2003). However, bacteria can stimulate the growth of fungal hyphae, especially at unfavorable conditions, e.g., during drought or high heavy metal concentrations, exemplarily due to impacting the gene expression of fungi (Haq et al., 2014). The OM dynamics in the mycorrhizosphere are driven by the secretion of plant-derived photosynthates catalyzed by mycorrhizal fungi (Frey, 2019), which lead to the release of energy-rich organic compounds, e.g., polysaccharides, fatty acids, and enzymes (Dakora and Phillips, 2002). In symbiotic or parasitic relationships in soil, fungi serve as or provide energy sources for bacteria and vice versa. In terms of litter decomposition, mutualistic strategies between fungi and bacteria enable the degradation of stable organic substrates, e.g., lignin (de Boer et al., 2005). Earthworms require the microbial community in their intestinal tract for an efficient OM decomposition: They take up from and release bacteria into the soil during cast formation (Lee and Foster, 1991). Furthermore, the biogenic OM-enriched earthworm-formed structures (e.g., casts, middens, and burrow linings) are locations of intensified microbial abundance and activity (Aira et al., 2009; Stromberger et al., 2012).

In summary, the OM excreting organisms are involved in both the degradation and formation processes of the OM produced by their symbiosis partners or decomposers. This implies that biogenic OM of the drilosphere or the mycorrhizosphere results from various and diverse sources in quantities that are difficult to estimate. For example, earthworms like *Lumbricus terrestris* L. affect a soil volume of up to 126.2 m^3/ha through burrowing (Schrader et al., 2007), and *Octolasion lacteum* Ö. releases up to 0.2–0.5% of total animal C daily by cast formation and mucus excretion (Scheu, 1991). However, most earthworms prefer humid locations with circumneutral to slightly alkaline pH (Schrader, 1994). In comparison, ectomycorrhizal fungi produce hyphae in a range between 2 and 200 g C/m^2 per year (Frey, 2019). Thus, they exist in a wide range of different biomes (Kjøller and Struwe, 1982), even in locations with extreme conditions (e.g., low pH, extreme temperature, drought, and high heavy metal concentrations) (Haq et al., 2014; Frac et al., 2018).Similarly, various bacterial strains are distributed unevenly across several habitats reaching from deep soil horizons to aquifers (Lazar et al., 2019).

Hence, a general assessment of the relative importance of organismic groups or taxa for the provision of OM_{BE} is not possible. Amount, type, and origin of OM_{BE} as well as its involvement in aggregation depend on the interplay of a hierarchy of factors starting from the "site legacy", including climate, parent rock, time, and relief which constrain the development of the local field conditions as well as pedogenetic and biotic characteristics. On the next hierarchical level, biotic factors (e.g., organism communities and OM_{BE} composition) interact with abiotic factors (e.g., milieu conditions and mineral composition) under the genesis of the characteristic biogeochemical interfaces (Totsche et al., 2018). Thus, many subprocesses, including the specific adsorption of OM_{BE} to soil minerals or the (im-)mobilization of organo-mineral associations, shape the locations of increased biogenic aggregation. To provide an insight into this complicated topic, we discuss the effect of plants, earthworms, microorganisms, and their mutualistic relationships on OM_{BE} supply, soil structuring, and aggregation. Finally, we elucidate the formation of biogenic aggregates shaped by OM_{BE} in detail at the mechanical level and according to their functionality in aggregation processes (Fig. 2).

3. Soil biota that facilitates aggregation

3.1. Plants

Plants provide aboveground carbon mainly as dead plant tissue (e.g., litter), incorporated into the soil by admixing processes. However, OM released by root exudation and decomposition of root litter is presumed to be more relevant in SOM stabilization and aggregation (e.g., Rasse et al., 2005). The supply of root tissue and exudates in the rhizosphere is a depth-dependent governing factor for forming organo-mineral associations (Angst et al., 2016). Gregory (2006) outlined that the multitude of processes at the transition zone between root and soil impacts the physicochemical properties of soil over variable distances, which provoke heterogeneities and spatial gradients in the rhizosphere. For example, the rhizosphere close to the root surface exhibits increased porosity (Helliwell et al., 2019). Recently, Burr-Hersey et al. (2020)

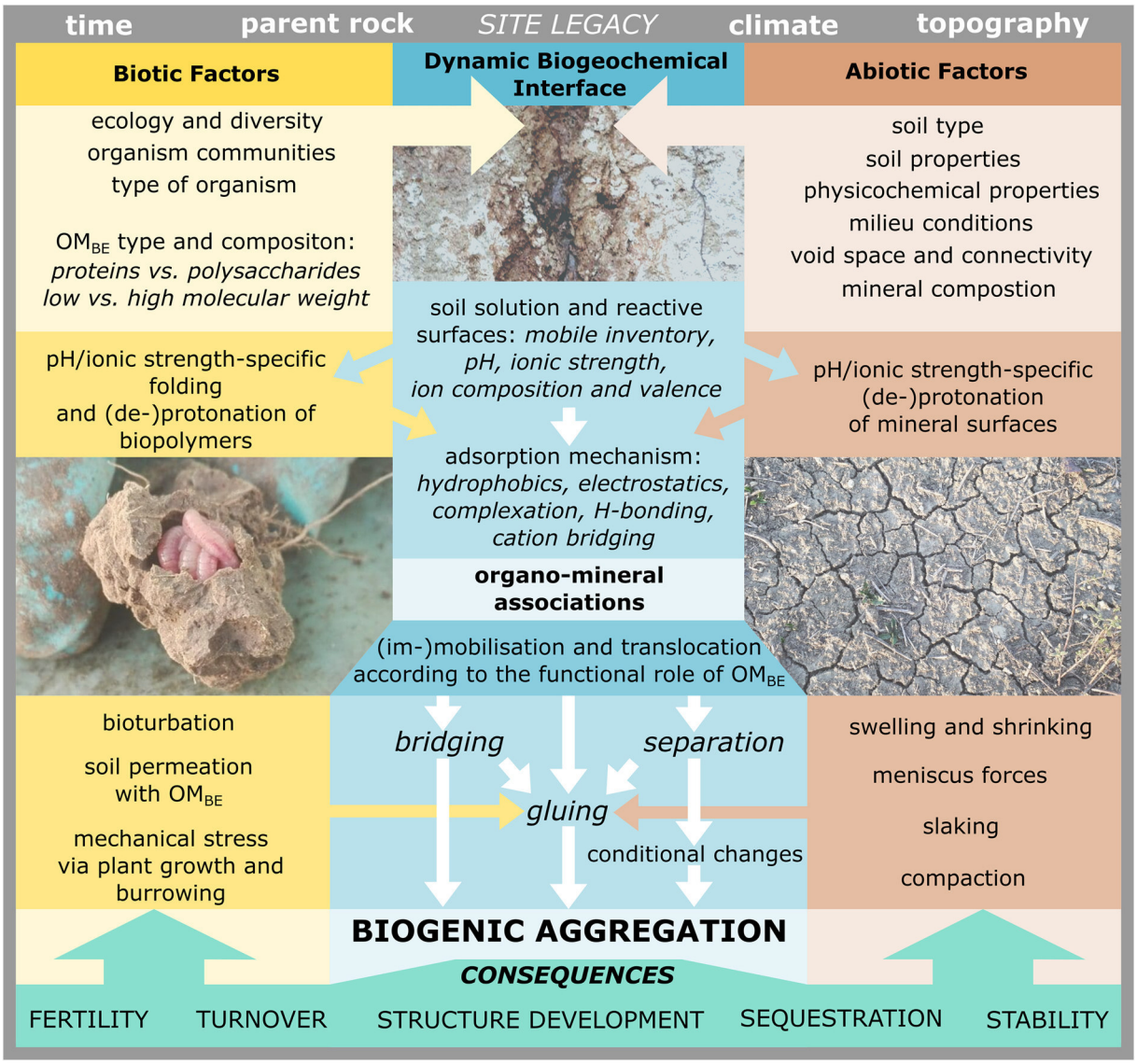

Fig. 2. Scheme visualizing the key relationships impacting biogenic aggregation. The site legacy (grey), including the superordinated pedogenetic factors, predefine the local biotic (yellow) and abiotic (orange) aggregation factors. Biotic factors include the ecology identified by the structural and functional biodiversity in the soil. The resulting communities and their interactions are resembled by the food webs and mutualistic relationships and feedbacks. The type of soil biota specifies the composition and properties of OM_{BE}. The abiotic factors comprise the physicochemical properties of the immediate soil environment and thus the milieu conditions. Included therein is the mineral assortment, which conditions the reactive surfaces of soil. These are located within the pore space network characterized by pore topology. The interaction zones between biotic and abiotic factors are the dynamic biogeochemical interfaces (blue) present, e.g., in the rhizosphere, the drilosphere, and the detritussphere. The coaction of abiotic and biotic factors governs the emergence and composition of the mobile inventory, including not only the (in-)organic solutes but colloidal and even larger sized particles of various origins (primary and secondary minerals, organo-mineral associations, microorganisms, biotic debris, biopolymers; Lehmann et al., 2021), which determines the composition and physicochemical properties of the soil solution and the reactive surfaces. The ionic strength, composition, valence, and pH of the soil solution affect interfacial and molecular properties requirements of the minerals, and OM_{BE} is decisive for the formation of organo-mineral associations. Depending on the functional role of the involved OM_{BE}, bridging, separation, or gluing between organo-mineral-associations is facilitated, which determines the fate (i.e., transport and (im-)mobilization) in soil. In addition, external forces of biotic and abiotic origin (e.g., bioturbation and the occurrence of meniscal forces) enforce an aggregation between organo-mineral associations and already existing aggregates by provoking a close approach of soil constituents. Vice versa, the biogenic aggregates influence the soil properties and soil biota via their fundamental roles in soil (green) structure development and stabilization and as critical elements within nutrient cycles involved in crucial turnover and sequestration processes.

revealed the probability of remediating compacted soils via root growth of (specialized) plant species, which cause an active formation of pores from micro- to centimeter scale. Aggregates formed in the direct vicinity of plant-formed biopores were of subpolyedric shape and can be distinguished clearly from earthworm-formed subplates originating from casts and burrow linings (Haas and Horn, 2018). However, since plant roots use earthworm burrows to facilitate their growth, the rhizosphere and drilosphere frequently overlap (Athmann et al., 2013; Han et al., 2015). After plant decay, root channels contribute to the entirety of biopores in soil and serve as preferential flow pathways (Jarvis, 2007; Kautz, 2014). The root litter inside biopores can contribute up to 48% of annual plant litter input into soil. Yet, root decay rates are lower than those of above-ground litter (Frescht et al., 2013) and depend on the associated mycorrhizal type (Jacobs et al., 2018). Thus, root litter is suggested as a source and driver of SOM dynamics (Frescht et al., 2013).

In turn, soil particles' size, physicochemical and surface properties influence root growth and exudation (Sasse et al., 2020). Hence,

composition and concentration of biopolymers, the conditions of the immediate environment (e.g., pH, moisture, and ionic strength), and the nature of the solid phases (e.g., mineral composition and OM coatings) the roots interact with (Violante and Caporale, 2015) control the biogeochemical processes in the rhizosphere. For example, roots affect the pH in their direct vicinity during the elongation process. Depending on plant species and required nutrients, the pH can be increased or decreased. Blossfeld et al. (2013) showed that the pH of the rhizosphere of chickpeas was decreasing by one unit during N_2 fixation. In contrast, the rhizosphere pH of wheat grassroots was increasing during nitrate uptake, resulting in a hydroxide(OH^-)-surplus (Hinsinger et al., 2003). Thus, the expression of rhizosphere properties results from the dynamic feedback between alternating and simultaneously occurring biological, chemical, and physical processes (Mueller et al., 2019) and ultimately causes the emergence of self-organized spatiotemporal patterns (Vetterlein et al., 2020), like the formation of aggregates.

Root exudates are a mixture of a wide variety of components from high molecular (>1 kDa) weight proteins (e.g., enzymes) and mucilage to low molecular weight compounds (<1 kDa) like sugars and organic acids (Oburger and Jones, 2018). Especially, mucilage is an often-discussed model component of root exudation. The composition of mucilage differs between plant species. However, carbohydrates and, in particular, polysaccharides are the dominant fraction (>90%) in comparison to proteins which seldomly exceed portions of 6% (Carminati and Vetterlein, 2013). However, root exudation is involved in the fixation of OM in aggregates and organo-mineral associations, which co-occurs with organic carbon release from mineral surfaces mediated by organic ligands. Previously fixed carbon is supplied to microbial decomposition and plant uptake (Keiluweit et al., 2015). Rodionov et al. (2019) demonstrated the local impact of plant material and root exudates on the carbon and OM turnover of soil (micro-)aggregates by laser-ablation-isotope-ratio mass spectrometry. Aggregation in the rhizosphere is affected by root growth (and hyphae growth of symbiotic fungi) through enmeshment, compaction, and simultaneous permeation with root exudates of soil particles (Hinsinger et al., 2009; Haq et al., 2014). Remarkably, the presence of mucilage results in a rapid formation of organo-mineral associations. Water stability increases once mucilage is incorporated into soil aggregates (Morel et al., 1991). Thus, the physicochemical properties and the aggregation in the rhizosphere are shaped by the mucilage availability, which facilitates the contact between the root surface and the solid phase and alters rhizosphere wettability due to a mucilage network and filament formations (Ahmadi et al., 2017; Carminati et al., 2017). Besides the direct impact of rooting and exudation, Wang et al. (2020) attributed an intensified aggregation stimulating microbial growth and EPS production by mucilage and root exudate supply. The mutualistic relationship between plants, rhizobacteria, and mycorrhizal fungi generates soil properties by OM_{BE} provision (Sher et al., 2020). It promotes plant growth by mediating salt and heavy metal stress reduction, moisture retention, outcompeting plant pathogens, and facilitating nutrient exchange and aggregate formation (Rillig and Mummey 2006; Saha et al., 2020).

3.2. Earthworms

Significant factors of aggregate formation are the presence, diversity, and activity of the soil fauna (Six et al., 2004). Organisms known to have a notable impact on soil structuring (Lee and Foster, 1991) and regulating soil's physical, chemical, and microbiological properties are earthworms (Bottinelli et al., 2015; Franco et al., 2020). Vice versa, soil properties affect the number, activity, and communities of invertebrates in the soil. On these grounds, the number and condition of invertebrates like earthworms are taken as indicators for soil quality (Lavelle et al., 2006; Bottinelli et al., 2015). For example, in the first 15 cm of tropic and temperate latitude soils, biogenic aggregates represent 40–60% of the soil weight (Lavelle et al., 2020). In humid regions, earthworms are common and important "ecosystem engineers" (Lavelle, 1988; Jones et al., 1994). Compared to social insects like termites and ants, which lead only to local modifications of the soil structure, the processing by "non-social" earthworms is more spread and locally unbound (Lee and Foster, 1991). Already Darwin (1881) emphasized the positive role of earthworms for soil structure and quality. Later, Lavelle (1988) described soil characteristics as determinants and consequences of earthworm activities. Exemplarily, earthworms change soil macroporosity, decompose OM, increase the humus content, and influence the energy and nutrient cycles (e.g., mineralization and humification) (Lavelle, 1988; Lee and Foster, 1991; Jones et al., 1994; Lemtiri et al., 2014). During soil processing (e.g., burrowing and soil ingestion), earthworms significantly influence aggregate turnover and SOM dynamics by destroying existing aggregates and forming biogenic (macro- and micro-) aggregates. These contain fine particulate OM, physically protected against microbial degradation (Pullman et al., 2005).

Three functional ecological groups of earthworms are known, which differ in their impact on soil structure and aggregate formation. Epigeic earthworms live in the litter layer on top of the mineral soil and feed on plant residues and litter-colonizing organisms (Brown et al., 2000). They mostly impact the soil by litter alteration or rare soil incorporation (Curry and Schmidt, 2007). In contrast, anecic and endogeic species impact the soil structure more actively. Anecic earthworms built up to several meters deep, durable, vertical burrows, which serve as preferential pathways for fluid flow and matter transport, including organic, biotic, and inorganic colloids (Lee and Foster, 1991; Edwards et al., 1993; Brown et al., 2000). Additionally, anecic earthworms actively translocate litter into the subsurface as food stock (Brown et al., 2000). To highlight the earthworm-driven macropore formation, Schrader et al. (2007) estimated for *L. terrestris* L. an annually affected burrow length of 82.3 km/ha. In contrast, the geophagous endogeic earthworms process the soil in approximately the first 30 cm by horizontal trenching of frequently collapsing burrows (Lee, 1985). By burrowing through the soil, earthworms form distinct zones, the so-called drilosphere (Bouché, 1975), which resembles a zone of up to 1 cm thickness around the burrows (Andriuzzi et al., 2013; Lipiec et al., 2015). The earthworms exert radial pressure on the adjacent soil, resulting in increased burrow stability due to burrow wall compaction and secrete cutaneous mucus as a lubricant (Lee, 1985; Six et al., 2004; Schrader et al., 2007). The radial force is anisotropic and leads to locally variable increased bulk densities in the drilosphere (up to 30%), which decrease from the burrow walls in the direction to the earthworm unaffected bulk soil (Rogasik et al., 2014). A reduced porosity also characterizes the earthworm-engineered surfaces of the burrow walls compared to the bulk soil due to compaction and cast deposition (burrow linings; Jégou et al., 2001). Middens deposited on the soil surface and casts are biogenic aggregates released by earthworms (Six et al., 2004). In the gastrointestinal tract of the earthworms, the ingested OM and soil material are mixed with intestinal mucus and symbiotic microorganisms, which are involved in the nutrient uptake of earthworms (Edwards and Fletcher, 1988). While passaging the gut, the ingested material is reorganized and subsequently excreted as aggregates containing microorganisms, plant debris, polysaccharides, and clay (Barois et al., 1993; Brown et al., 2000). Earthworm casts are one major fraction of aggregates in topsoil, stabilized by clay-organic matter complexes (Lee and Foster, 1991). Consequently, the earthworm-induced aggregate formation is associated with a recycling of the OM bound in initial soil aggregates, which are destroyed by the burrowing activity and the consumption of the soil material (Barois et al., 1993). However, binding agents (e.g., biopolymers like carbohydrates and proteins) and mineral components in casts come in contact upon aging and drying, which results in a strong intra-aggregate bonding of the biogenic (micro-) aggregates, and higher water stability than the aggregates in the bulk soil (Shipitalo and Protz, 1989). The casts are altered in pH and characterized by higher carbon, polysaccharides, Ca, Mg, and K contents, and a decreased porosity (Schrader, 1994; Jouquet et al., 2008). Additionally, the OM-enriched casts and burrow walls are water repellent (Don et al., 2008; Leue et al., 2015).

Consequently, earthworms alter the physicochemical properties of affected soil structures, which lead to implications for the soil properties and other soil organisms. For example, the heterogeneity of the bulk density (Rogasik et al., 2014) and hydrophobic OM (Jégou et al., 2001; Leue et al., 2015; Lipiec et al., 2015) along the burrow walls affect the lateral water transport, especially during rain events, causing ponding conditions inside burrows (Bastardie et al., 2005). Furthermore, earthworm casts, middens, and burrow linings are regions of increased microbial abundance and activity because of the enrichment in substrate and nutrient elements (Tiunov and Scheu, 1999; Brown et al., 2000; Aira et al., 2009; Stromberger et al., 2012). Microbial and faunal biomass (e.g., nematodes and protozoa) are enriched in earthworm burrows by up to 50% and 300%, respectively, compared to the adjacent soil. Additionally, the microbial community composition varies between burrows, resulting in the spatial differentiation of the soil community (Stromberger et al., 2012). Moreover, earthworms actively disperse microorganisms in the soil profile by cast excretion (Lee, 1985; Lemtiri et al., 2014). The interactions between microorganisms and earthworms provide plant-relevant nutrients (e.g., potassium and phosphorous) and thus facilitate plant growth (Edwards and Fletcher, 1988). Further studies showed that the stimulation of plant and root growth due to earthworms is intimately linked to soil aggregates' formation (Fonte et al., 2012).

3.3. Bacteria and fungi

Carbon enriched soil structures and aggregate surfaces (e.g., found in the topsoil and along preferential flow pathways) are potential habitats for microorganisms, the basis for biofilm formation, and involved in OM degradation and turnover (Guggenberger and Kaiser, 2003). Particulate and dissolved OM inputs into soil induce aggregate formation mediated by microbial processing (Bucka et al., 2019). Furthermore, the composition of aggregates, mainly the increased clay and OM contents, corresponds to improved aggregate stability against hydraulic stress (slaking). Recently, Felde et al. (2020) pointed out the possible role of the aggregate composition in structuring microbial communities. In line with that, Biesgen et al. (2020) reported the development of distinct microbial communities with increasing clay contents of (micro-)aggregates as well as community differences between free (copiotrophic bacteria) and occluded (oligotrophic bacteria) aggregates. For example, processes such as local compaction, micropore alteration (e.g., clogging and penetration), particle alignment, increase of water content, and aggregate stability can be assigned to the impact of microorganisms on soil structures at a small local scale of <20 μm due to the influence of fungal hyphae growth and the interaction with bacterial surfaces (Chenu and Cosentino, 2011).

Further studies indicated a strengthening of soil structural integrity by EPS-producing microorganisms up to the field scale, increasing the amount of water-stable aggregates (Redmile-Gordon et al., 2020). This strengthening is caused by microbially produced aggregation agents stabilizing (micro-)aggregates (Oades and Waters, 1991). For example, EPS is gluing and binding particles together by increasing the contact area of interparticle bonds. Fungal hyphae are also involved in macroaggregate formation by particle enmeshments (Six et al., 2004; Huang et al., 2005; Chenu and Cosentino, 2011; Costa et al., 2018). Furthermore, the attachment of cells to mineral surfaces and the active habitat formation of bacteria increases the aggregation of soil minerals in suspensions (Krause et al., 2019). In addition, microbial lyse products contribute to the OM pool in soil (Miltner et al., 2012) and aggregate formation (Krause et al., 2019). The aggregate stabilizing effect of microorganisms is a function of biologically available C and the dynamic environmental conditions (Baldock, 2002). This is particularly relevant if we additionally consider the presence/support of earthworms (Lemtiri et al., 2014) and plants (Wang et al., 2020), which stimulate the microbial communities (e.g., metabolic activity) by nutrient and habitat provision as well as the active dispersal of microorganisms within the soil profile during soil processing. In comparison, mycorrhizal fungi facilitate aggregation by shaping the composition of plant communities, the root growth of the host plant, and the direct effect of the mycelium growth (Rillig and Mummey, 2006).

To sustain their survival in soil, bacteria produce EPS inter alia to adapt their surrounding physicochemical properties by forming shelter-providing biofilms (Flemming et al., 2016). EPS is the biofilm matrix essential for habitat formation and structuring, including the genetic exchange, signaling, carbon source supply, nutrient source entrapment, cell adhesion, and aggregation (Costa et al., 2018). Furthermore, microbial EPS plays a crucial role in cell transport in the aqueous phase, attachment to soil particles, and increasing resistance against environmental and toxic stress (Tourney and Ngwenya, 2014). EPS composition and quantity (e.g., varying portions of carbohydrates, proteins, DNA, and RNA) depend on the environmental conditions, the type of bacteria, the bacterial growth stage, and functionality of EPS (e.g., tightly, loosely bound EPS or soluble EPS) (Wingender et al., 1999). In addition, fungi' EPS preserves the enzymes' functionality for SOM decomposition and contributes to fungal nutrient accumulation (Op De Beek et al., 2021). Thus, microbial EPS serves different purposes based on its variable composition: E.g., that can be utilized as a biogenic flocculant or biosorbent for wastewater treatment and soil remediation (More et al., 2014). Recently, Ivanov et al. (2020) showed that microbial-induced processes (e.g., biofilm formation and enmeshment) alter the engineering properties of technosols and increase the content of microaggregates, at least for the short term.

4. Adsorption to soil minerals and the formation of organo-mineral associations

Organo-mineral associations form by surface interactions (e.g., coprecipitation and adsorption: Kögel-Knabner et al., 2008) between OM and soil minerals (Christensen, 2001), and are essential for the provision and accumulation of nutrients (Jilling et al., 2018), the immobilization of toxic components and contaminants (Kleber et al., 2015), and the stabilization and binding of aggregates (Jastrow and Miller, 1998). Especially, humic substances, discussed as the stable part of organic matter in the soil, were in focus for decades (Gerke, 2018). There is a multitude of studies dealing with the interactions of humic substances with the soil mineral phase and their paths in soil (e.g., Amirbahman and Olson, 1995; Theng and Yuan, 2008; Aubry et al., 2013; Tiraferri et al., 2017; Yang et al., 2021). However, Kleber and Johnson (2010) pointed out that the term humic substances is blurred in definition and not representative of OM in soil. Alternatively, various studies investigated functionalized artificial polymers as surrogates for specific SOM, like polysaccharides and proteins (e.g., Theng, 1982; Donstova and Bigham, 2005; Philippe and Schaumann, 2014; Tan et al., 2014). Such studies are indispensable for the fundamental understanding of adsorption and aggregation processes in soil involving presumably more complexly composed OM_{BE}. For example, the formation of organo-mineral associations is an essential process in bacterial cell attachment to mineral surfaces and biofilm formation (Lower et al., 2000; Harimawan et al., 2011). Initial attachment and adsorption processes between (micro-)aggregate forming materials are controlled by the surface properties of the soil minerals and the functional groups of OM_{BE} (for microorganisms: Tourney and Ngwenya, 2014), which respond to the environmental conditions and their changes (e.g., pH, electric conductivity, type of electrolyte, and solution composition). The adsorption of OM like humic substances, high molecular weight proteins, or bacterial EPS to soil minerals leads to mineral surface screening and charge alteration (Tombácz et al., 2004; Flynn et al., 2012; Pen et al., 2015). In sum, the pathways of newly formed organo-mineral associations into the aggregates - and the soil - differ fundamentally from the corresponding pure minerals (Narvekar et al., 2017; Guhra et al., 2019; Yang et al., 2021).

4.1. Adsorption mechanisms

van der Waals interactions, H-bonding, cation bridging, complexation, hydrophobic interactions, and long-range electrostatic interactions (Philippe and Schaumann 2014) are presumed to govern OM adsorption (Kleber et al., 2015) and particle aggregation (c.f. Totsche et al., 2018, and references therein). In particular, the interplay between van der Waals interactions and electrostatic forces control particle attachment, aggregate formation, and aggregate properties like shape, size, and inner porosity in aquatic systems (Elimelech et al., 1995; Ritschel and Totsche, 2019). Specifically, electric conductivity and pH modify the surface charges of (micro-)aggregate forming materials. Hence, electrostatic repulsion between similar charged particles or attraction between oppositely charged particles emerges as indicated by their isoelectric point (IEP). Parks (1965) described the IEP as the pH value where the net charge of a mineral surface is zero due to an equivalent amount of positively and negatively charged surface groups (Kosmulski, 2016). For example, Fe-oxides (IEP: 6.4–9.1 in Kosmulski, 2020) are characterized by a variable surface charge with a positive charge at low to near neutral pH values (below the IEP), and a negative charge at higher values (above the IEP) (Cornell and Schwertmann, 2003). Variably charged surfaces can also be found for quartz (SiO_2) with low IEPs (IEP around pH 2 in Kosmulski, 2016) and for the edges of clay minerals, providing protonatable aluminol- and silanol-groups (Tombácz and Szekeres, 2006; Hong et al., 2013; Yu et al., 2013). However, the basal planes of clay minerals are negatively charged over the whole pH range (Kosmulski and Dahlsten 2006; Tombácz and Szekeres, 2006; Kosmulski, 2011).

Besides the inorganic soil constituents, interactions of OM_{BE} are also controlled by electric conductivity and pH. For example, EPS consists of a pH-controlled network of polymeric chains (Dogsa et al., 2005). Further studies suggested the swelling of EPS with increasing pH (Pen et al., 2015). Fourier transform infrared (FTIR) spectroscopy measurements of EPS conducted by Omoike and Chorover (2006) showed changes in the secondary structure of polymer chains, from ordered at low pH to unordered at high pH values. This structural dynamic is due to the protonation, deprotonation, and the interaction between the various functional groups of EPS constituents, predominantly proteins and polysaccharides (Wang et al., 2012; Dogsa et al., 2005). The EPS composition and the type of soil mineral control how much and which fraction of biogenic EPS is involved in adsorption and thus in the formation of organo-mineral associations (Lin et al., 2016; Guhra et al., 2019, 2020). For example, the adsorption of EPS to iron oxides like goethite is mediated by surface complexation due to the formation of Fe–O–P bonds (Omoike and Chorover, 2004, 2006). Hence, organic carbon and phosphorus compounds of the OM_{BE} enrich the newly formed organo-mineral associations with nutrient elements due to abiotic adsorption mechanisms (Scheu, 1987). For aluminum oxides, Mikutta et al. (2011) reported a fractionation of EPS constituents during adsorption as a function of pH and electric conductivity. The work of Lin et al. (2016) demonstrated differences between the adsorption of EPS to iron oxides (goethite) and clay minerals (e.g., montmorillonite and kaolinite) as a function of pH. Here, optimum adsorption is found around pH 5 for clay minerals and around pH 7 for goethite.

Cai et al. (2018) outlined the importance of the electric conductivity for EPS adsorption to goethite. They reported amide groups as more relevant at high electrolyte concentrations, whereas carboxyl and phosphoryl functional groups contribute to adsorption at low concentrations. Additionally, the conformation of proteinaceous EPS constituents turns away from random coil structure with increasing electrolyte content which facilitates adsorption. Mikutta et al. (2012) demonstrated that the type of mineral is also essential for specific EPS mineral interactions. The EPS adsorption to bentonite favors low-molecular-weight and N-rich compounds of EPS compared to ferrihydrite, which favors high-molecular-weight and P-rich compounds. The adsorption of the low molecular weight fractions was more substantial for goethite than for montmorillonite (Chen et al., 2021). The study of Liu et al. (2013) identified an unevenly distributed surface screening of protein- and lipid-rich spots after the adsorption of microbial EPS to goethite.

Only a few studies are available that explore the interactions of natural biopolymeric mixtures like root exudates (e.g., mucilage: Morel et al., 1987; Gaume et al., 2000; Grimal et al., 2001) and earthworm mucus (Guhra et al., 2020) with soil minerals. This imbalance of studies favouring microbial OM might be caused since it is repeatedly discussed as the predominant OM fraction in the silt and clay fraction of soil (e.g., Puget et al., 1999; Miltner et al., 2012; Wilpizeski et al., 2019). Kleber et al. (2007) highlighted proteins as the relevant fraction of organo-mineral associations found in soil, mainly attributed to microbial origin. Furthermore, Le Mer et al. (2020) reported that proteinaceous compounds formed by microorganisms were found in thermo-stable organo-mineral associations and aggregates, especially if the soil was processed by earthworms. This recent observation corroborates our inference that a wide variety of biota contribute to the presence and amount of biogenic OM in soils, and that a hierarchy of factors, including time, controls the proportions supplied by the different taxa. Accordingly, plant-derived exudates and earthworm-produced mucus are supposed to be the most dominant OM fractions in the rhizosphere (Haq et al., 2014) and drilosphere (Brown et al., 2000), where they permeate soil particles and shape their physicochemical properties (Six et al., 2004; Lavelle et al., 2020). Walker

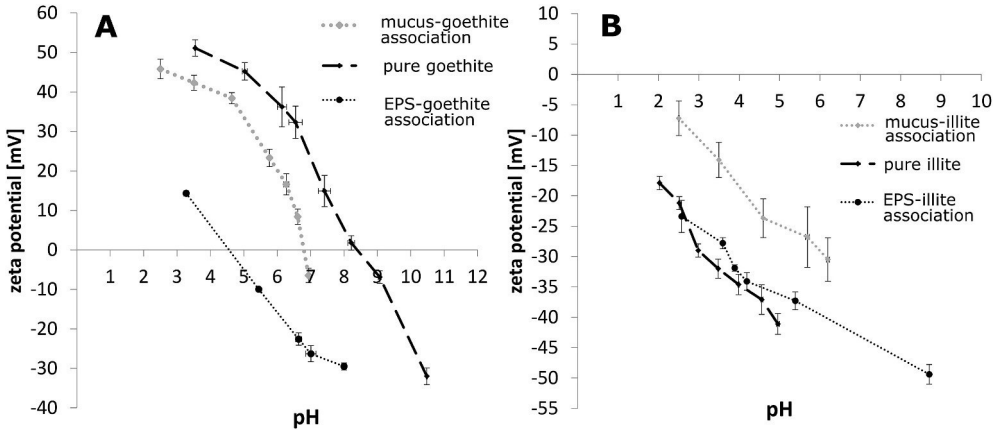

Fig. 3. Diversity in surface charge alteration after organo-mineral associations formation due to the impact of protein-rich earthworm mucus (according to Guhra et al., 2020) and carbohydrate- and polysaccharide-rich bacterial EPS (according to Guhra et al., 2019) shown by Zeta potential measurements as a function of pH for pure minerals (black dashed line), mucus-mineral associations (grey dotted line) and EPS-mineral association (black dotted line) for goethite (A) and illite (B).

et al. (2003) showed proteins as a relevant fraction of root exudates besides polysaccharides. Guhra et al. (2020) reported proteinaceous constituents of earthworm mucus (*L. terrestris* L. and *Aporrectodea caliginosa* Sav.) as an essential fraction involved in forming mucus-mineral associations via hydrophobic interactions. The earthworm mucus showed high similarities in composition and adsorption behavior of microbial EPS (*Bacillus subtilis*) of the early stationary phase to clay minerals and iron oxides. In contrast, late stationary phase EPS with a low protein content adsorbs to a lesser extent to clay minerals than iron oxides, resulting in a less effective surface screening of the first (Guhra et al., 2019, 2020). More effective screening of goethite was reached with EPS of late stationary phase, which is rich in polysaccharides and carbohydrates, compared to the protein-rich cutaneous earthworm mucus (Fig. 3.). Accordingly, considering clay minerals, Kleber et al. (2007) suggested that biogenic proteinaceous constituents are essential for forming organo-mineral associations via the interplay of electrostatic and hydrophobic interactions. Studies on the deposition of microbial EPS on a silicate surface (quartz crystal microbalance measurements) revealed preferential EPS adsorption when the EPS had a high protein to polysaccharide ratio (Zhu et al., 2009). In particular, proteins' functionality, orientation, and structure control their adsorption to mineral surfaces via conformation-specific characteristics (e.g., hydrophilic, hydrophobic, and type of charge) (Kubiak-Ossowska et al., 2016).

Furthermore, the adsorption of proteins to mineral surfaces is a function of pH, ionic strength, protein concentration, molecular weight, and the type of mineral (Violante et al., 1995; Barreto et al., 2020). It leads to conformation changes of adsorbed proteins which alter their reactivity in the environment. Proteins are frequently reported to adsorb during electrostatically unfavored conditions (Kubiak-Ossowska et al., 2016). Hydrophobic interactions enable adsorption if the protein and mineral surface's net-charge is similar (Kubiak-Ossowska et al., 2017). Hence, studies that focus on the predominant adsorption mechanisms and surface modification under representative soil conditions are necessary to elucidate the role of organism-specific proteins in complex mixtures like OM_{BE} during organo-mineral association and aggregate formation.

4.2. Biogenic aggregation

Biogenic-induced aggregation occurs on different scales and under the impact of and interaction between various organisms. The meta-analysis of Lehmann et al. (2017) highlighted bacteria and fungi in terms of aggregation but ascribed an improvement of aggregation to the interaction between different taxonomic groups and thus biodiversity. Similarly, Haydu-Houdeshell et al. (2018) identified no specific type of soil biota as the dominant initiator of aggregation. Exemplarily, the study of Lehndorff et al. (2021) showed the spatial dependency of microbial OM to carbon of plant residues as an energy source within the spatial organization of microaggregates by electron probe microanalysis of aggregate cross-sections. Local limitations are overcome during the growth of fungal hyphae and the distribution of microorganisms during the release of casts and burrow formation by earthworms (Brown et al., 2000; Chenu and Cosentino, 2011). Fungal OM (e.g., exudates and tissues) becomes stabilized through organo-mineral associations and aggregate formation, where hyphae enmesh soil particles physically, and fungal exudates serve as aggregation agents (Frey, 2019). Aggregate stabilization due to bacterial EPS release is typically found in the topsoil, which harbors the highest OM contents.

Furthermore, the study of Cania et al. (2019) found that the EPS-producing species varied with depth and that small changes in the bacterial communities (of EPS producers) can change the capacity of EPS to stabilize the soil structure against wetting. The stability of aggregates against wet sieving was more related to proteins than polysaccharides of EPS (Redmile-Gordon et al., 2020). Consequently, soil treatments with fungicides and bactericides lead to diminished aggregation (Tang et al., 2011). The interactions between microbial-produced EPS and plant-released exudates also result in altered hydraulic conditions (e.g., increased capacity to absorb water and hydrophobicity after drying out: Carminati et al., 2016). Besides, microbial EPS facilitates plant root growth, which forces aggregation in the rhizosphere (Costa et al., 2018). Rhizobacteria compensate for drought periods and promote root growth, which results in increased formation of root exudates. This, in turn, mediates adherence (aggregation mechanism) between root and soil, thereby improving nutrient and water uptake (Alami et al., 2000). Gras roots (*Panicum virgatum*) are involved in enhancing microbial activity, promoting microbial EPS production, improve water retention and aggregate formation due to the release of plant-derived EPS (high polysaccharide content) and rooting (Sher et al., 2020). The impact of root exudation on aggregation and C allocation throughout the soil profile is affected by the amount of released exudates, which was shown by the promotion of fungal growth and macroaggregate formation (also in the subsoil) if high concentrations of exudates were available (Baumert et al., 2018).

4.3. Biogenically excreted OM as bridging or separation agent

Biota-mediated aggregation and alteration of the soil structure and physicochemical properties have a lasting impact on the (im-)mobilization and the translocation of soil particles, organo-mineral associations, and small (micro-)aggregates. The release of soil components small enough to be susceptible to transport, like secondary minerals, OM, bacteria, and organo-mineral associations of various shapes and origin (McCarthy and McKay, 2004; Bin et al., 2011; Vlamakis et al., 2013; Lehmann et al., 2021) is due to the biological activity, the alternation and perturbation of geochemical (e.g., rapid changes in ionic strength and pH) and hydraulic conditions (e.g., wetting and drying) (Ryan and Elimelech 1996; Münch et al., 2002; de Jonge et al., 2004; DeNovio et al., 2004; Ranville et al., 2005). Once released and transported (Hotze et al., 2010), organo-mineral associations and small aggregates are prone to re-aggregation and immobilization if (i) the physical structure prohibits (further) transport, e.g., due to the narrowing of the pore aperture and the presence of dead-end pores, (ii) particle straining occurs due to hydraulic confinement in response to drying, (iii) the local milieu conditions get unfavorable. Local milieu changes may result from various processes, including the availability of new reactive surfaces offered by colloidal and even larger particles supplied by transport (Lehmann et al., 2021), the increase in electric conductivity, and changes in the pH buffering capacity. These translocation and reaggregation processes (Totsche et al., 2018) are crucial for aggregation in soils governed by illuviation, e.g., luvisols (Bronick and Lal, 2005; Ranville et al., 2005; Lehmann et al., 2021).

Long-range electrostatic forces are often discussed as aggregation controlling mechanisms in aqueous systems (e.g., Tombácz et al., 2004; Trefalt et al., 2014). The aggregation in biogenic OM-free systems containing various net-negatively charged (micro-)aggregate forming materials (e.g., illite and quartz at slightly acidic pH) is permitted by positively charged (micro-)aggregate forming materials (e.g., goethite) (Tombácz et al., 2001; Guhra et al., 2019). An optimum for electrostatically induced aggregation between mineral (micro-)aggregate forming materials can be found for systems with a net charge of zero (equivalent amount of positive and negative charges: Bansal et al., 2017; Dultz et al., 2019; Rupp et al., 2019). However, natural porous media contain OM, which interacts with the soil mineral phase and screens most of the potentially occurring positive surface charges (Kleber et al., 2015). In consequence, the adsorption of OM (Dultz et al., 2018) like humic substances (Tombácz et al., 2004), microbial EPS (Mikutta et al., 2012; Narvekar et al., 2017), or earthworm mucus (Guhra et al., 2020) leads to surface charge reversal/modifications of mineral surfaces screened with biogenic OM. As previously indicated, the formation of organo-mineral associations, and the extent of surface screening, depend on the composition of the OM_{BE} and the mineral type (Omoike and Chorover, 2004; Cao et al., 2011; Mikutta et al., 2011). This finding fits

with the observation of Zhang and Schrader (1993) for earthworm-produced intestinal mucus, where they suggested that the mucus composition is more important than its amount for aggregate stabilization. Shipitalo and Protz (1988) reported an enhanced dispersibility of fresh earthworm casts (found as linings in earthworm burrows) in comparison to the bulk soil. They attributed this to the disruption between interparticle bonds due to the incorporation by the earthworm and the reduced bonding between mucus-covered particles in an environment characterized by high water content and low water potential (Shipitalo and Protz, 1989). In conclusion, the fate of the resulting organo-mineral and mineral-mineral associations in the soil is controlled by the surface coverage of (micro-)aggregate forming materials, the resulting net charge of the surface, and the type of surface functional groups.

Extensive biogenic OM coatings (microbial EPS initially available in excess) can induce electrostatic repulsion between different sized, shaped, and charged mineral (micro-)aggregate forming materials, and inhibit aggregation in the liquid phase, which leads to a gravitative and size-specific separation of the (micro-)aggregate forming materials (Guhra et al., 2019). The experiments of Narvekar et al. (2017) showed that the attachment of EPS-modified hematite particles to a porous medium is related to the EPS loadings of the hematite particles. They reported a reduced interaction of hematite-EPS associations and silica surfaces with increasing EPS availability. However, for low EPS loadings, a strong aggregation between hematite-EPS associations due to the reduction of the IEP near to zero was found. Zhang and Schrader (1993) reported a saturation effect in aggregate stabilization with earthworm mucus coating. For bovine serum albumin as a surrogate for proteins, Flynn et al. (2012) showed an intensified colloid attachment when the adsorption of bovine serum albumin to goethite-covered sand reached its maximum while lower concentrations lead to repulsion between colloids and the immobile solid phase. They attributed this to a change in the bovine serum albumin configuration, leading to the availability of new adsorption sites.

In contrast, low amounts of okra mucilage (0.8 mg/l up to 3.2 mg/l) applied as a flocculant in wastewater treatment, induced a pH-dependent particle aggregation (Freitas et al., 2015). Further studies with high molecular weight bovine serum albumin in comparison to low molecular weight cytochrome C, revealed a fast hematite nanoparticle aggregation at low ionic strength, which exceeded the homo-aggregation of the nanoparticles caused by patchy-distributed polymer bridges (Sheng et al., 2016), a process they called patch-charge interactions (Szilagyi et al., 2014). Szewczuk-Karpisz and Wiśniewska (2019) showed that the aggregation of silica mediated by EPS, proteins, and polysaccharides was caused by hydrogen bonding, polymer bridging, and electrostatic interactions, yet strongly dependent on the biopolymer type and the pH. In sum, we conclude that the interplay of type and availability of OM_{BE}, minerals, and the environmental conditions controls whether OM_{BE} acts as a **bridging agent** promoting aggregation or as a **separation agent** inhibiting aggregation (Fig. 4).

4.4. Biogenically excreted OM as a gluing agent

Soils in humid regions are affected by temporal moisture variations due to wetting and drying. Consequently, soil aggregation is affected by contraction and expansion, surface (de-)hydration, formation of interparticle menisci, dissolution of (micro-)aggregate forming material, resuspension, and precipitation (Horn and Dexter, 1989; Ryan and Elimelech 1996; Hu et al., 2015; Totsche et al., 2018; Menon et al., 2020). During drying, water menisci between larger mineral particles or aggregates occur and pull small clay-sized (micro-)aggregate forming materials together. After complete drying, the smaller (micro-)aggregate forming materials (e.g., clays, metal oxides, and OM) become arranged between the greater particles and increase the number of contact points (Horn and Dexter, 1989; Semmel et al., 1991; Horn et al., 1994; Denef et al., 2002). Hence, the menisci forces can cause contraction, thereby reducing the distance between otherwise electrostatically repulsive (micro-)aggregate forming materials allowing solid bridges to create between them (Seiphoori et al., 2020).

Seiphoori et al. (2020) further demonstrated that the formation of hierarchically clustered aggregates during drying is more driven by mineral size than the type of mineral. Pen et al. (2015) showed for an EPS-covered bacteria cell strong attachment to a similarly charged silicon oxide surface (electrostatically repulsive) if the distance between each other was reduced by an external force (compression applied by an atomic force microscope). The strength of the adhesion was found to increase with approaching time and became increasingly independent of the pH. In addition, Chen et al. (2009) indicated improved surface attachment and deposition rates of bacterial cells caused by gravitational force. The study of Shipitalo and Protz (1988) stated the stabilization of biogenic aggregates due to external forces within earthworm

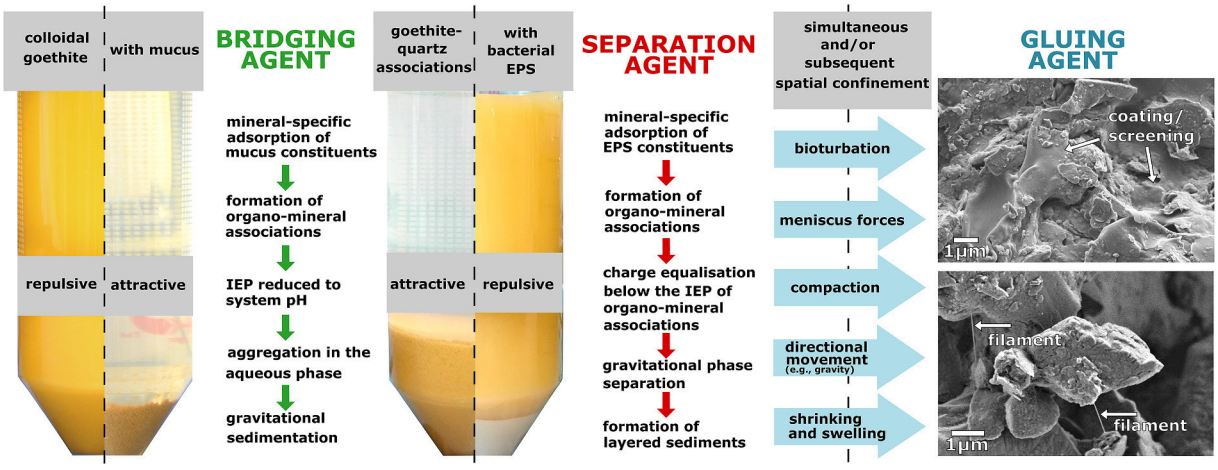

Fig. 4. The functional role of OM_{BE} as bridging and separation agent exemplified by batch experiments containing earthworm mucus and bacterial EPS with corresponding OM-free reference systems (according to Guhra et al., 2019, 2020). The formation of organo-mineral associations due to the adsorption of OM_{BE} like mucilage, mucus, or microbial EPS changes surface properties (e.g., isoelectric point: IEP), which control their further aggregation behavior. The simultaneous or subsequent occurrence of external forces can provoke spatial confinement, thereby outperforming repulsive long-range forces and accelerating aggregation. The resulting structures are stabilized by biogenic OM-induced surface coatings and OM filaments which interlink soil particles and serve as gluing agents (SEM images of biopore walls).

casts. They reported that the stability of earthworm casts increased after alteration and drying compared to the surrounding bulk soil due to interparticle bonding permitted by organic debris. Guhra et al. (2019) found that the aggregation between (micro-)aggregate forming materials was maximal if a drying step was conducted after treatment with bacterial EPS. The permeation of dry soil with chia mucilage increased soil aggregate stability (against wet sieving). As the controlling factors, soil type and the amount of mucilage were identified (Di Marsico et al., 2018). Carminati et al. (2017) showed that during desiccation, water menisci act as a template for developing mucilage filament networks between soil particles. Krause et al. (2019) reported aggregation mediation by bacteria cells and cell envelopes after lysis, primarily after multiple wetting and drying cycles.

We attribute this external force-induced aggregation with biogenic OM to the ability of biogenic OM to serve as a **gluing agent** (Fig. 4). In contrast to the function as a bridging or separation agent which are always controlled or at least influenced by surface charges, the function as a gluing agent is relatively independent of the surface charge of the (micro-)aggregate forming materials, i.e., the condition of soil solution like the pH and electric conductivity. Here, the OM_{BE} availability during drying influences the spatial configuration of solid bridges (filaments) between particles. Consequently, this leads to the substrates' altered wetting and hydraulic properties (Benard et al., 2019). For example, the rewetting of aggregates stabilized by gluing is derated due to the hydrophobic character of mucilage after drying (Carminati et al., 2016), which potentially enhances the aggregate stability against wet sieving (Morel et al., 1991). Earthworms exploit the increased water stability of aggregates as mainly anecic species use OM-enriched casts to stabilize their vertical burrows (Jégou et al., 2001). As a result of the cast application, earthworm burrow-walls feature heterogeneously distributed hydrophobic regions (Leue et al., 2015; Lipiec et al., 2015). Furthermore, earthworms facilitate particle confinement and agglutination by applying pressure to the burrow walls, which simultaneously get permeated with cutaneous mucus (Lee, 1985; Six et al., 2004; Schrader et al., 2007; Rogasik et al., 2014). Additionally, plants and fungi contribute to the functional role of OM_{BE} as gluing agent as they actively shape soil by root/hyphae growth, resulting in soil penetration, particle enmeshments, and pressure application combined with the secretion of fungal EPS and mucilage (Six et al., 2004; Nichols and Halvorson, 2013).

5. Approaches to explore the pathways and role of OM_{BE} in soil

Disclosing the role of OM_{BE} in the functioning of soils and tracing its intricate pathways into it requires consideration of a multitude of biotic and abiotic factors. A promising approach to achieve a mechanistic understanding of the processes leading to the incorporation of OM_{BE} into soil aggregates is to combine observational studies, laboratory experiments (experimental pedology), and a suite of complementary analytical techniques (e.g., compound-specific analytics, "Omics", spectroscopic, microscopic, and tomographic instrumental methods), with computational methods (Table 1). We thus advocate developing our understanding of the formation, structure, properties, and functional role of aggregates on sophisticated experiments conducted under defined conditions. Such investigations should aim to elucidate the complicated interactions between potentially (micro-)aggregate forming materials and to unravel the mechanisms and processes that drive the formation of organo-mineral association and aggregation in soil. Computational *in-silico* methods must complement the toolbox as they not only allow for performing thought experiments on a "digital twin", but are essential to validate theories inspired by observational *in-situ* studies, yet to be challenged by sophisticated lab experiments. Future efforts should aim to realize this paradigm for soil research from "scratch", yet, it will be more than rewarding to apply this paradigm with accomplished studies and re-use the results in a novel and widened context. In the field of biogenic aggregation and OM_{BE}, a by far not complete selection of suitable "study candidates" are reported here.

Observational studies: Sustainable soil fertilization strategies are inspired by attributing improved water retention of soil and aggregate stability through the symbiotic interaction between plants and microbial EPS producers (Sher et al., 2020). Using specifically designed lysimeters, the dynamics of the biotic and abiotic mobile inventory of soils (i.e., potential (micro-)aggregate forming materials) can be explored (e.g., Zhang et al., 2018; Lehmann et al., 2021). The role of macropores formed by plants and earthworms is investigated by brilliant-blue experiments that assess preferential flow pathways (e.g., Weiler and Naef, 2003; Cey et al., 2009). Further studies apply nondestructive endoscopic surveys of biopores to quantify the contact area between roots and soil (e.g., Kautz and Köpke, 2010; Athmann et al., 2013). Moreover, the beneficial role of soil biota on aggregate formation and stabilization as a function of the field treatment is assessed by quantifying the proportion of water-stable aggregates (e.g., Puget et al., 1999; Felde et al., 2020).

Sophisticated experimental approaches to explore OM_{BE} in soil (including experimental pedology): Pot experiments with well-defined artificial soils enable the control and exclusion of specific aggregation influencing factors (e.g., irrigation, substrate composition, or type of OM sources) and, thus, can be used for an assessment of structure development (e.g., Pronk et al., 2012; Bucka et al., 2021). In addition, column experiments reveal insights into the mobility of organo-mineral associations and bacteria/microorganisms in porous media under defined conditions (e.g., Flynn et al., 2012; Bai et al., 2016; Narvekar et al., 2017). Micro-structured soil chips were designed to simulate aggregate pore spaces and to study organism-specific colonialization of pores, competition within pores, biofilm-induced bypass-flows, and hyphal growth in micro-habitats (e.g., Drescher et al., 2013; Coyte et al., 2016; Aleklett et al., 2021). In batch experiments, the aggregation of particles and the interaction of OM_{BE} with primary and secondary soil minerals are illuminated. After batch treatments, solid and liquid phases can be investigated separately and compared to the corresponding stock solutions and bare mineral phases (e.g., Cao et al., 2011; Fang et al., 2012; Guhra et al., 2019, 2020). Furthermore, the rearrangement of newly formed organo-mineral associations inside the aqueous phase into aggregates can be monitored, e.g., by laser light scattering (e.g., Tan et al., 2012; Dultz et al., 2018).

Analytical techniques: Any assessment of the relative importance of sources of OM_{BE} has to be based on the identification and comparison of organism-specific biomarkers, for example, available for microorganisms and soil fauna (e.g., earthworms) via, e.g., phospholipid fatty acid analysis (Frostegård and Bååth, 1996; Sampedro et al., 2006; Ruess and Chamberlain, 2010; Schwab et al., 2019), amino sugars database reconciliation for necromass (Liang et al., 2019), or fluorescently labeled primers for viruses (Narr et al., 2017). Emerging techniques that aim to link microbial communities and their functions in ecosystems (e.g., soil and groundwater) are gene sequencing and metagenomics (Benk et al., 2019; Herrmann et al., 2020; Xenophontos et al., 2021). Methods like stable-isotope-probing (Taubert et al., 2019; Starke et al., 2021), metatranscriptomics (Carvalhais et al., 2012), and metaproteomics (Kleiner et al., 2018) are helpful to distinguish the actual active microbial community from the potential community as many of the microorganisms in soil are quiescent (Myrold et al., 2013; Bastida and Jehmlich, 2016). Employing computed X-ray micro-tomography (μCT), the impact of soil biota on biopore and aggregate formation, architecture, and soil restructuring can be visualized and quantified (e.g., Peth et al., 2014; Burr-Hersey et al., 2020). The habitat function of aggregates for microorganisms can be explored by combining imaging techniques like scanning electron microscopy, transmission electron microscopy, and fluorescence microscopy (e.g., Zhao et al., 2015; Watteau and Villemin et al., 2018; Krause et al., 2019) with tomographic approaches. The spatial organization of OM at aggregate surfaces and inside the aggregates (frequently requires the preparation of thin sections) can be revealed by electron probe micro analysis (e.g., Lehndorff et al., 2021) and nano secondary ion mass spectrometry (e.g., Remusat et al., 2012;

Liu et al., 2013). Methods as infrared spectroscopy, ^{13}C-nuclear magnetic resonance, X-ray photoelectron spectroscopy, and size-exclusion chromatography allow for the characterization of OM_{BE} and its functional groups (e.g., Omoike and Chorover, 2004; Metzger et al., 2009; Stewart et al., 2013). Zeta potential measurements can identify surface charge screenings of newly formed organo-mineral associations, e.g., the determination of the IEP as well as the characterization of current charge conditions in experiments and their response to changes in pH and electrolyte concentration (e.g., Tombácz, et al., 2004; Mikutta et al., 2012; Dultz et al., 2019). Furthermore, OM_{BE} adsorption and deposition kinetics can be revealed by calorimetric (e.g., Lin et al., 2016) and quartz crystal micro balance measurements (e.g., Kwon et al., 2006; Tong et al., 2011). The application of atomic force microscopy allows the detection of force-distance curves as an indicator for attractive and repulsive surface interactions between biogenic and mineral components (e.g., Huang et al., 2015; Pen et al., 2015).

Computational methods: Particle aggregation dynamics can be studied by numerical models that focus on physicochemical aspects of particle aggregation. For example, aggregation in the liquid phase was studied as a function of pH, electric conductivity (e.g., Praetorius et al., 2014; Liang et al., 2017), particle size/number mismatch (e.g., Olsen et al., 2005; Cerbelaud et al., 2017; Laganapan et al., 2018; Clavier et al.,

Table 1
Tool-box for the exploration of pathways of biogenically excreted OM into soil.

Research approaches	Technique	Scope	Selected references
observational studies	extraction of water stable and/or mechanical stable aggregates	evaluation of treatment effects on aggregate formation and stability	Puget et al. (1999); Spohn and Giani (2010); Krause et al. (2018); Wilpizeski et al. (2019); Sher et al. (2020); Felde et al. (2020)
	lysimeters	monitoring dynamics of the biotic and abiotic mobile inventory of the soil	Kaplan et al. (1993); Zhang et al. (2018); Lehmann et al. (2021)
	endoscopy of biopores	optical assessment of biopore topologies and genesis	Kautz and Köpke (2010); Athmann et al. (2013)
experimental investigations (including experimental pedology)	pot experiments	assessment of feedbacks between defined components	Pronk et al. (2012); Bucka et al. (2021)
	column experiments	transport of organo-mineral associations in porous media	Gargiulo et al. (2007); Flynn et al. (2012); Narvekar et al. (2017);
	micro-structured soil chips	microorganisms induced alteration of the pore space/fluid flow; growth and colonization in micropores	Drescher et al. (2013); Coyte et al. (2016); Aleklett et al. (2021)
	batch experiment	adsorption and aggregation behavior in the aqueous phase	Tombácz et al., 2004; Fang et al. (2012); Guhra et al. (2020)
	laser light scattering	colloidal aggregation; Structuring of excreted biogenic OM	Wang et al., 2012; Tan et al., 2012; Dultz et al., 2019
characterization, identification, and imaging/advanced instrumental techniques	analysis of biomarkers (e.g., phospholipid fatty acid analysis, amino sugars database reconciliation, fluorescent labeling)	identification of specific soil organisms in soil compartments	Narr et al., 2017; Benk et al. (2019); Liang et al. (2019); Schwab et al. (2019); Krause et al. (2019); Biesgen et al. (2020)
	DNA-extraction, metagenomics, metatranscriptomics, metaproteomics, stable-isotope-probing	identification of active microbial communities	Carvalhais et al. (2012); Kleiner et al. (2018); Herrmann et al., 2020; Taubert et al. (2019)
	X-ray micro-computed tomography	structural effects of bioturbation/root growth; pore architecture; aggregate pore network function and geometry; OM localization	Koebernick et al. (2014); Peth et al. (2014); Bacq-Labreuil et al. (2019); Burr-Hersey et al. (2020)
	scanning electron microscopy + energy-dispersive X-ray spectroscopy	visualization and characterization of micro aggregates	Zhao et al. (2015) Haas and Horn (2018); Guhra et al. (2019);
	transmission electron microscopy	morphological analysis of microstructures and characterization of micro-habitats	Chenu (1993); Watteau and Villemin (2018)
	fluorescence microscopy	spatial distribution of microorganisms in aggregates	Krause et al. (2019)
	electron probe microanalysis	spatial organization and relations of organic and inorganic constituents in aggregates	Lehndorff et al. (2021)
	nano secondary ion mass spectrometry	visualize and characterize organic matter on aggregate surfaces	Remusat et al. (2012); Liu et al. (2013)
	infrared spectroscopy	OM mapping on aggregate surfaces; compositional and structural information of OM	Omoike and Chorover (2004); Leue et al., (2010); Cao et al. (2011); Barreto et al. (2020)
	^{13}C-nuclear magnetic resonance spectroscopy	OM composition; component identification in soil samples	Kölbl and Kögel-Knabner (2004); Metzger et al. (2009); Le Mer et al. (2020)
	size-exclusion chromatography	characterization of OM for size and chemical functions	Huber et al. (2010); Stewart et al. (2013)
	X-ray photoelectron spectroscopy	characterization of OM	Omoike and Chorover (2004); Mikutta et al. (2011)
	zeta potential measurement or potentiometric acid-base titration	surface charge; determination of the isoelectric point/point of zero charge	Tombácz et al., 2004; Mikutta et al. (2012); Dultz et al. (2018)
	atomic force microscopy	cell attachment to mineral surfaces, force assessment between biogenic and mineral soil components	Assemi et al. (2004); Szilagyi et al. (2014); Huang et al. (2015); Pen et al. (2015);
	quartz crystal microbalance	deposition rates of OM to mineral surfaces	Kwon et al. (2006); Zhu et al. (2009); Tong et al. (2011)
	calorimetry	adsorption enthalpies	Lin et al. (2016)
computational methods	numerical models	particle aggregation dynamics, formation of aggregate structure and functions	Liang et al. (2017); Laganapan et al. (2018); Clavier et al. (2019); Lazzari et al. (2016); Ritschel and Totsche (2019); Zhang et al. (2019) Zech et al. (2021)

2019; Rupp et al., 2019) and impact of external fields (e.g., magnetic and gravitational) (Dukhin et al., 2007; Lazzari et al., 2016; Guhra et al., 2021). While recent models successfully linked these processes to the formation of aggregate structure and functions (Ritschel and Totsche, 2019), the impact of microbial communities and their exudates is still under development. Important biological aspects, including the attachment of bacterial cells to mineral particles controlled by hydrophobic substances (e.g., Hwang et al., 2012; Zhang et al., 2019) and the growth of microbial colonies (Ray et al., 2017), were recently addressed. Furthermore, microbial degradation kinetics were included in models at the microaggregate scale to simulate carbon turnover (Vogel et al., 2015; Portell et al., 2018; Zech et al., 2021). An explicit representation of OM_{BE} interactions in the soil might further help to establish a comprehensive numerical approach for aggregate formation, development, and function.

However, mechanistic studies are indispensable to entangle the mechanisms which lead to the phenomenology and structures observed *in situ*. Studies examining the specific adsorption of OM_{BE} onto soil minerals are a prominent example of the enrichment in nutrients and OM_{BE} protection and storage. In addition, lab-scale studies showed that OM_{BE} forms water- and mechanical-stable bonds between particles which explains the increased availability of water-stable aggregates for biota-treated study sites found on the field scale. This is the mechanistic basis for upcoming soil treatment strategies, which demonstrate that effective and sustainable soil fertilization can be achieved by biogenic aggregate formation triggered by EPS producers (Saha et al., 2020; Sher et al., 2020).

6. Future scope

Biogenically excreted OM in soil shapes (im-)mobilization and aggregation of (in-)organic soil constituents according to its three functional roles as gluing, bridging, and separation agents in soil. Given the current state of knowledge, we can only reconstruct fragmentarily who excreted OM or under which circumstances these functional roles apply in soil. Sophisticated studies are required to improve our mechanistic understanding: These studies should encompass varying conditions (e.g., controlled by pH, electrolyte concentration and type, biopolymer availability, and composition), favoring or inhibiting aggregation. In addition, we need to broaden our comprehension of how external forces (e.g., exerted by gravity, menisci, bioturbation, mechanical load) alter the distribution and formation of organo-mineral-associations and aggregates in saturated and unsaturated porous media. These external forces and stresses are of crucial importance for aggregate architecture and functions, hierarchic structuring, the formation of diagnostic horizons, aeration zone bypasses, nutrient fixation, and transport. Hence, it is long overdue that we combine dedicated experimental investigations with computational methods, which should be inspired and motivated by observational studies and field surveys to understand the functional role of OM_{BE} in aggregation and structure formation.

Furthermore, the identification of biogenic OM producers remains quite challenging despite innovative advances in this area. Yet, omics techniques like metagenomics, metatranscriptomics, and proteomics might point a way out as specific patterns and fingerprints of DNA, RNA, and proteins may allow for assessing the functionality and activity of soil (microbial) communities (Myrold et al., 2013). In addition, the multitude of mechanistic studies dealing with microbial EPS overshadows those of plant exudates and earthworm mucus. This is especially important considering the complex EPS extraction strategies which use, for example, ethanol, EDTA extractions, or cation-exchange-resins, which generate treatment-related compositional differences. By contrast, plant-derived mucilage or earthworm-formed cutaneous mucus are more easily and gently extractable and thus might represent less artificial surrogates of OM_{BE} in soil.

Furthermore, in the last decade, the focus turned from biogenically produced polysaccharides to proteins. They were frequently reported as the dominant fraction of stable organo-mineral associations and aggregates in soil. Suppose a specific adsorption and aggregation behavior of polysaccharides and proteins with secondary soil minerals is known. In that case, the protein-to-polysaccharide ratio of OM_{BE} could potentially be considered as a variable to prove/refer to their functionality as an aggregation agent in aggregation studies.

Finally, we should be careful with monocausal explanations since biogenically induced aggregation is triggered and mediated by the whole soil community. The challenge is to trace the essential interactions, nutrient cycles, and feedbacks between soil biota of different taxa leading to aggregate formation. This requires, for example, isotope labels bound in relevant SOM precursors. A deep understanding of the complex interplay (functional redundancy due to functional diversity) and the intricate feedback loops therein is mandatory to maintain and restore soil fertility as the basis of ecosystem services like GHG fixation and to accomplish the sustainable development goals “no hunger”, “climate action” and “clean water”.

7. Summary and conclusions

Soil organisms affect soil’s physicochemical properties and structure actively and passively during soil penetration, matter translocation, and OM_{BE} supply. The activity of soil biota is an essential driver of pedogenesis, structure dynamics, and nutrient and organic matter turnover in mature soils. The formation of biopores results in preferential pathways that connect the surface with deeper soil horizons and beyond, causing bypass flow of water and rapid transport of nutrients and pollutants even to surface-near aquifers. Hence, biota-induced and mediated alteration processes in soil are effective on a variety of spatial scales, from the micro- (predominantly surface-associated bacteria) to the pedon-scale (e.g., bioturbation), with significant effects on the landscape scale (soil fertility, crop yield, vulnerability of groundwater resources). However, biogenic (micro-)aggregation occurs in regions of high biological activity of organisms providing OM_{BE}, like the mycorrhizosphere and drilosphere. In particular, recent research focused on protein-like biogenic OM constituents as the dominant fraction of stable organo-mineral associations and aggregates in soil. The resulting biogenic aggregates affect soil functions, for instance, by increasing water repellency, enhancing water holding capacity, increasing nutrient and contaminant storage, and providing habitats. In the presence of OM_{BE}, aggregate formation results from screening, enmeshing, and agglutination of primarily mineral soil constituents (Fig. 1). However, there is convincing evidence that OM_{BE} may operate both as an aggregation inhibiting and mediating agent. These divergent observations result from monocausal derivations in terms of their functionality. They are provoked by experimental studies which considered a limited number of factors that influence aggregation. However, in nature, these factors coincide and interact in a changing and dynamic environment. In consequence, the functional roles of OM_{BE} co-occur or succeed each other, but to varying extent according to the environmental conditions. Thus, a more general conception should encompass the three different functional roles that OM_{BE} may play in aggregation (Fig. 4):

(I) **Bridging agents** permit the aggregation due to surface modifications and attraction, e.g., due to the formation of molecular bridges and surface coatings which provoke a balanced amount of positive and negative adsorption sides between interacting surfaces and by the environmental alterations (e.g., the composition of soil solution, water content, pH, and electrical conductivity) after OM supply to aggregation favoring conditions. The collision/attachment probability of particles is always impacted or controlled by the interplay of attractive and repulsive electrostatics.

(II) **Separation agents** inhibit aggregation and favor mobility and transport of organo-mineral associations inside natural porous media until environmental conditions change. The **separation**

agent acts antagonistically to the bridging agent. Thus, the inhibition of aggregation and fractionation is caused by surface screening, equalization of the surface charges, electrostatic repulsion, and steric interaction.

(III) **Gluing agents** mediate aggregate stability and a close approach of particles and OM after an external force supply, e.g., compaction, gravitative sedimentation, and menisci forces/drying. Thereby, the aggregation inhibiting effect of the **separation agents** can be compensated after an external force provokes a close approach of soil particles until attractive short-range forces like Van Der Waals interactions take over and aging/drying leads to the agglutination of particles (e.g., due to hydrophobic particle interlinkages which increase their water stability). Here, the strength and the duration of external forces or stresses control particles' collision/attachment probability.

We showed that a cascade of biotic and abiotic processes constrained by the hierarchy of interplaying factors (Fig. 2) shapes the pathways of OM_{BE} into aggregates. The contribution of OM_{BE} on the aggregation in soil operates across spatiotemporal scales and involves a large variety of soil biota. This further implies that the impact of soil biota on aggregation is not limited to specific soil taxonomic groups but is controlled by the interplay of the diverse soil biota and the particular community. Biogenic aggregate formation bolstered by mutualistic relationships can be utilized to counteract the deterioration of site conditions due to nutrient depletion, loss in biodiversity, soil contamination, and erosion. The growing understanding of OM-excreting biota's beneficial role and the effect of OM_{BE} for soil aggregation underpins the need to preserve or restore biodiversity and the biodiversity-linked functional redundancy for soil fertility and soil health. Ultimately, the overarching challenge is translating this understanding into recommendations and regulations for land-management practices for sustainable forestry and agriculture. These recommendations must aim to maintain and foster the functions of soils as the basis for ecosystem services, e.g., carbon storage and clean drinking water provision, under the conditions of climate change.

Author contributions

KT conceived the general idea of the manuscript. KT supervised, and TG developed the concept. TG and KS wrote the first draft. All authors carefully reviewed the manuscript.

Declaration of competing interest

The authors declare that they have no known competing financial interests or personal relationships that could have appeared to influence the work reported in this paper.

Acknowledgment

We kindly acknowledge financial support by the Deutsche Forschungsgemeinschaft within the framework of the research unit 2179 "MAD Soil - Microaggregates: Formation and turnover of the structural building blocks of soils" (Project no.: 193380941; www.madsoil.uni-jena.de). Katharina Stolze is funded by the International Max Planck Research School for Global Biogeochemical Cycles (www.imprs-gbgc.de). We thank Prof. Dr. Karl Ritz and two reviewers for their helpful comments and valuable suggestions.

References

Ahmadi, K., Zarebanadkouki, M., Ahmed, M.A., Ferrarini, A., Kuzyakov, Y., Kostka, S.J., Carminati, A., 2017. Rhizosphere engineering: innovative improvement of root environment. Rhizosphere 3, 176–184.

Aira, M., McNamara, N.P., Piearce, T.G., Domínguez, J., 2009. Microbial communities of *Lumbricus terrestris* L. middens: structure, activity, and changes through time in relation to earthworm presence. Journal of Soils and Sediments 9, 54–61.

Alami, Y., Achouak, W., Marol, C., Heulin, T., 2000. Rhizosphere soil aggregation and plant growth promotion of sunflowers by an exopolysaccharide-producing *Rhizobium* sp. strain isolated from sunflower roots. Applied and Environmental Microbiology 66, 3393–3398.

Aleklett, K., Ohlsson, P., Bengtsson, M., Hammer, E.C., 2021. Fungal foraging behaviour and hyphal space exploration in microstructured Soil Chips. The ISME Journal 15, 1782–1793.

Amelung, W., Brodowski, S., Sandhage-Hofmann, A., Bol, R., 2008. Combining biomarker with stable isotope analyses for assessing the transformation and turnover of soil organic matter. Advances in Agronomy 100, 155–250.

Amirbahman, A., Olson, T.M., 1995. Deposition kinetics of humic matter-coated hematite in porous media in the presence of Ca^{2+}. Colloids and Surfacces A 99, 1–10.

Andriuzzi, W.S., Bolger, T., Schmidt, O., 2013. The drilosphere concept: fine-scale incorporation of surface residuederived N and C around natural *Lumbricus terrestris* burrows. Soil Biology and Biochemistry 64, 136–138.

Angst, G., Kögel-Knabner, I., Kirfel, K., Hertel, D., Mueller, C.W., 2016. Spatial distribution and chemical composition of soil organic matter fractions in rhizosphere and non-rhizosphere soil under European beech (Fagus sylvatica L.). Geoderma 264, 179–187.

Asano, M., Wagai, R., Yamaguchi, N., Takeichi, Y., Maeda, M., Suga, H., Takahashi, Y., 2018. In search of a binding agent: nano-scale evidence of preferential carbon associations with poorly-crystalline mineral phases in physically-stable, clay-sized aggregates. MDPI Soil Systems 2. https://doi.org/10.3390/soilsystems2020032.

Assemi, S., Hartley, P.G., Scales, P.J., Beckett, R., 2004. Investigation of adsorbed humic substances using atomic force microscopy. Colloids and Surfacces A 248, 17–23.

Athmann, M., Kautz, T., Pude, R., Köpke, U., 2013. Root growth in biopores—evaluation with in situ endoscopy. Plant and Soil 371, 179–190.

Aubry, C., Gutierrez, L., Croue, J.P., 2013. Coating of AFM probes with aquatic humic and non-humic NOM to study their adhesion properties. Water Research 47, 3109–3119.

Bacq-Labreuil, A., Crawford, J., Mooney, S.J., Neal, A.L., Ritz, K., 2019. Phacelia (*Phacelia tanacetifolia* Benth.) affects soil structure differently depending on soil texture. Plant and Soil 441, 543–554.

Bai, H., Cochet, N., Drelich, A., Pauss, P., Lamy, E., 2016. Comparison of transport between two bacteria in saturated porous media with distinct pore size distribution. RSC Advances 6, 14602–14614.

Baldock, J.H., 2002. Interactions of organic materials and microorganisms with minerals in the stabilisation of soil structure. In: Huang, P.M., Bollag, J.M., Senesi, N. (Eds.), Interactions between Soil Particles and Microorganisms. John Wiley & Sons, pp. 85–131.

Bansal, P., Deshpande, A.P., Basavaraj, M.G., 2017. Hetero-aggregation of oppositely charged nanoparticles. Journal of Colloid and Interface Science 492, 92–100.

Barois, I., Villemin, G., Lavelle, P., Toutain, F., 1993. Transformation of the soil structure through *Pontoscolex corethrurus* (Oligochaeta) intestinal tract. Geoderma 56, 57–66.

Barreto, M.S.C., Elzinga, E.J., Alleoni, L.R.F., 2020. The molecular insights into protein adsorption on hematite surface disclosed by in-situ ATR-FTIR/2D-COS study. Scientific Reports 10. https://doi.org/10.1038/s41598-020-70201-z.

Bastardie, F., Ruy, S., Cluzeau, D., 2005. Assessment of earthworm contribution to soil hydrology: a laboratory method to measure water diffusion through burrow walls. Biology and Fertility of Soils 41, 124–128.

Bastida, F., Jehmlich, N., 2016. It's all about functionality: how can metaproteomics help us to discuss the attributes of ecological relevance in soil? Journal of Proteomics 144, 159–161.

Baumert, V.L., Vasilyeva, N.A., Vladimirov, A.A., Meier, I.C., Kögel-Knabner, I., Mueller, C.W., 2018. Root exudates induce soil macroaggregation facilitated by fungi in subsoil. Frontiers in Environmental Science 6. https://doi.org/10.3389/fenvs.2018.00140.

Benard, P., Zarebanadkouki, M., Brax, M., Kaltenbach, R., Jerjen, I., Marone, F., Couradeau, E., Felde, V.J.M.N.L., Kaestner, A., Carminati, A., 2019. Microhydrological niches in soils: how mucilage and EPS alter the biophysical properties of the rhizosphere and other biological hotspots. Vadose Zone Journal 18. https://doi.org/10.2136/vzj2018.12.0211.

Benk, S.A., Yan, L., Lehmann, R., Roth, V.-N., Schwab, V.F., Totsche, K.U., Küsel, K., Gleixner, G., 2019. Fueling diversity in the subsurface: composition and age of dissolved organic matter in the critical zone. Frontiers of Earth Science 7. https://doi.org/10.3389/feart.2019.00296.

Bin, G., Cao, X., Dong, Y., Luo, Y., Ma, L.Q., 2011. Colloid deposition and release in soils and their association with heavy metals. Critical Reviews in Environmental Science and Technology 41, 336–372.

Biesgen, D., Frindte, K., Maarastawi, S., Knief, K., 2020. Clay content modulates differences in bacterial community structure in soil aggregates of different size. Geoderma 376. https://doi.org/10.1016/j.geoderma.2020.114544.

Blossfeld, S., Schreiber, C.M., Liebsch, G., Kuhn, A.J., Hinsinger, P., 2013. Quantitative imaging of rhizosphere pH and CO_2 dynamics with planar optodes. Annals of Botany 112, 267–276.

Bottinelli, N., Jouquet, P., Capowiez, Y., Podwojewski, P., Grimaldi, M., Peng, X., 2015. Why is the influence of soil macrofauna on soil structure only considered by soil ecologists? Soil and Tillage Research 146, 118–124.

Bouché, M.B., 1975. Action de la faune sur les états de la matière organique dans les ecosystems. In: Kilbertius, G., Reisinger, O., Mourey, A., Cancela da Fonseca, J.A. (Eds.), Humification et biodégradation. Pierron, Sarreguemines, France, pp. 157–168.

Bronick, C.J., Lal, R., 2005. Soil structure and managment: a review. Geoderma 124, 3–22.

Brown, G.G., Barois, I., Lavelle, P., 2000. Regulation of soil organic matter dynamics and microbial activity in the drilosphere and the role of interactions with other edaphic functional domains. European Journal of Soil Biology 36, 177–198.
Bucka, F.B., Felde, V.J.M.N.L., Peth, S., Kögel-Knabner, I., 2021. Disentangling the effects of OM quality and soil texture on microbially mediated structure formation in artificial model soils. Geoderma 403. https://doi.org/10.1016/j.geoderma.2021.115213.
Bucka, F.B., Kölbl, A., Uteau, D., Peth, S., Kögel-Knabner, I., 2019. Organic matter input determines structure development and aggregate formation in artificial soils. Geoderma 354. https://doi.org/10.1016/j.geoderma.2019.113881.
Burr-Hersey, J.E., Ritz, K., Bengough, G.A., Mooney, S., 2020. Reorganisation of rhizosphere soil pore structure by wild plant species in compacted soils. Journal of Experimental Botany 71, 6107–6115.
Cai, P., Lin, D., Peacock, C.L., Peng, W., Huang, Q., 2018. EPS adsorption to goethite: molecular level adsorption mechanisms using 2D correlation spectroscopy. Chemical Geology 494, 127–135.
Cania, B., Vestergaard, G., Krauss, M., Fliessbach, A., Schloter, M., Schulz, S., 2019. A long-term field experiment demonstrates the influence of tillage on the bacterial potential to produce soil structure-stabilizing agents such as exopolysaccharides and lipopolysaccharides. Environmental Microbiome 14. https://doi.org/10.1186/s40793-019-0341-7.
Carminati, A., Vetterlein, D., 2013. Plasticity of rhizosphere hydraulic properties as a key for efficient utilization of scarce resources. Annals of Botany 112, 277–290.
Carminati, A., Zarebanadkouki, M., Kroener, E., Ahmed, M.A., Holz, M., 2016. Biophysical rhizosphere processes affecting root water uptake. Annals of Botany 118. https://doi.org/10.1093/aob/mcw113.
Carminati, A., Benard, P., Ahmed, M.A., Zarebanadkouki, M., 2017. Liquid bridges at the root-soil interface. Plant and Soil 417, 1–15.
Carvalhais, L.C., Dennis, P.G., Tyson, G.W., Schenk, P.M., 2012. Application of metatranscriptomics to soil environments. Journal of Microbiological Methods 91, 246–251.
Cao, Y., Wie, X., Cai, P., Huang, Q., Rong, X., Liang, W., 2011. Preferential adsorption of extracellular polymeric substances from bacteria on clay minerals and iron oxide. Colloids and Surfaces B 83, 122–127.
Cerbelaud, M., Videcoq, A., Rossignol, F., Piechowiak, M.A., Bochicchio, D., Ferrando, R., 2017. Heteroaggregation of ceramic colloids in suspensions. Advances in Physics X 2, 35–53.
Cey, E.E., Rudolph, D.L., Passmore, J., 2009. Influence of macroporosity on preferential solute and colloid transport in unsaturated field soils. Journal of Contaminant Hydrology 107, 45–57.
Chen, G., Hong, Y., Walker, S.L., 2009. Colloidal and bacterial deposition: role of gravity. Langmuir 26 (1), 314–319. https://doi.org/10.1021/la903089x.
Chen, Y., Wang, M., Zhou, X., Fu, H., Qu, X., Zhu, D., 2021. Sorption fractionation of bacterial extracellular polymeric substances (EPS) on mineral surfaces and associated effects on phenanthrene sorption to EPS-mineral complexes. Chemosphere 263. https://doi.org/10.1016/j.chemosphere.2020.128264.
Chenu, C., 1993. Clay- or sand-polysaccharide associations as models for the interface between microorganisms and soil: water related properties and microstructure. Geoderma 56, 143–156.
Chenu, C., Plante, A.F., 2006. Clay-sized organo-mineral complexes in a cultivation chronosequence: revisiting the concept of the 'primary organo-mineral complex. European Journal of Soil Science 57, 596–609.
Chenu, C., Cosentino, D.J., 2011. Microbial regulation of soil structural dynamics. In: Ritz, K., Young, I. (Eds.), The Architecture and Biology of Soils: Life in Inner Space. CABI, Wallingford, Oxfordshire, pp. 37–70.
Christensen, B.T., 2001. Physical fractionation of soil and structural and functional complexity in organic matter turnover. European Journal of Soil Science 52, 348–353.
Clavier, A., Praetorius, A., Stoll, S., 2019. Determination of nanoparticle heteroaggregation attachment efficiencies and rates in presence of natural organic matter monomers. Monte Carlo modelling. The Science of the Total Environment 650, 530–540.
Cornell, R.M., Schwertmann, U., 2003. The Iron Oxides. WILEY-VCH Verlag GmbH und Co. KGaA, Weinheim.
Cortez, J., Bouché, M., 1987. Compositionchimique du mucus cutané de *Allolobophora chaetophora* chaetophora (Oligochaeta: Lumbricidae). Écologie générale 305, 207–210.
Costa, O.Y.A., Raaijmakers, J.M., Kuramae, E.E., 2018. Microbial extracellular polymeric substances: ecological function and impact on soil aggregation. Frontiers in Microbiology 9, 1–14.
Coyte, K.Z., Tabuteau, H., Eamonn, A.G., Foster, K.R., Durham, W.M., 2016. Microbial competition in porous environments can select against rapid biofilm growth. Proceedings of the National Academy of Sciences 22, 161–170.
Curry, J.P., Schmidt, O., 2007. The feeding ecology of earthworms – a review. Pedobiologia 50, 463–477.
Dakora, F.D., Phillips, D.A., 2002. Root exudates as mediators of mineral acquisition in low-nutrient environments. Plant and Soil 245, 35–47.
Darwin, C.R., 1881. The Formation of Vegetable Mould through the Action of Worms, with Observations on Their Habits. John Murray, London.
de Boer, W., Folman, L.B., Summerbell, R.C., Boddy, L., 2005. Living in a fungal world: impact of fungi on soil bacterial niche development. FEMS Microbiology Reviews 795, 811.
de Jonge, L.W., Kjaergaard, C., Moldrup, P., 2004. Colloids and colloid-facilitated transport of contaminants in soils. Vadose Zone Journal 3, 321–325.
de Melo, T.R., Pereira, M.G., de Cesare Barbosa, G.M., da Silva Neto, E.C., Andrello, A.C., Filho, J.T., 2019. Biogenic aggregation intensifies soil improvement caused by manures. Soil and Tillage Research 190, 186–193.
DeNovio, N.M., Saiers, J.S., Ryan, J.N., 2004. Colloid movement in unsaturated porous media: recent advances and future directions. Vadose Zone Journal 3, 338–351.
Denef, K., Six, J., Merckx, R., Paustian, K., 2002. Short-term effects of biological and physical forces on aggregate formation in soils with different clay mineralogy. Plant and Soil 246, 185–200.
Di Marsico, A., Scrano, L., Labella, R., Lanzotti, V., Rossi, R., Cox, L., Perniola, M., Amato, M., 2018. Mucilage from fruits/seeds of chia (*Salvia hispanica L.*) improves soil aggregate stability. Plant and Soil 425, 57–69.
Dogsa, I., Krichbaum, M., Stopar, D., Laggner, P., 2005. Structure of bacterial extracellular polymeric substances at different pH values as determined by SAXS. Biophysics Journal 89, 2711–2720.
Don, A., Steinberg, B., Schöning, I., Pritsch, K., Joschko, M., Gleixner, G., Schulze, E.D., 2008. Organic carbon sequestration in earthworm burrows. Soil Biology and Biochemistry 40, 1803–1812.
Donstova, K.M., Bigham, J.M., 2005. Anionic polysaccharide sorption by clay minerals. Soil Science Society of America Journal 69, 1026–1035.
Drescher, K., Shen, Y., Bassler, B.L., Stone, H.A., 2013. Biofilm streamers cause catastrophic disruption of flow with consequences for environmental and medical systems. Proceedings of the National Academy of Sciences 110, 4345–4350.
Dukhin, A., Dukhin, S., Goetz, P., 2007. Gravity as a factor of aggregative stability and coagulation. Advances in Colloid and Interface Science 134, 35–71.
Dultz, S., Steinke, H., Mikutta, R., Woche, S., Guggenberger, G., 2018. Impact of organic matter types on surface charge and aggregation of goethite. Colloids and Surfaces A 554, 156–168.
Dultz, S., Woche, S.K., Mikutta, R., Schrapel, M., Guggenberger, G., 2019. Size and charge constraints in microaggregation: model experiments with mineral particle size fractions. Applied Clay Science 170, 29–40.
Edwards, A.P., Bremner, J.M., 1967a. Dispersion of soil particles by sonic vibration. European Journal of Soil Science 18, 47–63.
Edwards, A.P., Bremner, J.M., 1967b. Microaggregates in soil. European Journal of Soil Science 18, 64–73.
Edwards, C.A., Fletcher, K.E., 1988. Interactions between earthworms and microorganisms in organic-matter breakdown. Agriculture, Ecosystems & Environment 24, 235–247.
Edwards, W.M., Shipitalo, M.J., Owens, L.B., Dick, W.A., 1993. Factors affecting preferential flow of water and atrazine through earthworm burrows under continuous No-till corn. Journal of Environmental Quality 22, 453–457.
Elimelech, M., Gregory, J., Jia, X., Williams, R.A., 1995. Particle Deposition & Aggregation - Measurement, Modelling and Simulation. Butterworth-Heinemann, Woburn.
Eusterhues, K., Neidhardt, J., Hädrich, A., Küsel, K., Totsche, K.U., 2014. Biodegradation of ferrihydrite-associated organic matter. Biogeochemistry 119, 45–50.
Fang, L., Cao, Y., Huang, Q., Walker, S.L., Cai, P., 2012. Reactions between bacterial exopolymers and goethite: a combined macroscopic and spectroscopic investigation. Water Research 46, 5613–5620.
Felde, V.J.M.N.L., Schweizer, S.A., Biesgen, D., Ulbrich, A., Uteau, D., Knief, C., Graf-Rosenfellner, M., Kögel-Knabner, I., Peth, S., 2020. Wet sieving versus dry crushing: soil microaggregates reveal different physical structure, bacterial diversity and organic matter composition in a clay gradient. European Journal of Soil Science 72. https://doi.org/10.1111/ejss.13014.
Flemming, H.-C., Wingender, J., Szewzyk, U., Steinberg, P., Rice, S.A., Kjelleberg, S., 2016. Biofilms: an emergent form of bacterial life. Nature Reviews Microbiology 14, 563–575.
Flynn, R.M., Yang, X., Hofmann, T., von der Kammer, F., 2012. Bovine serum albumin adsorption to iron oxide coated sands can change microsphere deposition mechanisms. Environmental Science and Technology 46, 2583–2591.
Fonte, S.J., Quintero, D.C., Velásquez, E., Lavelle, P., 2012. Interactive effects of plants and earthworms on the physical stabilization of soil organic matter in aggregates. Plant and Soil 359, 205–214.
Frac, M., Hannula, S.E., Belka, M., Jedryczka, M., 2018. Fungal biodiversity and their role in soil health. Frontiers in Microbiology 9. https://doi.org/10.3389/fmicb.2018.00707.
Franco, A.L.C., Cherubin, M.R., Cerri, C.E.P., Six, J., Wall, D.H., Cerri, C.C., 2020. Linking soil engineers, structural stability, and organic matter allocation to unravel soil carbon responses to land-use change. Soil Biology and Biochemistry 150. https://doi.org/10.1016/j.soilbio.2020.107998.
Freitas, T.K.F.S., Oliveira, V.M., de Souze, M.T.F., Geraldino, H.C.L., Almeida, V.C., Fávaro, S.L., Garcia, J.C., 2015. Optimization of coagulation-flocculation process for treatment of industrial textile wastewater using okra (*A. esculentus*) mucilage as natural coagulant. Industrial Crops and Products 76, 538–544.
Frescht, G.T., Cornwell, W.K., Wardle, D.A., Elumeeva, T.G., Liu, W., Jackson, B.G., Onipchenko, V.G., Soudzilovskaia, N.S., Tao, J., Cornelissen, J.H.C., 2013. Linking litter decomposition of above- and below-ground organs to plant–soil feedbacks worldwide. Journal of Ecology 101, 943–952.
Frey, S.D., 2019. Mycorrhizal fungi as mediators of soil organic matter dynamics. Annual Review of Ecology, Evolution, and Systematics 50, 237–259.
Frostegård, A., Bååth, E., 1996. The use of phospholipid fatty acid analysis to estimate bacterial and fungal biomass in soil. Biology and Fertility of Soils 22, 59–65.
Gargiulo, G., Bradford, S.A., Simunek, J., Ustohal, P., Vereecken, H., Klumpp, E., 2007. Transport and deposition of metabolically active and stationary phase *Deinococcus radiodurans* in unsaturated porous media. Environmental Science & Technology 41, 1265–1271.

Gaume, A., Weidler, P.G., Frossard, E., 2000. Effect of maize root mucilage on phosphate adsorption and exchangeability on a synthetic ferrihydrite. Biology and Fertility of Soils 31, 525–532.
Gerke, J., 2018. Concepts and misconceptions of humic substances as the stable part of soil organic matter: a review. MDPI Agronomy 8. https://doi.org/10.3390/agronomy8050076.
Golchin, A., Baldock, J., Oades, J., 1998. A model linking organic matter decomposition, chemistry and aggregate dynamics. In: Lal, R., Kimble, J.M., Follett, R.F., Stewart, B. A. (Eds.), Soil Processes and the Carbon Cycle. CRC Press, Boca Raton, Boston, New York, Washington, London, pp. 245–266.
Guggenberger, G., Kaiser, K., 2003. Dissolved organic matter in soil: challenging the paradigm of sorptive preservation. Geoderma 113, 293–310.
Guhra, T., Ritschel, T., Totsche, K.U., 2019. Formation of mineral–mineral and organo–mineral composite building units from microaggregate-forming materials including microbially produced extracellular polymeric substances. European Journal of Soil Science 70, 604–615.
Guhra, T., Stolze, K., Schweizer, S., Totsche, K.U., 2020. Earthworm mucus contributes to the formation of organo-mineral associations in soil. Soil Biology and Biochemistry 145. https://doi.org/10.1016/j.soilbio.2020.107785.
Guhra, T., Ritschel, T., Totsche, K.U., 2021. The mechanisms of gravity-constrained aggregation in natural colloidal suspensions. Journal of Colloid and Interface Science 597, 126–136.
Gregory, P.J., 2006. Roots, rhizosphere and soil: the route to a better understanding of soil science? European Journal of Soil Science 57, 2–27.
Grimal, J.Y., Frossard, E., Morel, J.L., 2001. Maize root mucilage decreases adsorption of phosphate on goethite. Biology and Fertility of Soils 33, 226–230.
Han, E., Kautz, T., Perkons, U., Uteau, D., Peth, S., Huang, N., Horn, R., Köpke, U., 2015. Root growth dynamics inside and outside of soil biopores as affected by crop sequence determined with the profile wall method. Biology and Fertility of Soils 51, 847–856.
Haq, I.U., Zhang, M., Yang, P., van Elsas, J.D., 2014. The interactions of bacteria with fungi in soil: emerging concepts. Advances in Applied Microbiology 89, 185–215.
Harimawan, A., Rajasekar, A., Ting, Y.-P., 2011. Bacteria attachment to surfaces – AFM force spectroscopy and physicochemical analyses. Journal of Colloid and Interface Science 364, 213–218.
Haas, C., Horn, R., 2018. Impact of small-scaled differences in micro-aggregation on physico-chemical parameters of macroscopic biopore walls. Frontiers in Environmental Science 6. https://doi.org/10.3389/fenvs.2018.00090.
Haydu-Houdeshell, C.-A., Graham, R.C., Hendrix, P.F., Peterson, A.C., 2018. Soil aggregate stability under chaparral species in southern California. Geoderma 310, 201–208.
Helliwell, J.R., Sturrock, C.J., Miller, A.J., Whalley, W.R., Mooney, S.J., 2019. The role of plant species and soil condition in the structural development of the rhizosphere. Plant, Cell and Environment 42, 1974–1986.
Herrmann, M., Geesink, P., Yan, L., Lehmann, R., Totsche, K.U., Küsel, K., 2020. Complex food webs coincide with high genetic potential for chemolithoautotrophy in fractured bedrock groundwater. Water Research 170. https://doi.org/10.1016/j.watres.2019.115306.
Hinsinger, P., Plassard, C., Tang, C., Jaillard, B., 2003. Origins of root-mediated pH changes in the rhizosphere and their responses to environmental constraints: a review. Plant and Soil 248, 43–59.
Hinsinger, P., Bengough, A.G., Vetterlein, D., Young, I.M., 2009. Rhizosphere: biophysics, biogeochemistry and ecological relevance. Plant and Soil 321, 117–152.
Hong, Z., Chen, W., Rong, X., Cai, P., Dai, K., Huang, Q., 2013. The effect of extracellular polymeric substances on the adhesion of bacteria to clay minerals and goethite. Chemical Geology 360–361, 118–125.
Hooker, T.D., Stark, J.M., 2012. Carbon flow from plant detritus and soil organic matter to microbes—linking carbon and nitrogen cycling in semiarid soils. Soil Science Society of America Journal 76, 903–914.
Horn, R., Dexter, A.R., 1989. Dynamics of soil Aggregation in an irrigated desert loess. Soil and Tillage Research 13, 253–266.
Horn, R., Taubner, H., Wuttke, M., Baumgartl, T., 1994. Soil physical properties related to soil structure. Soil and Tillage Research 30, 187–216.
Hotze, E.M., Phenrat, T., Lowey, G.V., 2010. Nanoparticle aggregation: challenges to understanding transport and reactivity in the environment. Journal of Environmental Quality 39, 1909–1924.
Hu, F., Xu, C., Li, H., Li, S., Yu, Z., Li, Y., He, X., 2015. Particles interaction forces and their effects on soil aggregates breakdown. Soil and Tillage Research 147, 1–9.
Huang, P.-M., Wang, M.-K., Chiu, C.-Y., 2005. Soil mineral–organic matter–microbe interactions: impacts on biogeochemical processes and biodiversity in soils. Pedobiologia 49, 609–635.
Huang, Q., Wu, H., Cai, P., Fein, J.B., Chen, W., 2015. Atomic force microscopy measurements of bacterial adhesion and biofilm formation onto clay-sized particles. Scientific Reports 5. https://doi.org/10.1038/srep16857.
Huber, S.A., Balz, A., Abert, M., Pronk, W., 2010. Characterization of aquatic humic and non-humic matter with size-exclusion chromatography - organic carbon detection - organic nitrogen detection (LC-OCD-OND). Water Research 45, 879–885.
Hwang, G., Ahn, I.-S., Mhin, B.J., Kim, J.-Y., 2012. Adhesion of nano-sized particles to the surface of bacteria: mechanistic study with the extended DLVO theory. Colloids and Surfaces B: Biointerfaces 97, 138–144.
Ivanov, P., Manucharova, N., Nikolaeva, S., Safonov, A., Krupskaya, V., Chernov, M., Eusterhues, K., Totsche, K.U., 2020. Glucose-stimulation of natural microbial activity changes composition, structure and engineering properties of sandy and loamy soils. Engineering Geology 265. https://doi.org/10.1016/j.enggeo.2019.105381.
Jacobs, L.M., Sulman, B.N., Brzosteck, E.R., Feighery, J.J., 2018. Interactions among decaying leaf litter, root litter and soil organic matter vary with mycorrhizal type. Journal of Ecology 106, 502–513.
Jarvis, N.J., 2007. A review of non-equilibrium water flow and solute transport in soil macropores: principles, controlling factors and consequences for water quality. European Journal of Soil Science 58, 523–546.
Jastrow, J.D., Miller, R.M., 1998. Soil aggregate stabilization and carbon sequestation: feedbacks trough organomineral associations. In: Lal, R., Kimble, J.M., Follett, R.F., Stewart, B.A. (Eds.), Soil Processes and the Carbon Cycle. CRC Press, Boca Raton, Boston, New York, Washington, London, pp. 245–266.
Jégou, D., Schrader, S., Diestel, H., Cluzeau, D., 2001. Morphological, physical and biochemical characteristics of burrow walls formed by earthworms. Applied Soil Ecology 17, 165–174.
Jilling, A., Keiluweit, M., Contosta, A.R., Frey, S., Schimel, J., Schnecker, J., Smith, R.G., Tiemann, L., Grandy, A.S., 2018. Minerals in the rhizosphere: overlooked mediators of soil nitrogen availability to plants and microbes. Biogeochemistry 139, 103–122.
Jones, G.J., Lawton, J.H., Shachak, M., 1994. Organisms as ecosystem engineers. In: Knopf, F.L. (Ed.), Ecosystem Management. Springer, New York, pp. 373–386.
Jouquet, P., Bottinelli, N., Podwojewski, P., Hallaire, V., Duc, T.T., 2008. Chemical and physical properties of earthworm casts as compared to bulk soil under a range of different land-use systems in Vietnam. Geoderma 146, 231–238.
Kandeler, E., Gebala, A., Boeddinghaus, R.S., Müller, K., Rennert, T., Soares, M., Rousk, J., Marhan, S., 2019. The mineralosphere – succession and physiology of bacteria and fungi colonising pristine minerals in grassland soils under different land-use intensities. Soil Biology and Biochemistry 136. https://doi.org/10.1016/j.soilbio.2019.107534.
Kautz, T., Köpke, U., 2010. In situ endoscopy: new insights to root growth in biopores. Plant Biosystems 144, 440–442.
Kautz, T., 2014. Research on subsoil biopores and their functions in organically managed soils: a review. Renewable Agriculture and Food Systems 30, 318–327.
Kaplan, D.I., Bertsch, P.M., Adriano, D.C., Miller, W.P., 1993. Soil-borne mobile colloids as influenced by water flow and organic carbon. Environmental Science and Technology 27, 1193–1200.
Keiluweit, M., Bougoure, J.J., Nico, P.S., Pett-Ridge, J., Weber, P.K., Kleber, M., 2015. Mineral protection of soil carbon counteracted by root exudates. Nature Climate Change 5. https://doi.org/10.1038/NCLIMATE2580.
Kjøller, A., Struwe, S., 1982. Microfungi in ecosystems: fungal occurrence and activity in litter and soil. OIKOS 39, 391–422.
Kleber, M., Sollins, P., Sutton, R., 2007. A conceptual model of organo-mineral interactions in soils: self-assembly of organic molecular fragments into zonal structures on mineral surfaces. Biogeochemistry 85, 9–24.
Kleber, M., Johnson, M.G., 2010. Advances in understanding the molecular structure of soil organic matter: implications for interactions in the environment. In: Sparks, D.L. (Ed.), Advances in Agronomy. Academic Press, Burlington, pp. 77–142.
Kleber, M., Eusterhues, K., Keiluweit, M., Mikutta, C., Mikutta, R., Nico, P.S., 2015. Mineral–organic associations: formation, properties, and relevance in soil environments. Advances in Agronomy 130, 1–140.
Kleiner, M., Dong, X., Hinzke, T., Wippler, J., Thorson, E., Mayer, B., Strous, M., 2018. Metaproteomics method to determine carbon sources and assimilation pathways of species in microbial communities. Proceedings of the National Academy of Sciences 115. https://doi.org/10.1073/pnas.1722325115.
Koebernick, N., Weller, U., Huber, K., Schlüter, S., Vogel, H.-J., Jahn, R., Vereecken, H., Vetterlein, D., 2014. In situ visualization and quantification of three-dimensional root system Architecture and growth using X-ray computed tomography. Vadose Zone Journal 13. https://doi.org/10.2136/vzj2014.03.0024.
Kögel-Knabner, I., Guggenberger, G., Kleber, M., Kandeler, E., Kalbitz, K., Scheu, S., Eusterhues, K., Leinweber, P., 2008. Organo-mineral associations in temperate soil: integrating biology, mineralogy and organic matter chemistry. Journal of Soil Science and Plant Nutrition 171, 61–82.
Kölbl, A., Kögel-Knabner, I., 2004. Content and composition of free and occluded particulate organic matter in a differently textured arable Cambisol as revealed by solid-state 13C NMR spectroscopy. Journal of Plant Nutrition and Soil Science 167, 45–53.
Kosmulski, M., 2020. The pH dependent surface charging and points of zero charge. VIII. Update. Advances in Colloid and Interface Science 275. https://doi.org/10.1016/j.cis.2019.102064.
Kosmulski, M., Dahlsten, P., 2006. High ionic strength electrokinetics of clay minerals. Colloids and Surfaces A 291, 212–218.
Kosmulski, M., 2011. The pH-dependent surface charging and point of zero charge V. Update. Journal of Colloid and Interface Science 353, 1–15.
Kosmulski, M., 2016. Isoelectric points and points of zero charge of metal (hydr)oxides: 50 years after Parks' review. Advances in Colloid and Interface Science 238, 1–61.
Kramer, S., Dibbern, D., Moll, J., Huenninghaus, M., Koller, R., Krueger, D., Marhan, S., Urich, T., Wubet, T., Bonkowski, M., Buscot, F., Lueders, T., Kandeler, E., 2016. Resource partitioning between bacteria, fungi, and protists in the detritusphere of an agricultural soil. Frontiers in Microbiology 7. https://doi.org/10.3389/fmicb.2016.01524.
Krause, L., Rodinov, A., Schweizer, S.A., Siebers, N., Lehndorff, E., Klumpp, E., Amelung, W., 2018. Microaggregate stability and storage of organic carbon is affected by clay content in arable Luvisols. Soil and Tillage Research 182, 123–129.
Krause, L., Biesgen, D., Treder, A., Schweizer, S.A., Klumpp, E., Knief, C., Siebers, N., 2019. Initial microaggregate formation: association of microorganisms to montmorillonite-goethite aggregates under wetting and drying cycles. Geoderma 351, 250–260.

Kubiak-Ossowska, K., Jachimska, B., Mulheran, P.A., 2016. How negatively charged proteins adsorb to negatively charged surfaces: a molecular dynamics study of BSA adsorption on silica. Journal of Physical Chemistry B 120, 10463–10468.
Kubiak-Ossowska, K., Tokarczyk, K., Jachimska, B., Mulheran, P.A., 2017. Bovine serum albumin adsorption at a silica surface explored by simulation and experiment. Journal of Physical Chemistry B 121, 3975–3986.
Kwon, K.D., Vadillo-Rodriguez, V., Logan, B.E., Kubicki, 2006. Interactions of biopolymers with silica surfaces: force measurements and electronic structure calculation studies. Geochimica et Cosmochimica Acta 70, 3803–3819.
Laganapan, A., Cerbelaud, M., Ferrando, R., Tran, C.T., Crespin, B., Videcoq, A., 2018. Computer simulations of heteroaggregation with large size asymmetric colloids. Journal of Colloid and Interface Science 514, 694–703.
Landeweert, R., Hoffland, E., Finlay, R.D., Kuyper, T.W., Breemen, N., 2001. Linking plants to rocks: ectomycorrhizal fungi mobilize nutrients from minerals. Trends in Ecology & Evolution 16, 248–254.
Lavelle, P., 1988. Earthworm activities and the soil system. Biology and Fertility of Soils 6, 237–251.
Lavelle, P., Decaens, T., Aubert, M., Barot, S., Blouin, M., Bureau, F., Margerie, P., Mora, P., Rossi, J.-P., 2006. Soil invertebrates and ecosystem services. European Journal of Soil Biology 42, S3–S15.
Lavelle, P., Spain, A., Blouin, M., Brown, G., Decaens, T., Grimaldi, M., Jiménez, J.J., McKey, D., Mathieu, J., Velasquez, E., Zangerle, A., 2016. Ecosystem engineers in a self-organized soil: a review of concepts and future research questions. Soil Science 181, 91–109.
Lavelle, P., Spain, A., Fonte, S., Bedano, J.C., Blanchart, E., Galindo, V., Grimaldi, M., Jimenez, J.J., Velasquez, E., Zangerlé, A., 2020. Soil aggregation, ecosystem engineers and the C cycle. Acta Oecologica 105. https://doi.org/10.1016/j.actao.2020.103561.
Lazar, C.S., Lehmann, R., Stoll, W., Rosenberger, J., Totsche, K.U., Küsel, K., 2019. The endolithic bacterial diversity of shallow bedrock ecosystems. The Science of the Total Environment 679, 35–44.
Lazzari, S., Nicoud, L., Jaquet, B., Lattuada, M., Morbidelli, M., 2016. Fractal-like structures in colloid science. Advances in Colloid and Interface Science 235, 1–13.
Le Mer, G., Barthod, J., Dignac, M.-F., Berré, P., Baudin, F., Rumpel, C., 2020. Inferring earthworms' impact on the stability of organo-mineral associations by Rock-Eval pyrolysis and 13C NMR spectroscopy. Organic Geochemistry 144. https://doi.org/10.1016/j.orggeochem.2020.104016.
Lee, K.E., 1985. Earthworms, Their Ecology and Relationships with Soils and Land Use. Acadamic Press Inc., London.
Lee, K.E., Foster, R.C., 1991. Soil fauna and structure. Australian Journal of Soil Research 29, 745–775.
Lehmann, A., Zheng, W., Rillig, M., 2017. Soil biota contributions to soil aggregation. Nature Ecology and Evolution 1, 1828–1835.
Lehmann, K., Lehmann, R., Totsche, K.U., 2021. Event-driven dynamics of the total mobile inventory in undisturbed soil account for significant fluxes of particulate organic carbon. The Science of the Total Environment 756. https://doi.org/10.1016/j.scitotenv.2020.143774.
Lehndorff, E., Rodionov, A., Plümer, L., Rottmann, P., Spiering, B., Dultz, S., Amelung, W., 2021. Spatial organization of soil microaggregates. Goderma 386. https://doi.org/10.1016/j.geoderma.2020.114915.
Lemtiri, A., Colinet, G., Alabi, T., Zirbes, L., 2014. Impacts of earthworms on soil components and dynamics. A review. Biotechnology, Agronomy, Society and Environment 18, 121–133.
Leue, M., Ellerbrock, R.H., Gerke, H.H., 2010. DRIFT mapping of organic matter composition at intact soil aggregate surfaces. Vadose Zone Journal 9, 317–324.
Leue, M., Gerke, H.H., Godow, S.C., 2015. Droplet infiltration and organic matter composition of intact crack and biopore surfaces from clay-illuvial horizons. Journal of Soil Science and Plant Nutrition 178, 250–260.
Liang, C., Amelung, W., Lehmann, J., Kästner, M., 2019. Quantitative assessment of microbial necromass contribution. Global Change Biology 25. https://doi.org/10.1111/gcb.14781.
Liang, C., Kästner, M., Joergensen, R.G., 2020. Microbial necromass on the rise: the growing focus on its role in soil organic matter development. Soil Biology and Biochemistry 150. https://doi.org/10.1016/j.soilbio.2020.108000.
Liang, L., Wang, L., Nguyen, A.V., Xie, G., 2017. Heterocoagulation of alumina and quartz studied by zeta potential distribution and particle size distribution measurements. Powder Technology 309, 1–12.
Lin, D., Ma, W., Jin, Z., Wang, Y., Huang, Q., Cai, P., 2016. Interactions of EPS with soil minerals: a combination study by ITC and CLSM. Colloids and Surfaces B 138, 10–16.
Liu, X., Eusterhues, K., Thieme, J., Ciobota, V., Höschen, C., Mueller, C.W., Küsel, K., Kögel-Knabner, I., Rösch, P., Popp, J., Totsche, K.U., 2013. STXM and NanoSIMS investigations on EPS fractions before and after adsorption to goethite. Environmental Science and Technology 47, 3158–3166.
Lipiec, J., Brzezinska, M., Turski, M., Szarlip, P., Frac, M., 2015. Wettability and biogeochemical properties of the drilosphere and casts of endogeic earthworms in pear orchard. Soil and Tillage Research 145, 55–61.
Lower, S.K., Tadanier, J., Hochella, M.F., 2000. Measuring interfacial and adhesion forces between bacteria and mineral surfaces with biological force microscopy. Geochimica et Cosmochimica Acta 64, 3133–3139.
Lützow, M., Kögel-Knabner, I., Ekschmitt, K., Matzner, E., Guggenberger, G., Marschner, B., Flessa, H., 2006. Stabilization of organic matter in temperate soils: mechanisms and their relevance under different soil conditions – a review. European Journal of Soil Science 57, 426–445.
Machmuller, M.B., Kramer, M.G., Cyle, T.K., Hill, N., Hancock, D., Thompson, A., 2015. Emerging land use practices rapidly increase soil organic matter. Nature Communications. https://doi.org/10.1038/ncomms7995.
Mahapatra, S., Banerjee, D., 2013. Fungal exopolysaccharide: production, composition and applications. Microbiology Insights 6, 1–16.
Marschner, P., Marhan, S., Kandeler, E., 2012. Microscale distribution and function of soil microorganisms in the interface between rhizosphere and detritusphere. Soil Biology and Biochemistry 49, 174–183.
McCarthy, J.F., McKay, L.D., 2004. Colloid transport in the subsurface: past, present, and future challenges. Vadose Zone Journal 3, 326–337.
McMaster, T.J., 2012. Atomic Force Microscopy of the fungi–mineral interface: applications in mineral dissolution, weathering and biogeochemistry. Current Opinion in Biotechnology 23, 563–569.
Menon, M., Mawodza, T., Rabbani, A., Blaud, A., Lair, G.J., Babaei, M., Kercheva, M., Rousseva, S., Banwart, S., 2020. Pore system characteristics of soil aggregates and their relevance to aggregate stability. Geoderma 366. https://doi.org/10.1016/j.geoderma.2020.114259.
Metzger, U., Lankes, U., Fischpera, K., Frimmel, F.H., 2009. The concentration of polysaccharides and proteins in EPS of Pseudomonas putida and Aureobasidum pullulans as revealed by 13C CPMAS NMR spectroscopy. Applied Microbiology and Biotechnology 85, 197–206.
Mikutta, R., Zang, U., Chorover, J., Haumaier, L., Kalbitz, K., 2011. Stabilization of extracellular polymeric substances (Bacillus subtilis) by adsorption to and coprecipitation with Al forms. Geochimica et Cosmochimica Acta 75, 3138–3154.
Mikutta, R., Baumgärtner, A., Schippers, A., Haumaier, L., Guggenberger, G., 2012. Extracellular polymeric substances from Bacillus subtilis associated with minerals modify the extent and rate of heavy metal sorption. Environmental Science and Technology 46, 3866–3873.
Miltner, A., Bombach, P., Schmidt-Brücken, B., Kästner, M., 2012. SOM genesis: microbial biomass as a significant source. Biogeochemistry 111, 41–55.
Morales, V.L., Parlange, J.-Y., Steenhuis, T.S., 2010. Are preferential flow paths perpetuated by microbial activity in the soil matrix? A review. Journal of Hydrology 393, 29–36.
More, T.T., Yadav, J.S.S., Yan, S., Tyagi, R.D., Surampalli, R.Y., 2014. Extracellular polymeric substances of bacteria and their potential environmental applications. Australasian Journal of Environmental Management 144, 1–25.
Morel, J.L., Andreux, F., Habib, L., Guckert, A., 1987. Comparison of the adsorption of maize root mucilage and polygalacturonic acid on montmorillonite homoionic to divalent lead and cadmium. Biology and Fertility of Soils 5, 13–17.
Morel, J.M., Habib, L., Plantureux, S., Guckert, A., 1991. Influence of maize root mucilage on soil aggregate stability. Plant and Soil 136, 111–119.
Mueller, C.W., Carminati, A., Kaiser, C., Subke, J.-A., Gutjahr, C., 2019. Editorial: rhizosphere functioning and structural development as complex interplay between plants, microorganisms and soil minerals. Frontiers in Environmental Science 7. https://doi.org/10.3389/fenvs.2019.00130.
Münch, J.M., Totsche, K.U., Kaiser, K., 2002. Physicochemical factors controlling dissolved organic carbon release in forest subsois - a column study. European Journal of Soil Science 53, 311–320.
Myrold, D.D., Zeglin, L.H., Jansson, J.K., 2013. The potential of metagenomic approaches for understanding soil microbial processes. Soil Science Society of America Journal 78, 3–10.
Narr, A., Nawaz, A., Wick, L.Y., Harms, H., Chatzinotas, A., 2017. Soil viral communities vary temporally and along a land use transect as revealed by virus-like particle counting and a modified community fingerprinting approach (fRAPD). Frontiers in Microbiology 8. https://doi.org/10.3389/fmicb.2017.01975.
Narvekar, S.P., Ritschel, T., Totsche, K.U., 2017. Colloidal stability and mobility of extracellular polymeric substance amended hematite nanoparticles. Vadose Zone Journal 168, 1–10.
Nichols, K.A., Halvorson, J.J., 2013. Roles of biology, chemistry, and physics in soil macroaggregate formation and stabilization. The Open Agriculture Journal 7, 107–117.
Nwadialo, B.E., Mbagwu, J.S.C., 1991. An analysis of soil components active in microaggregate stability. Soil Technology 4, 343–350.
Oades, J.M., 1984. Soil organic matter and structural stability: mechanisms and implications for management. Plant and Soil 76, 319–337.
Oades, J.M., Waters, A.G., 1991. Aggregate hierarchy in soils. Australian Journal of Soil Research 29, 815–828.
Oburger, E., Jones, D.L., 2018. Sampling root exudates – mission impossible? Rhizosphere 6, 116–133.
Olsen, A., Franks, G., Biggs, S., Jameson, G.J., 2005. Bi-modal hetero-aggregation rate response to particle dosage. The Journal of Chemical Physics 123. https://doi.org/10.1063/1.2117027.
Omoike, A., Chorover, J., 2004. Spectroscopic study of extracellular polymeric substances from *Bacillus subtilis*: aqueous chemistry and adsorption effects. Biomacromolecules 5, 1219–1230.
Omoike, A., Chorover, J., 2006. Adsorption to goethite of extracellular polymeric substances from *Bacillus subtilis*. Geochimica et Cosmochimica Acta 70, 827-338.
Op De Beek, M., Persson, P., Tunlid, A., 2021. Fungal extracellular polymeric substance matrices – highly specialized microenvironments that allow fungi to control soil organic matter decomposition reactions. Soil Biology and Biochemistry 159. https://doi.org/10.1016/j.soilbio.2021.108304.
Pan, X., Song, W., Zhang, D., 2010. Earthworms (*Eisenia foetida, Savigny*) mucus as complexing ligand for imidacloprid. Biology and Fertility of Soils 46, 845–850.
Parks, G.A., 1965. The isoelectric points of solid oxides, solid hydroxides, and aqueous hydroxo complex systems. Chemical Reviews 65 (2), 177–198. https://doi.org/10.1021/cr60234a002.
Pen, Y., Zhang, Z.J., Morales-García, A.L., Mears, D.S., Tarmey, D.S., Edyvean, R.G., Banwart, S.A., Geoghegan, M., 2015. Effect of extracellular polymeric substances on

the mechanical properties of Rhodococcus. Biochimica et Biophysica Acta 1848, 518–526.
Peth, S., Chenu, C., Leblond, N., Mordhorst, A., Garnier, P., Nunan, N., Pot, V., Ogurreck, M., Beckmann, F., 2014. Localization of soil organic matter in soil aggregates using synchrotron-based X-ray microtomography. Soil Biology and Biochemistry 78, 189–194.
Philippe, A., Schaumann, G.E., 2014. Interactions of dissolved organic matter with natural and engineered inorganic colloids: a review. Environmental Science and Technology 48, 8946–8962.
Portell, X., Pot, V., Garnier, P., Otten, W., Baveye, P.C., 2018. Microscale heterogeneity of the spatial distribution of organic matter can promote bacterial biodiversity in soils: insights from computer simulations. Frontiers in Microbiology 9. https://doi.org/10.3389/fmicb.2018.01583.
Praetorius, A., Labille, J., Scheringer, M., Thill, A., Hungerbühler, K., Bottero, J.-Y., 2014. Heteroaggregation of titanium dioxide nanoparticles with model natural colloids under environmentally relevant conditions. Environmental Science and Technology 48, 10690–10698.
Pronk, G.J., Heister, K., Ding, G.-C., Smalla, K., Kögel-Knabner, I., 2012. Development of biogeochemical interfaces in an artificial soil incubation experiment; aggregation and formation of organo-mineral associations. Geoderma 189-190, 585–594. https://doi.org/10.1016/j.geoderma.2012.05.020.
Puget, P., Angers, D.A., Chenu, C., 1999. Nature of carbohydrates associated with water-stable aggregates of two cultivated soils. Soil Biology and Biochemistry 31, 55–63.
Pullman, M.M., Six, J., Uyl, A., Marinissen, J.C.Y., Jongmans, A.G., 2005. Earthworms and management affect organic matter incorporation and microaggregate formation in agricultural soils. Applied Soil Ecology 29, 1–15.
Ranville, F.J., Chittleborough, D.J., Beckett, R., 2005. Particle-size and element distributions of soil colloids: implications for colloid transport. Soil Science Society of America Journal 69, 1173–1184.
Rasse, D.P., Rumpel, C., Dignac, M.-F., 2005. Is soil carbon mostly root carbon? Mechanisms for a specific stabilization. Plant and Soil 269, 341–356.
Ray, N., Rupp, A., Prechtel, A., 2017. Discrete-continuum multiscale model for transport, biomass development and solid restructuring in porous media. Advances in Water Resources 107, 393–404.
Redmile-Gordon, M.A., Brookes, P.C., Evershed, R.P., Goulding, K.W.T., Hirsch, P.R., 2014. Measuring the soil-microbial interface: extraction of extracellular polymeric substances (EPS) from soil biofilms. Soil Biology and Biochemistry 72, 163–171.
Redmile-Gordon, M.A., Gregory, A.S., White, R.P., 2020. Soil organic carbon, extracellular polymeric substances (EPS), and soil structural stability as affected by previous and current land-use. Geoderma 363. https://doi.org/10.1016/j.geoderma.2019.114143.
Remusat, L., Hatton, P.-J., Nico, P.S., Zeller, B., Kleber, M., Derrin, D., 2012. NanoSIMS study of organic matter associated with soil aggregates: advantages, limitations, and combination with STXM. Environmental Science and Technology 46, 3943–3949.
Rillig, M.C., Mummey, D.L., 2006. Mycorrhizas and soil structure. New Phytologist 171, 41–53.
Ritschel, T., Totsche, K.U., 2019. Modeling the formation of soil microaggregates. Computational Geosciences 127, 36–43.
Rodionov, A., Lehndorff, E., Stremtan, C.C., Brand, W.A., Königshoven, H.-P., 2019. Spatial microanalysis of natural 13C/12C abundance in environmental samples using laser ablation-isotope ratio mass spectrometry. Analytical Chemistry 91, 6225–6232.
Rogasik, H., Schrader, S., Onasch, I., Kiesel, J., Gerke, H.H., 2014. Micro-scale dry bulk density variation around earthworm (*Lumbricus terrestris L.*) burrows based on X-ray computed tomography. Geoderma 213, 471–477.
Rupp, A., Guhra, T., Meier, A., Prechtel, A., Ritschel, T., Ray, N., 2019. Totsche, K.U. Application of a cellular automaton method to model the structure formation in soils under saturated conditions: a mechanistic approach. Frontiers in Environmental Science 7. https://doi.org/10.3389/fenvs.2019.00170.
Ruess, L., Chamberlain, P.M., 2010. The fat that matters: soil food web analysis using fatty acids and their carbon stable isotope signature. Soil Biology and Biochemistry 42, 1898–1910.
Ryan, J.N., Elimelech, M., 1996. Colloid mobilization and transport in groundwater. Colloids and Surfaces A 107, 1–56.
Saha, I., Datta, S., Biswas, D., 2020. Exploring the role of bacterial extracellular polymeric substances for sustainable development in agriculture. Current Microbiology 77, 3224–3239.
Sampedro, L., Jeannotte, R., Whalen, J.K., 2006. Trophic transfer of fatty acids from gut microbiota to the earthworm Lumbricus terrestris L. Soil Biology and Biochemistry 38, 2188–2198.
Sasse, J., Kosina, S.M., de Raad, M., Jordan, S.J., Whiting, K., Zhalnina, K., Northern, T. R., 2020. Root morphology and exudate availability are shaped by particle size and chemistry in *Brachypodium distachyon*. Plant Direct 4, 1–14.
Scheu, S., 1987. Microbial activity and nutrient dynamics in earthworm casts (Lumbricidae). Biology and Fertility of Soils 5, 230–234.
Scheu, S., 1991. Mucus excretion and carbon turnover of endogeic earthworms. Biology and Fertility of Soils 12, 217–220.
Schrader, S., 1994. Influence of earthworms on the pH conditions of their environment by cutaneous mucus secretion. Zoologischer Anzeiger 233, 211–219.
Schrader, S., Rogasik, H., Onasch, I., Jégou, D., 2007. Assessment of soil structural differentiation around earthworm burrows by means of X-ray computed tomography and scanning electron microscopy. Geoderma 137, 375–387.
Schwab, F.S., Nowak, M.E., Trumbore, S.E., Xu, X., Gleixner, G., Muhr, J., Küsel, K., Totsche, K.U., 2019. Isolation of individual saturated fatty acid methyl esters derived from groundwater phospholipids by preparative high-pressure liquid chromatography for compound-specific radiocarbon analyses. Water Resources Research 55, 2521–2531.
Seiphoori, A., Ma, X., Arratia, P.E., Jerolmack, D.J., 2020. Formation of stable aggregates by fluid-assembled solid bridges. Proceedings of the National Academy of Sciences 117, 3375–3381.
Semmel, H., Horn, R., Hell, U., Dexter, A.R., Schulze, E.D., 1991. The dynamics of soil aggregate formation and the effect on soil physical properties. Soil Technology 3, 113–129.
Sheng, A., Liu, F., Xie, N., Liu, J., 2016. Impact of proteins on aggregation kinetics and adsorption ability of hematite nanoparticles in aqueous dispersions. Environmental Science and Technology 50, 2228–2235.
Sher, Y., Baker, N., Herman, D., Fossum, C., Hale, L., Zhang, X., Nuccio, E., Saha, M., Zhou, J., Pett-Ridge, J., Firestone, M., 2020. Microbial extracellular polysaccharide production and aggregate stability controlled by switchgrass (*Panicum virgatum*) root biomass and soil water potential. Soil Biology and Biochemistry 143. https://doi.org/10.1016/j.soilbio.2020.107742.
Shipitalo, M.J., Protz, R., 1988. Factors influencing the dispersibility of clay in worm casts. Soil Science Society of America Journal 52, 764–769.
Shipitalo, M.J., Protz, R., 1989. Chemistry and micromorphology of aggregation in earthworm casts. Geoderma 45, 357–374.
Six, J., Bossuyt, H., Degryze, S., Denef, K., 2004. A history of research on the link between (micro)aggregates, soil biota, and soil organic matter dynamics. Soil and Tillage Research 79, 7–31.
Spohn, M., Giani, L., 2010. Water-stable aggregates, glomalin-related soil protein, and carbohydrates in a chronosequence of sandy hydromorphic soils. Soil Biology & Biochemistry 42, 1505–1511. https://doi.org/10.1016/j.soilbio.2010.05.015.
Starke, R., Schäpe, S.S., Jehmlich, N., Bergen, M., 2021. Protein stable isotope probing with H_2 ^{18}O differentiated cold stress response at permissive temperatures from general growth at optimal conditions in *Escherichia coli* K12. Rapid Communications in Mass Spectrometry 35. https://doi.org/10.1002/rcm.8941.
Stewart, T.J., Traber, J., Kroll, A., Behra, R., Sigg, L., 2013. Characterization of extracellular polymeric substances (EPS) from periphyton using liquid chromatography-organic carbon detection–organic nitrogen detection (LC-OCD-OND). Environmental Science and Pollution Research 20, 3214–3223. https://doi.org/10.1007/s11356-012-1228-y.
Stromberger, M.E., Keith, A.M., Schmidt, O., 2012. Distinct microbial and faunal communities and translocated carbon in *Lumbricus terrestris* drilospheres. Soil Biology and Biochemistry 46, 155–162.
Szewczuk-Karpisz, K., Wiśniewska, M., 2019. Adsorption layer structure at soil mineral/biopolymer/supporting electrolyte interface – the impact on solid aggregation. Journal of Molecular Liquids 284, 117–123.
Szilagyi, I., Trefalt, G., Tiraferri, A., Maroni, P., Borkovec, M., 2014. Polyelectrolyte adsorption, interparticle forces, and colloidal aggregation. Soft Matter 10, 2479–2502.
Tan, X., Zhang, G., Yin, H., Reed, A.H., Furukawa, Y., 2012. Characterization of particle size and settling velocity of cohesive sediments affected by a neutral exopolymer. International Journal of Sediment Research 27, 473–485.
Tan, X., Hu, L., Reed, A.H., Furukawa, Y., Zhang, G., 2014. Flocculation and particle size analysis of expansive clay sediments affected by biological, chemical, and hydrodynamic factors. Ocean Dynamics 64, 143–157.
Tang, J., Mo, Y., Zhang, J., Zhang, R., 2011. Influence of biological aggregating agents associated with microbial population on soil aggregate stability. Applied Soil Ecology 47, 153–159.
Taubert, M., Stähly, J., Kolb, S., Küsel, K., 2019. Divergent microbial communities in groundwater and overlying soils exhibit functional redundancy for plant-polysaccharide degradation. PLoS One 14 (3). https://doi.org/10.1371/journal.pone.0212937.
Theng, B.K.G., 1982. Clay-polymer interactions: summary and perspectives. Clays and Clay Minerals 30, 1–10.
Theng, B.K.G., Yuan, G., 2008. Nanoparticles in the soil environment. Elements 4, 395–399.
Tiraferri, A., Hernandez, L.A.S., Bianco, C., Tosco, T., Sethi, R., 2017. Colloidal behavior of goethite nanoparticles modified with humic acid and implications for aquifer reclamation. Journal of Nanoparticle Research 19. https://doi.org/10.1007/s11051-017-3814-x.
Tisdall, J.M., Oades, J.M., 1982. Organic matter and water-stable aggregates in soils. European Journal of Soil Science 33, 141–163.
Tiunov, A.V., Scheu, S., 1999. Microbial respiration, biomass, biovolume, and nutrient status in burrow walls of *Lumbricus terrestris* L. (Lumbricidae). Soil Biology and Biochemistry 31, 2039–2048.
Tombácz, E., Csanaky, C., Illés, E., 2001. Polydisperse fractal aggregate formation in clay mineral and iron oxide suspensions, pH and ionic strength dependence. Colloid and Polymer Science 279, 484–492. https://doi.org/10.1007/s003960100480.
Tombácz, E., Libor, Z., Illés, E., Majzik, A., Klumpp, E., 2004. The role of reactive surface sites and complexation by humic acids in the interaction of clay mineral and iron oxide particles. Organic Geochemistry 35, 257–267.
Tombácz, E., Szekeres, M., 2006. Surface charge heterogeneity of kaolinite in aqueous suspension in comparison with montmorillonite. Applied Clay Science 34, 105–124.
Tong, M., Zhu, P., Jing, X., Kim, H., 2011. Influence of natural organic matter on the deposition kinetics of extracellular polymeric substances (EPS) on silica. Colloids and Surfaces B 87, 151–158.
Totsche, K.U., Amelung, W., Gerzabek, M.H., Guggenberger, G., Klumpp, E., Knief, C., Lehndorff, E., Mikutta, R., Peth, S., Prechtel, A., Ray, N., Kögel-Knabner, I., 2018. Microaggregates in soils. Journal of Soil Science and Plant Nutrition 181, 104–136.
Tourney, J., Ngwenya, B.T., 2014. The role of bacterial extracellular polymeric substances in geomicrobiology. Chemical Geology 386, 115–132.

Trefalt, G., Ruiz-Cabello, F.J.M., Borkovec, M., 2014. Interaction forces, heteroaggregation, and deposition involving charged colloidal particles. Journal of Physical Chemistry B 118, 6346–6355.

Vetterlein, D., Carminati, A., Kögel-Knabner, I., Bienert, G.P., Smalla, K., Oburger, E., Schnepf, A., Banitz, T., Tarkka, M.T., Schlüter, S., 2020. Rhizosphere spatiotemporal organization–A key to rhizosphere functions. Frontiers in Agronomy 2. https://doi.org/10.3389/fagro.2020.00008.

Violante, A., de Cristofaro, A., Rao, M.A., Gianfreda, L., 1995. Physicochemical properties of protein-smectite and protein-Al(OH)x-Smectite complexes. Clay Minerals 30, 325–336.

Violante, A., Caporale, A.G., 2015. Biogeochemical processes at soil-root interface. Journal of Soil Science and Plant Nutrition 15, 422–448.

Vlamakis, H., Chai, Y., Beauregard, P., Losick, R., Kolter, R., 2013. Sticking together: building a biofilm the *Bacillus subtilis* way. Nature Reviews Microbiology 11, 157–168.

Vogel, L.E., Makowski, D., Garnier, P., Vieublé-Gonod, L., Coquet, Y., Raynaud, X., Nunan, N., Chenu, C., Falconer, R., Pot, V., 2015. Modeling the effect of soil meso- and macropores topology on the biodegradation of a soluble carbon substrate. Advances in Water Resources 83, 123–136.

Wagai, R., Kajiura, M., Asano, M., 2020. Iron and aluminum association with microbially processed organic matter via meso-density aggregate formation across soils: organometallic glue hypothesis. SOIL 6, 597–627.

Walker, T.S., Bais, H.P., Grotewold, E., Vivanco, J.M., 2003. Root exudation and rhizosphere biology. Plant Physiology 132, 44–51.

Wang, L.-L., Wang, L.-F., Ren, X.-M., Ye, X.-D., Li, W.-W., Yuan, S.-J., Sun, M., Sheng, G.-P., Yu, H.-Q., Wang, X.-K., 2012. pH dependence of structure and surface properties of microbial EPS. Environmental Science and Technology 46, 737–744.

Wang, X., Sale, P., Hayden, H., Tang, C., Clark, G., Armstrong, R., 2020. Plant roots and deep-banded nutrient-rich amendments influence aggregation and dispersion in a dispersive clay subsoil. Soil Biology and Biochemistry 141. https://doi.org/10.1016/j.soilbio.2019.107664.

Watteau, F., Villemin, G., 2018. Soil microstructures examined through transmission electron microscopy reveal soil-microorganisms interactions. Frontiers in Environmental Science 6. https://doi.org/10.3389/fenvs.2018.00106.

Weiler, M., Naef, F., 2003. An experimental tracer study of the role of macropores in infiltration in grassland soils. Hydrological Processes 17, 477–493.

Williamson, K.E., Fuhrmann, J.J., Wommack, K.E., Radosevich, M., 2017. Viruses in soil ecosystems: an unknown quantity within an unexplored territory. Annual Review of Virology 4, 201–219.

Wilpizeski, R.L., Aufrecht, J.A., Retterer, S.T., Sullivan, M.B., Graham, D.E., Pierce, E.M., Zablocki, O.D., Palumbo, A.V., Elias, D.A., 2019. Soil aggregate microbial communities: towards understanding microbiome interactions at biologically relevant scales. Applied and Environmental Microbiology 85. https://doi.org/10.1128/AEM.00324-19.

Wingender, J., Neu, T.R., Flemming, H.-C., 1999. Microbial Extracellular Polymeric Substances: Characterization, Structure and Function. Springer-Verlag, Berlin, Heidelberg.

Xenophontos, C., Taubert, M., Harpole, W.S., Küsel, K., 2021. Phylogenetic and metabolic diversity have contrasting effects on the ecological functioning of bacterial communities. Microbial Ecology 97. https://doi.org/10.1093/femsec/fiab017.

Yang, F., Tang, C., Antonietti, M., 2021. Natural and artificial humic substances to manage minerals, ions, water, and soil microorganisms. Chemical Society Reviews 50, 6221–6239.

Yu, W.H., Li, N., Tong, D.S., Zhou, C.H., Lin, C.X., Xu, C.Y., 2013. Adsorption of proteins and nucleic acids on clay minerals and their interactions: a review. Applied Clay Science 80–81, 443–453.

Yudina, A., Kuzyakov, Y., 2019. Saving the face of soil aggregates. Global Change Biology 25, 3574–3577.

Zech, S., Ritschel, T., Ray, N., Totsche, K.U., Prechtel, A., 2021. How water connectivity and substrate supply shape the turnover of organic matter - insights from simulations at the scale of microaggregates. Geoderma in revision.

Zhao, W., Yang, S., Huang, Q., Cai, P., 2015. Bacterial cell surface properties: role of loosely bound extracellular polymeric substances (LB-EPS). Colloids and Surfaces B128, 600–607.

Zhang, L., Lehmann, K., Totsche, K.U., Lueders, T., 2018. Selective successional transport of bacterial populations from rooted agricultural topsoil to deeper layers upon extreme precipitation events. Soil Biology and Biochemistry 124, 168–178. https://doi.org/10.1016/j.soilbio.2018.06.012.

Zhang, H., Schrader, S., 1993. Earthworm effects on selected physical and chemical properties of soil aggregates. Biology and Fertility of Soils 15, 229–234.

Zhang, D., Chen, Y., Ma, Y., Guo, L., Sun, J., Tong, J., 2016. Earthworm epidermal mucus: Rheological behavior reveals drag-reducing characteristics in soil. Soil and Tillage Research 158, 57–66.

Zhang, X., Zhou, X., Xi, H., Sun, J., Liang, X., Wei, J., Xiao, X., Liu, Z., Li, S., Liang, Z., 2019. Interpretation of adhesion behaviors between bacteria and modified basalt fiber by surface thermodynamics and extended DLVO theory. Colloids and Surfaces B: Biointerfaces 177, 454–461.

Zhu, P., Long, G., Ni, J., Tong, M., 2009. Deposition kinetics of extracellular polymeric substances (EPS) on silica in monovalent and divalent salts. Environmental Science and Technology 43, 5699–5704.

2.2. Publication 2 (P_{II}): Earthworm mucus contributes to the formation of organo-mineral associations in soil

Citation: Guhra, T., Stolze, K., Schweizer, S. and Totsche, K.U. 2020. Earthworm mucus contributes to the formation of organo-mineral associations in soil. *Soil Biology and Biochemistry*, 145, 107785.

DOI: 10.1016/j.soilbio.2020.107785

Rights and licensing: All (co-)authors agree that this article is permitted to be used in the dissertation presented here. This article is published under the terms of the creative commons CC BY-NC-ND license. Authors of this article retain the right to include it in a thesis or dissertation, provided it is not published commercially. The journal as the original source of the article is referenced above.

Authors: Tom Guhra[1*], Katharina Stolze[2*], Steffen Schweizer[3] and Kai Uwe Totsche[4]

[*]Authors contributed equally to the manuscript

P_{III}				
involved in:	**Author**			
	1	**2**	**3**	**4**
conception of research design	X	X		X
planning of research activities	X	X		
data acquisition	X	X	X	
data analyses and interpretation	X	X		X
manuscript writing	X	X		X
suggested publication equivalence value	**1.0**	1.0		

Soil Biology and Biochemistry 145 (2020) 107785

Contents lists available at ScienceDirect

Soil Biology and Biochemistry

journal homepage: http://www.elsevier.com/locate/soilbio

Earthworm mucus contributes to the formation of organo-mineral associations in soil

Tom Guhra [a,1], Katharina Stolze [a,1], Steffen Schweizer [b], Kai Uwe Totsche [a,*]

[a] Department of Hydrogeology, Institute of Geosciences, Friedrich Schiller University Jena, Germany
[b] Department of Ecology and Ecosystem Management, School of Life Sciences Weihenstephan, Technical University of Munich, Germany

ARTICLE INFO

Keywords:
Mucus adsorption
Alteration of surface properties
Completely mixed batch reactor experiments
Lumbricidae
FTIR-ATR
^{13}C-NMR

ABSTRACT

Earthworms are considered as "ecosystem engineers" impacting soil properties as well as nutrient and element cycles. As they move through soil, earthworms secrete cutaneous mucus which is metabolized by soil microorganisms and a source of plant-available nutrients. Earthworm-processed soil contains carbon enriched, earthworm-specific soil aggregates (e.g. casts and middens) in comparison to earthworm unaffected soil. The reason could be that organic polymeric substances in earthworm mucus bind to soil minerals. The objective of this study was to investigate the small-scale interactions between earthworm mucus and secondary soil minerals, e.g. goethite and illite, leading to the formation of organo-mineral associations. We characterized the chemical composition of earthworm mucus by FTIR and ^{13}C-NMR spectroscopy and compared spectra of mucus to microbial extracellular polymeric substances (EPS), an abundant and well-known type of organic matter that binds with soil minerals. Mucus from anecic (*Lumbricus terrestris* L.) and endogeic (*Aporrectodea caliginosa* Sav.) earthworm species was dominated by proteins and carbohydrates. Between 21 and 36% of the total organic carbon in the mucus containing treatments adsorbed to illite and goethite, and most of the binding with goethite was associated with phosphorus containing mucus compounds. The surface charge of newly-formed organo-mineral associations was determined by measuring the isoelectric point (IEP). The IEP of mucus-goethite associations was 6.8, which was lower than the bare goethite IEP of 8.4. The zeta potential of mucus-illite associations was greater than bare illite. We conclude that the specific adsorption of earthworm mucus constituents to soil minerals leads to the formation of mucus-mineral associations. These associations contribute to retention of organic substances from earthworm mucus in soil (micro-)aggregates and explain the altered physicochemical properties of earthworm-formed aggregates in comparison to the earthworm unaffected "bulk" soil material.

1. Introduction

The soil fauna significantly contributes to the formation of stable soil aggregates, impacting the turnover rates, porosity and coherence of soil as well as water infiltration (Lee and Foster, 1991). Among the ecological groups, anecic and endogeic earthworms affect the soil structure as "ecosystem engineers" (Jones et al., 1994) by forming casts, middens or burrow wall linings, and serve as important biogenic agents of aggregation (Six et al., 2004). Specifically, the drilosphere (Bouché, 1975), defined as the zone of 2 mm to 1 cm thickness around the burrow walls (Andriuzzi et al., 2013; Lipiec et al., 2015) is directly affected by earthworm activity due to the deposition of earthworm-formed soil aggregates (Six et al., 2004).

When earthworms burrow through soil, they deposit nutrient-rich mucus, and excrete casts, a mixture of digested soil material, organic matter (OM) and microorganisms, on the burrow walls (Lee, 1985; Brown et al., 2000). The released cutaneous mucus is a lubricant to facilitate earthworm movement through the soil and protects the earthworm from being encased by soil particles (Lee, 1985). The cutaneous and intestinal mucus consist of water, carbohydrates, proteins, lipids and polysaccharides (Pan et al., 2010; Zhang et al., 2016). In consequence, earthworm activity and mucus excretion shape soil and soil aggregate properties and processes (physically, chemically and biologically) e.g. nutrient element storage (P and C accumulation), habitat formation (beneficial conditions for microbial growth and root penetration), infiltration and transport (burrows as preferential flow

* Corresponding author.
E-mail address: kai.totsche@uni-jena.de (K.U. Totsche).
[1] Authors contributed equally to the manuscript.

https://doi.org/10.1016/j.soilbio.2020.107785
Received 10 July 2019; Received in revised form 24 February 2020; Accepted 14 March 2020
Available online 17 March 2020
0038-0717/© 2020 The Authors. Published by Elsevier Ltd. This is an open access article under the CC BY-NC-ND license (http://creativecommons.org/licenses/by-nc-nd/4.0/).

pathways) (Lee and Foster, 1991; Brown et al., 2000; Six et al., 2004). The OM inside the drilosphere and earthworm-formed aggregates is attributed to cutaneous and intestinal mucus, together with earthworm processed plant debris (Shipitalo and Protz, 1989; Six et al., 2004; Brown et al., 2000) and builds the fundament for microbial hotspots in earthworm formed structures (Edwards and Fletcher, 1988; Aira et al., 2009). The incorporation of OM is reported to cause changes of the physicochemical properties of the earthworm-formed aggregates in comparison to the surrounding soil material (Brown et al., 2000; Six et al., 2004).

Earthworms may release 0.2–0.5% of total animal C per day via mucus excretion or cast formation (for *Octolasion lacteum,* sees Scheu, 1991). Given this impressive numbers, we intend to expand the studies on biogenic OM by identifying the role of earthworm mucus with respect to microbial EPS, a well-studied fraction of OM in soil. The objective of our study is to elucidate the formation of mucus-mineral associations due to adsorption, as so far neglected but essential process during the formation of earthworm-formed soil structures. We aim to contribute to a better understanding of the role of earthworm derived mucus-mineral associations in the element cycling and as reactive component in soil. Several authors demonstrated the complex interactions of microbially produced OM, especially extracellular polymeric substances (EPS) of bacterial origin, with typical constituents of the soil mineral phase like iron oxides, clay minerals and quartz (Omoike and Chorover, 2004; Cao et al., 2011; Fang et al., 2012). We hypothesize, regarding their specific composition, a comparability between microbial EPS and earthworm mucus in terms of their interaction with the soil mineral phase and the formation of organo-mineral associations. Additionally, we presume a similar composition and mucus-mineral interactions of mucus obtained from different ecological functional groups due to maintaining their function as drag reducing lubricant found for mucus of different earthworm species (Zhang et al., 2016).

Specifically, we investigated the interactions between earthworm cutaneous mucus extracts of *Lumbricus terrestris* L. (anecic) and *Aporrectodea caliginosa* Sav. (endogeic) with goethite and illite, i.e., typical secondary minerals of temperate soils. We compared our results with results obtained for EPS from *Bacillus subtilis* of the late (Narvekar et al., 2017; Guhra et al., 2019) and early stationary phase (Liu et al., 2013). The mucus composition was characterised by spectrometric methods. We conducted completely mixed batch adsorption experiments of earthworm cutaneous mucus with the named secondary soil minerals. The composition of mucus before and after reaction with minerals was investigated by attenuated total reflection-Fourier-transform infrared spectroscopy (ATR-FTIR). The potential adsorption of mucus compounds to the bare mineral phase of illite or goethite was measured as change of the total organic carbon (TOC) concentration (TOC analyzes) as well as the change of element concentration like phosphorus and potassium by inductively coupled plasma optical emission spectrometry (ICP-OES). The formation of organo-mineral associations was indirectly evidenced by the determination of an altered surface-charge of organo-mineral associations in comparison to the bare minerals by zeta potential measurements.

2. Material and methods

2.1. Earthworm mucus extraction

Earthworms were sampled on pasture and cropland sites located within the Hainich Critical Zone Exploratory (Küsel et al., 2016) in north-west Thuringia, Germany. Soil groups varied between Rendzic Leptosols, Cambisols and Luvisols originating from limestone and Loess cover (Kohlhepp et al., 2017). Endogeic earthworms were sampled by hand-sorting of the top 15 cm of the soil. Anecic earthworms were sampled after Chan and Munro (2001), applying a mustard solution which was poured into the remaining soil pit. Earthworm species were determined according to Sims and Gerard (1999). Cutaneous earthworm mucus of endogeic (EN) *A. caliginosa* and anecic (AN) *L. terrestris* was extracted according to Eisenhauer et al. (2009). To prevent contamination of mucus with cast material, earthworm species were kept separately on wetted pulp (XXL2 Blue; Roth, Karlsruhe, Germany) to void their guts for approximately 60 h. Coprophagy was prevented by regular exchange of the pulp. Before the extraction, the earthworms were washed with pure water (Milli-Q, Integral 5, Elix Technology Inside, Merck Millipore, Darmstadt, Germany) and placed inside beakers. According to Eisenhauer et al. (2009), we utilized 30 individuals of *L. terrestris* for mucus extraction and used the equivalent biomass of *A. caliginosa* to maintain comparability between the two treatments. Hence, the extraction took place with the resulting ratio of 1.3 g (earthworm biomass):1 ml (pure water). Pure water was added to the beakers and earthworms were stirred with a glass rod for 15 min (every third minute for 1 min). This leads to tactile skin irritation, which provoked the mucus release. The extract was centrifuged twofold at 20,000 g at 20 °C for 30 min (Sorvall RC 6 Plus Zentrifuge, Thermo Scientific, Waltham, USA) to remove remaining mineral particles. The obtained mucus was frozen (temp.: −20 °C) overnight and subsequently freeze-dried (Alpha 1–4 LSC, CHRIST, Osterode am Harz, Germany).

2.2. Characterization of mucus

The freeze-dried stocks of anecic and endogeic mucus were analyzed by Fourier-transform infrared spectroscopy (FTIR) (Nicolet iS10 spectrometer, Thermo Fisher Scientific, Dreieich, Germany) with the attenuated-total-reflection (ATR) option (Smart iTX, Thermo Fisher Scientific, Dreieich, Germany), CHNS elemental analyser (Euro EA, Eurovecector, Pavia, Italy) and solid-state ^{13}C-nuclear magnetic resonance (NMR) (DSX 200, Bruker, Billerica, USA) spectroscopy. Measurements of the chemical shifts were done at a resonance frequency of 50.3 MHz with cross-polarization magic angle spinning technique. We measured at a spinning speed of 6.8 kHz and pulse delays of 0.4 s. A line broadening of 50 Hz was applied to the spectra. We compared the NMR spectra with data obtained at similar acquisition conditions as for EPS from *Bacillus subtilis* 168 (DSM 402), in the late (Narvekar et al., 2017; Guhra et al., 2019) and early stationary phase (Liu et al., 2013). We computed the integrals of chemical shift regions of aliphatic C (0–45 ppm), αC of amino acids (45–65 ppm), O-alkyl-C (65–90 ppm), anomeric C (90–110 ppm), aromatic as well as olefinic C (160-110 ppm) and amides as well as carboxyl C (160–200 ppm) according to Metzger et al. (2009).

2.3. Mineral characterization

Goethite was synthesized according to Schwertmann and Cornell (2000). In short, a solution of 1M Fe(III)nitrate-nonahydrate (EMSURE 99–101% for analysis, Merck, Germany) was prepared and rapidly mixed with 5M NaOH (from sodium hydroxide pellets $\geq$ 98%, CARL ROTH, Karlsruhe, Germany). Subsequently, ultrapure water was added in a ratio of 100:16. The precipitated ferrihydrite was aged to goethite by storage in a drying chamber (Binder, Tuttlingen, Germany) at 60 °C. Needle-shaped goethite was obtained from this procedure with an average length of 0.9 ± 0.3 µm as measured by scanning electron microscopy (see Guhra et al. (2019) for details). To remove nitrate, the material was rinsed repeatedly with deionized water and freeze-dried (Alpha 1–4 LSC, CHRIST, Osterode am Harz, Germany) for storage.

Chunks of Illite (INTER-ILI, Mérnöki Iroda, Általános és Kereskedelmi Kft, Hungary) were crushed and dry sieved to a maximum size of <36 µm. Mid particle size of illite was 9.0 ± 0.6 µm as measured by laser diffraction (Analysette 22 compact, Fritsch, Nagytarcsa, Hungary). Minerals were characterized by X-ray diffraction (XRD, D8 Advance, Bruker, Karlsruhe, Germany) and specific surface area by N_2-BET (Autosorb-1, Quantachrome, Odelzhausen, Germany) (see Guhra et al. (2019) for details).

2.4. Mucus-mineral adsorption experiment

The adsorption of mucus to the mineral phases of illite and goethite was investigated with a series of completely mixed batch reactor experiments using aqueous suspensions of mucus and illite or goethite. To produce the mucus-extract suspension, freeze-dried mucus was successively dispersed in 1 mM NaCl solution (99.7%, VWR, Leuven, Belgium) in a cooled ultrasonic bath (VWR ultrasonic cleaner; ratio: 1 mg mucus/7.5 ml $NaCl_{aq}$). Illite and goethite was suspended in 1 mM sodium chloride solutions with/without mucus. The solid (mg):liquid (ml)-ratio of the batch-experiments containing illite and goethite was adjusted to 2.5:1.

As reference, blank samples consisting of only endogeic mucus and anecic mucus as well as bare mineral phases mixed with sodium chloride solution were processed in the same way as the mineral-mucus containing variants. Batches of mucus-free and mucus-containing variants were shaken (115 rounds/minute) for 24 h. Afterwards, the solid and liquid phase were separated by centrifugation at 20,000 g at 20 °C for 30 min (Fang et al., 2012; Cao et al., 2011) to estimate the adsorbed amount of carbon and phosphate originating from endogeic and anecic mucus. For this, the supernatant was analyzed with a TOC- and DOC-Analyzer (Multi N/C 2100s, Analytic Jena GmbH, Jena, Germany) and inductively coupled plasma optical emission spectrometry (ICP-OES) (Varian, Varian 725 ES, Darmstadt, Germany). An aliquot of the supernatant was freeze-dried and analyzed by ATR-FTIR. As reference for any amendments in the band intensities within the mucus spectra of mineral treated and untreated samples, the band assigned to the carboxylic groups at 1402 cm^{-1} (Abdulla et al., 2010) was used for normalization. The P:C ratio was calculated by the P concentrations (in mmol/l) divided by the TOC-values (in mmol/l). The standard deviations given as a measure for uncertainty result from the measurements of three replicates. The significance of treatment effects was tested by Student's two-tailed *t*-test with $p < 0.05$.

2.5. Surface charge and isoelectric point

The isoelectric point (IEP) of the pure and mucus-associated minerals as well as endogeic and anecic mucus references was calculated from zeta potential measurements (Nano ZS, Malvern Instruments, Malvern, UK) as function of the pH. We used freeze-dried and resuspended pellets of minerals and organo-mineral associations after the conduction of the batch experiments. These were washed for several times with pure water to remove loosely bound mucus to obtain potentially strong mucus-mineral associations. Suspensions of 100 mg/l pure minerals (goethite or illite) and the mucus-mineral associations were prepared in 10 mM sodium chloride solution. Subsequently, the pH was adjusted by the addition of HCl (from hydrochloric acid 37%, VWR AnalaR NORMAPUR, Paris, France) or NaOH (from sodium hydroxide pellets $\geq$ 98%, CARL ROTH, Karlsruhe, Germany) to the mucus references and the mineral or organo-mineral associations containing suspensions. To equilibrate the surface charges of bare minerals and the associations (Kosmulski, 2016), the suspensions were shaken (115 rounds/minute) for 24 h. After equilibration, pH (WTW pH 197 with PLUS WTW, pH-Elektrode Sen Tix 41, Weilheim, Germany) and zeta potential (Nano ZS, Malvern Instruments, Malvern, UK) were measured. The intersection of the stepwise linear interpolation of zeta potentials as a function of pH was used to calculate the IEP.

3. Results

3.1. Mucus characterization and comparison to microbial EPS

The freeze-dried stock endogeic and anecic earthworm mucus provided narrow C:N ratios of 5.1 ± 0.2 (endogeic mucus) and 3.67 ± 0.03 (anecic mucus) and were composed of a mixture of proteins, carbohydrates and polysaccharides as attributed to the chemical composition by ATR-FTIR analysis. In both mucus samples, typical bands of the stretching vibration of O–H bonds assigned to surface water (Socrates, 2001) were observed with high extinctions between approximately 3500 to 3100 cm^{-1} (Fig. 1). Bands at 2920 cm^{-1} and 2860 cm^{-1} are typical for C–H asymmetric and symmetric stretching vibrations of methylene groups (Socrates, 2001). The most prominent bands in both samples were at 1631 cm^{-1} (Amid I) and 1544 cm^{-1} (Amid II), which represent typical bands of proteins as the stretching vibration of C═O (Amid I) and the N–H deformation and C–N stretching in –CO–NH (Amid II) (Omoike and Chorover, 2004; Jiang et al., 2018). These bands were more distinct in anecic mucus. The band at 1449 cm^{-1} is attributed to symmetrical deformations of CH_2 and C–OH (Omoike and Chorover, 2004) and more apparent in anecic mucus as in endogeic mucus. The band at 1402 cm^{-1} represents COO-groups (symmetric stretching) in both samples (Abdulla et al., 2010). The band at 1347 cm^{-1} is assigned to O–H in-plane bending vibration of carbohydrates (Abdulla et al., 2010). Both bands were more pronounced in endogeic mucus. The band at 1300 cm^{-1} is attributed to the Amid III band (Socrates, 2001). The wavenumber of 1242 cm^{-1} was allocated to the asymmetric stretching vibration P═O of the phosphodiester backbone of nucleic acid or phosphorylated proteins (Omoike and Chorover, 2004). The band at 1078 cm^{-1} is attributed to phosphate symmetric stretching bands C–O–P as well as C–O–C ring vibration of polysaccharides and the band at 1028 cm^{-1} to an asymmetric stretching of C–O (Omoike and Chorover, 2004; Abdulla et al., 2010).

The results of the ATR-FTIR spectroscopy were supplemented by NMR measurements. According to Metzger et al. (2009), the two chemical shift regions between 110 and 65 ppm (anomeric C and O-alkyl C) are mainly assigned to carbohydrates. Similar proportions of anomeric C (110-90 ppm) values were found in anecic and endogeic mucus, whereas the proportion of O-alkyl C (90-65 ppm) was slightly higher in endogeic mucus (Table 1). In comparison to the carbohydrate related regions, higher proportions mainly referred to proteins, fatty acids and peptidoglycan (amides, carboxyl C, aliphatic C, aromatic C, olefinic C and αC of amino acids) were detected in mucus samples. Anecic and endogeic mucus had similar proportions of αC of amino acids, which can be predominantly related to the proteins, whereas the proportions of aromatic C and olefinic C were the highest in anecic mucus. Amides, carboxyl C and aliphatic C were similar for both mucus samples.

Additionally, we compared the NMR data of mucus samples with EPS samples from previous studies of the early (Liu et al., 2013) and late stationary phase (Fig. S1; Narvekar et al., 2017; Guhra et al., 2019). The microbial EPS of the early stationary phase exhibited relations of anomeric C and O-alkyl C in the same magnitude as anecic mucus, whereas the EPS of the late stationary phase showed approximately twofold higher values of the chemical shift regions of carbohydrates. Proportions of αC of amino acids were slightly higher in microbial EPS of both phases compared to the mucus samples (Table 1). One of the most distinct differences between mucus and EPS could be verified for aromatic C and olefinic C, where approximately only half of the proportion of the mucus was found in microbial EPS. The early stationary phase EPS showed highest values for the chemical shift regions of amides and carboxyl C, whereas the EPS of the late stage had the lowest amounts of carboxyl C and aliphatic C.

3.2. Completely mixed batch reactor experiments

3.2.1. Experimental conditions

The initial total and dissolved anecic and endogeic mucus-C concentrations in the mucus references were higher for anecic mucus than for endogeic mucus (Table 2). In comparison to TOC and DOC concentrations, P, Ca, S, Mg, Si, Mn, Fe and Al concentrations exhibited lower amounts (Table 2). The concentration of K was highest between the inorganic constituents in both samples.

The highest pH were detected in the anecic mucus containing

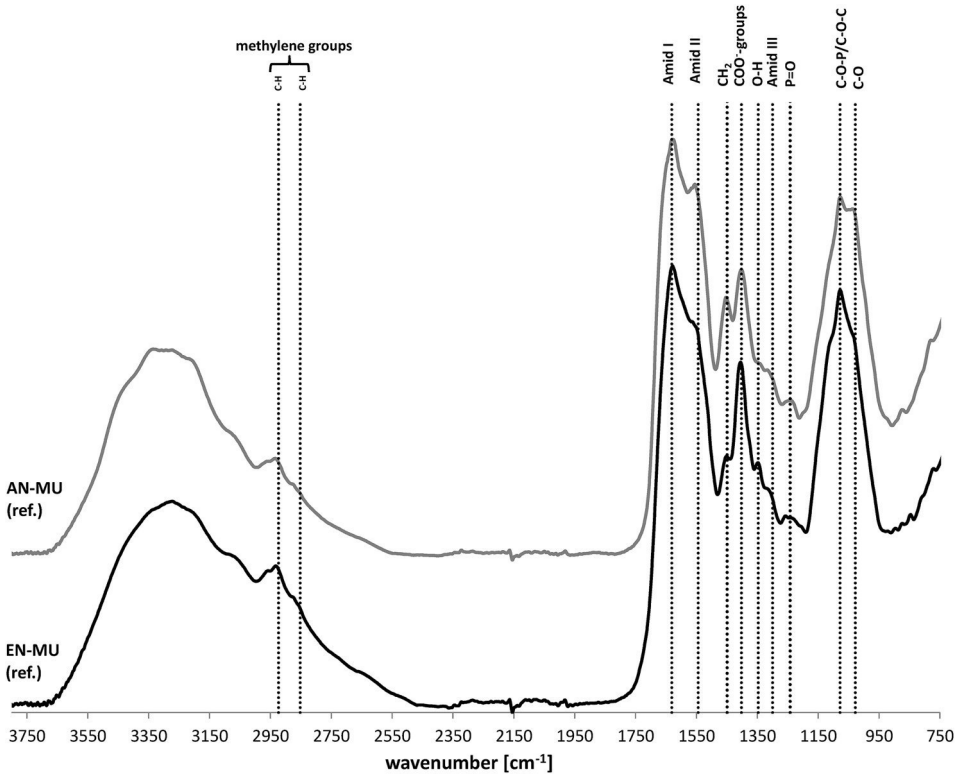

Fig. 1. Attenuated total reflection – Fourier-transform infrared spectroscopy (ATR-FTIR) spectra of the freeze-dried anecic *L. terrestris* (AN-MU) and endogeic *A. caliginosa* (EN-MU) mucus reference (ref.).

Table 1
Integral regions of solid-state^{13}C-nuclear magnetic resonance spectroscopy (NMR) of the freeze-dried mucus of anecic *L. terrestris* and endogeic *A. caliginosa* after extraction. For comparison, additional spectra of microbial EPS were added from previous studies: *Bacillus subtilis* 168 (DSM 402) (EPS), late (Narvekar et al., 2017; Guhra et al., 2019) and early (Liu et al., 2013) stationary phase.

Sample	percent [%]					
	chemical shift [ppm]					
	200–160	160–110	110–90	90–65	65–45	45–0
	amides, carboxyl C	aromatic, olefinic C	anomeric C	O-alkyl C	αC of amino acids	aliphatic C
anecic mucus	16.6	18.4	5.6	11.7	18.4	29.3
endogeic mucus	17.6	12.1	5.6	17.0	19.4	28.2
EPS (early growth)	21.7	7.5	3.4	10.9	23.8	32.8
EPS (late growth)	7.4	4.4	12.0	43.7	21.2	11.3

Table 2
Total organic carbon (TOC) and dissolved organic carbon (DOC) as well as inductively coupled plasma optical emission spectrometry (ICP-OES) measured element concentrations of K, P, Ca, S, Mg, Si, Mn, Fe and Al in the dispersed anecic *L. terrestris* and endogeic *A. caliginosa* mucus references. Uncertainty is given as standard deviation (n = 3).

Sample	[mg/l]										
	TOC	DOC	K	P	Ca	S	Mg	Si	Mn	Fe	Al
anecic mucus	23.12 ± 0.05	16.5 ± 1.0	5.65 ± 0.04	1.065 ± 0.005	0.973 ± 0.007	0.83 ± 0.01	0.342 ± 0.003	0.06 ± 0.01	0.0231 ± 0.0001	0.0211 ± 0.0006	LOD
endogeic mucus	15.37 ± 0.07	14.8 ± 0.3	4.77 ± 0.06	0.653 ± 0.004	0.54 ± 0.04	0.551 ± 0.009	0.233 ± 0.009	0.125 ± 0.001	0.0080 ± 0.0001	0.053 ± 0.008	0.011 ± 0.001

treatments followed by endogeic mucus containing treatments and the bare minerals without mucus (Table 3). Between the different treatments (anecic mucus, endogeic mucus and mucus-free), goethite-containing batches showed the highest pH in comparison to illite and the mucus references.

3.2.2. Mucus adsorption

In goethite-containing treatments, 35 ± 1% of anecic mucus TOC and 35.8 ± 0.4% of endogeic mucus TOC were adsorbed (Fig. 2). For illite, an adsorption of 32 ± 2% and 21 ± 4% was detected. Phosphorus (P) vanished almost entirely (P concentration below the limit of detection of 0.03 mg/l) in anecic and endogeic mucus containing batches. We explain this by a rather complete adsorption of P to goethite. For illite, 5

Table 3
Physicochemical parameters, pH and electrical conductivity of mucus-free and -containing batches treated with goethite and illite as well as mineral-free references (ref.) of mucus of anecic *L. terrestris* and endogeic *A. caliginosa* after conducting the batch reactor experiments. Uncertainty is given as standard deviation (n = 3).

Type	Sample	pH	Electric conductivity [µS/cm]
anecic mucus	ref.	6.76 ± 0.05	183.0 ± 0.1
	goethite	7.10 ± 0.04	183.3 ± 0.2
	illite	6.77 ± 0.02	183.7 ± 0.1
endogeic mucus	ref.	5.69 ± 0.02	192.4 ± 0.4
	goethite	6.71 ± 0.08	192.5 ± 0.4
	illite	5.84 ± 0.09	194.9 ± 0.6
bare minerals	goethite	6.3 ± 0.1	125.9 ± 0.2
	illite	5.90 ± 0.06	127.2 ± 0.3

± 1% and 7.5 ± 0.6% adsorption of P was observed. In comparison to P, only 24 ± 3% and 47 ± 2% of sulfur (S) were adsorbed to goethite. The adsorption to illite was below 5% for anecic and endogeic mucus.

The P:C ratio of the anecic mucus reference was slightly higher than that of endogeic mucus. If mucus was treated with illite, the P:C ratio was higher in comparison to the mucus reference solution. However, the calculation of the P:C ratios of goethite treated samples was not possible due to P concentrations below the limit of detection (LOD). Consequently, low P:C ratios can be assumed and were estimated by the utilization of the LOD of 0.03 mg/l P as minimum value (Fig. 2). The S:C ratios of the mucus reference and illite were similarly to the respective P:C ratios (Fig. 2). For the goethite treated system, higher values were observed for anecic mucus and reduced values for endogeic mucus in comparison to the mineral-free mucus reference.

3.2.3. ATR-FTIR spectra of freeze-dried supernatants

For the freeze-dried references and supernatants after the batch experiments, three main constituents were attributed to the bands between 1750 and 900 cm^{-1}: proteins (1700–1500 cm^{-1}), carbohydrates (1460–1200 cm^{-1}) and polysaccharides as well as nucleic acids (1300–900 cm^{-1}) (Fig. 3; Socrates, 2001; Jiao et al., 2010). In comparison to goethite treated samples, for illite only small changes were observed in the protein area of anecic and endogeic mucus, which does not allow for a clear distinction of Amid I and Amid II bands. In the wavenumbers related to polysaccharides and carbohydrates, only slight changes could be established. For anecic and endogeic mucus containing batches treated with goethite, clear intensity decreases were noticeable in the protein and polysaccharide region in comparison to the carboxyl groups within the carbohydrate area. The bands assigned to proteins decreased in their intensity near (anecic mucus) or below (endogeic mucus) the level of the carboxylic groups. This observation was more pronounced for polysaccharides which are notably below the reference level for both treatments. In comparison to the anecic mucus, endogeic mucus treatments containing illite or goethite showed clear intensity decreases in the Amid I band of the protein area in relation to the Amid II band.

Dominant protein related FTIR bands were also found for EPS of the early stationary phase. The bands allocated to the asymmetric stretching vibration P═O (1242 cm^{-1}), P–O symmetric stretching (1031 cm^{-1}) and asymmetric stretching of C–O (1028 cm^{-1}) (Abdulla et al., 2010; Cao et al., 2011) were slightly more pronounced in early stationary phase EPS than mucus. The EPS sample from the late stationary phase revealed dominantly polysaccharide assigned bands in relation to those attributed to proteins and carbohydrates (Fig. S2).

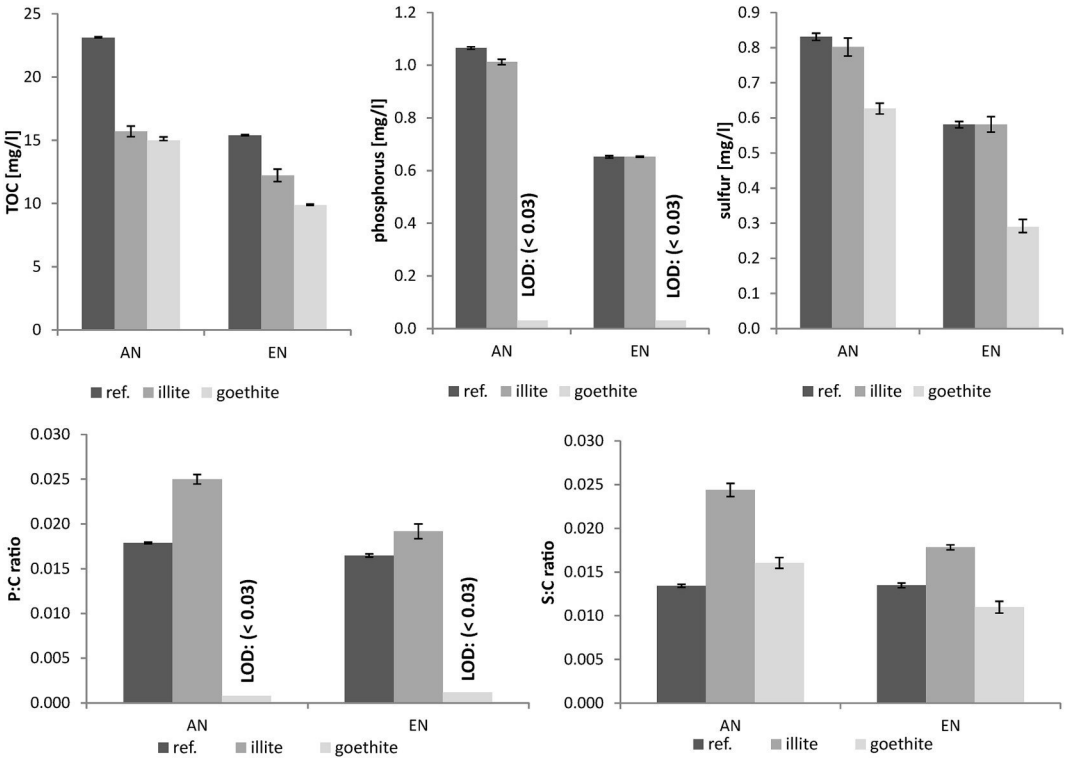

Fig. 2. Total organic carbon (TOC) and inductively coupled plasma optical emission spectrometry (ICP-OES)-measured P and S from the mineral phase separated supernatants after batch adsorption experiments of treatments containing anecic *L. terrestris* (AN-MU) and endogeic *A. caliginosa* (EN-MU) mucus. The reference (ref.) is assigned to the mineral-free solution which was processed in the same way then the other treatments. The P:C ratio and S:C ratio was calculated for mineral-free and -containing treatments of AN and EN-MU. For the calculation of the P:C ratio of the goethite-containing treatment the limit of detection (LOD) of the device was used for the estimation for P concentration.

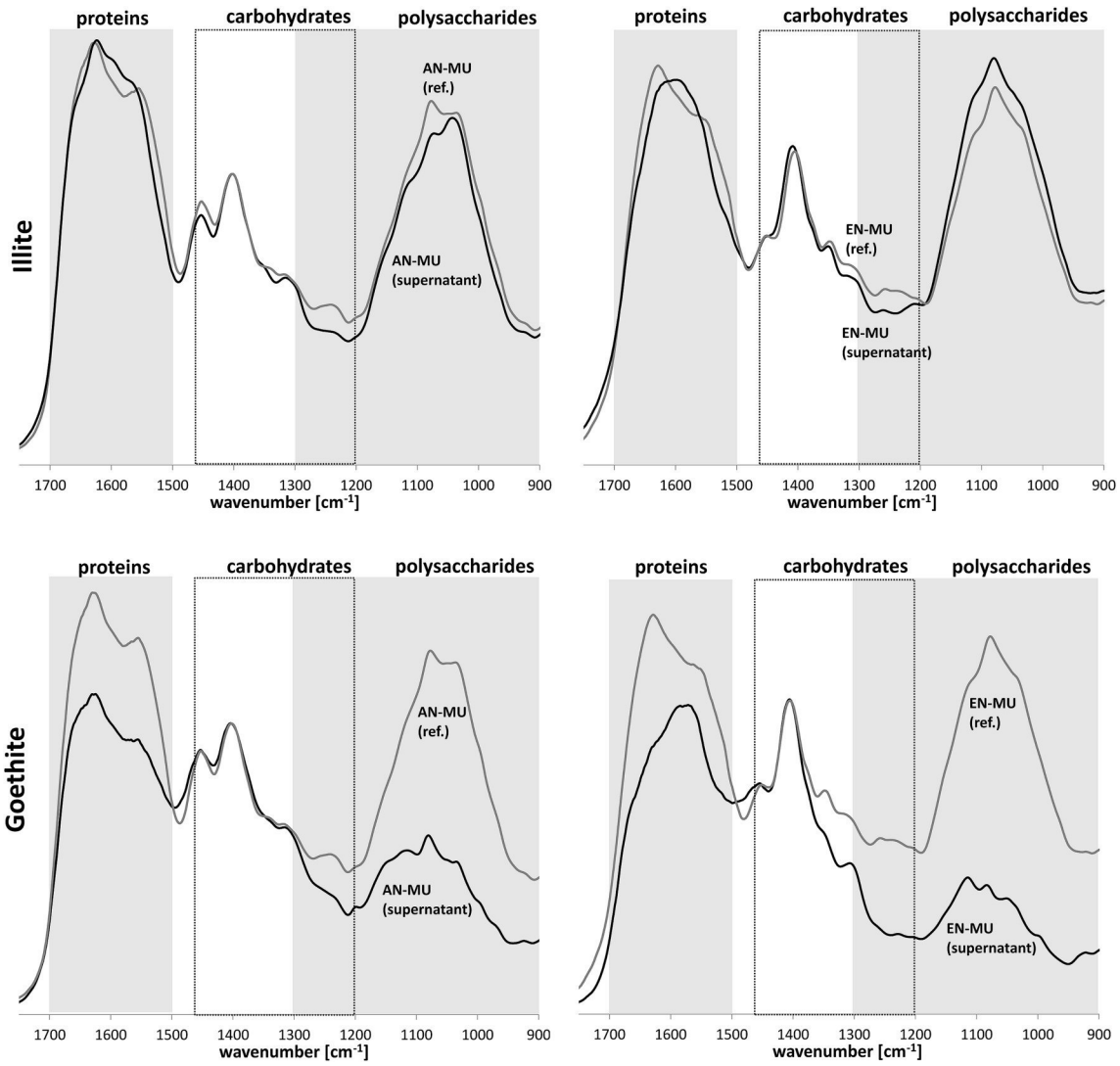

Fig. 3. Attenuated total reflection – Fourier-transform infrared spectroscopy (ATR-FTIR) spectra of the anecic *L. terrestris* (AN-MU: left) and endogeic *A. caliginosa* (EN-MU: right) mucus treated (black) with goethite (Gt: top) and illite (Il: bottom) as well as reference (ref.) without a mineral treatment (grey). For comparison of spectra, intensities were normalized to the carboxylic group (1402 cm^{-1}). Main composites were classified in proteins (1700–1500 cm^{-1}), carbohydrates (1460–1200 cm^{-1}) and polysaccharides as well as nucleic acids (1300–900 cm^{-1}) according to Jiao et al. (2010) and Socrates (2001).

3.3. Surface charge of organo-mineral associations

The surface charge of pure illite was net negative in comparison to the positively charged goethite at experimental pH (range between grey vertical dashed lines, Fig. 4). Zeta-potentials near pH of 2 were not measurable due to the limitations of the device. The mucus reference samples exhibited an IEP at 2.4 for anecic mucus and values below 2 for endogeic mucus. In comparison, bare goethite showed an ongoing decrease from 51 ± 2 mV (pH: 3.5) to −32 ± 2 mV (pH: 10.5) with an IEP at 8.4, the IEP of endogeic mucus-goethite associations and anecic mucus-goethite associations decreased in a parallel manner with approximately 10 mV lower zeta potentials for the same pH and reached the IEP at 6.8. The lowest zeta potential was observed for illite. The zeta potentials of anecic mucus-illite associations and endogeic mucus-illite associations were above the values of bare illite and below mineral untreated anecic mucus and endogeic mucus. All samples containing illite showed an IEP below 2.

4. Discussion

4.1. Mucus composition

We show by NMR spectroscopy, that cutaneous mucus samples extracted from *L. terrestris* and *A. caliginosa* were composed of chemical moieties assigned to proteins, peptidoglycans, fatty acids and carbohydrates. The dominance of proteinaceous molecules in the mucus (Cortez and Bouché, 1987) of both ecological groups was ascertained, too, by ATR-FTIR spectra which exhibited distinct amid bands typical for proteins (Socrates, 2001). The application of spectroscopic methods showed a coexistence of different structural groups (e.g. amides, aliphatic C and carboxyl groups) in cutaneous mucus of *L. terrestris* and *A. caliginosa* which corroborates the suggestions of a rather complex composition reported by Richards (1978) for mucus of lumbricids based on wet chemical methods.

Despite the high similarity between anecic and endogeic mucus, we observed higher carbohydrate contents in endogeic mucus as highlighted by the peaks of methyl groups of polysaccharides between 62 and 55 ppm (Mao et al., 2007), while more aromatic and olefinic C as potential hydrophobic parts of proteins and nucleic acids were found in

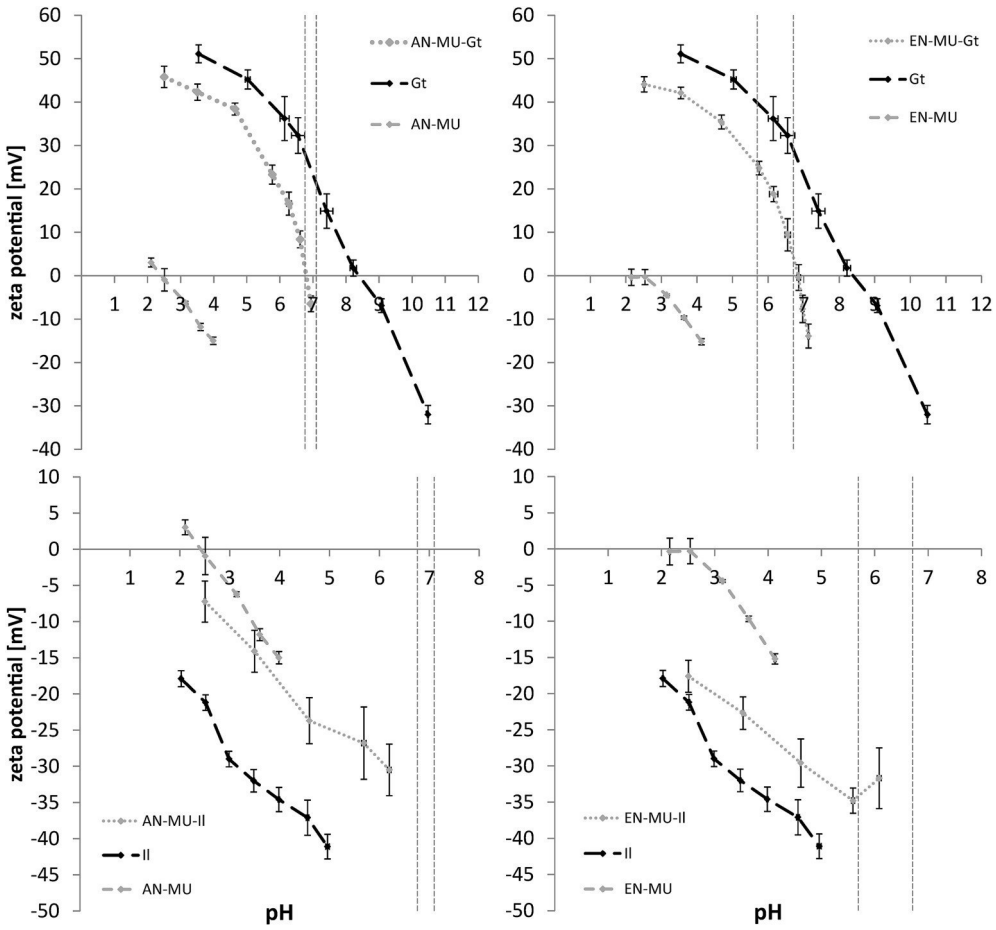

Fig. 4. Zeta potential measurements as function of pH for bare minerals (black dashed line), mucus (grey dashed line) and mucus-mineral association (grey pointed line) for anecic *L. terrestris* (AN-MU) mucus (left) and endogeic *A. caliginosa* (EN-MU) mucus (right) as well as for goethite (Gt) (top) and illite (Il) (bottom). Areas between vertical grey dashed lines indicate pH during the experiments.

anecic mucus. Hydrophobic mucus components are reported as beneficial for stabilization of permanent vertical burrows which are characterized by higher water repellency in comparison to the bulk soil (Ellerbrock et al., 2009; Leue et al., 2015). Compositional differences in cutaneous mucus could originate from the adaption to different digging and feeding behavior of ecological groups. This was proposed already by Zhang et al. (2016) who connected amino acid composition to different rheological properties of cutaneous mucus.

We found that the ATR-FTIR and NMR spectra of cutaneous earthworm mucus were similar to those of microbial EPS of the common soil microorganism *Bacillus subtilis* obtained from the early stationary phase (Liu et al., 2013) in comparison to those of the late stationary phase (Narvekar et al., 2017; Guhra et al., 2019). Compared to earthworm mucus, however, both EPS types showed fewer structural groups assigned to proteins and nucleic acids between 160 and 110 ppm as revealed by NMR. Additionally, as shown by ATR-FTIR, the amide bands of EPS were shifted in comparison to those of mucus, which suggests different composition and structures of proteins (Socrates, 2001). The high number of structural groups assigned to amino acids (65-45 ppm) which are similar in both EPS types can be attributed besides proteins to glycosaminoglycans, typically produced by bacteria (Metzger et al., 2009). Based on our findings we substantiate the hypothesis of compositional similarities between mucus and microbial EPS of the early stationary phase. This implies a similar fate in soil, similar functionalities for soil microorganisms and interactions with the soil mineral phase. Consequently, the findings of microbial EPS and their environmental relevance might also apply for mucus. Yet, we need to take into account that both the amount and the composition of microbial EPS strongly depends on various factors, e.g., microbial strain and growth phase, wetting/drying cycles, temperature, elemental composition of the environment and pH (More et al., 2014; Costa et al., 2018). In contrast, a much more uniform and stable composition is to be expected for the cutaneous earthworm mucus to preserve the function as lubricant (Lee, 1985). We thus suggest that earthworm mucus provides a compositionally less variable and - due to earthworm's active soil processing - a more readily available and widespread source of biotic OM in soil. This, in turn, may point to a more important role of earthworm mucus than microbial EPS in the formation of organo-mineral associations and even larger aggregated soil structures.

The investigation of freeze-dried anecic and endogeic mucus exhibited high contents of total N and C which lead in turn to low C:N ratios around 3.7 (anecic mucus) and 5.1 (endogeic mucus). These low C:N ratios of cutaneous mucus are in line with the results of Scheu (1991) and are reported as beneficial for microbial activity, increasing respiration and mineralization rates in the burrow system (Tiunov and Scheu, 1999; Brown et al., 2000; Don et al., 2008). Besides organic constituents, earthworm mucus contains a variety of electrolytes (Pan et al., 2010). Within the inorganic mucus constituents, K showed the highest concentrations. As outlined by Lemtiri et al. (2014), K can be released from clay minerals due to a pH decrease in the earthworm gut passage and thus serves as nutrients benefiting plant growth.

4.2. Mucus adsorption to secondary soil minerals

In relation to the FTIR bands attributed to proteins and polysaccharides, the band assigned to the carboxylic groups at 1402 cm^{-1}

(Abdulla et al., 2010) remained rather unchanged in the supernatants after adsorption. This coincides with the findings for EPS of Omoike and Chorover (2004): They did not find any evidence for the contribution of carboxyl groups to the adsorption of EPS to goethite. Furthermore, the decreased P:C-ratio of the goethite-treatment indicates a preferential adsorption of phosphorus-containing mucus constituents. We explain this by the specific adsorption via the formation of Fe–O–P bonds. These are likely formed due to the complexation between phosphoryl groups and Fe metal centers on the goethite surface as known for microbial EPS (Omoike and Chorover, 2006). Additionally, hydroxyl groups are released from the goethite surface during the formation of such complexes, which results in an increase of the pH in the solution (Omoike and Chorover, 2006). This is consistent with the increased pH in treatments containing goethite and mucus in comparison to the goethite-free or mucus-free treatments. Consequently, this affinity of phosphorus-containing mucus constituents to goethite points to the immobilization of P on the soil mineral phase (containing secondary iron oxides) in earthworm-formed aggregates and thus supports the suggestions of Scheu (1987) that P-immobilization in earthworm casts is mainly caused by abiotic processes.

In contrast, ATR-FTIR spectra of illite-containing samples showed only minor compositional change in response to the adsorption. Yet, we observed a clear increase of the P:C- and S:C-ratios for the illite treated anecic and endogeic mucus-samples compared to goethite treated samples and the untreated mucus reference. Hence, we conclude a reduced contribution of P- and S-containing mucus constituents in the adsorption to illite. A fractionation of phosphorus was also reported for microbial EPS, where a reduced adsorption of P to clay minerals in comparison to goethite occurred (Cao et al., 2011; Lin et al., 2016). The most conspicuous change of ATR-FTIR spectra of illite-containing mucus treatments in comparison to the mucus references was the absence of the separation of the bands corresponding to amid I and amid II of proteins (Socrates, 2001). Clay minerals provide variably charged silanol and aluminol groups on the edges and constantly negatively charged siloxane groups on the basal planes as adsorption sites (Hong et al., 2013; Yu et al., 2013). The basal planes contribute massively to the net charge of illite. Consequently, we observed negative charges for illite at ambient pH of the batch experiments where mucus was also negatively charged. Thus, we assign the adsorption between proteins and the basal planes of clay minerals to the impact of hydrophobic interactions. This may counterbalance the electrostatic repulsion between the equal charges (Yu et al., 2013). Additionally, a preferred adsorption of amino groups, as part of proteins, to variably charged clay mineral aluminol groups under the formation of hydrogen bonding and electrostatic interaction (Cao et al., 2011; Lin et al., 2016) could cause these changes in amid band distribution. Additionally, the high S:C ratio suggests that S-containing mucus constituents like the amino acids cysteine and methionine, which are common in the mucus of different earthworm species (Zhang et al., 2009, 2016), are unfavored in the adsorption processes to illite, in turn leading to the compositional fractionation of dispersed mucus.

Considering that earthworm-formed and physically stabilised organo-mineral associations inside casts and burrows may outlast their creating earthworms (Brown et al., 2000), the observed adsorption of molecules from mucus contributes to nutrient element storage and fertilisation due to earthworm activity (Lee and Foster, 1991). The selectivity of adsorption of cutaneous mucus of both earthworm species to goethite and in lesser extent to illite ascertains our proposition on similar mucus-mineral interactions of mucus obtained from different ecological functional groups. These mineral specific interactions are particularly relevant considering the mineral composition of the interacting soil material and potential release and translocation of unassociated mucus constituents inside earthworm burrows (Edwards et al., 1993; Simard et al., 2000).

4.3. The role of earthworm mucus for the formation of organo-minerals associations

Brown et al. (2000) outlined that earthworm-produced structures provide physicochemical and biologically changed properties in comparison to the initial soil materials. Schrader (1994) reported a buffering effect of cutaneous mucus on soil substrates to circumneutral pH, which we found for the anecic mucus extract (pH: ~6.8) in comparison to the endogeic mucus extract (pH: ~5.7). At this pH, the net charge of anecic and endogeic mucus (IEP: anecic mucus 2.4; endogeic mucus >2) was negative in comparison to goethite (IEP 8.4) which suggests additional adsorption via electrostatic attraction. The acidic IEP of mucus implies the contribution of carboxylic groups which are known to protonate at low pH in microbial EPS (Wang et al., 2012). Omoike and Chorover (2006) also showed an increased adsorption of microbial derived molecular mixtures if opposite charges are present. The amount of adsorbed OM to illite (IEP < 2) was like that of goethite, despite net negative charges of mucus and illite during the experimental conditions which force electrostatic repulsion. However, Illite-mucus associations are formed during electrostatically unfavourable conditions which points to mechanisms other than electrostatic interactions and specific adsorption which we expected for goethite. For instance, Kwon et al. (2006) demonstrated that hydrogen bonds provided by lipids are important for the adsorption to silanol groups of silica surfaces. Those lipids were also found in mucus as peak near to 30 ppm attributed to lipids as part of the NMR integral region for aliphatic C (Metzger et al., 2009). In addition, hydrophobic interactions with the constant negatively charged basal planes caused by long-chained aliphatic compounds such as lipids and high molecular weight OM like proteins (Yu et al., 2013; Kleber et al., 2015) could be an explanation for the, in comparison to endogeic mucus, higher adsorption of anecic mucus to illite due to its higher content of proteinaceous mucus constituents. This agrees with the findings on the preferred accumulation of proteins on clay mineral surfaces reported by Lin et al. (2016) for microbial EPS. The interaction between mucus and minerals is additionally affected by earthworm mucus provided electrolytes (Pan et al., 2010) such as K, polyvalent cations (Ca and Mg) as well as water-rich molecules which are known to bridge between organic and inorganic soil constituents and permit the formation of organo-mineral associations, i.e. via cation bridging (Shipitalo and Protz, 1989; Totsche et al., 2018). In summary, the physicochemical properties of mucus shape the reaction environment during the formation of earthworm-generated soil structures like casts and the innermost burrow walls of up to 1 cm soil volume (extended drilosphere) (Schrader, 1994; Andriuzzi et al., 2013; Lipiec et al., 2015).

Organo-mineral associations formed during our experiments revealed altered IEPs in comparison to the pure minerals, even after conducting a threefold washing step. This implies the formation of water stable organo-mineral associations. Hence, the formation of a surface coating and screening of the charge of the bare minerals due to mucus adsorption is suggested. Similarly, an alteration of the surface charge of goethite by the adsorption of microbial EPS of the early stationary phase (Fang et al., 2012) or humic substances (Assemi et al., 2004) led to a charge reversal under constant experimental conditions. However, EPS of the late stationary phase was shown to adsorb in a clearly lesser extend to illite and alter the surface charge of illite inconsiderably (Guhra et al., 2019). In this study, we provide evidence for the screening of the surface charge of illite due to the formation of mucus-mineral associations. This points additionally to the importance of a higher content of proteinaceous mucus constituents for the adsorption to clay minerals.

5. Conclusion

We found that earthworm cutaneous mucus was similar in its chemical composition, adsorption behavior and ability to form organo-mineral associations as microbial EPS secreted in the early stationary

phase. Yet, earthworm mucus had similar chemical composition in two ecological groups (anecic and endogeic), whereas microbial EPS composition varies according to the microbial growth stage and environmental conditions. This implies that the functions of earthworm mucus in soil could be consistent and predictable. Adsorption of earthworm cutaneous mucus depended on the type of soil mineral, which could determine how much and which fraction of mucus becomes associated with nascent organo-mineral associations. The unassociated mucus potentially remains in the soil liquid phase where it could be used for microbial metabolism or is transported in the soil pore system. Under field conditions, earthworm mucus will be deposited throughout the soil profile. For instance, the vertical digging of anecic earthworms forms biopores that are coated with mucus and operate as preferential flow-paths, while the horizontally burrowing endogeic species are known to form stable, OM-enriched (micro-)aggregates during their bioturbation process. The preferential adsorption of the organic carbon and organic phosphorus compounds in the mucus on soil minerals could enrich the newly-formed organo-mineral associations with biogenic nutrient elements. If this occurs in field environments, it suggests that earthworm mucus contributes to nutrient redistribution throughout the soil profile and implies a biogeochemical mechanism to retain the phosphorus secreted in earthworm mucus. Furthermore, the screened surface charge of mucus-mineral associations could explain the often discussed, but unsubstantiated claim that earthworm-processed soil has unique (micro-)aggregation and altered physicochemical properties when compared to bulk soil that was not in contact with earthworms. In conclusion, our work on the small-scale interactions among earthworm mucus and soil minerals provides an intriguing explanation for the beneficial effects of earthworms on pedogenesis and soil quality that were observed repeatedly in lab and field scale studies.

Declaration of competing interest

The authors declare that they have no known competing financial interests or personal relationships that could have appeared to influence the work reported in this paper.

Acknowledgment

We kindly acknowledge financial support by the Deutsche Forschungsgemeinschaft within the framework of the research unit 2179 “MAD Soil - Microaggregates: Formation and turnover of the structural building blocks of soils” (Project no.: 193380941; www.madsoil.uni-jena.de). Katharina Stolze is funded within the framework of the International Max Planck Research School for Global Biogeochemical Cycles (www.imprs-gbgc.de). We thank the CRC AquaDiva (www.aquadiva.uni-jena.de) to provide their test sites to sample the earthworm community. Dr. Sneha Pradip Narvekar helped in producing extracellular polymeric substances. Arnold Wonneberger and Niklas Sebastian van Wickeren are acknowledged for their support of the lab and field work.

Appendix A. Supplementary data

Supplementary data to this article can be found online at https://doi.org/10.1016/j.soilbio.2020.107785.

References

Abdulla, H.A.N., Minor, E.C., Dias, R.F., Hatcher, P.G., 2010. Changes in the compound classes of dissolved organic matter along an estuarine transect: a study using FTIR and 13C NMR. Geochem. Cosmochim. Acta 74, 3815–3838.
Aira, M., McNamara, N.P., Piearce, T.G., Domínguez, J., 2009. Microbial communities of Lumbricus terrestris L. middens: structure, activity, and changes through time in relation to earthworm presence. J. Soils Sediments 9, 54–61.
Andriuzzi, W.S., Bolger, T., Schmidt, O., 2013. The drilosphere concept: fine-scale incorporation of surface residuederived N and C around natural Lumbricus terrestris burrows. Soil Biol. Biochem. 64, 136–138.
Assemi, S., Hartley, P., Scales, P., Beckett, R., 2004. Investigation of adsorbed humic substances using atomic force microscopy. Colloids Surf., A 248, 17–23.
Bouché, M.B., 1975. Action de la faune sur les états de la matière organique dans les ecosystems. In: Kilbertius, G., Reisinger, O., Mourey, A., Cancela da Fonseca, J.A. (Eds.), Humification et biodégradation. Pierron, Sarreguemines, France, pp. 157–168.
Brown, G.G., Barois, I., Lavelle, P., 2000. Regulation of soil organic matter dynamics and microbial activity in the drilosphere and the role of interactions with other edaphic functional domains. Eur. J. Soil Biol. 36, 177–198.
Cao, Y., Wie, X., Cai, P., Huang, Q., Rong, X., Liang, W., 2011. Preferential adsorption of extracellular polymeric substances from bacteria on clay minerals and iron oxide. Colloids Surf., B 83, 122–127.
Chan, K.-Y., Munro, K., 2001. Evaluating mustard extracts for earthworm sampling. Pedobiologia 45, 272–278.
Cortez, J., Bouché, M., 1987. Compositionchimique du mucus cutané de Allolobophora chaetophora chaetophora (Oligochaeta: lumbricidae). Écologie générale 305, 207–210.
Costa, O.Y.A., Raaijmakers, J.M., Kuramae, E.E., 2018. Microbial extracellular polymeric substances: ecological function and impact on soil aggregation. Front. Microbiol. 9, 1–14.
Don, A., Steinberg, B., Schöning, I., Pritsch, K., Joschko, M., Gleixner, G., Schulze, E.D., 2008. Organic carbon sequestration in earthworm burrows. Soil Biol. Biochem. 40, 1803–1812.
Edwards, C.A., Fletcher, K.E., 1988. Interactions between earthworms and microorganisms in organic-matter breakdown. Agric Ecosys. Environ. 24, 235–247.
Edwards, W.M., Shipitalo, M.J., Owens, L.B., Dick, W.A., 1993. Factors affecting preferential flow of water and atrazine through earthworm burrows under continuous No-till corn. J. Environ. Qual. 22, 453–457.
Eisenhauer, N., Shuy, M., Butenschoen, O., Scheu, S., 2009. Direct and indirect effects of endogeic earthworms on plant seeds. Pedobiologia 52, 151–162.
Ellerbrock, R.H., Gerke, H.H., Böhm, C., 2009. In situ DRIFT characterization of organic matter composition on soil structural surfaces. Soil Sci. Soc. Am. J. 73, 531–540.
Fang, L., Cao, Y., Huang, Q., Walker, S.L., Cai, P., 2012. Reactions between bacterial exopolymers and goethite: a combined macroscopic and spectroscopic investigation. Water Res. 46, 5613–5620.
Guhra, T., Ritschel, T., Totsche, K.U., 2019. Formation of mineral–mineral and organo–mineral composite building units from microaggregate-forming materials including microbially produced extracellular polymeric substances. Eur. J. Soil Sci. 70, 604–615.
Hong, Z., Chen, W., Rong, X., Cai, P., Dai, K., Huang, Q., 2013. The effect of extracellular polymeric substances on the adhesion of bacteria to clay minerals and goethite. Chem. Geol. 360–361, 118–125.
Jiang, L., Yang, Y., Jia, L.X., Liu, Y., Pan, B., Lin, Y., 2018. Effects of earthworm casts on sorption-desorption, degradation, and bioavailability of nonylphenol in soil. Environ. Sci. Pollut. Res. Int. 25, 7968–7977.
Jiao, Y., Cody, G.D., Harding, A.K., Wilmes, P., Schrenk, M., Wheeler, K.E., Banfield, J.F., Thelen, M.P., 2010. Characterization of extracellular polymeric substances from acidophilic microbial biofilms. Appl. Environ. Microbiol. 76, 2916–2922.
Jones, G.J., Lawton, J.H., Shachak, M., 1994. Organisms as ecosystem engineers. In: Knopf, F.L. (Ed.), Ecosystem Management. Springer, New York, pp. 373–386.
Kleber, M., Eusterhues, K., Keiluweit, M., Mikutta, C., Mikutta, R., Nico, P.S., 2015. Mineral–organic associations: formation, properties, and relevance in soil environments. Adv. Agron. 130, 1–140.
Kohlhepp, B., Lehmann, R., Seeber, P., Küsel, K., Trumbore, S.E., Totsche, K.U., 2017. Aquifer configuration and geostructural links control the groundwater quality in thin-bedded carbonate–siliciclastic alternations of the Hainich CZE, central Germany. Hydrol. Earth Syst. Sci. Discuss. 21, 6091–6116.
Kosmulski, M., 2016. Isoelectric points and points of zero charge of metal (hydr)oxides: 50 years after Parks’ review. Adv. Colloid Interface Sci. 238, 1–61.
Küsel, K., Totsche, K.U., Trumbore, S.E., Lehmann, R., Steinhäuser, C., Herrmann, M., 2016. How deep can surface signals Be traced in the critical zone? Merging biodiversity with biogeochemistry research in a central German muschelkalk landscape. Front. Earth Sci. 4, 1–18.
Kwon, K.D., Vadillo-Rodriguez, V., Logan, B.E., Kubicki, J.D., 2006. Interactions of biopolymers with silica surfaces: force measurements and electronic structure calculation studies. Geochem. Cosmochim. Acta 70, 3803–3819.
Lee, K.E., 1985. Earthworms, Their Ecology and Relationships with Soils and Land Use. Acadamic Press Inc., London.
Lee, K.E., Foster, R.C., 1991. Soil fauna and structure. Aust. J. Soil Res. 29, 745–775.
Lemtiri, A., Colinet, G., Alabi, T., Zirbes, L., 2014. Impacts of earthworms on soil components and dynamics. A Rev. Biotechnol. Agron. Soc. Environ. 18, 121–133.
Leue, M., Gerke, H.H., Godow, S.C., 2015. Droplet infiltration and organic matter composition of intact crack and biopore surfaces from clay-illuvial horizons. J. Plant Nutr. Soil Sci. 178, 250–260.
Lin, D., Ma, W., Jin, Z., Wang, Y., Huang, Q., Cai, P., 2016. Interactions of EPS with soil minerals: a combination study by ITC and CLSM. Colloids Surf., B 138, 10–16.
Liu, X., Eusterhues, K., Thieme, J., Ciobota, V., Höschen, C., Mueller, C.W., Küsel, K., Kögel-Knabner, I., Rösch, P., Popp, J., Totsche, K.U., 2013. STXM and NanoSIMS investigations on EPS fractions before and after adsorption to goethite. Environ. Sci. Technolog 47, 3158–3166.
Lipiec, J., Brzezinska, M., Turski, M., Szarlip, P., Frac, M., 2015. Wettability and biogeochemical properties of the drilosphere and casts of endogeic earthworms in pear orchard. Soil Tillage Res. 145, 55–61.
Mao, J., Cory, R.M., McKnight, D.M., Schmidt-Rohr, K., 2007. Characterization of a nitrogen-rich fulvic acid and its precursor algae from solid state NMR. Organic Geochem. 38, 1277–1292.

Metzger, U., Lankes, U., Fischpera, K., Frimmel, F.H., 2009. The concentration of polysaccharides and proteins in EPS of Pseudomonas putida and Aureobasidum pullulans as revealed by 13C CPMAS NMR spectroscopy. Appl. Microbiol. Biotechnol. 85, 197–206.
More, T.T., Yadav, J.S.S., Yan, S., Tyagi, R.D., Surampalli, R.Y., 2014. Extracellular polymeric substances of bacteria and their potential environmental applications. J. Environ. Manag. 144, 1–25.
Narvekar, S.P., Ritschel, T., Totsche, K.U., 2017. Colloidal stability and mobility of extracellular polymeric substance amended hematite nanoparticles. Vadose Zone J. 168, 1–10.
Omoike, A., Chorover, J., 2004. Spectroscopic study of extracellular polymeric substances from Bacillus subtilis: aqueous chemistry and adsorption effects. Biomacromolecules 5, 1219–1230.
Omoike, A., Chorover, J., 2006. Adsorption to goethite of extracellular polymeric substances from Bacillus subtilis. Geochem. et Cosmochim. Acta 70, 827-338.
Pan, X., Song, W., Zhang, D., 2010. Earthworms (Eisenia foetida, Savigny) mucus as complexing ligand for imidacloprid. Biol. Fertil. Soils 46, 845–850.
Richards, K.S., 1978. Epidermis and cuticle. In: Mill, P.J. (Ed.), Physiology of Annelids. Academic Press, London, pp. 33–61.
Scheu, S., 1987. Microbial activity and nutrient dynamics in earthworm casts (Lumbricidae). Biol. Fertil. Soils 5, 230–234.
Scheu, S., 1991. Mucus excretion and carbon turnover of endogeic earthworms. Biol. Fertil. Soils 12, 217–220.
Schrader, S., 1994. Influence of earthworms on the pH conditions of their environment by cutaneous mucus secretion. Zoologischer Anzeiger 233, 211–219.
Schwertmann, U., Cornell, R.M., 2000. Iron Oxides in the Laboratory: Preparation and Characterization. WILEY-VCH Verlag GmbH, Weinheim.
Shipitalo, M.J., Protz, R., 1989. Chemistry and micromorphology of aggregation in earthworm casts. Geoderma 45, 357–374.
Simard, R.R., Beauchemin, S., Haygarth, P.M., 2000. Potential for preferential pathways of phosphorus transport. J. Environ. Qual. 29, 97–105.
Sims, R.W., Gerard, B.M., 1999. Earthworms: Keys and Notes for the Identification of the Species. Brill, London.
Six, J., Bossuyt, H., Degryze, S., Denef, K., 2004. A history of research on the link between (micro)aggregates, soil biota, and soil organic matter dynamics. Soil Tillage Research 79, 7–31.
Socrates, G., 2001. Infrared and Raman Characteristic Group Frequencies: Tables and Charts. John Wiley & Sons Ltd, Chichester.
Tiunov, A.V., Scheu, S., 1999. Microbial respiration, biomass, biovolume and nutrient status in burrow walls of Lumbricus terrestris L. (Lumbricidae). Soil Biol. Biochem. 31, 2039–2048.
Totsche, K.U., Amelung, W., Gerzabek, M.H., Guggenberger, G., Klumpp, E., Knief, C., Lehndorff, E., Mikutta, R., Peth, S., Prechtel, A., Ray, N., Kögel-Knabner, I., 2018. Microaggregates in soils. J. Plant Nutr. Soil Sci. 181, 104–136.
Wang, L.-L., Wang, L.-F., Ren, X.-M., Ye, X.-D., Li, W.-W., Yuan, S.-J., Sun, M., Sheng, G.-P., Yu, H.-Q., Wang, X.-K., 2012. pH dependence of structure and surface properties of microbial EPS. Environ. Sci. Technol. 46, 737–744.
Yu, W.H., Li, N., Tong, D.S., Zhou, C.H., Lin, C.X., Xu, C.Y., 2013. Adsorption of proteins and nucleic acids on clay minerals and their interactions: a review. Appl. Clay Sci. 80–81, 443–453.
Zhang, S., Hu, F., Li, H., Li, X., 2009. Influence of earthworm mucus and amino acids on tomato seedling growth and cadmium accumulation. Environ. Pollut. 157, 2737–2742.
Zhang, D., Chen, Y., Ma, Y., Guo, L., Sun, J., Tong, J., 2016. Earthworm epidermal mucus: rheological behavior reveals drag-reducing characteristics in soil. Soil Tillage Res. 158, 57–66.

Earthworm mucus contributes to the formation of organo-mineral associations in soil

Running title: *Earthworm mucus interactions with soil minerals*

Tom Guhra[a*], Katharina Stolze[a*], Steffen Schweizer[b] and Kai Uwe Totsche[a]

[a]*Department of Hydrogeology, Institute of Geosciences, Friedrich Schiller University Jena, Germany*

[b]*Department of Ecology and Ecosystem Management, School of Life Sciences Weihenstephan, Technical University of Munich, Germany*

**Authors* contributed equally *to the manuscript*

Correspondence: K. Totsche. E-mail: kai.totsche@uni-jena.de

Key words: Mucus adsorption, alteration of surface properties, completely mixed batch reactor experiments, Lumbricidae, FTIR-ATR, ^{13}C-NMR

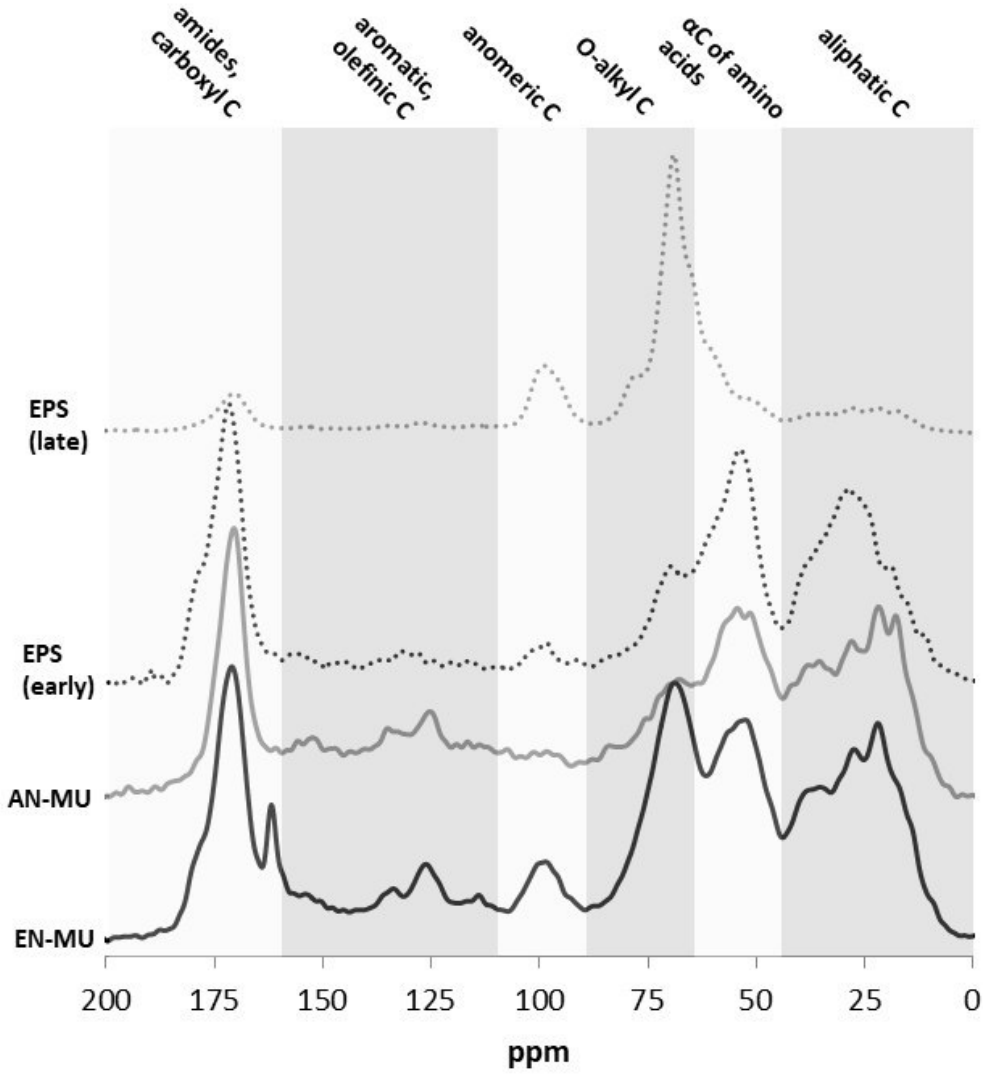

Figure S1: Solid-state ^{13}C-nuclear magnetic resonance spectra of anecic *L. terrestris* mucus (AN-MU), endogeic *A. caliginosa* mucus (EN-MU), extracellular polymeric substances (EPS) of *Bacillus subtilis* obtained from the early stationary phase (early) (Liu et al., 2013) and from the late stationary phase (late) (Guhra et al., 2019). Integral regions are shown by alternating grey values and classified according to Metzger et al. (2009).

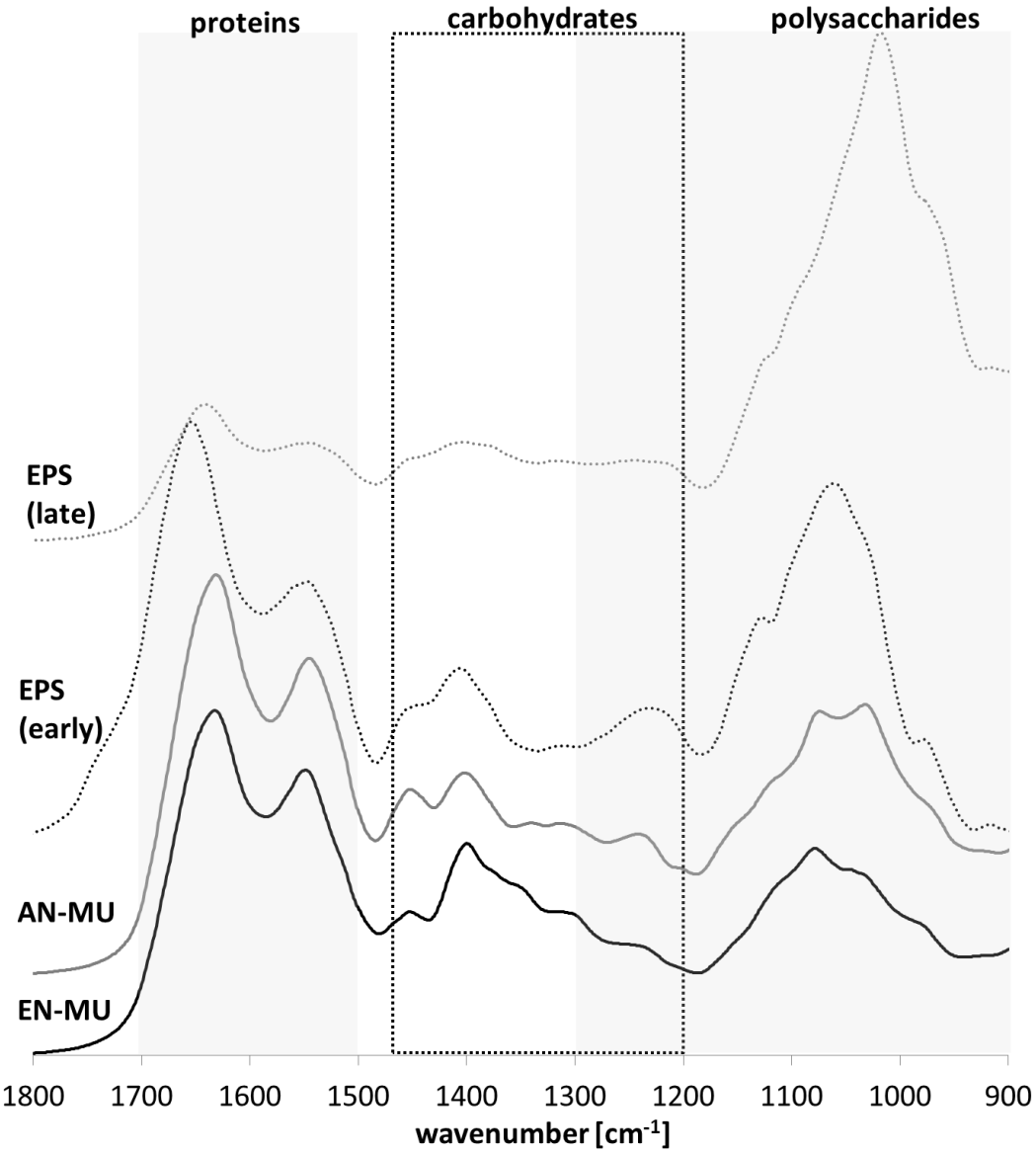

Figure S2: Attenuated total reflection – Fourier-transform infrared spectroscopy (ATR-FTIR) spectra of anecic *L. terrestris* mucus (AN-MU), endogeic *A. caliginosa* mucus (EN-MU), extracellular polymeric substances (EPS) of *Bacillus subtilis* obtained from the early stationary phase (early) (Liu et al., 2013) and from the late stationary phase (late) (Guhra et al., 2019). Main composites were classified in proteins (1700 to 1500 cm $^{-1}$), carbohydrates (1460 to 1200 cm^{-1}) and polysaccharides as well as nucleic acids (1300 to 900 cm^{-1}) according to Jiao et al. (2010) and Socrates (2010).

2.3. Publication 3 (P_{III}): Formation of mineral–mineral and organo–mineral composite building units from microaggregate-forming materials including microbially produced extracellular polymeric substances

Citation: Guhra, T., Ritschel, T. and Totsche, K.U. 2019. Formation of mineral–mineral and organo–mineral composite building units from microaggregate-forming materials including microbially produced extracellular polymeric substances. *European Journal of Soil Science*, 70, 604-615.

DOI: 10.1111/ejss.12774

Rights and licensing: All (co-)authors agree that this article is permitted to be used in the dissertation presented here. The license to use this article in this dissertation was obtained from John Wiley and Sons (date: Jan 19, 2022; format: print and electronic; portion: full article). The journal as the original source of the article is referenced above.

Authors: Tom Guhra[1], Thomas Ritschel[2] and Kai Uwe Totsche[3]

P_{III}			
involved in:	**Author**		
	1	**2**	**3**
conception of research design	X		X
planning of research activities	X		X
data acquisition	X		
data analyses and interpretation	X	X	X
manuscript writing	X	X	X
suggested publication equivalence value	**1.0**		

Received: 13 March 2018 | Revised: 20 September 2018 | Accepted: 6 November 2018

DOI: 10.1111/ejss.12774

WILEY European Journal of Soil Science

ORIGINAL ARTICLE

Formation of mineral–mineral and organo–mineral composite building units from microaggregate-forming materials including microbially produced extracellular polymeric substances

Tom Guhra | Thomas Ritschel | Kai Uwe Totsche

Department of Hydrogeology, Institute for Geosciences, Friedrich Schiller University Jena, Jena, Germany

Correspondence
Tom Guhra.
Email: tom.guhra@uni-jena.de

Funding information
Deutsche Forschungsgemeinschaft, Grant/Award Number: 193380941

Structures of colloidal compounds in soil, including organo–mineral and mineral–mineral associations, are considered as composite building units (CBUs) that may combine into soil microaggregates. Despite the ubiquitous occurrence of CBUs, the major formation mechanisms are rather obscure and little is known about whether they form primarily during weathering of the parent rocks or by aggregation processes from the soil suspension. We studied the formation of CBUs from suspensions composed of minerals and organic matter typical for temperate soils (i.e. quartz, goethite, illite and extracellular polymeric substances [EPS]). Without EPS, we found CBUs formed as mineral–mineral associations by hetero coagulation of illite and quartz that is bridged by goethite. The presence of EPS, in contrast, led to the formation of a stable suspension of clay-sized CBUs with no involvement of quartz. We explained this by the rapid formation of organo–mineral CBUs made of EPS-associated goethite and EPS-associated illite. The sorption of EPS to goethite screened its surface charge, thereby reducing the electrostatic attraction between goethite and illite. This interaction effectively impeded the formation of mineral–mineral CBUs. Moreover, interactions of EPS with goethite resulted in a marked decrease of the phosphorus/carbon ratio in the suspension. This suggested a preferred adsorption of phosphorus-containing EPS constituents to goethite and in turn to a compositional fractionation of EPS constituents between the solid and liquid phase as shown by Fourier-transform infrared spectroscopy with attenuated total reflection (FTIR–ATR). Laser light diffraction measurements revealed a shift from the fine silt fraction to that of the fine sand that also supports the role of EPS as a 'binding' agent.

Highlights

- Composite building units (CBUs) form in suspensions with different mineral and organic components.
- Both, hetero mineral–mineral and organo–mineral CBUs were formed.
- The initial composition of the suspension controls type and properties of resulting CBUs.
- Depending on the mineral surfaces, EPS may serve as a separation or binding agent.

KEYWORDS

alteration of surface properties, completely mixed batch reactor experiments, EPS adsorption, FTIR–ATR, hetero aggregation, SEM-EDX

 © 2018 British Society of Soil Science

1 | INTRODUCTION

Microaggregates are composite structural units of all soils (Totsche et al., 2018) involved in all fundamental functions, including water retention, habitat and element cycling (Six, Bossuyt, Degryze, & Denef, 2004; Totsche et al., 2018). The existence and presence of soil microaggregates, however, is based mainly on the observation that the mechanical destruction of macroaggregates (e.g. by ultrasound of increasing energy) results in rather stable fractions (cf. Six et al., 2004) of sizes that depend on applied mechanical stress. Based on such fractionation experiments, a hierarchy of aggregates has been derived with microaggregates at the smaller size range operationally defined to be smaller than 250 μm (Christensen, 2001; Tisdall & Oades, 1982). Bronick & Lal (2005) suggested that besides the turnover of macroaggregates, microaggregates are formed by the progressive bonding of clays, soil organic matter and cations. Accordingly, a closer look at microaggregates reveals that they have formed from a variety of smaller, but frequently composite, compound structures, recently termed "composite building units" (CBUs, Totsche et al., 2018). These CBUs have formed from clay minerals, pedogenic oxides and organic substances of different provenance and in particular include mineral–mineral associations (Tisdall & Oades, 1982), organo–mineral associations (e.g. Kögel-Knabner, Guggenberger, Kleber et al., 2008; Lehmann, Kinyangi, & Solomon, 2007) or "mineral–organic associations" (Kleber, Eusterhues, Keiluweit, Mikutta, Mikutta, & Nico,2015). Christensen (2001) outlined that the surface interactions between organic matter (OM), organisms and minerals are crucial in regulating the formation of organo–mineral associations as basic units in soil. The CBUs result from persistent and strong binding agents such as microbial products, root exudates, aluminium and iron oxide cements and polyvalent cations (Christensen, 2001; Tisdall & Oades, 1982), and are frequently characterized by marked stability against mechanical and chemical stress. Accordingly, Lehmann et al. (2007) suggested that the association of microbial metabolites with mineral surfaces is especially crucial for the formation of stable microaggregates, rather than the occlusion of organic debris by minerals. However, inorganic constituents such as iron oxides and amorphous aluminium silicates also result in strong bonding and therefore mediate stability (Tisdall & Oades, 1982).

Considering the stability and size of small CBUs <2 μm (Totsche et al., 2018), it is not surprising that they frequently appear as a major fraction of the mobile suspended colloids. An early study by Kaplan, Bertsch, Adriano, and Miller (1993) showed that colloidal materials exported from lysimeters were composed of organo–mineral associations with iron oxides and clay minerals that had more organic carbon (OC) than the bulk soil. In line with this, Totsche, Jann, and Kögel-Knabner (2007) found a considerable amount of suspended matter, of both organic and mineral composition, in the 0.7 to 200-μm size fraction in the seepage of undisturbed lysimeters in a field study. In general, the presence of colloids such as clay minerals, primary silicates, sesquioxides and organic macromolecules is well documented in relation to carrier-affected transport (de Jonge, Kjaergaard, & Moldrup, 2004; Totsche, Danzer, & Kögel-Knabner, 1997). Extensive vertical particle movement is also related to natural soil-forming processes such as eluviation and illuviation, resulting in the formation of diagnostic horizons (Bronick & Lal, 2005) characteristic for Luvisols or Podzols. During these pedogenic processes, OM-associated minerals (e.g. Kleber et al., 2015), clay minerals and metal oxides are translocated (de Jonge et al., 2004) and can be regarded as a mobile fraction of CBUs in natural soils. In summary, the void system of soils contains aqueous suspensions rather than solutions, which are composed of a large variety of organic and inorganic materials that must be considered microaggregate-forming materials (MFM, Totsche et al., 2018) with the potential to form CBUs or already constitute CBUs.

Despite the ubiquitous occurrence and importance of CBUs in soil, their formation is rather obscure. Moreover, their relation to structural properties and functions of microaggregates has not been examined sufficiently. The presence of these materials in the soil suspension may be attributed to surface erosion and, thus, the destruction and disintegration of microaggregates (de Jonge et al., 2004), relating CBU formation to the immobile soil matrix. It remains unclear, however, what type of CBU could also be formed in soil solution from a mobile fraction of MFM that is formed in situ (Fritzsche et al., 2015) or released from the soil matrix.

Here, we present a study on the initial formation of CBUs from aqueous suspensions. We explored the properties of the CBUs (size and composition) formed from representative mineral and organic compounds of temperate soils at different background electrolyte concentrations. The effect of type and concentration of ions (i.e. electrolyte or specific ion effect) on colloid- or clay-sized particle aggregation or interaction has been studied extensively (e.g. Tombácz, Libor, Illés, Majzik, & Klumpp, 2004; Tombácz & Szekeres, 2006; Trefalt, Ruiz-Cabello, & Borkovec, 2014); therefore, we focused our approach on the role of an important fraction of the soil organic matter (i.e. the extracellular polymeric substance [EPS]). Furthermore, wetting–drying cycles have been shown to increase the stability of aggregates (cf. Denef, Six, Merckx, & Paustian, 2002) and, thus, we also investigated the effect of drying. For microaggregate-forming materials, we used minerals typical of temperate soils (i.e. goethite as a representative of iron-oxihydroxides, illite as a representative of clay minerals and quartz). We chose an EPS because it is an abundant organic binding agent (Chenu, 1993; Puget, Angers, & Chenu, 1999) representative of microbial products, which are presumed to be the

most important materials in the stabilization of microaggregates smaller than 20 μm (Oades & Waters, 1991). Furthermore, Puget et al. (1999) suggested that microbial carbohydrates, common constituents of EPS, act as organic binding agents that force aggregation and aggregate stability.

The interaction forces between minerals and organic substances can be attractive; therefore, we hypothesized that stable CBUs might form from suspension. Furthermore, the adsorption of EPS to the mineral surface results in surface alteration and could have a considerable effect on the aggregation processes, with consequences for structure and function.

2 | MATERIAL AND METHODS

2.1 | Materials and mineral characterization

Goethite (Gt) was synthesized according to Schwertmann and Cornell (2000). Specifically, 1 M Fe(III)-solution was prepared from Fe(III)nitrate-nonahydrate (EMSURE 99–101% for analysis, Merck, Germany) and mixed rapidly with 5 M NaOH (≥98%, Pharmacopoea Europaea, USP, BP, in pellets, ROTH, Karlsruhe, Germany). After the addition of ultrapure water (Milli-Q, Integral 5, Elix Technology Inside, Merck Millipore, Darmstadt, Germany) at a ratio of 100:16, the ferrihydrite-containing suspension was aged to goethite by storage in a drying chamber (Binder, Tuttlingen, Germany) at 60°C. The procedure resulted in needle-shaped Gt with an average length of 0.9 ± 0.3 μm as shown by scanning electron microscopy (SEM). Prior to use, the material was rinsed repeatedly with deionized water to remove nitrate.

Quartz (Qz) was purchased from Haltern Quarzwerke GmbH (W11 Millisil, Quarzwerke GmbH, Haltern, Germany) and illite (Il) from INTER-ILI (Mérnöki Iroda, Általános és Kereskedelmi Kft, Nagytarcsa, Hungary). Quartz was dry sieved to a size <63 μm and washed with 10% HCl and ultrapure water. Illite chunks were crushed and dry sieved to a maximum size of <36 μm. Mean particle sizes of 9.0 ± 0.6 μm for Il and 17.0 ± 0.9 μm for Qz were observed by laser diffraction. Minerals were characterized by X-ray diffraction (XRD) (D8 Advance, Bruker, Karlsruhe, Germany) and specific surface area measured by N_2-BET (Autosorb-1, Quantachrome, Odelzhausen, Germany).

2.2 | Bacterial EPS isolation and purification

The EPS of the strain *Bacillus subtilis* 168 (DSM 402) was harvested according to Omoike & Chorover (2004). To isolate free EPS, bacteria were grown to the late stationary phase under aerobic conditions. The cells were separated from solution by centrifugation at 10 000 *g* at 4°C for 20 mins. The EPS was isolated from the supernatant by mixing with cold ethanol and stored immediately at −18°C for 24 hrs. To extract the EPS, the suspension was centrifuged again for 30 mins at 12 000 *g* at 4°C. The EPS pellet obtained was dissolved with sterilized ultrapure water and transferred in dialysis tubing (Spectra/Por 7, Spectrum, Los Angeles, California, USA) of 1 kDa for purification. Dialysis was carried out with ultrapure water changed every 24 hr until the electrical conductivity was constant. The dialysed EPS was freeze-dried for storage. The EPS stock solutions for batch experiments were obtained by dissolving EPS over 3 hr in a chilled ultrasonic bath (ultrasonic cleaner, VWR, Leuven, Belgium). This EPS solution was then centrifuged at 20 000 *g* at 20°C for 30 mins to remove undissolved large particulate EPS flocs.

2.3 | Completely mixed match reactor experiments and chemical analyses

A series of completely mixed batch reactor experiments was conducted with different aqueous suspensions. Specifically, a mixture of Qz, Il and Gt was suspended in 1 and 100 mM sodium chloride (99.7%, VWR, Leuven, Belgium) solutions in the absence and presence of approximately 50 mg(EPS-C)/L^{-1} with three replications. A blank consisting of the EPS stock solution, which was processed in the same way as the batches containing the minerals, was used as reference. The mineral mixture consisted of 75 wt.% Qz, 20 wt.% Il and 5 wt.% Gt and the solid (g) to liquid (mL) amounts were adjusted to 1:20. The EPS-free and EPS-containing variants were shaken (115 revolutions per minutes [rpm]) for 24 hr at a pH between 5.8 and 6.8. Subsequently, the suspension was split into aliquots for further processing and chemical analysis. Some of the mineral suspensions showed an instantaneous separation after shaking from sedimentation; therefore, we sampled each distinctly different sedimented layer (Figure 1) separately for Fourier-transform infrared spectroscopy with attenuated total reflection (FTIR–ATR) and scanning electron microscopy (SEM). One aliquot was dried at 40°C and resuspended for 24 hr in ultrapure water at the same solid/liquid ratio to determine the effect of drying. To estimate the adsorbed amount of carbon (EPS-C) and phosphate (EPS-P) originating from EPS in the supernatants, the solid and liquid phase were separated by centrifugation at 20 000 *g* at 20°C for 30 mins (Cao, Wie, Cai et al., 2011; Fang, Cao, Huang, Walker, & Cai, 2012). The supernatant obtained was used for chemical analysis with inductively coupled plasma optical emission spectrometry (ICP-OES) (Varian, Varian 725 ES, Darmstadt, Germany) and a TOC analyser (Analytic Jena multi N/C 2100s, Jena, Germany). In addition, each single mineral phase was suspended in a replicate EPS solution according to the mass ratios from the batch experiments with a background electrolyte of 100 mM NaCl. These samples were processed in the same way as described above and supernatants were analysed for TOC and element content. The sedimented material produced during the centrifugation step of the single mineral suspensions containing EPS was washed several times to remove loosely

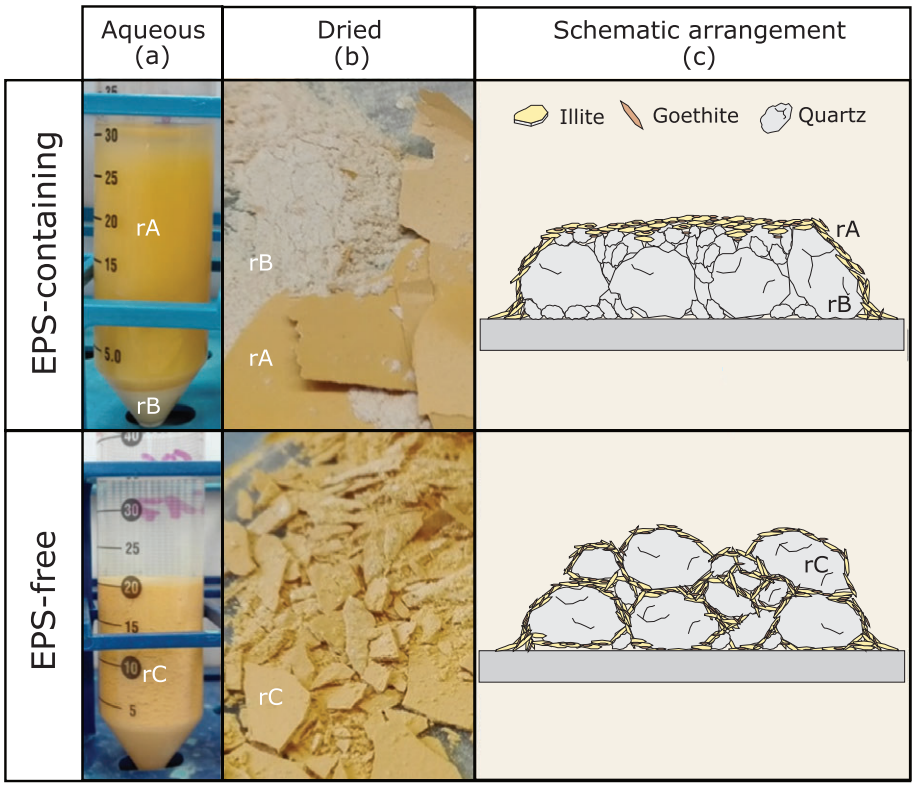

FIGURE 1 Series of images of extracellular polymeric substance (EPS)-containing and -free treatments: (a) suspension after shaking, (b) dried suspension and (c) schematic image of microaggregate-forming materials (MFMs) (needle-shaped goethite [brown], illite sheets [beige] and quartz particles [grey]) distribution after drying. Clay-sized brownish material (rA), sedimented quartz-rich material (rB) and hetero coagulated material (rC) are seen throughout the processing steps

bound EPS and to obtain EPS–mineral associations if any existed. Uncertainties are given as standard errors for $n = 3$. Significance of the treatment effects was tested by the Student's two-tailed t-test at $p = 0.05$.

2.4 | Surface charge and isoelectric point

Zeta-potential measurements (Nano ZS, Malvern Instruments, Malvern, UK) as a function of the pH were used to estimate the isoelectric point (IEP) for the pure and EPS-associated minerals. For measurements of the IEP, 100 $mgL^{-1}$of the pure mineral phase was suspended in 10 mM sodium chloride solution and the pH was adjusted by the addition of HCl or NaOH. The mineral suspension was shaken for 24 hr for equilibration (Kosmulski, 2016). Immediately before the zeta potential was measured, the pH values of the suspensions were checked (pH 197 with pH-electrode Sen Tix 41, WTW, Weilheim, Germany). Finally, the IEP was calculated as the intersection of the stepwise linear interpolation of zeta potentials as a function of pH.

2.5 | Composition, size and properties of minerals and CBUs

The composition of minerals and CBUs was assessed with FTIR spectroscopy (Nicolet iS10 spectrometer, Thermo Fisher Scientific, Dreieich, Germany) with the ATR option (Smart iTX, Thermo Fisher Scientific). The FTIR–ATR measurements are used to characterize the pure and EPS-associated mineral phases of Gt, Il and Qz and the mineral mixture before and after the batch experiments. In addition, the blank with EPS and the supernatants obtained from the batch experiments were freeze-dried for the ATR measurements and comparison of the spectra of the blank and composition of the EPS remaining in the supernatant after adsorption. Particle-size distributions of all batches before and after drying were determined by laser diffraction (Analysette 22 compact, Fritsch, Idar-Oberstein, Germany) at a measurement range between 0.3 and 300 μm with ultrasonication deactivated to prevent the destruction of water-stable CBUs.

An aliquot from the batch experiments was dialysed (Spectra/Por Dialysis Membrane Biotech CE Tubing MWCO: 1000 kD, Spectrum, Los Angeles, CA, USA) to remove sodium chloride for the investigation with SEM (ULTRA PLUS, Zeiss, Jena, Germany) on air-dried samples prepared on a silicon sheet. Distributions of elements were mapped by energy-dispersive X-ray (EDX) at approximately 1-μm resolution at three different randomly selected locations for every sample. Element distribution was attributed to minerals according to: silicon (Si) to quartz (Qz), aluminum (Al) and potassium (K) to illite (Il) and iron (Fe) to goethite (Gt). The Pearson correlation coefficients (r) of element distribution EDX maps (i.e. a cross-correlation between the

pixel-wise greyscale information of two different elemental maps obtained from one spot) were calculated using the Fiji plugin CorrelationJ (Chinga & Syverud, 2007). In addition, element overlap maps were prepared from binarized EDX maps, which were segmented by manual thresholding.

3 | RESULTS

3.1 | Completely mixed batch reactor experiments

For the experiment with the mixed mineral suspensions, the initial EPS-C concentration of the EPS-containing blank was 49.4 ± 0.1 mgL^{-1} for 100 mM and 46.5 ± 0.3 mgL^{-1} for 1 mM background electrolyte. Furthermore, the EPS-P concentration for the blank was between 6.15 ± 0.02 mgL^{-1} for 100 mM and 5.18 ± 0.03 mgL^{-1} for 1 mM background electrolyte**.** The blank of the EPS stock solution used for the batch experiments containing the single mineral phases of Gt, Il and Qz, had an EPS-C and EPS-P concentration of 64.7 ± 0.7 mgL^{-1} and 5.36 ± 0.02 mgL^{-1} at pH 6.7 ± 0.3.

After 24 hr of shaking, the silt-sized fraction mainly attributed to quartz sedimented immediately from the mineral mixture when EPS was present (Figure 1). Consequently, two distinct regions evolved: a brownish supernatant (rA) stabilized in suspensions above a mostly white sediment (rB). After drying, rA formed a thin brownish layer above rB. Without EPS, brownish flocs formed that did not show any separation after sedimentation; therefore, drying at 40°C resulted in unlayered brownish agglomerations (rC).

3.2 | Adsorption of EPS

The EPS-C in solutions containing the mineral mixture decreased from 49.4 ± 0.1 to 25.79 ± 0.09 mgL^{-1} for 100 mM background solution and from 46.5 ± 0.3 to 25.23 ± 0.08 mgL^{-1} for 1 mM background solution. This corresponds to an adsorption of 47.7 ± 0.2% (100 mM) and 45.5 ± 0.4% (1 mM). The P concentration was measured by ICP-OES to obtain EPS-P of the blank in comparison to the supernatants after the batch experiments (Figure 2). The concentration of P decreased from 6.15 ± 0.02 to 0.467 ± 0.006 mg L^{-1} (100 mM) and from 5.18 ± 0.03 to 0.406 ±

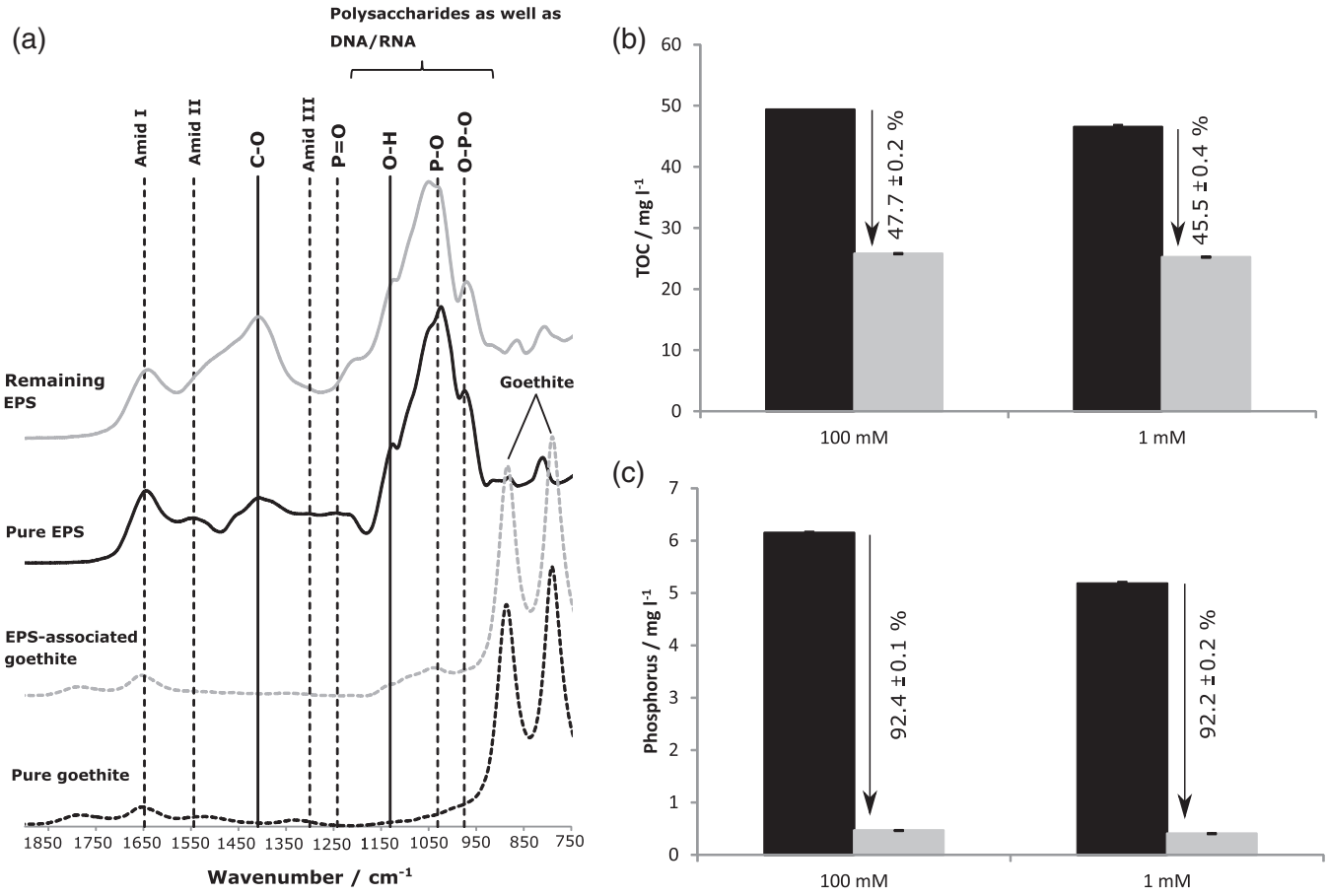

FIGURE 2 (a) The Fourier-transform infrared spectroscopy with attenuated total reflection (FTIR–ATR) spectra of freeze-dried extracellular polymeric substance (EPS) from stock solution (black line) and supernatants (grey line), pure goethite (black dashed line) and EPS-associated goethite (grey dashed line). (b) Amounts of adsorbed carbon (by total organic carbon [TOC] measurements) and (c) adsorbed phosphorus (measured by inductively coupled plasma optical emission spectrometry [ICP-OES]) for 100 mM and 1 mM sodium chloride electrolyte are shown as differences between mineral-containing (grey) and mineral-free treatments (black)

TABLE 1 The measured EPS-C (TOC) and EPS-P (ICP-OES) concentrations and the P/C ratio before and after the batch experiments for suspensions including the mineral mixture (mixed) and the single minerals (single) of goethite, illite and quartz at different background electrolyte concentrations

Sample	Background electrolyte NaCl mM^{-1}	EPS-C mg^{-1} L^{-1}	EPS-P mg^{-1} L^{-1}	P/C ratio
Blank[a] (mixed)	100	49.4 ± 0.1	6.15 ± 0.03	0.0483 ± 0.0002
Blank[a] (mixed)	1	46.5 ± 0.3	5.18 ± 0.05	0.0432 ± 0.0006
Mineral mix	100	25.79 ± 0.09	0.467 ± 0.006	0.0070 ± 0.0001
Mineral mix	1	25.23 ± 0.08	0.406 ± 0.008	0.0062 ± 0.0001
Blank[a] (single)	100	64.7 ± 0.7	5.36 ± 0.02	0.0325 ± 0.0006
Gt	100	41.4 ± 1.1	0.86 ± 0.10	0.0081 ± 0.0008
Il	100	62.6 ± 0.2	4.59 ± 0.04	0.0284 ± 0.0003
Qz	100	64.8 ± 0.4	5.29 ± 0.02	0.0317 ± 0.0002

Uncertainty is given as standard error for $n = 3$.
EPS, extracellular polymeric substance; EPS-C, EPS-carbon; TOC, total organic carbon; EPS-P, EPS-phosphorus; ICP-OES, inductively coupled plasma optical emission spectrometry; Gt, goethite; Il, illite; Qz, quartz.
[a] Blank (mixed) and blank (single) are the EPS-containing and mineral-free references for the treatments containing the mineral mixture and the single minerals.

0.008 mg L^{-1} (1 mM). This is equivalent to an adsorption of 92.4 ± 0.1% (100 mM) and 92.2 ± 0.2% (1 mM). The calculation of the P/C ratio of the EPS-C and EPS-P resulted in 0.0483 ± 0.0002 for 100 mM and 0.0432 ± 0.0006 for 1 mM for the blank. In turn, the P/C ratio of the supernatant decreased by one order of magnitude (0.0070 ± 0.0001 [100 mM] and 0.0062 ± 0.0001 [1 mM]) (Table 1).

The adsorption of EPS to the single mineral phases of Gt, Il and Qz showed a decrease in adsorbed amounts of EPS-C and EPS-P in the order Gt > Il > Qz (Table 1). The largest adsorption was for Gt, with 36 ± 2% EPS-C and 84 ± 2% EPS-P. In comparison, Il adsorbed 3 ± 1% EPS-C and 14.3 ± 0.8% EPS-P. The smallest adsorption was observed for Qz, with no traceable amounts of EPS-C and 1.2 ± 0.5% EPS-P. According to the adsorbed amounts of EPS-C and EPS-P, the P/C ratio increased from Gt to Qz.

3.3 | Characterization of the microaggregate-forming materials (MFMs) and composite building units (CBUs)

The measured BET-specific surface areas were 41.7 ± 0.2 m^2g^{-1} for Gt, 34.47 ± 0.05 m^2g^{-1} for Il and 2.4 ± 0.1 m^2g^{-1} for Qz. The Gt and Qz showed pure mineral phases according to the XRD measurements. Diffractograms of Il indicated small amounts of Qz and feldspar (Supporting Information Figure S1).

The FTIR–ATR spectra of Il showed no additional phases and all bands could be attributed to Il references. There were also pure mineral phases for Gt and Qz (Supporting Information Figure S2). The FTIR–ATR measurements of the dried material of the mineral mixtures showed that rC (i.e. the EPS-free material) was mainly a mixture of Il and Qz, with the main band assigned to a signal overlap of the dominant Qz band at 1045 cm^{-1} and νSi–O of Il at 989 cm^{-1} as shown in Figure S4, Supporting Information (Chukanov, 2014). In addition, Il bands between 825 cm^{-1} and 696 cm^{-1} were superposed by the strong Qz bands at 798, 779 and 696 cm^{-1}. Analysis of rB revealed that the white material was predominantly Qz and contained smaller amounts of Il compared with the materials that formed in rA, which were more strongly enriched in Il. No traces of Gt were detected in the mineral mixtures because the quantities were small.

The freeze-dried EPS of the blank showed FTIR–ATR bands typical for proteins (C=O of amides associated with proteins, 1660 cm^{-1}; N–H and C–N in –CO–NH– of proteins, 1544 cm^{-1}; P=O, 1300 to 1150 cm^{-1}; P=O of phosphate diester or phosphorylated proteins, 1242 cm^{-1}; P–O–C, 1050 to 950 cm^{-1}; P–O symmetric stretching, 1031 cm^{-1}; O–P–O asymmetric stretching of ester, 975 cm^{-1}) and carbohydrates (1200 to 1000 cm^{-1} typical area for overlapping sugar bands, C–H attributed to aldehydes, 1450 to 1350 cm^{-1}; C–O of COO^- groups, 1404 cm^{-1}; OH deformation and C–O ring vibration of polysaccharides, 1127 cm^{-1}; C–H vibrations, 900 to 700 cm^{-1}) (Cao et al., 2011; Omoike & Chorover, 2006; Socrates, 2001). In general, the same bands were detected in the freeze-dried material from the supernatants after the batch experiment, but there was a notable decrease in intensity at wave numbers 1660, 1242 and 975 cm^{-1} in comparison to those at 1404 and 1127 cm^{-1} (Figure 2).

Zeta potentials of the pure mineral phases Il and Qz were negative at experimental conditions compared with the positively charged Gt (Figure 3). The zeta potentials of the EPS-associated single mineral phases had negative surface charges at experimental conditions for all minerals. The IEP was estimated as 8.4 for Gt, whereas the EPS-associated Gt showed a strong decrease in the zeta potentials and the IEP decreased to 4.4. For Qz and Il, zeta potential measurements at pH < 2, which would have been required to determine the IEP, were not possible because of the limitations of the device. From that we concluded that the IEPs of Qz and Il, if they existed, were below pH = 2 (Kosmulski, 2016; Sondi, Biscan, & Pravdic, 1996). Zeta potential measurements of EPS-associated Il and Qz revealed no clear increases in the zeta potentials compared with EPS-free samples (Supporting Information Figure S3).

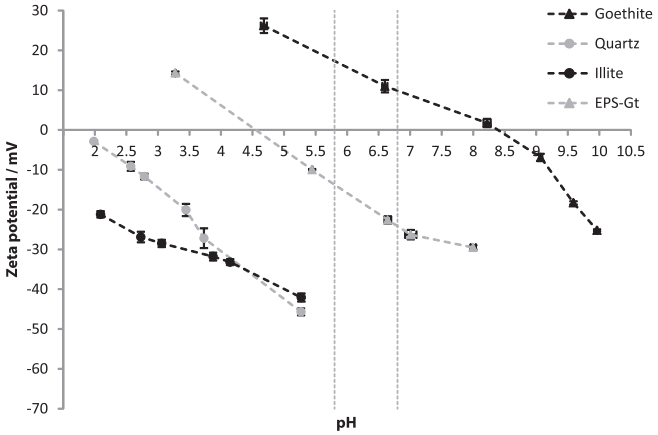

FIGURE 3 The pH-dependent zeta potential measurements of the pure mineral phases of goethite (Gt), illite (Il) and quartz (Qz) and the composite building units (CBUs) composed of extracellular polymeric substance-associated goethite (EPS-Gt) in 10 mM sodium chloride solution. The area between the vertical grey dashed lines represents the pH range during the experiments

3.4 | Development of particle and aggregate sizes

In comparison to the EPS-free mixtures, the particle-size distributions of those with EPS increased significantly in size from the clay and fine silt fractions to coarse silt and fine sand fractions (Table 2). The division diameters D10, D50 and D90 from the cumulative particle-size distributions (i.e. the diameter of the investigated particles that divides the sample mass into a percentage of 10, 50 and 90%) also showed an increase in particle size if an EPS was present. A significant increase in D90 for the EPS-containing treatment compared with the EPS-free treatment was more pronounced if the samples were subject to a drying step. Independent of the EPS availability, samples with a background electrolyte concentration of 100 mM had a significantly larger coarse silt fraction than for the electrolyte concentration of 1 mM (Table 2).

3.5 | Spatial distribution of MFMs

Air-dried samples from the batch experiments were investigated by scanning electron microscopy (SEM-EDX) with 1-μm resolution to search for differences between the spatial arrangement of MFMs in the air-dried aliquots of the EPS-containing and EPS-free treatments. The Pearson correlation coefficient *r* was positive for all element combinations in the EPS-containing treatment, except for Si and Fe, which were negatively correlated (Figure 4). Furthermore, Si and K, Fe and Al as well as Fe and K showed only weak positive correlations. In comparison to rC, rA had stronger negative correlations between Si and Fe and negative correlations between Fe and Al, and Fe and K. The *r* values of rB were close to zero, which suggests that the MFMs were uncorrelated. The *r* value of Al and K was strongly positive for all samples. Element overlap maps showed that Al, Si and Fe almost never overlapped in rA. Only Al and Si showed overlapping areas. The Fe signal was mainly separated from the rest. The correlation values near zero reflected strong element separation in rB. Compared with the EPS-containing treatment, the EPS-free treatment showed large areas of simultaneous occurrence of all mineral MFMs, Si and Fe, as well as overlap of Al and Si.

4 | DISCUSSION

4.1 | Formation of mineral–mineral associations

The EPS-free treatments showed independence from the monovalent NaCl background electrolyte concentration, a clear supernatant and hetero coagulated brownish sediments. This separation occurred almost immediately after shaking of the solution was stopped. This points to small or non-existent repulsive forces that could stabilize the suspension and favours, in turn, the formation of rather large particles. We explain this by the formation of Qz–Gt, Il–Gt and Qz–

TABLE 2 Particle-size classes and division diameter (D10, D50 and D90) for the EPS-containing and EPS-free treatments shaken in 1 and 100 mM sodium chloride solution with and without a drying step followed by subsequent resuspension

Size class /μm	EPS-free (100 mM)/(%)	EPS-containing (100 mM)/(%)	EPS-free (1 mM)/(%)	EPS-containing (1 mM)/(%)	EPS-free dried (100 mM)/(%)	EPS-containing dried (100 mM)/(%)	EPS-free dried (1 mM)/(%)	EPS-containing dried (1 mM)/(%)
<2	12.6 ± 0.3	9.80 ± 0.07	13.6 ± 0.3	11.6 ± 0.3	12.7 ± 0.1	10.0 ± 0.2	11.6 ± 0.1	10.6 ± 0.1
2–6.3	21.0 ± 0.5	17.4 ± 0.2	23.4 ± 0.6	19.4 ± 0.4	22.3 ± 0.3	18.0 ± 0.3	23.8 ± 0.6	19.4 ± 0.1
6.3–20	31.3 ± 0.3	30.7 ± 0.2	30.5 ± 0.4	30.66 ± 0.07	32.3 ± 0.4	30.5 ± 0.2	35.4 ± 0.6	30.8 ± 0.3
20–63	34.7 ± 0.5	39.7 ± 0.4	31.6 ± 0.9	36.4 ± 0.5	32.64 ± 0.05	37.7 ± 0.1	29.2 ± 1.2	36.4 ± 0.8
63–200	0.5 ± 0.4	2.41 ± 0.087	0.9 ± 0.5	2.0 ± 0.2	0.09 ± 0.08	3.6 ± 0.5	0.01 ± 0.01	2.8 ± 0.5
>200	0.006 ± 0.006	0.012 ± 0.005	0.02 ± 0.02	0.008 ± 0.003	BDL[a]	0.2 ± 0.2	BDL[a]	0.05 ± 0.04
				Size /μm				
D10	1.62 ± 0.03	2.04 ± 0.01	1.53 ± 0.02	1.75 ± 0.04	1.63 ± 0.01	2.01 ± 0.04	1.76 ± 0.03	1.89 ± 0.03
D50	13.0 ± 0.4	16.3 ± 0.2	11.2 ± 0.5	14.4 ± 0.4	12.0 ± 0.1	15.9 ± 0.3	10.9 ± 0.4	14.7 ± 0.3
D90	36.3 ± 0.9	42.2 ± 0.2	36.1 ± 1.5	40.2 ± 0.6	34.4 ± 0.4	44.2 ± 1.3	32.3 ± 1.0	42.1 ± 0.7

Uncertainty is given as standard error for $n = 3$.
EPS, extracellular polymeric substance; D, division diameter.
[a] BDL, below detection limit.

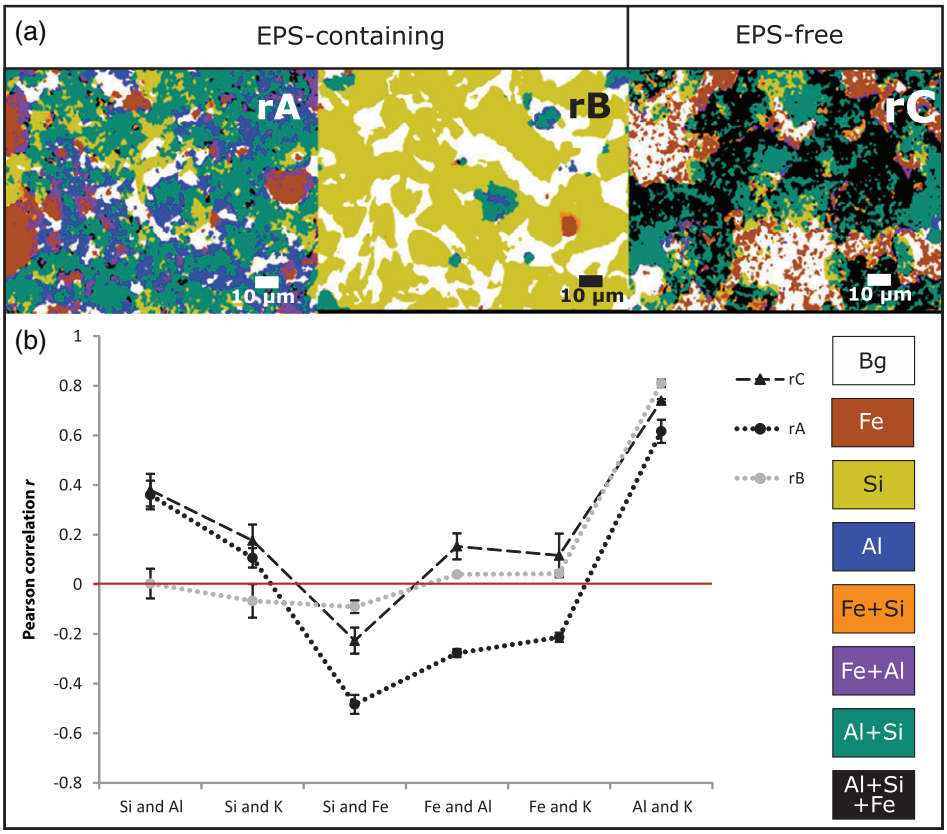

FIGURE 4 (a) Maps of element overlap based on energy-dispersive X-ray (EDX) measurements of air-dried extracellular polymeric substance (EPS)-free treatments containing hetero-coagulated material (rC) and EPS-containing treatments showing the different regions of clay-sized brownish material (rA) and sedimented quartz-rich material (rB) with background (Bg) shown in white, and (b) the Pearson correlation (r) ($n = 3$) of element distribution maps obtained from EDX shown for six element combinations: Si and Al, Si and K, Si and Fe, Fe and Al, Fe and K, and Al and K

Gt–Il mineral–mineral associations as a basic type of hetero-mineral CBU because of strong electrostatic attraction between the small positively charged Gt needles and the negatively charged silica surface of Qz and Il basal planes (Tombácz & Szekeres, 2006). Similarly, Tombácz et al. (2004), for example, also described particle aggregation resulting from attraction between clay minerals and iron oxides if no OM was present at acidic pH conditions. The clear supernatant and, thus, the absence of colloidally stable particles also provided evidence for the attachment of Il to Qz from hetero aggregation by bridging with Gt particles, reported for clay minerals and metal oxides by Tombácz (2003). In addition, reduction of the diffuse double layer by increasing the concentration of the background electrolyte could increase the effect of the variable-charged edges of illite for hetero aggregation (Tombácz & Szekeres, 2006). The resulting mineral–mineral associations were rather large because of the quartz particles. Therefore, these CBUs were prone to rapid sedimentation. Thus, large quartz particles might be scavengers for otherwise colloidally stable clay-sized particles by net attractive forces if the surfaces were not screened by organic compounds such as EPS (Figure 5). The immobilization of colloidal haematite particles on an oppositely charged porous quartz media surface was also shown by Narvekar, Ritschel, and Totsche (2017) if the haematite particles were not coated with EPS. The formation of these mineral–mineral CBUs is relevant for initial and OM-depleted soils characterized by mineral MFMs obtained from bedrock or pedogenic formation.

The resolution of the EDX maps only permits an assessment of mean CBU composition, whereas the exact spatial distribution of single MFMs inside the CBU was not resolved by the EDX beam. The maps of element overlap (Figure 4) for the EPS-free treatment showed large areas where all mineral MFMs overlap, which corresponded with the positive Pearson correlations, r, of Il and Qz as well as Il and Gt from the aforementioned attractive forces. The r values of Al and K were strongly positive for all samples because both elements could be assigned to Il. In addition, ATR measurements showed that the associations in rC were a mixture of Il and Qz, which supports the observation of an unseparated net attractive system that tends towards hetero mineral–mineral aggregation.

4.1.1 | Formation of organo–mineral associations

Composition

Measurements of TOC and ICP-OES in suspensions containing the single mineral MFMs showed consistently that the

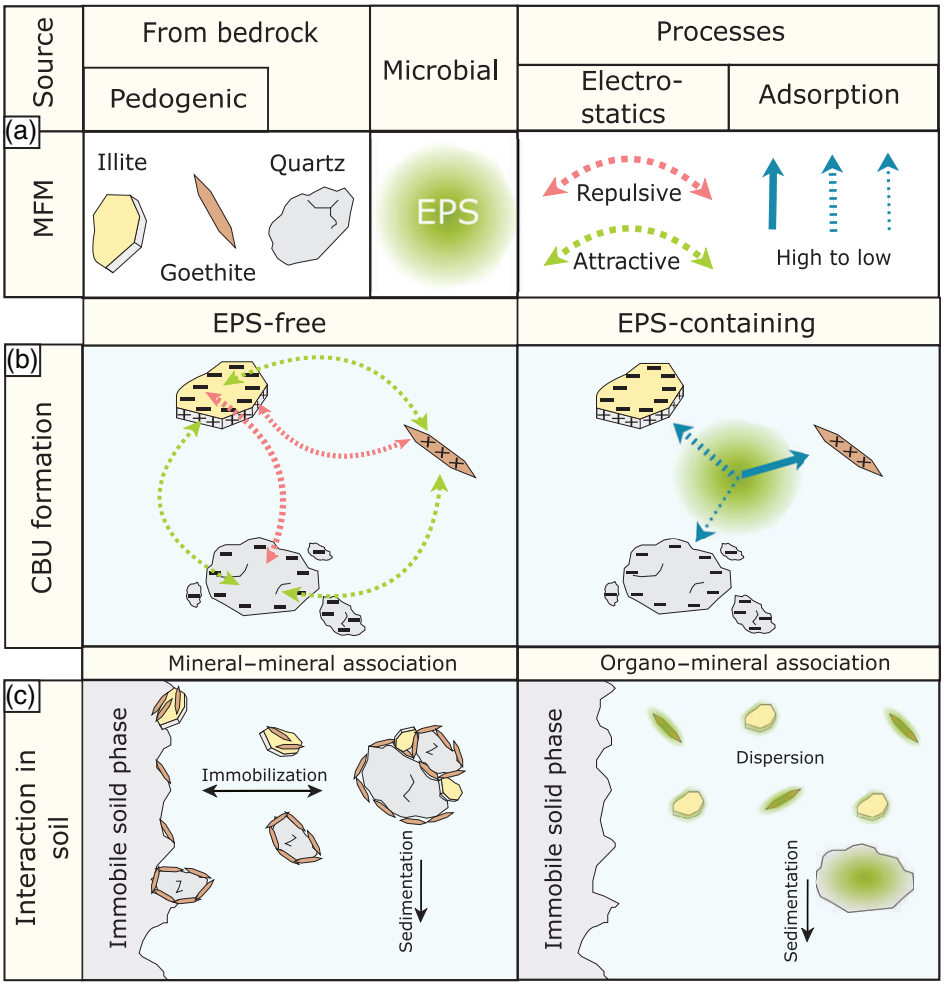

FIGURE 5 (a) Simplified scheme of composite building unit (CBU) formation from microaggregate-forming materials (MFMs) and formation pathways in the aqueous phase of soils based on experimental observations with an overview of interacting MFMs and processes involved in CBU formation, (b) the formation of CBUs inside an extracellular polymeric substance (EPS)-free and -containing liquid phase, and (c) the formation pathways of mineral–mineral and organo–mineral associations inside the soil

adsorption of EPS-C and EPS-P to the mixed mineral phases was mainly attributed to Gt, despite its small mass fraction in the mineral mixtures. The observations showed the expected magnitudes of EPS-C adsorbed to Gt for neutral pH shown by Fang et al. (2012) and Cao et al. (2011). This preferred adsorption to Gt is explained by the large specific surface area and positively charged Gt surfaces, which are known for their strong affinity towards EPS (Cao et al., 2011; Lin, Ma, Jin, Wang, Huang, & Cai, 2016; Omoike & Chorover, 2004, 2006). Compared with Gt, notably smaller amounts of EPS-C and EPS-P adsorbed to Il at the experimental pH values, which could be a result of the specific shape of illite because only the edges of Il provide aluminol groups (Cao et al., 2011; Hong, Chen, Rong, Cai, Dai, & Huang, 2013) with an affinity for proteinaceous EPS constituents also above the IEP of clay minerals (Lin et al., 2016). No adsorption of EPS was observed for Qz, which is consistent with previous findings (Omoike & Chorover, 2004). In summary, EPS forms associations with Gt and, to a lesser extent, Il and thus initiates the formation of organo–mineral associations as another basic type of CBU.

The EPS adsorption to Gt also led to a strong decrease in the P/C ratio of EPS remaining in solution, which was not observed for EPS reacting with Il and Qz. Furthermore, the comparison between ATR spectra of freeze-dried supernatants of the EPS containing the blank and mixed mineral batches revealed a decrease in the band size for phosphorus-containing groups, such as phosphate diesters and phosphorylated proteins, compared with typical bands of polysaccharides and carboxyl groups. This observation supports the findings of Omoike & Chorover (2004) that the contribution of carboxylate groups to the adsorption process was not evident. Thus, we explain the preferred adsorption of phosphorus-containing EPS constituents, such as phosphorylated proteins, phosphodiesters and nucleic acids, shown by ATR measurements by the association of EPS-phosphate groups with surface hydroxyl groups of Gt (Cao et al., 2011; Lin et al., 2016). Consequently, there was a fractionation of EPS constituents between the solid and liquid phase, also known for aluminum oxides (Mikutta, Zang, Chorover, Haumaier, & Kalbitz, 2011). The stability of Gt-associated EPS was confirmed by FTIR–ATR bands typical for EPS

(Figure 2), which were still present after several washing steps to remove any loosely bound fractions, suggesting an inner-sphere bonding of EPS phosphate groups as described by Cao et al. (2011). This points to a close relation of EPS–mineral CBUs to microaggregates because OM in microaggregates was described as mostly of microbial provenience and organic P accumulated within microaggregates compared with organic C (cf. Elliott, 1986). Lehmann et al. (2007) also showed that the association of microbial metabolites with mineral surfaces (also CBUs) was particularly crucial for microaggregate formation and for stabilization of this microbially derived OM by physical occlusion of these CBUs within microaggregates. Therefore, the initial formation of EPS-Gt CBUs observed here might be the decisive factor in controlling the P content of microaggregates. Furthermore, Qin, Hu, He, Dong, Cui, & Wang, (2010) reported an increase in phosphomonoesterases in the silt- and clay-sized fractions of soil, which pointed to the presence of enhanced microbial activity and, thus, the function of microaggregates as a microbial habitat that benefits from the supply of P.

Surface properties

The strong association of EPS with minerals also led to the alteration of net surface charges of EPS–mineral CBUs and therefore controls their interaction with each other. Specifically, there was a decrease in the IEP and negative zeta potentials of EPS–Gt CBUs compared with pure Gt for neutral to slightly acidic pH values (Figure 3),which was also reported by Fang et al. (2012). There were no changes in Qz and Il surface charges according to zeta potential measurements (Supporting Information Figure S3). As a result, all particles were net-negatively charged in the EPS-containing treatment at the experimental pH, resulting in effective repulsion and a colloidally stable suspension. Therefore, the CBUs formed were mobile in porous media, as also illustrated by Narvekar et al. (2017) for haematite covered with EPS that impeded any attractive forces to glass porous media. At the field scale, such conditions could lead to an export of organo–mineral CBUs with the seepage water (e.g. Kaplan et al., 1993) (Figure 5).

After shaking the mineral mixture with EPS, we observed two distinct regions: the colloidally stable clay-sized particles (rA) were deposited above the sedimented quartz material (rB) with sample preparation for EDX analysis. The element distribution maps showed that the correlations between the minerals in rB tended to zero because Il and Gt were enriched in rA and depleted in rB, which mainly consisted of Qz. In region rA, we could not detect any region with colocalization of all mineral MFMs (i.e. Qz, Il and Gt). On the contrary, Gt was in separate spots and negatively correlated with Il and Qz. The ATR measurements showed that compared with rC, which was a mixed region of Il and Qz, the EPS-containing treatment showed a fractionation of Il and Qz between rA and rB in accord with previous results and fitted well with the separation between rA and rB observed macroscopically in the tubes (Figure 1). In summary, EPS rapidly reacted with Gt because of a strong affinity caused by specific adsorption of phosphorus-containing EPS constituents and formed EPS–Gt associations. Consequently, the formation of these constituents dominated further interactions in a system containing three fractions: Qz, EPS–Gt and EPS–Il associations.

Furthermore, there was a small but significant increase in adsorbed amounts of EPS-C with increasing background electrolyte concentration of NaCl in our experiments that pointed to a reduction in the spread of the diffuse double layer around a charged particle and, thus, the increased interaction between EPS and the minerals (Cao et al., 2011).

Effect of EPS availability, background electrolyte concentration and drying on CBU size

Laser light diffraction showed a significant increase in particle size for background electrolyte concentration of 100 mM compared with 1 mM NaCl in the batch experiments. We explain this by the effect of the larger electrolyte concentration, which resulted in a less expanded diffuse layer around the particles and an increased attraction between two charged particles, which is consistent with the expected electrostatic interactions (Trefalt et al., 2014). There was also an increase in particle size from silt to fine sand fraction if EPS was present, which suggested that Qz, which solely comprised this size fraction in our experiments, also forms EPS-associated CBUs. Although difficult to detect in changes in the element composition by batch adsorption experiments (Kwon, Green, Bjöörn, & Kubicki, 2006), there was a marginal deposit of EPS to silica surfaces in the study of Zhu, Long, Ni, and Tong (2009). Thus, we suggest that Qz forms associates in suspension that result either from bridging by EPS or the reduction of electrostatic repulsion from EPS attachment. Puget et al. (1999) revealed a positive correlation between the carbohydrate content and the stability of aggregates. Pen, Zhang, Morales-García, Mears, Tarmey, Edyvean, & Geoghegan, (2015) showed an EPS-induced attachment between two repulsive surfaces (EPS-enclosed cell against a silicon wafer) with atomic force microscopy when a certain distance between the two components had been overcome. Kwon, Vadillo-Rodriguez, Logan, and Kubicki (2006) outlined the particular relevance of phosphorus-containing EPS constituents for the attachment of EPS to silanol groups by H-bonds at low to neutral pH values. Thus, phosphorus-containing groups seem to be the key element in the formation of organo–mineral CBUs irrespective of the minerals involved.

In the presence of EPS, the increase in large particles was even more pronounced when the mineral mixtures were dried and resuspended. We attribute this to menisci forces that occur during drying and pull smaller particles into the

interstitial space formed by larger particles, which results in an enlargement of the contact points between the particles (Denef et al., 2002; Horn & Dexter, 1989). In addition, OM is known to stabilize aggregates in soil against slaking by their hydrophobic properties and the formation of additional intermolecular associations upon drying (Bronick & Lal, 2005; Six et al., 2004).

5 | CONCLUSIONS

In heterogeneous aqueous suspensions, composite building units (CBUs) are expected to form under diverse conditions. The type and abundance of microaggregate-forming materials (MFMs) are therefore decisive for the size, composition and stability of formed CBUs. In suspensions free of mobile organic matter such as EPS, electrostatic attraction between oppositely charged minerals controls the formation of mineral–mineral CBUs in which pedogenic minerals like goethite take the role of 'bridging mineral'. In the presence of EPS, the formation of organo–mineral CBUs with altered surface properties is enforced, whereas the formation of mineral–mineral associations is inhibited. Thus, we conclude that in natural aqueous environments, which provide a large variety of MFMs, homo aggregation is of minor importance because minerals are expected to associate rapidly with oppositely charged minerals as well as organic MFMs. The strong attachment of EPS to minerals suggests that organo–mineral CBUs are the basic unit that facilitate carbon and phosphorus storage in microaggregates. Furthermore, EPS can act as both an agglomerative and dispersive agent because we also observed an increase in particle size for EPS-containing suspensions. Yet, our experiments did not provide evidence for the initiation of aggregation in aqueous environments with a single MFM acting as the nucleus.

ACKNOWLEDGEMENTS

We acknowledge financial support by the Deutsche Forschungsgemeinschaft within the framework of the research unit 2179 "MAD Soil - Microaggregates: Formation and turnover of the structural building blocks of soils" (Project no 193380941; www.madsoil.uni-jena.de). The authors thank Lydia Pohl for measuring the specific surface area by N_2-BET.

ORCID

Tom Guhra https://orcid.org/0000-0003-4587-0635

Thomas Ritschel https://orcid.org/0000-0002-9922-1107

Kai Uwe Totsche https://orcid.org/0000-0002-2692-213X

REFERENCES

Bronick, C. J., & Lal, R. (2005). Soil structure and management: A review. *Geoderma*, *124*, 3–22.

Cao, Y., Wie, X., Cai, P., Huang, Q., Rong, X., & Liang, W. (2011). Preferential adsorption of extracellular polymeric substances from bacteria on clay minerals and iron oxide. *Colloids and Surfaces B: Biointerfaces*, *83*, 122–127.

Chenu, C. (1993). Clay- or sand-polysaccharide associations as models for the interface between micro-organisms and soil: Water related properties and microstructure. *Geoderma*, *56*, 143–156.

Chinga, G., & Syverud, K. (2007). Quantification of paper mass distributions within local picking areas. *Nordic Pulp & Paper Research Journal*, *22*, 441–446.

Christensen, B. T. (2001). Physical fractionation of soil and structural and functional complexity in organic matter turnover. *European Journal of Soil Science*, *52*, 348–353.

Chukanov, N. V. (2014). *Infrared Spectra of Mineral Species: Extended Library*. Dordrecht, The Netherlands: Springer Science+Business Media.

de Jonge, L. W., Kjaergaard, C., & Moldrup, P. (2004). Colloids and colloid-facilitated transport of contaminants in soils. *Vadose Zone Journal*, *3*, 321–325.

Denef, K., Six, J., Merckx, R., & Paustian, K. (2002). Short-term effects of biological and physical forces on aggregate formation in soils with different clay mineralogy. *Plant and Soil*, *246*, 185–200.

Elliott, E. T. (1986). Aggregate structure and carbon, nitrogen, and phosphorus in native and cultivated soils. *Soil Science Society of America Journal*, *50*, 627–633.

Fang, L., Cao, Y., Huang, Q., Walker, S. L., & Cai, P. (2012). Reactions between bacterial exopolymers and goethite: A combined macroscopic and spectroscopic investigation. *Water Research*, *46*, 5613–5620.

Fritzsche, A., Schröder, C., Wieczorek, A. K., Händel, M., Ritschel, T., & Totsche, K. U. (2015). Structure and composition of Fe-OM co-precipitates that form in soil-derived solutions. *Geochimica et Cosmochimica Acta*, *169*, 167–183.

Hong, Z., Chen, W., Rong, X., Cai, P., Dai, K., & Huang, Q. (2013). The effect of extracellular polymeric substances on the adhesion of bacteria to clay minerals and goethite. *Chemical Geology*, *360–361*, 118–125.

Horn, R., & Dexter, A. R. (1989). Dynamics of soil aggregation in an irrigated desert loess. *Soil & Tillage Research*, *13*, 253–266.

Kaplan, D. I., Bertsch, P. M., Adriano, D. C., & Miller, W. P. (1993). Soil-borne mobile colloids as influenced by water flow and organic carbon. *Environmental Science & Technology*, *27*, 1193–1200.

Kleber, M., Eusterhues, K., Keiluweit, M., Mikutta, C., Mikutta, R., & Nico, P. S. (2015). Mineral–organic associations: Formation, properties and relevance in soil environments. *Advances in Agronomy*, *130*, 1–140.

Kögel-Knabner, I., Guggenberger, G., Kleber, M., Kandeler, E., Kalbitz, K., Scheu, S., & Leinweber, P. (2008). Organo-mineral associations in temperate soils: Integrating biology, mineralogy, and organic matter chemistry. *Journal of Plant Nutrition and Soil Science*, *171*, 61–82.

Kosmulski, M. (2016). Isoelectric points and points of zero charge of metal (hydr)oxides: 50 years after Parks´ review. *Advances in Colloid and Interface Science*, *238*, 1–61.

Kwon, K. D., Green, H., Bjöörn, P., & Kubicki, J. D. (2006). Model bacterial extracellular polysaccharide adsorption onto silica and alumina: Quartz crystal microbalance with dissipation monitoring of Dextran adsorption. *Environmental Science & Technology*, *40*, 7739–7744.

Kwon, K. D., Vadillo-Rodriguez, V., Logan, B. E., & Kubicki, J. D. (2006). Interactions of biopolymers with silica surfaces: Force measurements and electronic structure calculation studies. *Geochimica et Cosmochimica Acta*, *70*, 3803–3819.

Lehmann, J., Kinyangi, J., & Solomon, D. (2007). Organic matter stabilization in soil microaggregates: Implications from spatial heterogeneity of organic carbon contents and carbon forms. *Biogeochemistry*, *85*, 45–57.

Lin, D., Ma, W., Jin, Z., Wang, Y., Huang, Q., & Cai, P. (2016). Interactions of EPS with soil minerals: A combination study by ITC and CLSM. *Colloids and Surfaces B: Biointerfaces*, *138*, 10–16.

Mikutta, R., Zang, U., Chorover, J., Haumaier, L., & Kalbitz, K. (2011). Stabilization of extracellular polymeric substances (*Bacillus subtilis*) by adsorption to and coprecipitation with Al forms. *Geochimica et Cosmochimica Acta*, *75*, 3138–3154.

Narvekar, S. P., Ritschel, T., & Totsche, K. U. (2017). Colloidal stability and mobility of extracellular polymeric substance amended hematite nanoparticles. *Vadose Zone Journal*, *168*, 1–10.

Oades, J. M., & Waters, A. G. (1991). Aggregate hierarchy in soils. *Australian Journal of Soil Research*, *29*, 815–828.

Omoike, A., & Chorover, J. (2004). Spectroscopic study of extracellular polymeric substances from *Bacillus subtilis*: Aqueous chemistry and adsorption effects. *Biomacromolecules*, *5*, 1219–1230.

Omoike, A., & Chorover, J. (2006). Adsorption to goethite of extracellular polymeric substances from *Bacillus subtilis*. *Geochimica et Cosmochimica Acta*, *70*, 827–838.

Pen, Y., Zhang, Z. J., Morales-García, A. L., Mears, M., Tarmey, D. S., Edyvean, R. G., & Geoghegan, M. (2015). Effect of extracellular polymeric substances on the mechanical properties of *Rhodococcus*. *Biochimica et Biophysica Acta*, *1848*, 518–526.

Puget, P., Angers, D. A., & Chenu, C. (1999). Nature of carbohydrates associated with water-stable aggregates of two cultivated soils. *Soil Biology & Biochemistry*, *31*, 55–63.

Qin, S., Hu, C., He, X., Dong, W., Cui, J., & Wang, Y. (2010). Soil organic carbon, nutrients and relevant enzyme activities in particle-size fractions under conservational versus traditional agricultural management. *Applied Soil Ecology*, *45*, 152–159.

Schwertmann, U., & Cornell, R. M. (2000). *Iron Oxides in the Laboratory: Preparation and Characterization*. Weinheim, Germany: Wiley-VCH Verlag GmbH & Co, KGaA.

Six, J., Bossuyt, H., Degryze, S., & Denef, K. (2004). A history of research on the link between (micro)aggregates, soil biota, and soil organic matter dynamics. *Soil & Tillage Research*, *79*, 7–31.

Socrates, G. (2001). *Infrared and Raman Characteristic Group Frequencies: Tables and Charts*. Chichester, England: John Wiley & Sons Ltd.

Sondi, I., Biscan, J., & Pravdic, V. (1996). Electrokinetics of pure clay minerals revisited. *Journal of Colloid and Interface Science*, *178*, 514–522.

Tisdall, J. M., & Oades, J. M. (1982). Organic matter and water-stable aggregates in soils. *European Journal of Soil Science*, *33*, 141–163.

Tombácz, E. (2003). Effect of environmental relevant organic complexants on the surface charge and the interaction of clay mineral and metal oxide particles. In S. Barany (Ed.), *Role of Interfaces in Environmental Protection* (pp. 397–424). Dordrecht, The Netherlands: Springer Science+Business Media.

Tombácz, E., Libor, Z., Illés, E., Majzik, A., & Klumpp, E. (2004). The role of reactive surface sites and complexation by humic acids in the interaction of clay mineral and iron oxide particles. *Organic Geochemistry*, *35*, 257–267.

Tombácz, E., & Szekeres, M. (2006). Surface charge heterogeneity of kaolinite in aqueous suspension in comparison with montmorillonite. *Applied Clay Science*, *34*, 105–124.

Totsche, K. U., Amelung, W., Gerzabek, M. H., Guggenberger, G., Klumpp, E., Knief, C., & Kögel-Knabner, I. (2018). Microaggregates in soils. *Journal of Plant Nutrition and Soil Science*, *181*, 104–136.

Totsche, K. U., Danzer, J., & Kögel-Knabner, I. (1997). Dissolved organic matter-enhanced retention of polycyclic aromatic hydrocarbons in soil miscible displacement experiments. *Journal of Environmental Quality*, *26*, 1090–1100.

Totsche, K. U., Jann, S., & Kögel-Knabner, I. (2007). Single event–driven export of polycyclic aromatic hydrocarbons and suspended matter from coal tar–contaminated soil. *Vadose Zone Journal*, *6*, 233–243.

Trefalt, G., Ruiz-Cabello, F. J. M., & Borkovec, M. (2014). Interaction forces, heteroaggregation, and deposition involving charged colloidal particles. *The Journal of Physical Chemistry B*, *118*, 6346–6355.

Zhu, P., Long, G., Ni, J., & Tong, M. (2009). Deposition kinetics of extracellular polymeric substances (EPS) on silica in monovalent and divalent salts. *Environmental Science & Technology*, *43*, 5699–5704.

SUPPORTING INFORMATION

Additional supporting information may be found online in the Supporting Information section at the end of the article.

How to cite this article: Guhra T, Ritschel T, Totsche KU. Formation of mineral–mineral and organo–mineral composite building units from microaggregate-forming materials including microbially produced extracellular polymeric substances. *Eur J Soil Sci*. 2019;1–12. https://doi.org/10.1111/ejss.12774

Supporting information

Formation of mineral–mineral and organo–mineral composite building units from microaggregate-forming materials microbially produced extracellular polymeric substances

Running title: *(Organo–)mineral composite building unit formation*

T. Guhra[*,a], T. Ritschel[a] & K.U. Totsche[a]

[a]*Department of Hydrogeology, Institute for Geosciences, Friedrich Schiller University Jena, Germany*

*Correspondence: T. Guhra. E-mail: tom.guhra@uni-jena.de

Key words: hetero aggregation, EPS adsorption, alteration of surface properties, completely mixed batch reactor experiments, FTIR–ATR, SEM-EDX

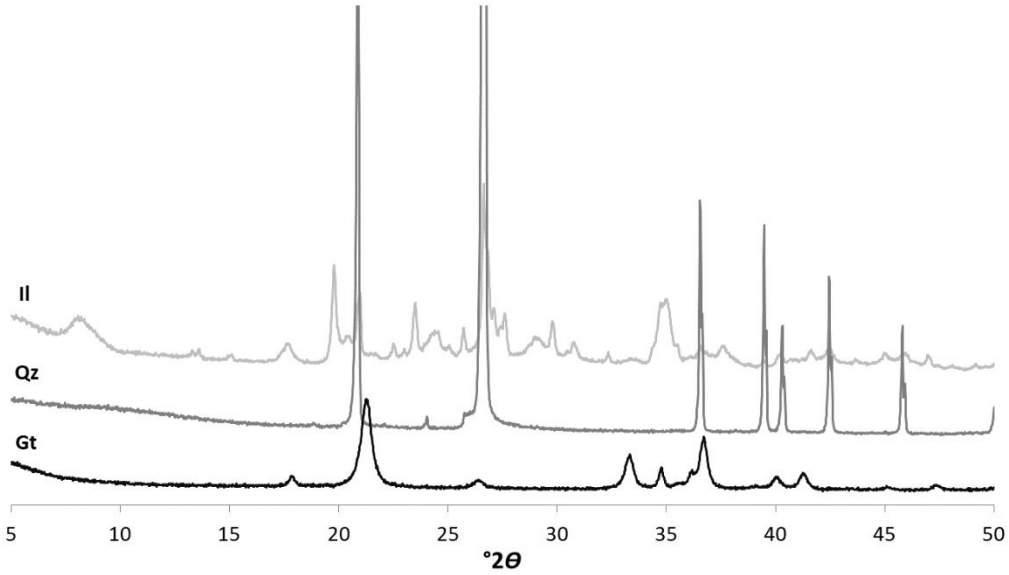

Figure S1 Diffractograms (primary optics: 0.3 °, axial soller 5.1 °, detector: 1 D mode 2.93, step size 0.02 °2θ, measurement time per step 0.5 s) of pure mineral phases of goethite (Gt), quartz (Qz) and illite (Il).

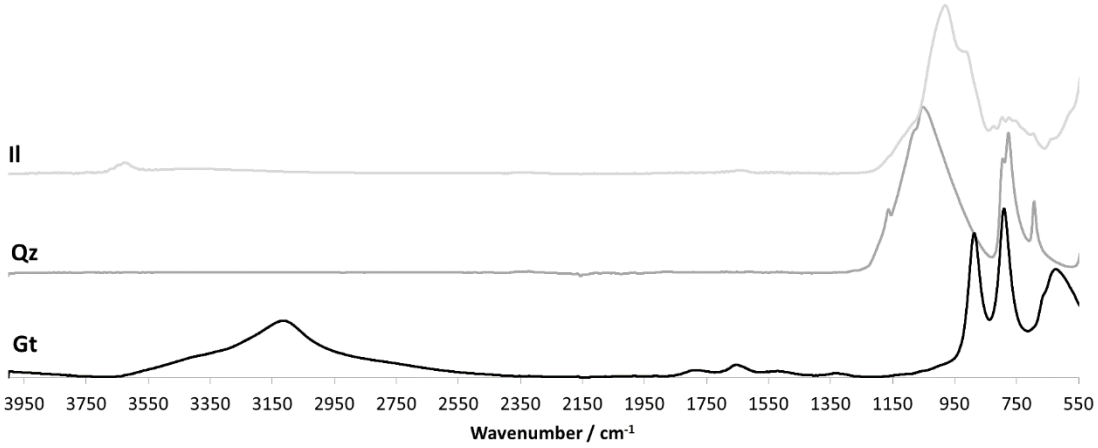

Figure S2 The FTIR–ATR spectra of pure mineral phases of goethite (Gt), quartz (Qz) and illite (Il).

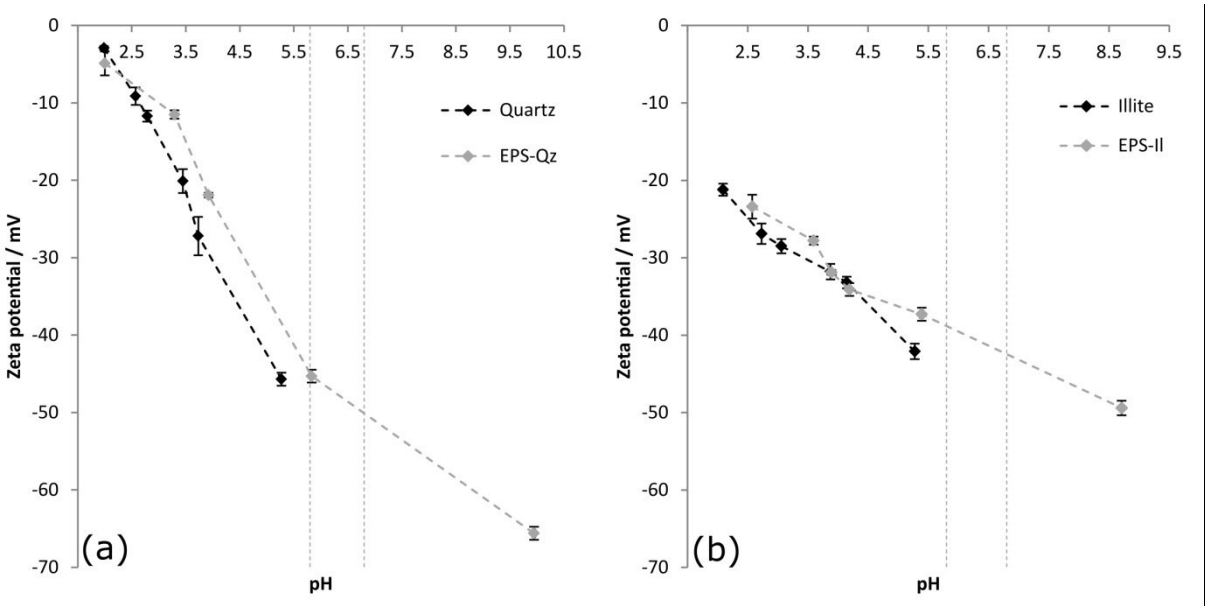

Figure S3 (a) The pH dependent zeta potential measurements of the pure mineral phases of quartz and EPS-associated quartz (EPS-Qz) and (b) illite and EPS-associated illite (EPS-Il) in 0.01 M sodium chloride solution. The area between the vertical grey dashed lines represents the pH range during the experiments.

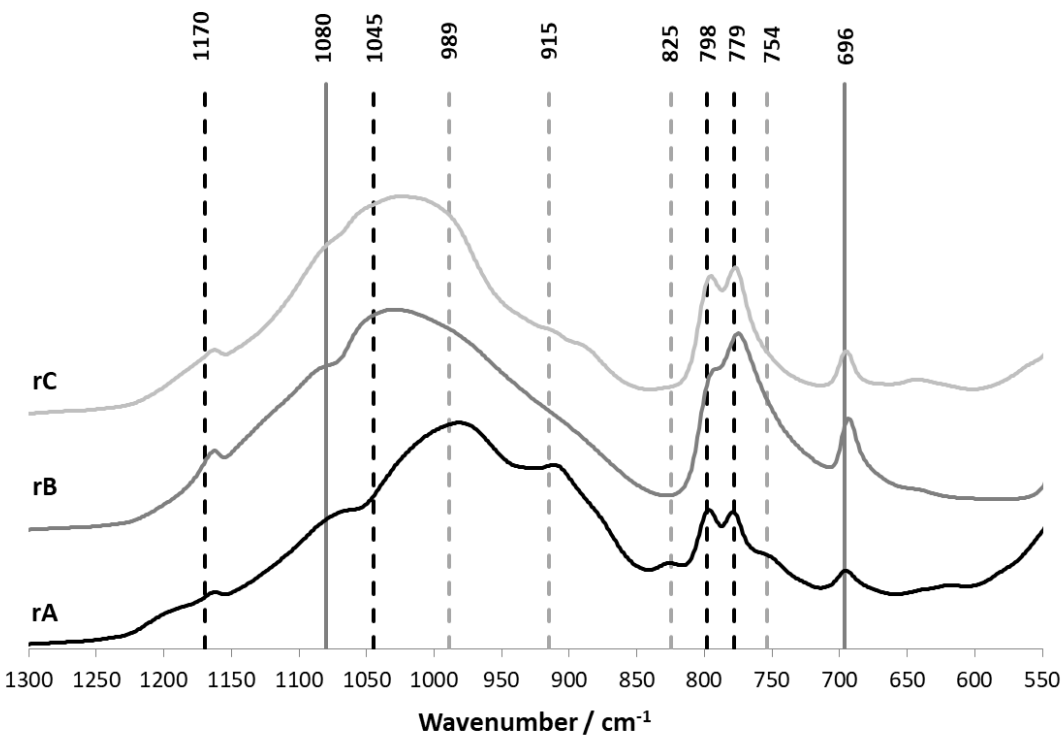

Figure S4. The FTIR–ATR spectra of region rC from the dried EPS-free treatment and regions rA and rB from the dried EPS-containing treatment. Vertical dashed lines represent the band position for pure quartz (black) and illite (grey) phases. Continuous grey lines reveal the position of bands that could be attributed to illite and quartz.

2.4. Publication 4 (P_{IV}): Application of a cellular automaton method to model the structure formation in soils under saturated conditions: A mechanistic approach

Citation: Rupp, A., Guhra, T., Meier, A., Prechtel, A., Ritschel, T., Ray, N. and Totsche, K.U. 2019. Application of a cellular automaton method to model the structure formation in soils under saturated conditions: A mechanistic approach. *Frontiers in Environmental Science*, 7, 170.

DOI: 10.3389/fenvs.2019.00170

Rights and licensing: All (co-)authors agree that this article is permitted to be used in the dissertation presented here. This article is published under the terms of the creative commons CC-BY license, thus no permission to reuse the article is required. The journal as the original source of the article is referenced above.

Authors: Andreas Rupp[1], Tom Guhra[2], Andreas Meier[3], Alexander Prechtel[4], Thomas Ritschel[5], Nadja Ray[6] and Kai Uwe Totsche[7]

P_{IV}							
involved in:	**Author**						
	1	**2**	**3**	**4**	**5**	**6**	**7**
conception of research design				X		X	X
planning of research activities	X	X		X	X	X	X
data acquisition	X		X				
data analyses and interpretation		X			X		X
manuscript writing	X	X		X	X	X	
suggested publication equivalence value		**0.5**					

frontiers in Environmental Science

ORIGINAL RESEARCH
published: 01 November 2019
doi: 10.3389/fenvs.2019.00170

Application of a Cellular Automaton Method to Model the Structure Formation in Soils Under Saturated Conditions: A Mechanistic Approach

Andreas Rupp[1], *Tom Guhra*[2], *Andreas Meier*[1], *Alexander Prechtel*[1], *Thomas Ritschel*[2], *Nadja Ray*[1]* *and Kai Uwe Totsche*[2]

[1] *Chair of Applied Mathematics I, Department of Mathematics, Friedrich-Alexander University Erlangen-Nürnberg, Erlangen, Germany,* [2] *Chair of Hydrogeology, Institute of Geosciences, Friedrich-Schiller University Jena, Jena, Germany*

Soil functions are closely related to the structure of soil microaggregates. Yet, the mechanisms controlling the establishment of soil structure are diverse and partly unknown. Hence, the understanding of soil processes and functions requires the connection of the concepts on the formation and consolidation of soil structural elements across scales that are hard to observe experimentally. At the bottom level, the dynamics of microaggregate development and restructuring build the basis for transport phenomena at the continuum scale. By modeling the interactions of specific minerals and/or organic matter, we aim to identify the mechanisms that control the evolution of structure and establishment of stationary aggregate properties. We present a mechanistic framework based on a cellular automaton model to simulate the interplay between the prototypic building units of soil microaggregates quartz, goethite, and illite subject to attractive and repulsive electrostatic interaction forces. The resulting structures are quantified by morphological measures. We investigated shielding effects due to charge neutralization and the aggregate growth rate in response to the net system charge. We found that the fraction as well as the size of the interacting oppositely charged constituents control the size, shape, and amount of occurring aggregates. Furthermore, the concentration in terms of the liquid solid ratio has been shown to increase the aggregation rate. We further adopt the model for an assessment of the temporal evolution of aggregate formation due to successive formation of particle dimers at early stages in comparison to higher order aggregates at later stages. With that we show the effect of composition, charge, size ratio, time, and concentration on microaggregate formation by the application of a mechanistic model which also provides predictions for soil aggregation behavior in case an observation is inhibited by experimental limitations.

Keywords: individual based modeling, microaggregate formation, mineral surface charge, morphological characteristics, soil structure simulation, self-organization, cellular automaton

OPEN ACCESS

Edited by:
Ali Ebrahimi,
Massachusetts Institute of Technology, United States

Reviewed by:
Bin Wang,
University of California, Irvine, United States
Jing Yan,
University of California, Merced, United States
Nasrollah Sepehrnia,
Leibniz University Hannover, Germany

***Correspondence:**
Nadja Ray
ray@math.fau.de

Specialty section:
This article was submitted to Soil Processes, a section of the journal Frontiers in Environmental Science

Received: *26 July 2019*
Accepted: *09 October 2019*
Published: *01 November 2019*

Citation:
Rupp A, Guhra T, Meier A, Prechtel A, Ritschel T, Ray N and Totsche KU (2019) Application of a Cellular Automaton Method to Model the Structure Formation in Soils Under Saturated Conditions: A Mechanistic Approach. Front. Environ. Sci. 7:170. doi: 10.3389/fenvs.2019.00170

INTRODUCTION

Soil structure is organized in a hierarchy of patterns and properties, as e.g., found in pores and aggregates at different scales. To unravel the interplay between the macroscopic functions provided by soils and the sub-micron scale of surface interactions observed between minerals and organic constituents of the soil solution may be regarded as one of the grand challenges of soil science

(Totsche et al., 2010). Conceptual models for the turnover of aggregate classes date back to the research work by Tisdall and Oades (1982), see also Six et al. (2004). In the context of carbon balances, quantitative investigations have been conducted using multipool/compartment concepts (e.g., Segoli et al., 2013; Stamati et al., 2013). Due to the large scales, on which these models are defined, they do not account for any spatial structure of the (micro-)aggregates besides a size class. Also, mechanistic process based transformation rates are missing. For a review of aggregation model approaches see also section 6 in Totsche et al. (2018). While simulations on explicit pore structures of soils have become feasible in the last decade (e.g., Blunt et al., 2013) they do not account for an evolution of the rigid structures. Portell et al. (2018), e.g., established an individual based model approach to account for growth of microbial species on explicit pore geometries, and combined it with solute transport realized by a Lattice Boltzmann method. The solid structure is fixed, however. Cellular automaton model (CAM) methods have already successfully been used to describe the structural development of biofilms at the pore scale (Tang and Valocchi, 2013; Tang et al., 2013) or self-organization of soil-microbe systems (Crawford et al., 2012). On a smaller interaction scale, DLVO theory and the fractal growth of diffusion-limited aggregation has been used recently to illustrate the detailed interplay of molecular forces between particles in the formation of microaggregates (Ritschel and Totsche, 2019).

The model as presented in Ray et al. (2017) and Rupp et al. (2018) approaches the task of unraveling the interplay between scales by the coupling of continuum-scale transport phenomena and a local scale able to represent mineral surface interactions and the consolidation of microaggregates. The effective transport parameters required at the continuum-scale can be derived by an upscaling of micro-scale morphological properties that translates the formation and restructuring of microaggregates to their impacts on, e.g., the hydraulic conductivity (Schulz et al., 2019) or the effective diffusion (Ray et al., 2018). However, how and even whether stable effective properties on the continuum scale emerge from the dynamics at the local scale is not investigated yet. In addition, the factors that control the establishment of stationary structures are to be identified. In Rupp et al. (2018), electrostatics were introduced as surface interactions that control colloidal stability and the aggregation by opposing the attractive van der Waals forces (for two likely charged particles) or electrostatic attraction which leads to fast aggregation (for two oppositely charged particles, Fermin and Riley, 2010; Trefalt et al., 2014). However, the interactions between minerals are not only controlled by surface forces, but also by their physical properties, e.g., size, density, compactness, rigidity, complex shapes, surface roughness (Buffle and Leppard, 1995; McCarthy and McKay, 2004; Bin et al., 2011). As a result, the interaction of constituents of the soil solution is quite diverse and leads to complex structures and structural properties (McCarthy and McKay, 2004; Bin et al., 2011).

A simultaneous investigation of the impact of mineral size, shape, composition, concentration, and charge for the formation of microaggregates is a challenge that is experimentally elaborate or sometimes impossible. Numerous experimental studies consider only selected aspects of aggregation simultaneously e.g., the hetero-aggregation of two similar sized and shaped nanoparticles in different relations (e.g. Bansal et al., 2017) or the hetero-aggregation of two dissimilar sized and shaped mineral particles (Tombácz et al., 2004). Totsche et al. (2018) outline that mathematical aggregation models could support the development of new ways for dedicated and theory-guided experiments and explorative instrumental studies. Additionally, mathematical aggregation models could provide an insight into the time scale of aggregation processes (Bremer et al., 1995) which can avoid immense experimental efforts as well as the development of different aggregate structures as function of time (Szilagyi et al., 2014). Models also allow discriminating the influence of single mechanisms on aggregate formation, which cannot be separated experimentally.

In this study, we present the systematic application and evaluation of a 2D mechanistic, mathematical model (Ray et al., 2017; Rupp et al., 2018; Rupp, 2019) to elucidate the influence of varying sizes, shapes, and charge distributions of prototypic building units on structure formation. The building units are directly implemented with specific properties such as charge distributions, sizes, or shapes. This contrasts with concepts dealing with averaged concentrations in representative elementary volumes where the spatial structure of particles or the porous medium is not resolved explicitly.

Our model also allows for an analysis of the temporal evolution of the formation of microaggregates by investigating whether particle suspensions lead to stable potentially dispersed structures. We adopt this model with a focus on systems, in which electric forces, van der Waals forces, and random Brownian motion are supposed to have a major impact on aggregation as, e.g., in initial soils, subsoil horizons, and ground water systems. Such natural multi-particle systems provide a variety of inorganic mineral particles which are probable to interact which each other. Their charge properties are a function of the prevailing boundary conditions, pH and electric conductivity (Tombácz et al., 2001; Guhra et al., 2019). Three surrogates are designed *in silico* inspired by secondary mineral phases like goethite (Gt) and illite (Il) as well as quartz (Qz) as a persistent primary mineral, which are all typical for temperate soils.

With this, we simulated the aggregate development in differently composed suspensions to provide a comprehensive overview of optimal growth rates, final aggregate sizes, and structural properties.

MATERIALS AND METHODS

For our numerical experiments, we apply the CAM as presented in Ray et al. (2017), Rupp et al. (2018), and Rupp (2019) to study structure formation in soils at the scale of microaggregates. We do not investigate the influence of organic matter or biofilms but focused on abiotic interactions to avoid a superposition of contrasting processes that cannot be identified uniquely. Readers might refer to Tang et al. (2013), who explicitly studied biofilm growth with CAM models.

In general CAM are based on decision rules that move or transform cells on rectangular grids to new states or locations. We use a two-dimensional, periodic computational domain consisting of 200 × 200 quadratic unit cells which are the smallest discrete objects in our simulations. For verification, calculations were also performed with a resolution of 500 × 500 cells (not shown here). The results confirmed that the chosen domain is considered representative. For our study, we designed three morphological prototypes to resemble typical minerals of humid latitudes, i.e., the secondary minerals goethite (Gt) and illite (Il) as well as quartz (Qz) as persistent primary mineral. On their surfaces we uniformly apply charges occurring at stationary circumneutral pH. Gt as a needle shaped variable charge metal hydroxide is represented by a positively charged rectangle with an area of 1 × 5 squares, although a negative charge at pH values above their specific point of zero charge (PZC) is also possible (Cornell and Schwertmann, 2003; Kosmulski, 2011). Il is represented by plates of 2 × 3 squares. A typical length scale for the unit cell could thus be 1 μm. Due to its variably charged edges and negatively charged basal planes (Tombácz and Szekeres, 2006) we allowed the charge of Il to be either uniformly positive or negative. This will be specified below in the respective simulation scenarios (section Simulation Scenarios and Results). Qz has negative charges at circumneutral pH (Kosmulski, 2011). Its spherical shape is approximated by unit cells with a diameter of 11 for the prototype (resulting in a particle area of 97). When investigating the influence of the size, we also used Qz with a diameter of 21 (area 349), and 41 (area 1257).

We distinguish between microaggregate forming materials (MFM), i.e., single particles of Qz, Gt and Il, and composite building units (CBUs), i.e., the composition of two or more prototypes called MFMs (for details of the used terminology, see Totsche et al., 2018). The interplay between the MFMs and their composites follows the cellular automaton rules as described in Ray et al. (2017) and Rupp et al. (2018). The range of potential movement for MFMs and/or CBUs are defined analogously within the computational domain and is characterized by stencils in the context of the CAM which are motivated by physical laws. Note that we expand the approach presented in Ray et al. (2017) and Rupp et al. (2018) further as follows: In the current research, we distinguish between the movement within a range of attraction due to electric forces (Trefalt et al., 2014) and random movement due to Brownian motion. These potential movements, encoded in the respective stencil sizes as discussed below, depend on size and charge of the MFMs/the CBUs themselves. The range of electric attraction/repulsion is modeled by r_{el}, while the range of diffusion is given by r_{df}:

$$r_{el} = \left\lfloor c_{el} \left| \frac{NC_p}{a_p} \right| \right\rfloor, r_{df} = \left\lfloor \frac{c_{df}}{\sqrt{a_p}} \right\rfloor, \quad (1)$$

where $\lfloor x \rfloor$ is the floor function (greatest integer less than or equal to x), and NC_p and $a_p$denote the net charge and the area of a particle (either MFM or CBU), respectively. In our investigations, both stencils may be balanced through their respective constants c_{el} and c_{df}. Unless stated otherwise, the constants in the definition of the stencils are set to 10. This would correspond to time steps of about 0.5 s, relating the mean path length of particles to it. The respective stencils of our approach are abstract theoretical entities. One may interpret their physical meaning as follows: The diffusion stencil may be derived from the expected value of squared diffusive displacement which is $2Dt$ and Stokes-Einstein equation that linearly relates the diffusion coefficient D of a particle to its inverse radius. Hence, the mean displacement caused by diffusion requires a $\frac{1}{\sqrt{a_p}}$ dependence, which we multiplied by an effective parameter that combines all further physical constants that are involved. Consequently, r_{df} decreases when CBUs grow. This is a more realistic characterization of the movement of (larger) composites than in Ray et al. (2017) and Rupp et al. (2018). Likewise, the range of electric attraction/repulsion depends on the net charge and may change for composites that are created if MFMs/CBUs of various charges aggregate. The net charge NC_p is the sum of the charges of all unit cells this particle is composed of. Thus, the electrostatic stencil and its size relates to the electrostatic potential (Coulomb potential) that is proportional to the charge density represented by $\frac{NC_p}{a_p}$. Again, the constant combines the physical constants that are involved. Along this line, a fully dynamic situation is considered throughout the numerical investigations. In each time step, MFMs are allowed to move in accordance with their stencils first, followed by composites. To this end, the sizes of the corresponding electro and random stencils are evaluated dynamically. First, each MFM moves to the closest void space within the electro stencil r_{el} where the affinity A_i is maximal. The affinity A_i of a potential target position Y^i in the fluid (which has to be inside the range of the stencil r_{el}) is calculated according to the following formula, with $Y_s^{\hat{i}}$ being the location of the solid MFM under consideration:

$$A_i = NN - \min_{\bar{Y}_s^{\hat{i}} \text{ is a rotation of } Y_s^{\hat{i}}} \left\{ \sum_{\substack{neighbors \\ Y_s^j \neq Y_s^{\hat{i}} of\, Y^i}} \int_{\partial \bar{Y}_s^{\hat{i}} \cap \partial\, Y_s^j} \rho^{\bar{Y}_s^{\hat{i}}} \rho^{Y_s^j} d\sigma \right\} \quad (2)$$

NN is the number of (new) solid neighbors $\neq Y_s^{\hat{i}}$ in position Y^i. ρ is the surface charge density, evaluated at the common edges of $Y_s^{\hat{i}}$ and Y_s^j which we denote with $\partial Ys^{\hat{i}} \cap \partial Y_s^j$.The affinity A_i is thus a combination of uniform attraction and repulsive/attractive electric forces between particles with charges, for a detailed definition and illustration of a similar mechanism see Rupp et al. (2018). If there are several equally advantageous target positions, one is chosen randomly. Only if the current position is optimal within its electro stencil, the diffusion stencil is evaluated additionally. Then, this procedure is repeated for CBUs without considering rotations. We conduct numerical experiments under varying conditions to investigate the effect of composition, charge, size ratio, and concentration on microaggregate formation (cf. scenarios 1–3 in section Simulation Scenarios and Results). Moreover, the temporal evolution of microaggregate formation is illuminated.

A quantitative analysis of the resulting structures using the subsequent morphological characteristics then follows.

***Morphological characteristics*:**

- The total area of CBUs is defined as the sum of the areas of all composites and increases if MFMs form composites (Isolated single MFMs are ignored in this calculation). The total area can be interpreted as a measure of mass.
- The total surface is defined as the length of the solid-fluid interface. The total surface of CBUs is the length of the interface between CBUs and the fluid.
- The number of particles/composites is defined as the number of isolated particles/composites.
- The average particle size (PS) is defined as the arithmetic average of the area of all particles (MFMs and CBUs), i.e., the total area over the number of particles. Likewise, the average particle size of CBUs is defined as the total area of composites over the number of isolated composites.
- The compactness ratio (CR) of CBUs (in two dimensions) is defined as the total surface of CBUs to the power of 2 over the total area of CBUs. Note that any circle has the minimal CR of 4π, any square 16. The prototypes of our MFMs have CR of 16.7 (Il), 28.8 (Gt), and the imperfect approximations of the circular Qz of 20.0/20.2/21.4 (for small, medium and large size Qz).
- The net electric charge (NC) of the scenarios is defined as the sum of all charges according to all MFMs in the observed system.

Further measurements may be derived from these definitions such as the specific surface (total surface over total area). Moreover, the dynamics of theses quantities can be reported, i.e., the temporal evolution of the aggregation process can be characterized according to different descriptive quantities.

SIMULATION SCENARIOS AND RESULTS

We conducted the following numerical experiments to illustrate the impact of composition, surface charge, particle size ratio, and concentration on microaggregate formation. All simulations start with a random uniform distribution of the solid MFMs in the fluid. We performed 1,000 steps of the CAM, and repeated each scenario 10 times. Longer runs (4,000 steps) revealed no additional information (not shown here).

Variation of Composition

As first scenario, we considered a fixed (area) fraction of 20% of solids in the computational domain and vary the composition of the solid in portions of Qz, Gt, and Il. We started with a solid phase consisting of Qz only (i.e., 0% of the solid is Gt and Il, 100% of the solid is Qz) and equally increase the portions of Il and Gt stepwise until no Qz remains in the solid (i.e., 50% of the solid is each Il and Gt, while 0% is Qz). Additionally, we investigated the effect of the net electric charge (NC) in the observed systems, including the sum of negative charged Qz and positive charges Gt as well as positively (Il_{pos}) or negatively (Il_{neg}) charged Il.

Figure 1 shows the effect of composition and charge on the average particle size (PS). If Il is positively charged, both Il and Gt can attach to Qz to form aggregates. PS for Il_{pos} (**Figure 1**) increases for compositions of 0 (i.e., only Qz) to 10% Gt/Il from 97 to a maximum PS of 896 (gray shaded in **Figure 1**). Mixtures with higher portions of Gt/Il then lead to smaller CBUs again (e.g., PS = 73 for 20%Gt/20%Il/60%Qz), down to a minimal PS of 6 for a mixture of 50% of (likely charged) Gt and Il, where all particles appear un-associated. In the scenarios with negatively charged Il_{neg} also the small BUs of Gt and Il can attach to form composites. The PS increases now from 97 (free Qz) to 761 (10% Gt/Il) and further to a maximum PS of 2027 at a composition of 36% of each Gt and Il (cp. **Figure 1**). The maximal reached PS corresponds to scenarios with the NC of zero in both systems (**Figure 1**). Hence these zero charge scenarios represent the composition of MFMs that leads to the strongest aggregation due to charge neutralization by a balanced amount of positive and negative charged MFMs in the observed systems. Compositions deviating from this optimum, i.e., with higher positive or negative net charges, produce lower PS.

The aggregate distributions and structures obtained after 1,000 CAM steps for 10, 20, and 44% Il/Gt portions that correspond to scenarios with clearly different PS (**Figure 1**), including negatively and positively charged Il scenarios are exemplarily shown in **Figure 2**. First we observe that for Il_{pos} at a composition of 10%Gt/10%Il/80%Qz all MFMs are bound in CBUs. With increasing portions of Il_{pos}/Gt (20 and 44%) a shielding is visible by positive charged Il and Gt surrounding one negative charged Qz. The fact that smaller particles move faster than larger ones strengthens this effect. In contrast to this case, Il_{neg} can also bind to Gt (**Figure 2**). Thus, the isolation of large particles by shielding does not occur, and composites with several Qz MFMs form. Consequently PS grows up to a maximum of 2027, and does not fall below 550 even without Qz (cf. **Figure 1**). Furthermore, we want to emphasize that similar PS can correspond to considerably distinct phenotypes of CBUs. Exemplary, we observe short coiled chain like CBUs whose PS is in the same magnitude for mixtures of around 10% Gt/10% Il_{pos}/80% Qz (∼897) and 20% Gt/20% Il_{neg}/60% Qz (∼1,049). But for 44% Gt/44% Il_{neg}/12% Qz (∼915) and higher Gt/Il concentrations structures of thin long chains are observed with increasing content of associated smaller Il and Gt particles. However, the phenotypes of the CBUs are very different (see **Figure 2**), with long branches of Gt/Il_{neg} stacks or single Qz only associated to Gt and Il_{pos} with increasing Gt and Il contents.

Variation of the Size of MFMs

The second scenario considers a fixed (area) fraction of 20% solid and additionally a fixed composition of 6% Gt, 6% Il_{pos} and 88% Qz that has shown to produce high aggregation according to **Figure 1**. However, the diameter of Qz now varies from 11 to 21 to 41 (resulting in areas of 97, 349, and 1,257, respectively), i.e., the effect of size ratio of the MFMs was investigated: We compared the effect of less but larger Qz particles to the situation of more but smaller Qz particles building aggregates with Gt/Il_{pos}. **Figure 3** illustrates the evolution of the average particle size PS and the compactness ratio CR over 1,000 CAM steps for the different Qz sizes (Green line: small Qz, red: medium size Qz, black: large Qz). First we observed that the

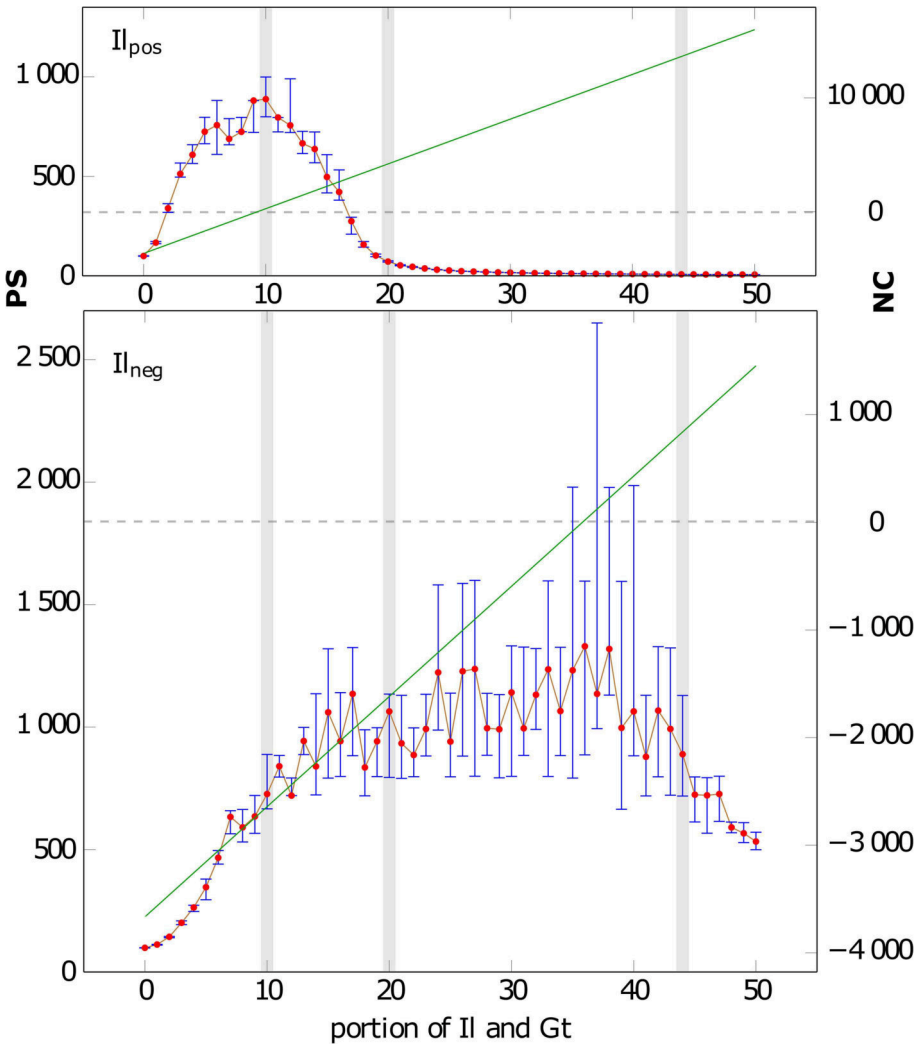

FIGURE 1 | Average particle sizes (PS) for various compositions of the solid after 1,000 CAM steps: X-axis: number denotes the (equal) portions of Il and Gt, the remaining portion is Qz (i.e., 10 represents a composition of 10% Gt, 10% Il, and 80% Qz particles). (**Top**) Il is positively charged (Il_{pos}), (**Bottom**) Il is negatively charged (Il_{neg}). The red dots show the median of 10 runs, the blue bars indicate the lower and upper quartile of the 10 runs. The green lines depict the net electric charge (NC) of the system and correspond to the second y-axis. The intersection of the gray dashed line and the green line marked the NC of zero and the highest PS in both systems. The gray shaded areas correspond to the three compositions shown in **Figure 2**.

amplitude of variations is largest for large Qz, because the aggregation or separation of a Qz MFM changes the area of a composite by at least 1,257. As the large Qz MFMs or CBUs diffuse very slowly, the much smaller Gt/Il_{pos} MFMs attach fast to Qz, but the formation of composites with several Qz MFMs has a low probability. With small Qz the movement is faster and the formation of structures with several Qz MFMs is facilitated. The PS grows over a larger number of time steps (compare the slopes of the PS curves in **Figure 3**) and CR decreases with MFM size with spherical structures having the lowest CR. Smaller Qz MFMs result in chain-like structures with highest CR, see also the exemplary configurations after 1,000 steps in **Figure S1** in the Supplementary Material. Low CR are achieved for large Qz, which reflects the fact that the CBUs including large Qz are more compact, and closer to spherical structures.

We repeated these calculations for other compositions. If we compare to a scenario with an unfavorable aggregate formation (MFM compositions of 24% Gt, 24% $Il_{pos,}$ and 52% Qz see **Figure 1**) we obtain aggregates with the similar PS independent of initial size of Qz. During these scenarios only compact and short chain structures are formed for small and medium Qz and scenarios containing large Qz are characterized by totally separated spheres coated with Il and Gt, which are not linked to each other. Hence, the formation of dense surface coatings (shielding: inhibits dendritic growth of aggregates) with Il and Gt (over 1,000 CAM-steps) leads to the formation compact structures in all scenarios independent of initial size of Qz. As

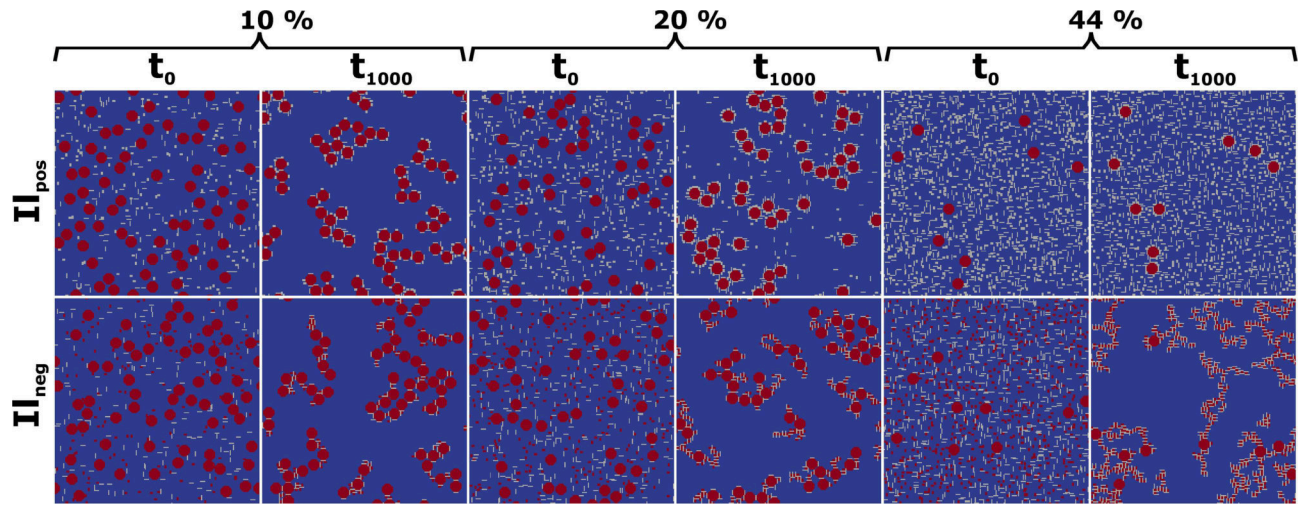

FIGURE 2 | Initial (t_0) and final state ($t_{1,000}$) of a simulation with 10, 20 and 44% of positive (Il_{pos}) or negative (Il_{neg}) charged Il and Gt. Positively charged MFMs in gray, negatively charged in red.

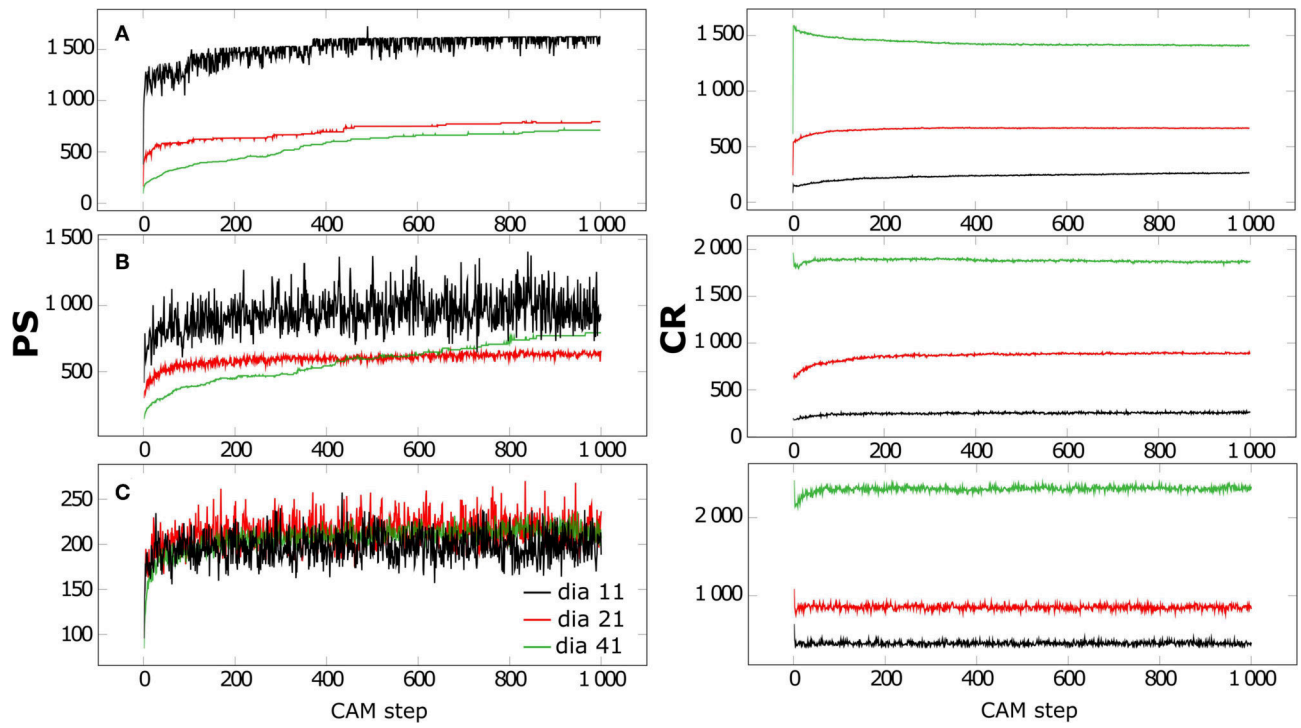

FIGURE 3 | Average particle sizes (PS) and compactness ratios (CR) for CBUs plotted as function of time. The initial conditions were set to an area fraction of 20% and a composition of 6% Gt, 6% Il_{pos} and 88% Qz **(A)**, 12% Gt, 12% Il_{pos} and 76% Qz **(B)** as well as 24% Gt, 24% Il_{pos} and 52% Qz **(C)** of different sizes: small diameter of 11 (green), medium diameter of 21 (red) and large diameter of 41 (black).

described above, scenarios containing large Qz leading to more compact structures because of their structure close to an ideal sphere (**Figure S1**). Intermediate scenarios of 12% Gt, 12% Il_{pos} and 76% Qz representing an overlapping of effects observed for scenarios with optimal (6% Gt, 6% Il_{pos} and 88% Qz) and reduced (24% Gt, 24% Il_{pos} and 52% Qz) aggregation. In these scenarios the number of particles (Il and Gt) in relation to the size and surface of the Qz particles is a distinct parameter which leads to a continuous increase in PS for small Qz. In the small Qz scenario the amount of Il and Gt is not enough to cover the whole Qz surfaces and consequently support aggregation due to bridging. If the Qz size increases, the ratio between the number of particles

and the surface of Qz decline and comprehensive surface coatings are formed, which lead to an inhibited aggregation for medium and large Qz scenarios due to the Il and Gt surface coverage (**Figure S1**).

Variation of Concentration

As third scenario, we varied the solid concentration through changing the porosities to 95, 80, and 50% in the computational domain, equivalent to solid concentrations of 5, 20, and 50%. The composition of the solid phase is again constant with an area fraction of 6% Il_{neg}, 6% Gt, and 88% Qz (small size) within the solid phase (**Figure 4**). Note that now also the small MFMs Gt and Il_{neg} attract each other. We observe that PS increases with higher solid concentration in a non-linear manner. Concentration rises from 5 to 20 to 50% by factors of 4 and 10, respectively, but PS at $t_{1,000}$ rises only from 174 to 372 and 645 (factors of 2.1 and 3.7). Furthermore, **Figure 4** shows a fast initial aggregation for all concentration levels followed by a long transition interval and with fluctuations up to $t_{1,000}$. Again, fluctuations are larger for high PS. The occurring aggregate shapes after 1,000 time steps are also a function of the porosity shown by short chain like and only single bound aggregates (porosity of 95%) over long and branched chains (porosity of 80%) to strongly coiled aggregates (porosity of 50%) (**Figure 5**). We also observed different shapes as function of time which suggest an increasing complexity as well as size of aggregates with ongoing aggregation time.

We also repeated these simulations with 3% Il_{neg}, 3% Gt, and 94% Qz (3/3/94), as well as ratios of 12/12/76, and 24/24/52. In all simulations the succession of the three curves was identical to simulations with 6% Il_{neg}, 6% Gt, and 88% Qz, i.e., the higher the concentrations the larger the aggregate sizes (**Figure 4**). Only the absolute values differed (**Figure S2**). In particular, increasing portions of small oppositely charged Gt lead to increasing PS values in all scenarios. However, this effect scales non-linearly to porosity due to the different number of oppositely charged clay-sized interaction partners that increase faster in number than large particles with decreasing porosities. Hence, they act more efficiently as possible bridges between equally charged MFMs.

DISCUSSION

We can clearly see that the composition of the solid phase (proportions of Qz and Il/Gt) affects the average particle sizes (cf. **Figures 1**, **2**). If Il is considered as net positively charged, Il_{pos} and Gt associate to the oppositely charged Qz surface and permit a bridging between greater Qz spheres. In comparison, if Il is net negatively charged, Gt associates to the oppositely charged II_{neg} and Qz, which results in a bridging due to three different combinations via Gt: Qz-Gt-Il, Il-Gt-Il, and Qz-Gt-Qz. Similar associations are also suggested by completely mixed batch reactor experiment studies due to electrostatic interactions as result of the specific surface charges of interacting compounds (Guhra et al., 2019). Also small Il-Gt-Il aggregates are attached to Qz surfaces (**Figure 2**). We observe clear differences for Il_{neg} and Il_{pos} in PS as function of the composition (c.f. **Figure 1**). However, for an area fraction of ∼10% (Il/Gt), the PS values (896 for Il_{pos}; 761 for Il_{neg}) are in the same magnitude explained by the dominance of bridging via Gt. The observation of the highest PS for Il_{pos} at low portions of approximately 10% Il/Gt fits very well with the observations of Goldberg and Glaubig (1987), reporting that small amounts of Al- or Fe-oxides (net pos. charged) may greatly improve the flocculation of negative charged particles. For higher area fractions of Il_{pos} shielding effects lead to the formation of small aggregates consisting of Gt and Il_{pos} covered Qz spheres. The inhibition of further associations is due to neutralization of the surface charge of Qz as consequence of the association of positively charged particles, if these are present in excess (c.f. **Figure 3**). Ohtsubo et al. (1991) report that positively charged Fe-oxides remain in solution as soon as the negative surface charges of the counterpart are neutralized. Such shielding effects could not be observed for Il_{neg} due to the coexistence of equivalent amounts of positively charged Gt and negatively charged Il particles which permits the association of Gt with Il or Qz over an entire range of different Il/Gt area fractions (except 0%). The size and shape of resulting aggregates have shown to depend on the proportions of oppositely charged particles (**Figure 2**) and are limited by the surface available for association. Consequently, we observe highest PS (c.f. **Figure 1**) for small amounts of bridging particles (Gt and Il_{pos}) which corresponds to a NC of the system around zero. This observation is in line with the study of Bansal et al. (2017), who observe the largest structures arise due to reaching a zeta-potential near zero for the investigated two-component system. They also find formation of different aggregate shapes as function of the mixing fractions of pos. and neg. charged nanoparticles at constant volume fractions which is also shown by our results (**Figure 2**).

We also note that for 0% (in Il_{pos} and Il_{neg}) and 50% (in Il_{pos}) no aggregation occurs in our simulations. As homo-aggregation is limited to very specific conditions like achieving a pH near the PZC or charge neutrality (Tripathy and De, 2006) for single compound systems of minor relevance in nature, we did not include it here. However, this could be changed by assigning a stronger weight to the attraction of likely charged particles. Dale et al. (2015) also state that there is an increasing consensus between modelers and experimentalists that homo-aggregation can be ignored in natural systems due to vast variety of influencing variables like ionic strength, pH and composition of the media, in particular dissolved organic species, as well as the different sizes, shapes and surface coatings of interaction components (Guhra et al., 2019).

Considering the influence of the size ratio of particles on the resulting structures, the simulations demonstrate a huge impact on the compactness of particles, which reaches a stationary state much faster than the average particle size. We found the formation of the largest aggregates if the size of Qz is maximal in scenarios which were characterized by optimal aggregation (**Figure 1**). This is also shown by experimental studies as, e.g., by Yates et al. (2008), who observed a similar effect due to variably sized silica spheres (neg. charged) attaching to Al-oxide (pos. charged) spheres of a constant size. This highlights the importance of the initial size relation between the interacting constituents for *in vitro* and *in silico* aggregation processes.

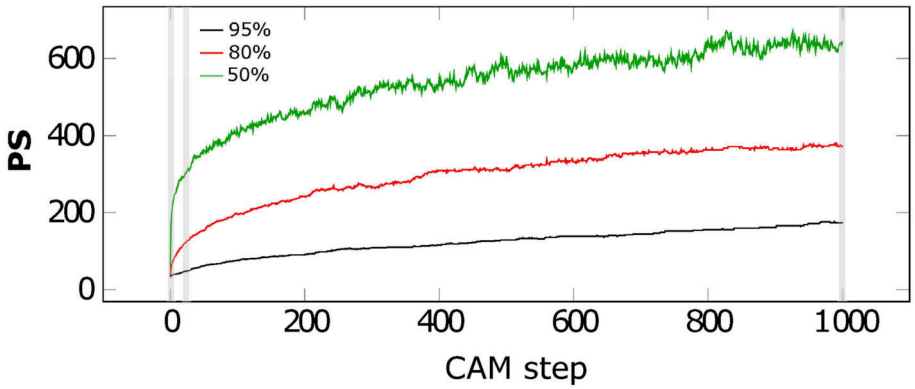

FIGURE 4 | Average particle sizes (PS) over CAM time steps for a composition of 6%Gt/6%Il_{neg}/88%Qz for porosity of 50% (green), 80% (red), and 95% (black). The gray shaded areas correspond to three time steps shown in **Figure 5**.

Additionally, we observe a faster aggregation for small Qz particles in comparison to larger Qz. This is explained by the amount of interacting positive and negative charged particles at constant area fractions of 20%. With increasing size, the number and specific surface area of Qz particles decrease at constant area fractions. Consequently, the interaction distances increase between oppositely charged interaction partners and the small similar charged particles competing each other to find free interaction partners, which decelerate the aggregation process (see **Figure S1**). In our numerical experiments, the increase in Qz size in comparison to Il and Gt corresponds to an increased compactness. This result is also observed in laboratory studies which report higher aggregate compactness if the size difference between the oppositely charged particles (aluminum-silica system) is increased (Cerbelaud et al., 2017). But if we simulate more aggregation unfavorable MFM compositions dominated by previously mentioned shielding effects due to an oversupply of Il and Gt, which force the formation of surface coatings, we limit the formation of greater aggregate structures independent of initial Qz particle size (**Figure S1**). In this case the aggregation is a function of surface coverage (Yates et al., 2005) and scales with the decreasing surface of Qz (in relation to Il and Gt particles) with increasing Qz particle size at fixed (area) fraction of 20% solid.

It is clearly visible that the portion of solid to fluid plays an important role for aggregation. As the interactions for particles are limited to the distance given by the stencil, the long-range interactions are solely driven by random Brownian motion until the particles approach each other (Gregory, 2006). Thus, we observe initially the most rapid aggregation for the model configurations with the lowest porosity and consequently short distances to find and associate to an interaction partner. Comparable concentration effects are typically reported from lab scale if constant boundary conditions are given but increasing initial particle concentrations are used in experiments (He et al., 2008). Additionally, Szilagyi et al. (2014) describe different stages of aggregation as function of time, whereby particle dimers are formed at early stages in comparison to higher order aggregates at later stages, which is supported by the observed sizes and shapes of aggregates formed due to our numerical experiments which are prone to become more complex and increase in aggregate size as function of CAM time steps (**Figure 5**). We also suggest that—although the composition and thus the portion of binding partners is the same—the structures at higher concentrations are not only an extrapolated view of the lower concentrations.

CONCLUSION

Soil is known to contain a vast variety of inorganic and organic MFMs like minerals, rock fragments, microorganisms, viruses, organo-mineral associations, and macro/micro-molecules that are mobilized due to the perturbation of geochemical and hydraulic settings (Ryan and Elimelech, 1996; de Jonge et al., 2004). These particles are hugely different in terms of shape, size, roughness, charge, and many further factors (McCarthy and McKay, 2004; Bin et al., 2011). With this model, we approached this natural diversity by studying a three mineral component system that was successfully used to relate the amount of differently shaped/sized and charged MFMs to the size and the structure of resulting aggregates. It was shown that our model can be used to systematically identify compositions that promote certain structural features and aggregate growth rates that, e.g., largely depend on the number of clay-sized particles. Furthermore, our model clearly reflects how surface properties, as e.g., the surface charge controlled by pH and electric conductivity (Tombácz et al., 2004; Trefalt et al., 2014) as well as the corresponding number of equal and unequal charged MFMs, facilitate the electrostatic interactions and thus the strength and kinetics of aggregation (Goldberg and Glaubig, 1987). Consequently, we obtain an evolution of small and dense structures as a result of increasing shielding effects (surface coating with counter charge MFMs) during a high charge difference between interacting MFMs or dendritic grown large structures for systems with equivalent amounts of oppositely charged MFMs where the net charge of the system tend to

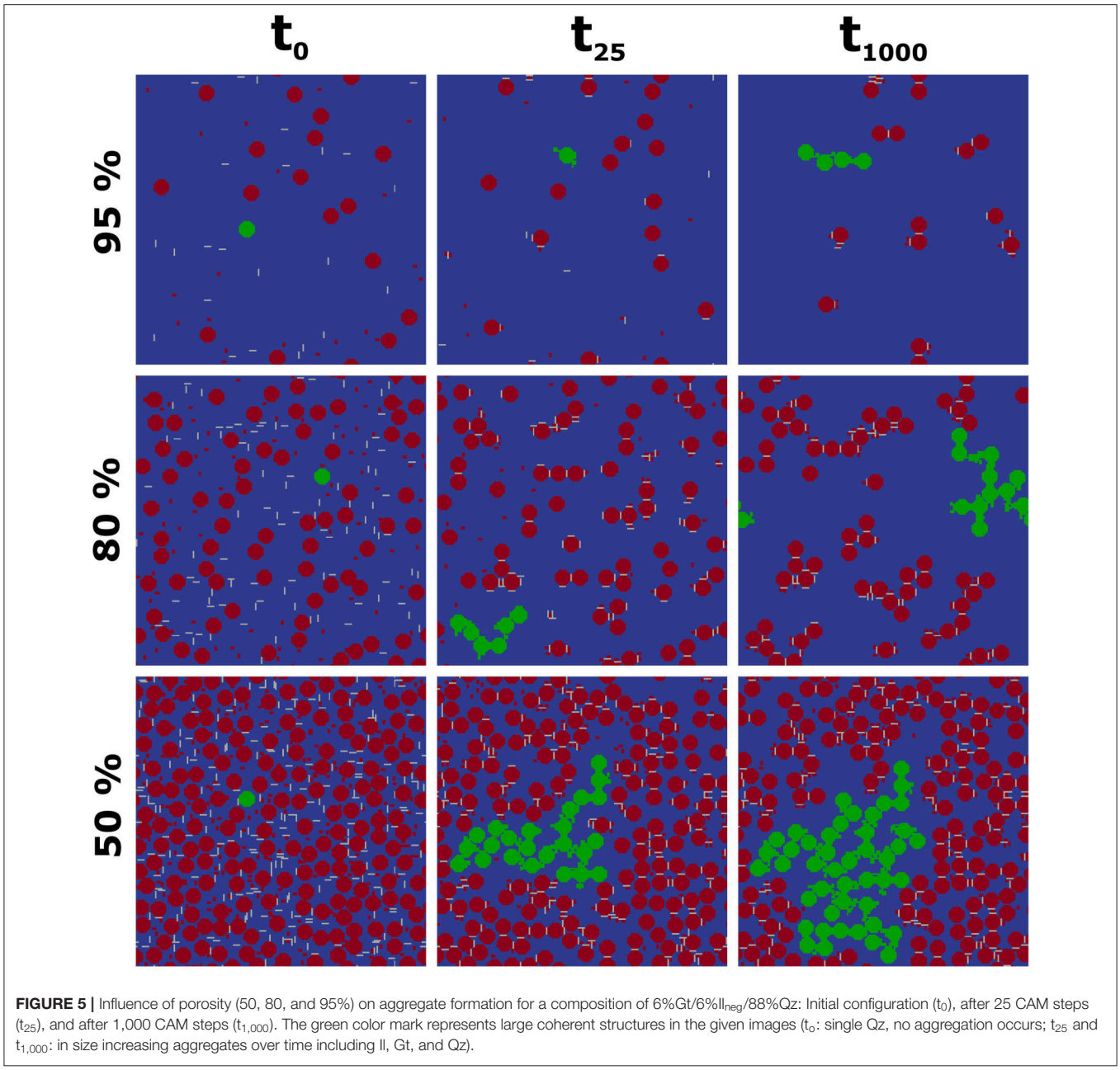

FIGURE 5 | Influence of porosity (50, 80, and 95%) on aggregate formation for a composition of 6%Gt/6%Il_{neg}/88%Qz: Initial configuration (t_0), after 25 CAM steps (t_{25}), and after 1,000 CAM steps ($t_{1,000}$). The green color mark represents large coherent structures in the given images (t_o: single Qz, no aggregation occurs; t_{25} and $t_{1,000}$: in size increasing aggregates over time including Il, Gt, and Qz).

zero. Thus, the surface charge essentially decides on the type of aggregate that is formed. Additionally, the MFM size and especially the size relation between MFMs control how many oppositely charged MFMs are needed to neutralize the surface charge of their interaction partner and how they arrange as aggregates (Yates et al., 2005). As typical boundary conditions found in natural aqueous suspensions readily translate to the model framework, we think that the presented model is a promising tool to investigate the complex spatial and temporal interplay of aggregation mechanisms that is hard to tackle experimentally.

OUTLOOK

Although soil is characterized as a dynamic multi-phase and -component system, it was possible to assess selected processes of aggregation and structure formation by the systematic application of mechanistic 2D CAM. Still, an extension to 3D is implied for more complex scenarios that include organic matter, microbes or a solid pore network. The size, charge, concentration, and the composition of interacting components controlled the aggregation in water-saturated systems and determined the size, shape, amount and assembly of emerging microaggregates.

Consequently, the provided model produces aggregates *in silico* mimicking water saturated systems dominated by hetero-aggregation due to electrostatic interactions. Especially, the net charge of the observed systems has shown to be a valuable measure to assess the rate of aggregation which is also available experimentally with zeta-potential measurements. The similarities found for the modeled aggregates in comparison to aggregates formed in lab-scale environments, encourage the application of mechanistic models to investigate further scenarios, such as the impact of higher diversity of minerals and the interaction with organic matter typically found in soil solutions that require high experimental effort. The application of the model to aggregate formation experiments under precise conditions as Guhra et al. (2019), or Dultz et al. (2019) seems promising and is work under progress. Furthermore, the available methods to upscale morphological information into effective properties of higher scales have the potential to provide a link between the hierarchy of aggregates and the phenomena of flow and transport at the continuum scale in soils. With this, we may further study the path and fate of nutrients and the development of microbial habitats of *in silico* aggregates as surrogates for *in vitro* evolving structures due to morphological analyses of their compactness, size, porosity as well as charges which are important fur microbial attachment. We could also confirm that the timescale of formation is highly relevant considering the transient conditions inside a dynamic system like initial soils, deep soil horizons and ground water systems. Thus, the slow establishment of equilibrium and the different dynamics caused by various size, charge, concentration and the composition of interacting components renders the observation of end members of aggregates also unlikely in natural environments.

DATA AVAILABILITY STATEMENT

The datasets generated for this study are available on request to the corresponding author.

AUTHOR CONTRIBUTIONS

KT perceived the general concept. AR, NR, and AP developed and elaborated the modeling approach. AR and AM performed the simulations. KT, TG, and TR provide the parameter constraints and scenarios for the model runs. AR, NR, and TG wrote the manuscript. All authors carefully reviewed the manuscript.

FUNDING

This research was kindly supported by the DFG RU 2179 MAD Soil - Microaggregates: Formation and turnover of the structural building blocks of soils.

SUPPLEMENTARY MATERIAL

The Supplementary Material for this article can be found online at: https://www.frontiersin.org/articles/10.3389/fenvs.2019.00170/full#supplementary-material

REFERENCES

Bansal, P., Deshpande, A. P., and Basavaraj, M. G. (2017). Hetero-aggregation of oppositely charged nanoparticles. *Colloid Interface Sci.* 492, 92–100. doi: 10.1016/j.jcis.2016.12.059

Bin, G., Cao, X., Dong, Y., Luo, Y., and Ma, L. Q. (2011). Colloid deposition and release in soils and their association with heavy metals. *Crit. Rev. Environ. Sci. Technol.* 41, 336–372. doi: 10.1080/10643380902871464

Blunt, M. J., Bijeljic, B., Dong, H., Gharbi, O., Iglauer, S., Mostaghimi, P., et al. (2013). Pore-scale imaging and modelling. *Adv. Water Resour.* 51, 197–216. doi: 10.1016/j.advwatres.2012.03.003

Bremer, L. G. B., Walstra, P., and van Vliet, T. (1995). Estimations of the aggregation time of various colloidal systems. *Colloids Surf. A* 99, 121–127. doi: 10.1016/0927-7757(95)03159-B

Buffle, J., and Leppard, G. G. (1995). Characterization of aquatic colloids and macromolecules. 1. Structure and behaviour of colloidal material. *Environ. Sci. Technol.* 29, 2169–2175. doi: 10.1021/es00009a004

Cerbelaud, M., Videcoq, A., Rossignol, F., Piechowiak, M. A., Bochicchio, D., and Ferrando, R. (2017). Heteroaggregation of ceramic colloids in suspensions. *Adv. Phys. X* 2, 35–53. doi: 10.1080/23746149.2016.1254064

Cornell, R. M., and Schwertmann, U. (2003). *The Iron Oxides*. Weinheim: WILEY VCH Verlag.

Crawford, J., Deacon, L., Grinev, D., Harris, J., Ritz, K., Singh, B., et al. (2012). Microbial diversity affects self-organization of the soil - microbe system with consequences for function. *J. R. Soc.* Interface 9, 1302–1310. doi: 10.1098/rsif.2011.0679

Dale, A. L., Casman, E. A., Lowry, G. V., Lead, J. R., Viparelli, E., and Baalousha, M. (2015). Modeling nanomaterial environmental fate in aquatic systems. *Environ. Sci. Technol.* 49, 2587–2593. doi: 10.1021/es505076w

de Jonge, L. W., Kjaergaard, C., and Moldrup, P. (2004). Colloids and colloid-facilitated transport of contaminants in soils. *Vadose Zone J.* 3, 321–325. doi: 10.2113/3.2.321

Dultz, S., Woche, S. K., Mikutta, R., Schrapel, M., and Guggenberger, G. (2019). Size and charge constraints in microaggregation: model experiments with mineral particle size fractions. *Appl. Clay Sci.* 170, 29–40. doi: 10.1016/j.clay.2019.01.002

Fermin, D., and Riley, J. (2010). "Charge in colloidal systems," in *Colloid Science Principles, Methods and Applications*, ed T. Cosgrove (Chichester, UK: John Wiley & Sons), 45–59.

Goldberg, S., and Glaubig, R. A. (1987). Effect of saturating cation, pH, and aluminium and iron oxide on the flocculation of kaolinite and montmorillonite. *Clays Clay Miner.* 3, 220–227. doi: 10.1346/CCMN.1987.0350308

Gregory, J. (2006). *Particles in Water: Properties and Processes*. Boca Raton, FL: CRC Press.

Guhra, T., Ritschel, T., and Totsche, K. U. (2019). Formation of mineral-mineral and organo-mineral composite building units from microaggregate-forming materials including microbially produced extracellular polymeric substances. *Eur. J. Soil Sci.* 70, 604–615. doi: 10.1111/ejss.12774

He, Y. H., Wan, J., and Tokunaga, T. (2008). Kinetic stability of hematite nanoparticles: the effect of particle sizes. *J. Nanopart. Res.* 10, 321–332. doi: 10.1007/s11051-007-9255-1

Kosmulski, M. (2011). The pH-dependent surface charging and points of zero charge V. Update. *J. Colloid Interf. Sci.* 353, 1–15. doi: 10.1016/j.jcis.2010.08.023

McCarthy, J. F., and McKay, L. D. (2004). Colloid transport in the subsurface: past, present, and future challenges. *Vadose Zone J.* 3, 326–337. doi: 10.2113/3.2.326

Ohtsubo, M., Yoshimura, A., Wada, S.-I., and Yong, R. N. (1991). Particle interaction and rheology of illite-iron oxide complexes. *Clays Clay Miner.* 39, 347–354. doi: 10.1346/CCMN.1991.0390402

Portell, X., Pot, V., Garnier, P., Otten, W., and Baveye, P. C. (2018). Microscale heterogeneity of the spatial distribution of organic matter can promote bacterial biodiversity in soils: insights from computer simulations. *Front. Microbiol.* 9:1583. doi: 10.3389/fmicb.2018.01583

Ray, N., Rupp, A., and Prechtel, A. (2017). Discrete-continuum multiscale model for transport, biomass development and solid restructuring in porous media. *Adv. Water Resour.* 107, 393–404. doi: 10.1016/j.advwatres.2017.04.001

Ray, N., Rupp, A., Schulz, R., and Knabner, P. (2018). Old and new approaches predicting the diffusion in porous media. *Transp. Porous Med.* 124, 803–824. doi: 10.1007/s11242-018-1099-x

Ritschel, T., and Totsche, K. U. (2019). Modeling the formation of soil microaggregates. *Comput. Geosci.* 127, 36–43. doi: 10.1016/j.cageo.2019.02.010

Rupp, A. (2019). *Simulating structure formation in soils across scales using discontinuous Galerkin methods* (Ph.D. Thesis). Germany: Shaker, Düren.

Rupp, A., Totsche, K. U., Prechtel, A., and Ray, N. (2018). Discrete-continuum multiphase model for structure formation in soils including electrostatic effects. *Front. Environ. Sci.* 6:96. doi: 10.3389/fenvs.2018.00096

Ryan, J. N., and Elimelech, M. (1996). Colloid mobilization and transport in groundwater. *Colloids Surf. A.* 107, 1–56. doi: 10.1016/0927-7757(95)03384-X

Schulz, R., Ray, N., Zech, S., Rupp, A., and Knabner, P. (2019). Beyond Kozeny–Carman: predicting the permeability in porous media. *Transp. Porous Med.* 130, 487–512. doi: 10.1007/s11242-019-01321-y

Segoli, M., De Gryze, S., Dou, F., Lee, J., Post, W. M., Denef, K., et al. (2013). AggModel: a soil organic matter model with measurable pools for use in incubation studies. *Ecol. Model.* 263, 1–9. doi: 10.1016/j.ecolmodel.2013.04.010

Six, J., Bossuyt, H., Degryze, S., and Denef, K. (2004). A history of research on the link between (micro)aggregates, soil biota, and soil organic matter dynamics. *Soil Till. Res.* 79, 7–31. doi: 10.1016/j.still.2004.03.008

Stamati, F. E., Nikolaidis, N. P., Banwart, S., and Blum, W. E. H. (2013). A coupled carbon, aggregation, and structure turnover (CAST) model for topsoils. *Geoderma* 211–212, 51–64. doi: 10.1016/j.geoderma.2013.06.014

Szilagyi, I., Szabo, T., Desert, A., Trefalt, G., Oncsik, T., and Borkovec, M. (2014). Particle aggregation mechanisms in ionic liquids. *Phys. Chem. Chem. Phys.* 16, 9515–9524. doi: 10.1039/C4CP00804A

Tang, Y., and Valocchi, A. (2013). An improved cellular automaton method to model multispecies biofilms. *Water Res.* 47, 5729–5742. doi: 10.1016/j.watres.2013.06.055

Tang, Y., Valocchi, A., Werth, C., and Liu, H. (2013). An improved pore-scale biofilm model and comparison with a microfluidic flow cell experiment. *Water Resour. Res.* 49, 8370–8382. doi: 10.1002/2013WR013843

Tisdall, J. M., and Oades, J. M. (1982). Organic matter and water-stable aggregates in soils. *J. Soil Sci.* 33, 141–163. doi: 10.1111/j.1365-2389.1982.tb01755.x

Tombácz, E., Casanky, C., and Illés, E. (2001). Polydisperse fractal aggregate formation in clay mineral and iron oxide suspensions, pH and ionic strength dependence. *Colloid Polym. Sci.* 279, 484–492. doi: 10.1007/s003960100480

Tombácz, E., Libor, Z., Illés, E., Majzik, A., and Klumpp, E. (2004). The role of reactive surface sites and complexation by humic acids in the interaction of clay mineral and iron oxide particles. *Org. Geochem.* 35, 257–267. doi: 10.1016/j.orggeochem.2003.11.002

Tombácz, E., and Szekeres, M. (2006). Surface charge heterogeneity of kaolinite in aqueous suspension in comparison with montmorillonite. *Appl. Clay Sci.* 34, 105–124. doi: 10.1016/j.clay.2006.05.009

Totsche, K. U., Amelung, W., Gerzabek, M. H., Guggenberger, G., Klumpp, E., Knief, C., et al. (2018). Microaggregates in soils. *J. Plant Nutr. Soil Sci.* 181, 104–136. doi: 10.1002/jpln.201600451

Totsche, K. U., Rennert, T., Gerzabek, M. H., Kögel-Knabner, I., Smalla, K., Spiteller, M., et al. (2010). Biogeochemical interfaces in soil: the interdisciplinary challenge for soil science. *J. Plant Nutr. Soil Sci.* 173, 88–99. doi: 10.1002/jpln.200900105

Trefalt, G., Ruiz-Cabello, F. J. M., and Borkovec, M. (2014). Interaction forces, heteroaggregation, and deposition involving charged colloidal particles. *J. Phys. Chem. B* 118, 6346–6355. doi: 10.1021/jp503564p

Tripathy, T., and De, B. R. (2006). Flocculation: a new way to treat the waste water. *J. Phys. Sci.* 10, 93–127.

Yates, P. D., Franks, G. V., Biggs, S., and Jameson, G. J. (2005). Heteroaggregation with nanoparticles: effect of particle size ratio on optimum particle dose. *Colloids Surf. A* 255, 85–90. doi: 10.1016/j.colsurfa.2004.12.035

Yates, P. D., Franks, G. V., and Jameson, G. J. (2008). Orthokinetic heteroaggregation with nanoparticles: effect of particlesize ratio on aggregate properties. *Colloids Surf. A* 326, 83–91. doi: 10.1016/j.colsurfa.2008.05.030

Conflict of Interest: The authors declare that the research was conducted in the absence of any commercial or financial relationships that could be construed as a potential conflict of interest.

Copyright © 2019 Rupp, Guhra, Meier, Prechtel, Ritschel, Ray and Totsche. This is an open-access article distributed under the terms of the Creative Commons Attribution License (CC BY). The use, distribution or reproduction in other forums is permitted, provided the original author(s) and the copyright owner(s) are credited and that the original publication in this journal is cited, in accordance with accepted academic practice. No use, distribution or reproduction is permitted which does not comply with these terms.

Supplementary Material

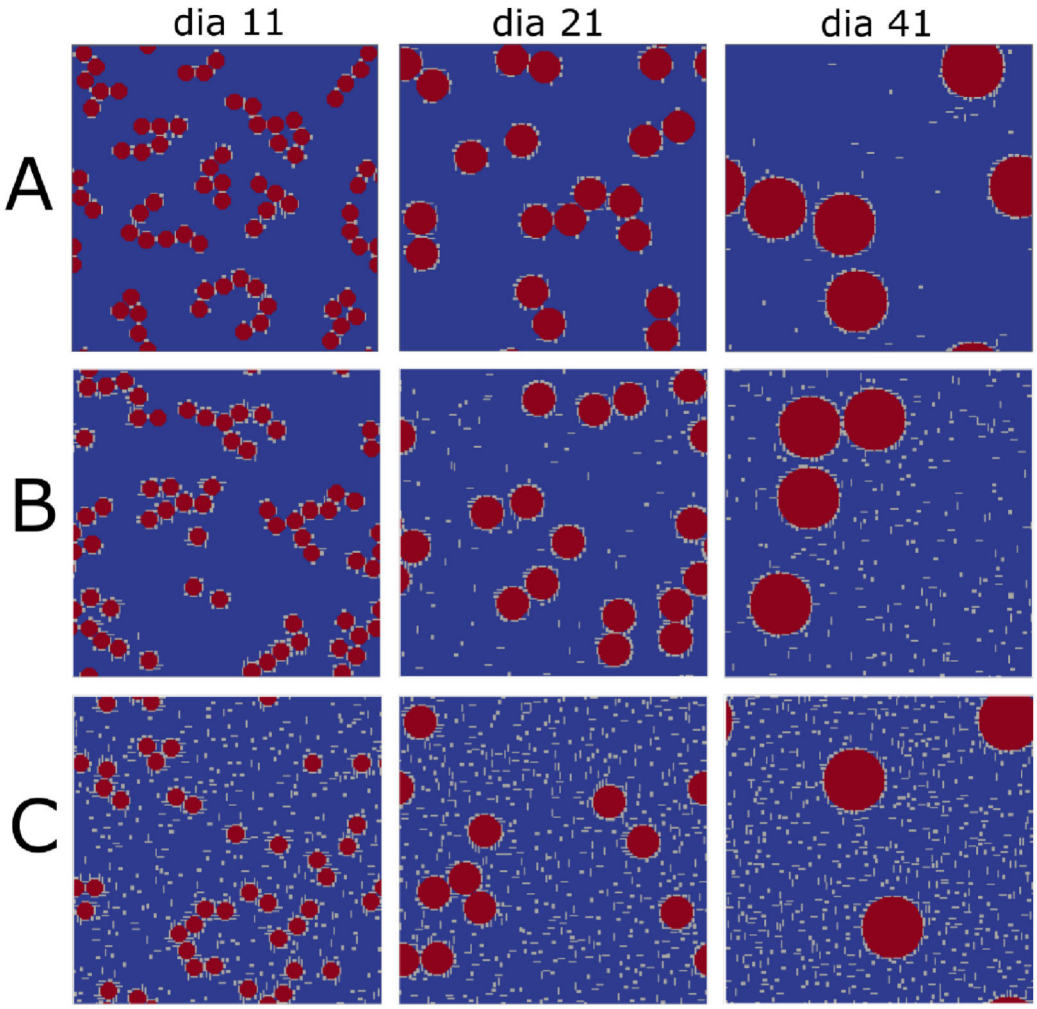

Supplementary Figure S1: Exemplary configuration after 1000 steps for small (diameter: 11), medium (diameter: 21) and large (diameter: 41) Qz (red MFMs). The initial conditions were set to an area fraction of 20% and a composition of 6% Gt, 6% Il_{pos} and 88% Qz (A), 12% Gt, 12% Il_{pos} and 76% Qz (B) as well as 24% Gt, 24% Il_{pos} and 52% Qz (C). This figure supplements Fig. 3 of the original article and compares different compositions of minerals according to scenario 2.

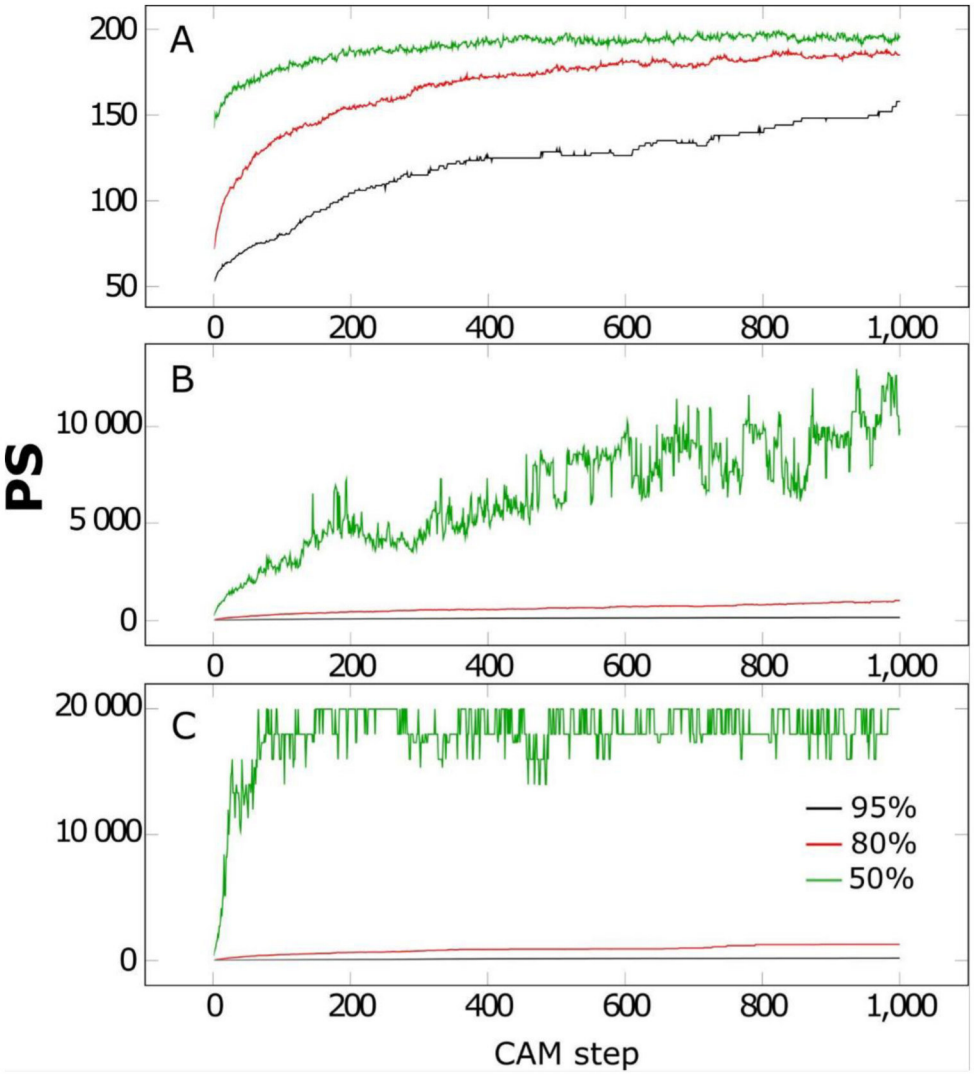

Supplementary Figure S2: Average particle sizes (PS) for CBUs plotted as function of time for a porosity of 50% (green), 80% (red) and 95% (black) at compositions of 3% Gt, 3% Il_{neg} and 94% Qz (A), 12% Gt, 12% Il_{neg} and 76% Qz (B) as well as 24% Gt, 24% Il_{neg} and 52% Qz (C). This figure extends Fig. 4 (6% Gt, 6% Il_{neg} 88% Qz) of the original article for other compositions: Note that in these scenarios Illite is negatively charged and thus is also attracted by Gt. This leads to large PS values for growing amounts of small particles (subfigures B and C, compared to A and Fig. 4).

2.5. Publication 5 (P_V): The mechanisms of gravity-constrained aggregation in natural colloidal suspensions

Citation: Guhra, T., Ritschel, T. and Totsche, K.U. 2021. The mechanisms of gravity-constrained aggregation in natural colloidal suspensions. *Journal of colloid and interface science*, 597, 126-136.

DOI: 10.1016/j.jcis.2021.03.153

Rights and licensing: All (co-)authors agree that this article is permitted to be used in the dissertation presented here. This article is published under the terms of the creative commons CC BY-NC-ND license. Authors of this article retain the right to include it in a thesis or dissertation, provided it is not published commercially. The journal as the original source of the article is referenced above.

Authors: Tom Guhra[1], Thomas Ritschel[2] and Kai Uwe Totsche[3]

P_V			
involved in:	**Author**		
	1	**2**	**3**
conception of research design		X	X
planning of research activities	X	X	X
data acquisition	X	X	
data analyses and interpretation	X	X	X
manuscript writing	X	X	X
suggested publication equivalence value	**1.0**		

Journal of Colloid and Interface Science 597 (2021) 126–136

Contents lists available at ScienceDirect

Journal of Colloid and Interface Science

journal homepage: www.elsevier.com/locate/jcis

Regular Article

The mechanisms of gravity-constrained aggregation in natural colloidal suspensions

Tom Guhra, Thomas Ritschel, Kai Uwe Totsche *

Department of Hydrogeology, Institute of Geosciences, Friedrich Schiller University Jena, 07749, Germany

GRAPHICAL ABSTRACT

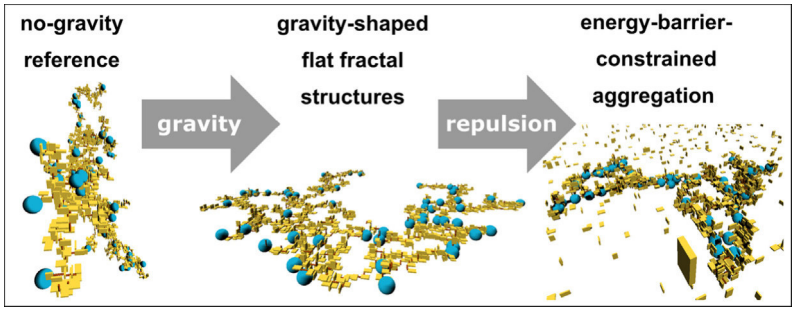

ARTICLE INFO

Article history:
Received 15 December 2020
Revised 26 February 2021
Accepted 26 March 2021
Available online 29 March 2021

Keywords:
pH
Stochastic model
Derjaguin-Landau-Verwey-Overbeek (DLVO) theory
Visualization tool
Hierarchic structures
Fractal dimension
Graphical user interface (GUI)

ABSTRACT

Colloidal settlement in natural aqueous suspensions is effectively compensated by diffusive movement if particles resist aggregation – a state known as colloidal stability. However, if the settling velocity increases upon aggregation, complex structural features emerge from the directional movement induced by gravity. We present a comprehensive modeling study on the evolution of an aggregated three-dimensional structure due to diffusion, surface interactions, and gravity. The systematic investigation of particle geometry and size revealed three mechanisms: (I) aggregation due to spatial confinement of settled particles, (II) aggregation due to differential settling, whereby fast and slow particles collide, (III) inhibition of aggregation due to fractionation of particles with different settling velocity. A 3D visualization tool allowed us to follow the subtle interplay of these mechanisms and the highly dynamic hierarchical self-assembly of aggregates. It revealed how the balance of the different interactions determines the actual rate of aggregation.

© 2021 The Author(s). Published by Elsevier Inc. This is an open access article under the CC BY-NC-ND license (http://creativecommons.org/licenses/by-nc-nd/4.0/).

1. Introduction

Among the fundamental physical forces, gravity is by far the weakest with a relative strength nearly 40 orders of magnitude lower than electromagnetism. Unlike electric charges that are usually compensated by the same number of opposing charges at a scale above nanometers, gravity cannot be shielded and reaches out infinitely into space. Consequently, distant interactions are dominated by gravity, while electromagnetism mainly controls local chemical processes. Therefore, the interactions between reactive surfaces of colloidal particles are frequently described without gravity, and, e.g., the tendency of soil-borne particles to form aggregates is commonly discussed solely in terms of their surface properties [1-6]. However, the evolution of an aggregated structure also requires transport mechanisms to bring particles into contact. At a small scale, diffusion is the driving force of the so-called

* Corresponding author at: Department of Hydrogeology Institute of Geosciences Friedrich Schiller University Jena, Burgweg 11, 07749 Jena, Germany.
E-mail address: kai.totsche@uni-jena.de (K.U. Totsche).

https://doi.org/10.1016/j.jcis.2021.03.153
0021-9797/© 2021 The Author(s). Published by Elsevier Inc.
This is an open access article under the CC BY-NC-ND license (http://creativecommons.org/licenses/by-nc-nd/4.0/).

perikinetic aggregation and leads to a "self-assembly" of particles [7,8]. In colloidal and material sciences, this self-organization is exploited to produce nanostructures with desired properties by changing particle composition, size, and shape [6,9,10] at different hierarchical levels [11-13]. In particular the work by Witten, Sander [14], and Meakin [8,15] provided a fundamental mechanistic framework on the fractal growth universally observed in perikinetic colloidal aggregation [7]. These ideas have been developed and extended intensely over the last decades [16-18], leading to a variety of diffusion-limited aggregation models including the simultaneous growth in cluster–cluster aggregation, and the combination with population balance equations [19,20]. However, less attention has been paid to gravity as its effect are supposedly negligible for small colloids [21], and sedimentation has been discussed controversially in colloidal sciences [22]. This is partly caused by the requirement of a "no-gravity-reference" for comparison, which is hard to achieve experimentally and extraordinarily expensive, e.g., on the international space station (informal experiments) [23] and on free-fall flights. Nonetheless, aggregated colloids easily exceed the sub-micrometer range and are susceptible to settling [24], as revealed by several experimental [23,25-27] as well as theoretical studies [28-30]. In particular, the work by Dukhin et al. (2007) [31] on the influence of gravity on the aggregation of colloidal suspensions provided an overview of the major controls and mechanisms behind gravity-driven aggregation. So far, the primary focus has been on the effect of gravity on aggregation rates [32], and not on how an explicit three-dimensional structure is formed in response to the subtle interplay of electrostatics, Brownian motion, and sedimentation. As shown by recent discussions about the involved mechanisms [33], such a framework is particularly required to understand the evolution of soil microaggregates, whose structure controls their stability, their function as microbial habitat, and their ability to store and turnover nutrients and contaminants. To this date, the numerical models used to simulate soil aggregate formation build on approaches from colloid and polymer sciences [34,35] using cellular automatons [36,37] and diffusion-limited aggregation [38], yet they do not consider gravity.

To fundamentally explore gravity's impact on aggregation, we developed a modeling framework that anneals diffusion-limited aggregation [38] with sedimentation. We performed a systematic analysis of aggregate formation and kinetics due to gravity compared to a no-gravity-reference. Furthermore, visualization helps to develop an understanding of the complex feedback and dynamics of self-organization, as, e.g., reported by Tateno and Tanaka (2019) [13] for congeneric colloids. Thus, we augmented the model with a real-time visualization and exploration tool to disentangle the gravity-driven aggregation dynamics and to derive a classification scheme of the involved mechanisms.

2. Material and methods

2.1. Model development

We decided to use a spatially discrete equidistant cubic grid with cell size Δx for a numerical implementation that allows for stochastic Brownian movement and DLVO-type surface interactions. The model represents primary particle geometries (spheres, rods, and plates) as mineral prototypes. These prototypes are defined by their surface potential, Hamaker constant, and shape in terms of the number of occupied cells and the grid cell length. Diffusion is represented by a random walk of clusters and particles on the grid. Applying the central limit theorem to the random walk yields the following relation of the discrete diffusive time step Δt_d, spatial step Δx, and diffusion coefficient [39]:

$$\Delta t_d = \frac{2pq\Delta x^2}{D_{max}} \tag{1}$$

where p and q are the probabilities of movement in forward or backward direction, and D_{max} is the largest diffusion coefficient expressed by one of the clusters. Upon contact, we used the DLVO theory to balance van der Waals attraction and electrostatic interactions – that may be attractive or repulsive depending on the sign of the surface potential – in order to derive the total energy of interaction [40,41]. Each primary particle shape follows a distinct geometry/energy relationship as detailed in Ritschel & Totsche (2019) [38]. Total interactions energies were used to calculate the energy barrier ΔE and the chance of attachment according to $\kappa h_{min}\exp(-\frac{\Delta E}{k_B T})$, where κ is the inverse Debye length, h_{min} is the minimal distance between the center of masses of attaching particles, k_B is the Boltzmann constant, and T is the temperature [40]. Hence, aggregation is controlled by diffusive transport as well as attachment, both modeled in a non-deterministic manner that reveals the three-dimensional spatial arrangement of primary particles inside the aggregates.

In addition, the known hydrodynamic radii r_h and cluster volumes V allowed us to model sedimentation by a balance of forces due to gravity F_g, buoyancy F_b, and drag F_d [25]:

$$F_g = \rho_p V g \tag{2a}$$

$$F_b = \rho_f V g \tag{2b}$$

$$F_d = 6\pi r_h \mu v_s \tag{2c}$$

Here, ρ_p is the density of the primary particles which – in accordance to the mean density of soil minerals – we set equal to 2.65 g cm^{-3}, ρ_f is the fluid density equal to 1 g cm^{-3}, μ is the dynamic viscosity of the fluid equal to 1 g m^{-1} s^{-1}, g is the gravitational acceleration, and v_s is the sedimentation velocity. A rearrangement towards v_s assuming $F_d = F_g - F_b$ then yields

$$v_s = \frac{(\rho_p - \rho_f)Vg}{6\pi r_h \mu} \tag{3}$$

The cluster volume was calculated as $V = n\Delta x^3$ with n being the number of grid cells occupied by the cluster. To save computation time, the time step was adaptively adjusted to allow exactly one grid cell transition for the fastest cluster. The largest time step allowed by sedimentation is given as $\Delta t_s = \frac{\Delta x}{v_s^{max}}$, where v_s^{max} is the largest sedimentation velocity of all clusters. To ensure also the constraint given by equation (1), the smallest time step was used in the simulation according to $\Delta t = \min(\Delta t_s, \Delta t_d)$. An appropriate implementation of a non-discrete velocity that only occasionally results in exactly one cell transition on the regular cubic grid requires a stochastic approach to represent the expected value of v_s appropriately. Hence, the aggregate is translocated one grid-cell in downward direction when a uniform random draw in [0,1] is smaller than $\frac{v_s \Delta t}{\Delta x}$.

We condensed the spatio-temporal evolution of the various variables into three significant characteristics, which we calculated as mass-weighted means of all aggregates and primary particles at each time step:

(1) the mass represented by the volume of the aggregate,
(2) the radius of gyration calculated according to

$$r_g = \sqrt{\frac{1}{n}\sum_i (r_i - r_0)^2} \tag{4}$$

where $r_i - r_0$ is the distance between grid cells i belonging to the cluster and the center of mass r_0,

(3) the fractal dimension calculated using the box-counting algorithm [42].

The balance between gravity and diffusion was calculated as the Péclet number [43] using the mean hydrodynamic radius:

$$Pé = \frac{v_s L}{D} = \frac{(\rho_p - \rho_f) V g L}{k_B T}, \quad (5)$$

where L is the characteristic length taken as the aggregate radius. The diffusion coefficient D is calculated with the Stokes-Einstein equation [40]

$$D = \frac{k_B T}{6\pi r_h \mu}. \quad (6)$$

To derive aggregation rates, we modeled the number of remaining free, i.e., non-aggregated primary particles n_i by a simplified form of Smoluchowskis coagulation equation [40]. Since primary particles cannot be formed by aggregation, the production term can be ignored, and Smoluchowskis coagulation equation reduces to

$$\frac{\partial n_i}{\partial t} = -\sum_j K_{ij} n_i n_j \ (i,j \text{ are spheres, rods, plates}), \quad (7)$$

where K_{ij} is the aggregation rate between particles of type i and j and n_j is the number of potential aggregation partners of type j. However, particularly scenarios with sedimentation showed an aggregation behavior with two stages that necessitate the introduction of two particle fractions with separate aggregation rates. We decided to refer to the initial aggregation stage as the α-stage that is followed by a second β-stage. With this modification, equation (7) now reads

$$\frac{\partial n_i^\alpha}{\partial t} = -\sum_j K_{ij}^\alpha n_i^\alpha n_j \quad (8a)$$

$$\frac{\partial n_i^\beta}{\partial t} = -\sum_j K_{ij}^\beta n_i^\beta n_j \quad (8b)$$

$$f_i n_i = n_i^\alpha \quad (8c)$$

$$(1 - f_i) n_i = n_i^\beta \quad (8d)$$

where $f_i \in [0,1]$ is the initial fraction of particles aggregating in the α-stage, K_{ij}^α is the aggregation rate of the α-stage and K_{ij}^β is the aggregation rate of the β-stage between particles of type i and j. These parameters were fitted using the Levenberg-Marquardt [44] algorithm applied to the modeled number of free particles in each scenario.

Each basic geometry was adjusted in size and surface properties to represent a mineral class typically found in soils, i.e., weathered silicates with spherical shape, secondary clay minerals with platy shape, and pedogenic iron oxides with a rod-like shape in analogy to Ritschel & Totsche (2019) [38]. The Hamaker constant represents the strength of van-der-Waals forces interactions between the primary particles according to the mineral analogues [45-47]. The sizes of the primary particle types were set according to the grid cell length Δx in a mesh of 500x500x500 grid cells (Table 1). We simulated a monovalent 1 mM NaCl background solution containing 1500 (plates), 500 (rods), and 50 (spheres). The resulting modeling domain had a solid/liquid volume ratio of 0.0005, which is in the range of experimental and natural reference systems [48].

Notably, each model run will differ in its trajectories of diffusion and realized attachments in case of energy barriers due to the stochastic nature of the algorithm. Furthermore, particles were initialized randomly over the entire computational grid regarding position as well as rotational conformation. Hence, we computed three model runs to calculate the mean and standard deviation of all results produced by the model. As a consequence of the ongoing aggregation, the number of separate objects decreases throughout the model runs and the sample population from which we calculate the mean radius of gyration and fractal dimension is getting smaller. Due to the randomness of the structural conformations, meaningful averaging requires a large sample population. Consequently, we stopped the simulations once the number of separate objects decreased to 20 (approximately 1% of the initial number of objects).

Table 1
Mineral prototype (plate, rod and sphere) dimension (h = height; l = length; b = broadness; ø = diameter), Hamaker constant, zeta potentials as function of the pH (3, 6 and 9) and Péclet number as function of grid size (Δx: 0.075, 0.15 and 0.3 μm).

	plate	rod	sphere
	Size (grid cells)		
	h × l × b = 1 × 6 × 4	l × ø=6 × 1	ø =10
	Hamaker constant (J)		
	[a] 2.5 x 10^{-20}	[b] 2.29 x 10^{-20}	[c] 1.02 x 10^{-20}
pH	**Zeta potential (mV)**		
3	−25	+27.5	+2.5
6	−40	+12.5	−12.5
9	−55	−2.5	−27.5
Grid size [μm]	**Péclet number**		
0.075	0.010	0.0022	0.42
0.15	0.17	0.035	6.8
0.3	2.7	0.56	109

[a] according to Novich and Ring (1984)
[b] according to Xu et al. (2015)
[c] according to Bergström (1997)

We analysed the aggregation dynamics as a function of the strength of gravity and surface interactions with the following simulation sets.

2.2. Simulation set "gravity series":

We conducted two aggregation scenarios: diffusion with gravity (+G) and diffusion only (-G). We explored the importance of gravity by analyzing the critical transition between Brownian and Brownian-gravitational aggregation for spherical primary particles at the upper limit of the size of colloids and clays [3,31]. Specifically, we modeled spheres above and below 1–2 μm by using grid cell sizes of Δx = 0.3 μm ($S_{0.3}$), Δx = 0.15 μm ($S_{0.15}$), and Δx = 0.0 75 μm ($S_{0.075}$), that result in spheres with a diameter of 3 μm, 1.5 μm, and 0.75 μm, respectively. By changing the grid cell size instead of the number of occupied grid cells, the influence of gravity was changed while all particle shapes and the mass ratio of primary particles remained constant. Nonetheless, the initial Péclet number increased by the fourth power of the relative spatial change (cf. equation (5) where V and L are affected). The time corresponding to one simulation step also relates to the spatial scale via the diffusion coefficient. Thus, for each scenario, we simulated a separate, gravity-free reference. Noteworthy, the strength of surface interactions and, in turn, the aggregation kinetics are affected by the changes in the charge density and the reach of the van-der-Waals forces, which also scale with particle size.

2.3. Simulation set "pH series":

We explored the aggregation at different pH-dependent surface potentials that are expected for the mineral prototypes at pH values of 3, 6, and 9 for Δx = 0.075 μm ($S_{0.075}$). These scenarios refer to an overall attractive situation (S_{pH3}), a situation controlled by a "bridging agent" (S_{pH6}), and a situation with considerable energy

barriers between the bridging agent and further particles (S_{pH9}). We assigned distinct isoelectric points (IEP) to the three mineral prototypes to represent pH dependent interactions by corresponding surface potentials. Specifically, we selected an IEP of 3.5 for the spherical mineral prototype typical for tectosilicates like quartz [49]. The platy structures are chosen to have strong negative charge (-20 mV) even at pH = 2, as typically reported for clay minerals [27,50]. The rod-like prototypes (IEP: 8.5) are inspired by secondary Fe-oxides which are characterized by high IEP around 5.5–9.7 [27,49]. For intercomparability between the scenarios, we used surface potentials (Table 1) that we determined by linear extrapolations of the surface potential as a function of the pH (Figure S1).

3. Results and discussion

3.1. General classification of aggregation dynamics

3.1.1. Gravity series

In our numerical simulations, the susceptibility of colloidal suspensions to sedimentation largely depends on the particle size that directly follows from the different cell sizes of the numerical grid (Fig. 1). With increasing size, the movement of colloids becomes increasingly dominated by gravity. This is indicated by the corresponding Péclet numbers of the single mineral prototypes (Table 1). We found initial Péclet numbers above unity for plates and spheres in $S_{0.3}$ and only for spheres in $S_{0.15}$, whereas rods start with the diffusion-dominated movement in all three scenarios as well as all particles in scenario $S_{0.075}$ and plates in $S_{0.15}$. However, due to the proceeding aggregation of particles, the aggregate size increases for all scenarios. Gravity gets more effective as shown by a gradual increase of the Péclet numbers over time [51] (cf. Figure S2). Consequently, scenario $S_{0.3}$ is governed by sedimentation from the very beginning, while $S_{0.15}$ and $S_{0.075}$ exhibit a transition from diffusion- to gravity-dominated regimes once the size of the aggregates approaches 1 μm. This reflects the critical transition between Brownian and Brownian-gravitational aggregation [3]. In the long term, all simulations converge to a state where all particles and aggregates are settled.

No homo-aggregation was found in the gravity series due to high energy barriers between particles of equal type (Table S1). In all cases, the positive charge of rods constitutes their role as bridging agent between negatively charged plates and spheres. Hence, the probability of collision with rods controls the growth rate of aggregates.

In terms of aggregate mass, radius of gyration, and fractal dimension (Fig. 2), the aggregation dynamics are similar to the gravity-free reference scenarios (-G) in the first 50 to 100 s. During this stage, more time is required to overcome the initial distances between particles before any effect of gravity emerges. After that, the aggregation dynamics diverged compared to the reference situation and between the different size scenarios.

3.1.2. pH series

In analogy to the gravity series, rods always act as a bridging agent, independent of the pH range. This agrees with experimental observations of, e.g., Goldberg and Glaubig (1987) [52]. They report that small numbers of Al- or Fe-oxides may significantly promote the flocculation of negatively charged particles. However, in the

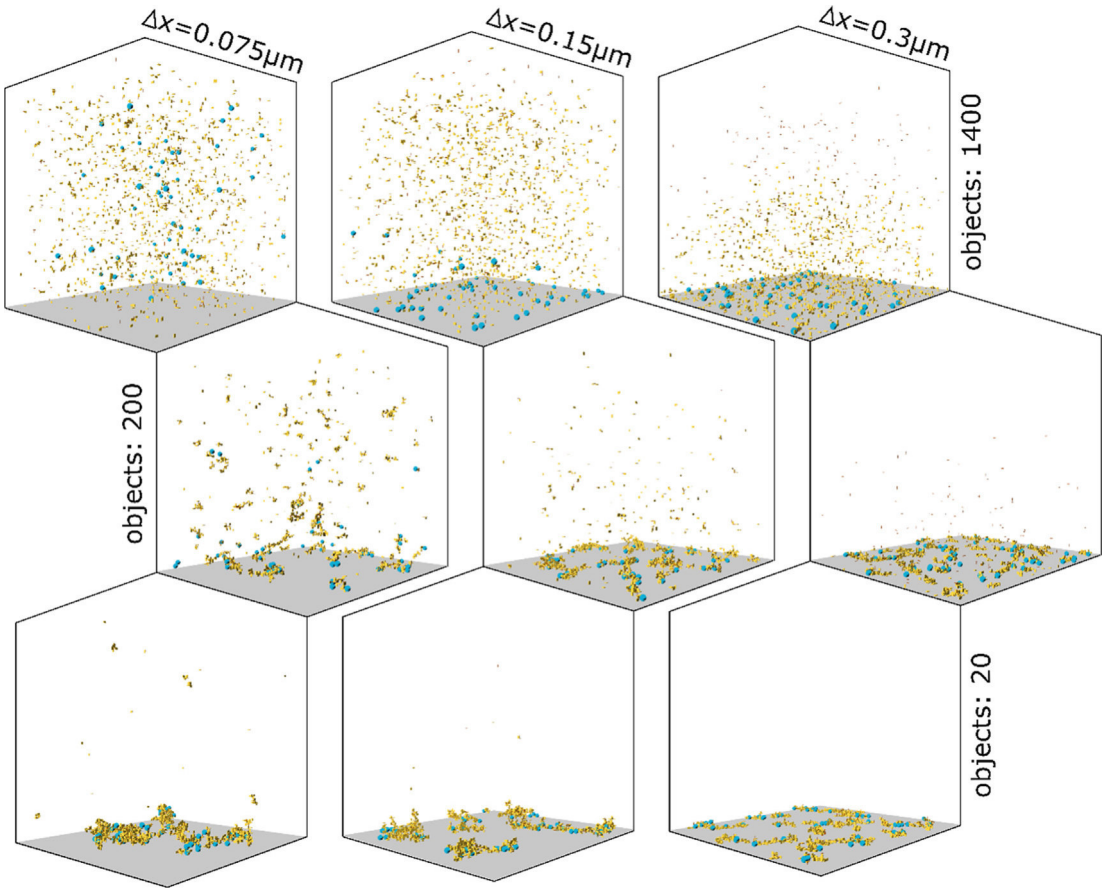

Fig. 1. Snapshots of the modeling domain of 500x500x500 cells for Δx = 0.075 μm ($S_{0.075}$), 0.15 μm ($S_{0.15}$) and 0.3 μm ($S_{0.3}$) for simulations progressed to 1400, 200 and 20 objects, respectively.

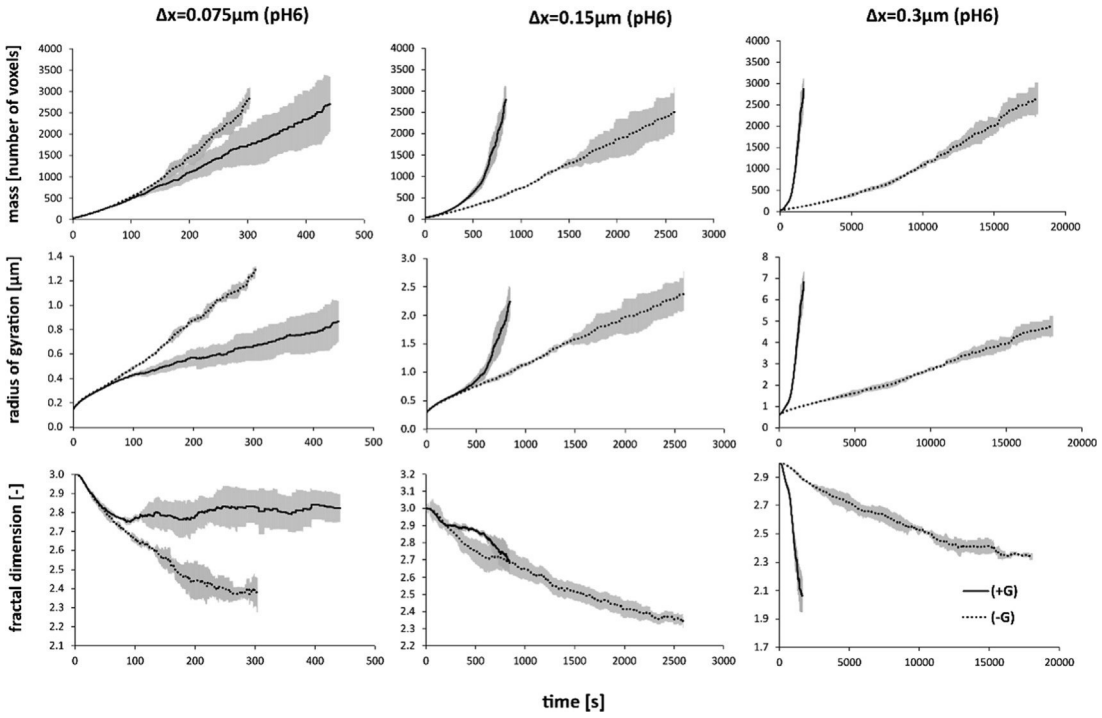

Fig. 2. Temporal development of the mean aggregate mass, radius of gyration, and fractal dimension for gravity-impacted (+G) and gravity-free (-G) scenarios with different particle sizes Δx = 0.075 µm ($S_{0.075}$), 0.15 µm ($S_{0.15}$) and 0.3 µm ($S_{0.3}$) until the number of 20 objects is reached. The standard deviation was calculated for n = 3 (grey shaded error bar).

scenario at low pH (S_{pH3}), also plates and spheres might directly attach due to the slightly positive surface potential of the spheres near to their IEP. In contrast, in S_{pH6} and S_{pH9} an aggregation of spheres and plates is prohibited due to strong negative charges. Yet, near-neutral rods can form homo-aggregates at high pH (up to 25% of inter-particle bonds) that substantially limits their availability as a bridging agent. Hence, overall aggregation is slowest at high and near-neutral pH values (S_{pH6}, S_{pH9}) due to high energy barriers between the mineral prototypes, and the increase in both aggregate mass and radius of gyration (Fig. 3) is fastest at low pH (S_{pH3}). This renders reaction-limited aggregation caused by energy barriers less decisive in our simulations and aggregation is dominated by the mechanisms of gravitational aggregation, as presented in detail in the following sections.

As all separate objects will ultimately combine into one single cluster, we also assessed the overall progress of aggregation as a function of separate objects left in the simulation. In this way, we can explore whether the dynamics of aggregation are different independent of the actual aggregation rate. For instance, despite the strong difference in aggregation rate, the increase in Péclet numbers for S_{pH3} and S_{pH6} is identical during aggregate formation when plotted against the number of objects, and Péclet numbers of 1 are reached once 90% of objects are aggregated. In contrast, the Péclet number approaches 1 already after 70% of objects are aggregated at high pH (S_{pH9}). This is due to the intermediate energy barrier of approximately 8 k_BT between rods and plates that results in a limitation of plate aggregation in comparison to S_{pH3} and S_{pH6}. Hence, S_{pH9} features the simultaneous occurrence of free, unassociated plates driven by diffusion and few large gravity driven aggregates.

3.2. Aggregation rates

Each scenario is characterized by a subtle interplay of diffusion, particle interaction and sedimentation that results in strong chances of aggregation rates in response to initial particle sizes and surface potentials (Table 2). A single stage aggregation model was not able to reproduce our observations and the introduction of a second stage as represented by equation (8) was necessary. Such a dual-stage behavior was already suggested by Allain et al. (1995) [53]. In our simulations, the β-stage is found to significant fractions in scenarios that are not only dominated by diffusion-limited aggregation. For example, we found the diffusive collision of particles delayed by the fractionation of potential interaction partners by sedimentation or the presence of energy barriers between particles which requires a bridging agent. Consequently, the impossibility to fit a one-stage model satisfactorily is a strong indication for the presence of processes beyond perikinetic, i.e. diffusive, aggregation.

Both stages are well described by a second-order model typically found for aggregation processes. In the "gravity series", only rods (indexed as r) facilitate aggregation with spheres (indexed as s) and plates (indexed as p), and we could reduce the number of rate constants in equation (8) to K^{α}_{sr}, K^{β}_{sr}, K^{α}_{pr}, and K^{β}_{pr} in our scenarios.

With this two-stage model, we could well describe the behavior found in all our simulations for rapid aggregation, e.g., spheres in $S_{0.3}$ (Table 2), and slow aggregation, e.g., plates in $S_{0.075}$. Furthermore, the rates provide a direct way of quantifying and comparing the aggregation behavior between scenarios.

3.3. How gravity promotes aggregation

We exemplify the promoting effect of gravity with scenarios $S_{0.3}$ and $S_{0.15}$. Here, aggregates and part of the primary particles settle rapidly ($S_{0.3}$: plates and spheres; $S_{0.15}$: spheres). Thus, the aggregation rates for the α-stage K^{α}_{sr} and K^{α}_{pr} are larger when sedimentation is allowed. Likewise, we found a more rapid increase in the aggregate mass and radius of gyration (Fig. 2), implying that not only particles aggregate faster, but initially also the aggregates grow lar-

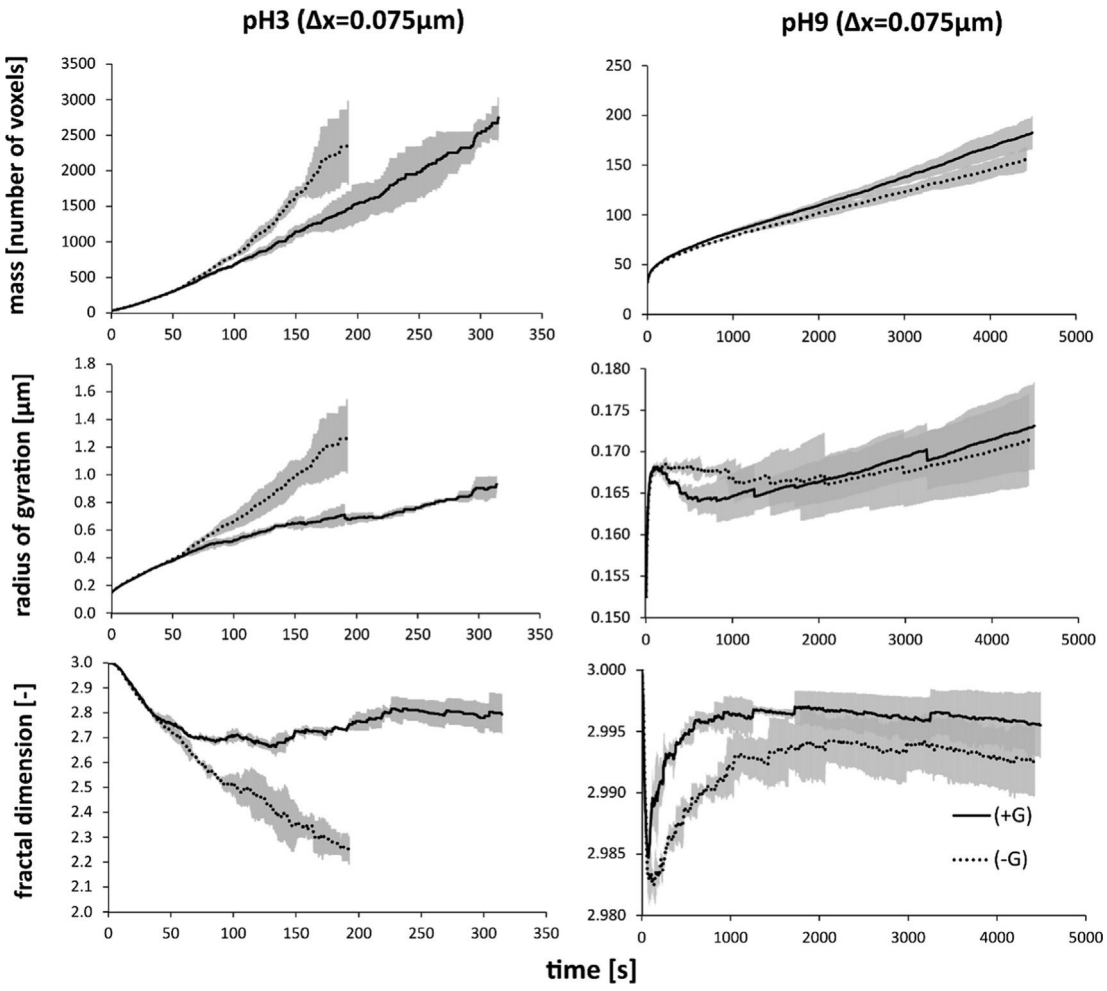

Fig. 3. Temporal development of the mean aggregate mass, radius of gyration and fractal dimension for gravity impacted (+G) and free (-G) scenarios at different pH (3 and 9: Δx = 0.075 µm). The standard deviation was calculated for n = 3.

Table 2
Aggregation rates (in 10^{-4} s^{-1}) of rods with spheres (K_{sr}^{α} and K_{sr}^{β}) and plates (K_{pr}^{α} and K_{pr}^{β}) for Δx = 0.075 µm ($S_{0.075}$), 0.15 µm ($S_{0.15}$) and 0.3 µm ($S_{0.2}$) with (+G) and without (-G) gravity and using the mean diffusion length in $S_{0.075}$ as reference (with confidence interval of 0.95) . The contribution of α-phase and β-phase on the aggregation process of primary particles spheres (f_s), rod (f_r) and plates (f_p). Uncertainty is represented by the 0.95-confidence interval from the fitting procedure.

	Δx = 0.3 µm		**Δx = 0.15 µm**		**Δx = 0.075 µm**	
	G+	**G-**	**G+**	**G-**	**G+**	**G-**
K_{sr}^{α}	18.7 ± 1.4	2.85 ± 0.05	6.93 ± 0.16	2.10 ± 0.05	4.30 ± 0.13	3.13 ± 0.04
K_{sr}^{β}	2.21 ± 0.09	0.155 ± 0.004	1.20 ± 0.02	0.142 ± 0.004	0.432 ± 0.011	0.090 ± 0.002
K_{pr}^{α}	5.21 ± 0.10	2.70 ± 0.05	2.69 ± 0.03	2.39 ± 0.07	2.05 ± 0.03	2.69 ± 0.04
K_{pr}^{β}	0.76 ± 0.02	0.405 ± 0.011	0.600 ± 0.011	0.37 ± 0.02	0.189 ± 0.006	0.406 ± 0.010
f_s	0.53	0.80	0.59	0.78	0.67	0.86
f_r	0.43	0.93	0.85	0.94	0.99	0.94
f_p	1.00	0.70	0.68	0.75	0.84	0.71

ger under gravity. In $S_{0.075}$, the primary particles are hardly affected by gravity, as seen in the initial Pé numbers (Table 1), until they form aggregates with spheres that grow large enough to settle. Hence, the initial aggregation process for rods with spheres or plates is only slightly impacted by gravity in the $S_{0.075}$ scenario as they nonetheless predominantly aggregate due to diffusion.

The scenarios showed different mechanisms that might result in aggregation (Fig. 4):

Mechanism I - Indirect promotion due to space confinement: Particles that have settled increase the particle density at the bottom of the domain, which reduces the mean particle distance. This results in a squared reduction of the corresponding diffusion time since $\Delta x^2 = 2Dt$, and a likewise increase in collision rate. Furthermore, as the movement is constrained to two dimensions, particles and aggregates effectively lose one spatial degree of freedom. The indirect promotion of aggregation can be observed in $S_{0.3}$ and $S_{0.15}$ as a rapid increase in aggregate mass and gyration radius compared to the gravity-free reference situation (-G) (Fig. 2). Furthermore, rapid sedimentation of all three types of primary particles causes a large decrease in mean particle distances and, thus, a larger α-aggregation rate. Especially plates are affected by this mechanism in $S_{0.3}$ as they settle down more rapidly and early reach the

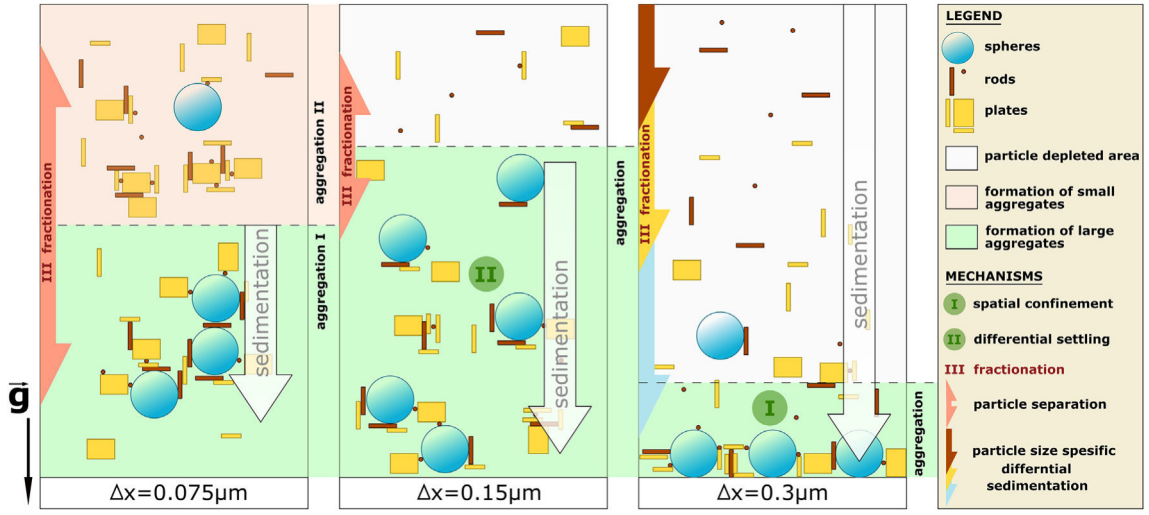

Fig. 4. Scheme of mineral prototype (blue spheres, yellow plates, and brown rods) size dependent indirectly promoting (I. due to space confinement), directly (II. due to sedimentation) and inhibiting (III. due to fractionation) mechanisms of aggregation for three different scenarios Δx = 0.075 μm ($S_{0.075}$, left), 0.15 μm ($S_{0.15}$, middle) and 0.3 μm ($S_{0.3}$, right). (For interpretation of the references to colour in this figure legend, the reader is referred to the web version of this article.)

lower modeling domain with a high particle density seen in large K_{pr}^{α} (Table 2). A promoting effect is not observed at $\Delta x = 0.075$ unless the pH value is high (S_{pH9}) and the homo-aggregation of rods produces aggregates fast enough to significantly settle in the timeframe of our simulations (Fig. 3).

Mechanism II - Direct promotion due to sedimentation: Large particles settle faster and may collide with other particles intersecting their trajectory [28]. This effect has been referred to as, e.g., differential sedimentation [40] or differential settling [31]. The direct aggregation-promoting effect of gravity is prominently visible in $S_{0.15}$ where, in contrast to $S_{0.3}$, aggregation is not dominated by mechanism I. In $S_{0.15}$, gravity increases aggregate mass, the radius of gyration, and the aggregation rates in particular before most of the particles have settled and mechanism I becomes apparent (Table 2). We explain this by the sedimentation of aggregates that could grow to a considerable size before they started to settle and passed a particular volume in which they collided with smaller particles (plates and rods) that settle slower [54]. Thus, the differential settling provokes large aggregation rates during the β-stage which is more pronounced for all three primary particle types in comparison to the gravity-free reference.

3.4. How gravity inhibits aggregation

Gravity will not always favor aggregation. From our numerical analysis, it becomes evident that gravity can significantly delay aggregation due to the following mechanism (Fig. 4):

Mechanism III - Inhibition of aggregation due to separation: Primary particles may "escape" aggregation if they are separated from each other due to sedimentation before they collide. Furthermore, the settling velocity increases with ongoing aggregation and forms aggregates that settle faster than the remaining particles. This may result in diffusion-dominated and sedimentation-dominated particles/aggregates in spatially distinct domains simultaneously, i.e., a size fractionation of the particles.

The separation of potential interaction partners results in an extended aggregation time. For instance, in $S_{0.075,}$ fractionation occurs after an initial diffusion-driven formation of aggregates that are large enough to settle and separate from unassociated particles. Consequently, the growth of aggregates in terms of mass and radius of gyration is slower in $S_{0.075}$ when sedimentation is allowed. In contrast, sedimentation accelerates aggregate growth in $S_{0.15}$ and $S_{0.3}$ due to the above discussed mechanisms I and II (Fig. 2). In particular, plates are subject to fractionation in $S_{0.075}$, which are repulsive for spheres and, thus, require rods for aggregation. In turn, the availability of rods is reduced as soon as they start to settle upon being incorporated into large aggregates. This process further depletes potential interaction partners for plates and causes the smallest aggregation rates (K_{pr}^{α} and K_{pr}^{β}) for the plates in comparison to all scenarios (Table 2).

A dominant fractionation is also present in $S_{0.3}$, where the spheres settle rapidly, and their aggregation with plates and rods takes place predominantly at the bottom of the domain, once the more slowly settling plates and rods have arrived. This leads to a delay between sedimentation and aggregation compared to $S_{0.075}$ and $S_{0.15}$ (Fig. 1). However, in $S_{0.3}$ this fractionation is masked by the indirect promotion of aggregation due to sedimentation at the bottom of the domain (mechanism I), and the aggregation rates are largest in $S_{0.3}$ despite fractionation. Still, fractionation is evident in the fraction of particles following the α-stage. The contribution of the α-stage of spheres f_s and rods f_r is the smallest in comparison to all other scenarios. Hence, as soon as the scenarios do not start under conditions where all rods can aggregate diffusively, spheres and plates will settle before all rods are integrated into aggregates. As singular rods are the smallest particles in our scenarios and therefore feature the smallest settling velocity, part of the rods remain in the upper domain where they cannot attach further. In contrast, when the particle movement is initially dominated by diffusion, the rods largely aggregate in the α-stage, independent of the presence of gravity due to the high chance of finding potential interaction partners (Table S1).

The separation between particles of different type and size during aggregation (Fig. 1) results from a delicate interplay of diffusion, fractionation, strength of interaction, and availability of particles in excess. Depending on the exact setting, different particles (plates in $S_{0.075}$, rods in $S_{0.3}$) might be subject to fractionation or promotion by gravity. The findings might be transferable to phase separation studies which deal with the gravitational fractionation according to the physicochemical properties of multicomponent mixtures (including density and hydrophobicity differences) [55,56]. Exemplarily, de las Heras and Schmid (2013) [57] report that gravity unfolds a rich phenomenology in terms of particle fractionation, sedimentation, and layer formation even if aggregation is not considered. Hence, we can conclude that

gravity-constrained aggregation is an initiator for phase separation (Fig. 1), but is highly dynamic (Figure S3) and does not lead to a stable phase stacking sequence due to ongoing aggregation and changing sedimentation velocities.

3.5. How gravity shapes the aggregate structure

3.5.1. Fractal dimension

The scenarios start with randomly distributed, separated primary particles that individually exhibit a dense structure with a fractal dimension of 3. During aggregation, branched structures evolve with fractal dimensions between 1.5 and 1.8 (Fig. 5), typically reported for fractal aggregates [7]. We found the most rapid decrease in the fractal dimension in $S_{0.3}$ due to spatially constrained aggregation on the bottom boundary (mechanism I). The mean fractal dimensions in $S_{0.15}$ and $S_{0.075}$ are significantly larger than those without gravity and $S_{0.3}$ until the number of objects reduces to 20 (Fig. 5). We explain this phenomenon by the simultaneous, but spatially separated formation of small compact aggregates that settle slowly, and the growth of large and branched aggregates that already settled. Hence, aggregates with large and small fractal dimensions appear simultaneously, and the mean fractal dimension remains stable, which is in line with the suggestions of González (2016) [51], who describes coexistence of large and small aggregates/particles caused by gravity. In turn, small aggregates and primary particles with high fractal dimensions are preserved longer. The formation of fractal structures with long branches is delayed until all aggregates accumulate at the bottom boundary, clearly pointing to multiple temporal steps of aggregation with distinct mechanisms and aggregate properties in a hierarchical order. This observation fits with Szilagyi et al. (2014) [58], reporting different stages and complexity of aggregates and the ongoing development of already existing aggregates [59]. We identified this situation as being strongly affected by gravity.

3.5.2. Bond formation

The particle size also controls the aggregation dynamics of primary particles and aggregates to each other (Fig. 6). Generally, all scenarios start with the formation of bonds between primary particles as no aggregates yet exist. Over time, individual particles increasingly collide with existing aggregates, and particle-aggregate bonds develop while aggregates more intensively attach to each other with progressing simulation time (Fig. 6b). The temporal development of bond formation is hardly affected by gravity in $S_{0.075}$, although the dynamics regarding the evolution of mass, radius of gyration, and fractal dimension are significantly different (Fig. 2). Similarly, the formation of bonds between primary particles is not affected by gravity in $S_{0.15}$. However, slightly fewer particle-aggregate bonds are formed and an increased number of aggregate-aggregate bonds are generated instead due to increased collision-probability of aggregates at the bottom boundary (mechanism I) and during sedimentation (mechanism II). In contrast, the strength of gravity in $S_{0.3}$ reduces the ability of primary particles to find each other in suspension before they settle. Thus, the number of corresponding particle–particle bonds decreases and primary particles show an increased chance to attach to aggregates that are already settled. Hence, $S_{0.3}$ features a growth of existing aggregates with primary particles instead of a parallel formation of small aggregates that subsequently combine.

The reduction of energy barriers [60] between spheres and plates at low pH (S_{pH3}) only leads to small changes in the aggregation dynamics, as seen by slightly increased formation of particle–particle and aggregate-aggregate bonds in comparison to near-neutral pH (S_{pH6}). The reduced energy barrier between spheres and other particles in S_{pH3} supports the formation of aggregates

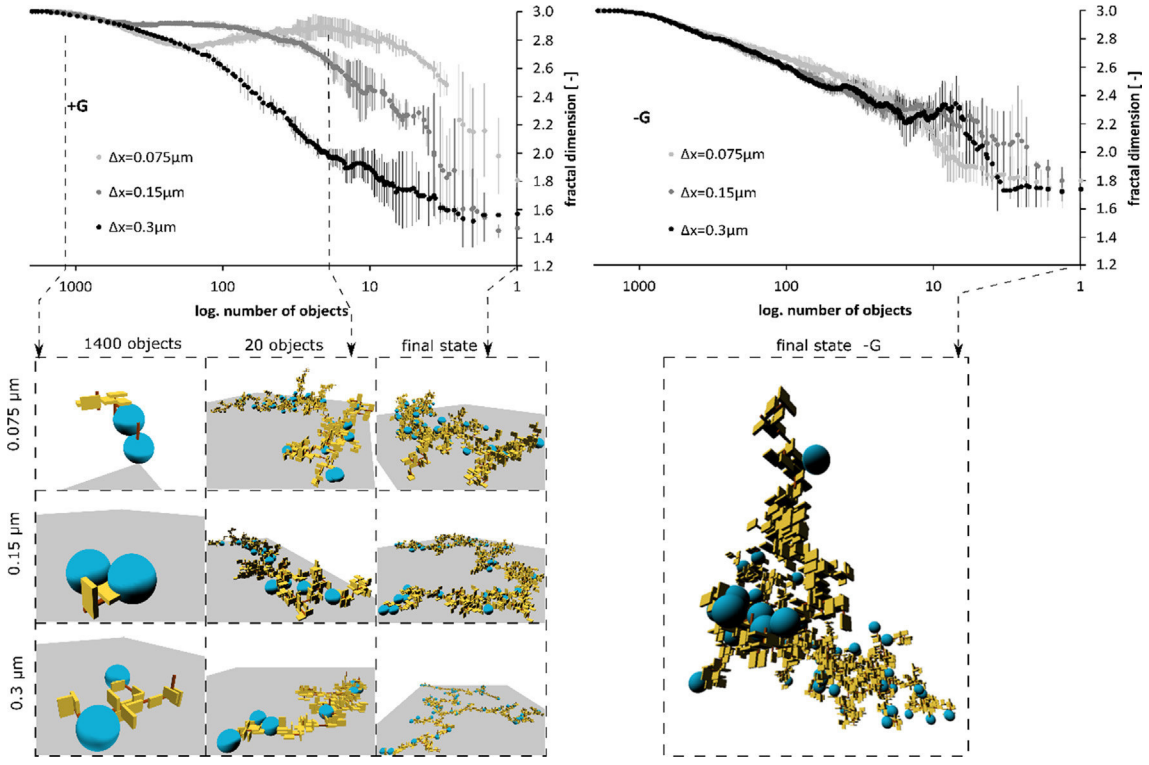

Fig. 5. Fractal dimension as function of number of objects for Δx = 0.075 µm ($S_{0.075}$), 0.15 µm ($S_{0.15}$) and 0.3 µm ($S_{0.3}$) with gravity (+G, top left) and without (-G, top right) gravity. The three-dimensional structures show the largest aggregate in the system at a number of 1400, 20 objects and the final state consisting of blue spheres, brown rods, and yellow plates, when gravity is allowed (+G, left), and the final state aggregate which is reached independent of the grid cell size without gravity (-G, right). The standard deviation was calculated for n = 3 (error bar). (For interpretation of the references to colour in this figure legend, the reader is referred to the web version of this article.)

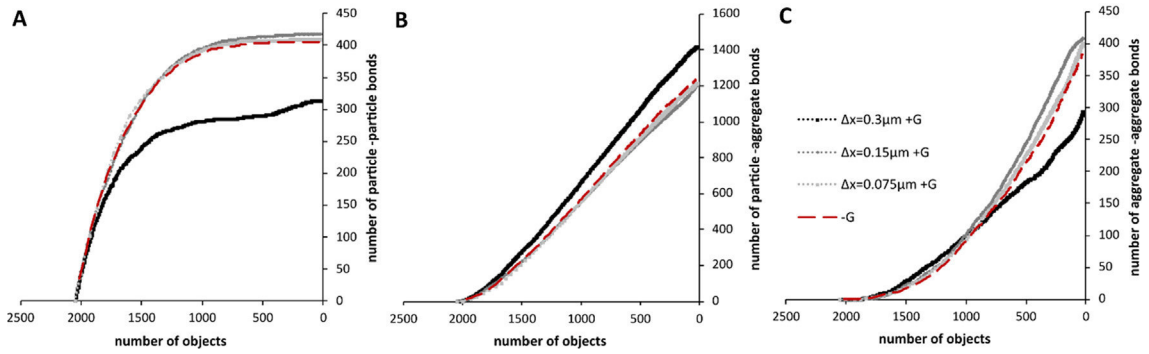

Fig. 6. Increasing number of particle–particle (A), particle-aggregate (B) and aggregate-aggregate bonds (C) as function of number of objects for 0.075 μm ($S_{0.075}$), 0.15 μm ($S_{0.15}$) and Δx = 0.3 μm ($S_{0.3}$) with gravity (+G) and without (-G) gravity.

from primary particles and favors the subsequent aggregation between already exiting aggregates but reduces the formation of particle-aggregate bonds (Figure S4). In contrast, if energy barriers are high (S_{pH9}), the initial aggregation occurs predominantly between spheres and rods. The formation of particle–particle and aggregate-aggregate bonds is finished as soon as spheres and rods are incorporated into aggregates. In the following, the formation of particle-aggregate bonds becomes dominant by single plates that still find configurations at aggregate surfaces where rods are exposed and permit further plate attachment. With the ongoing aggregation of plates, the number of available aggregation sites decreases and the aggregate gets screened against further interactions with remaining plates (Figure S4). A succession of dominant aggregation mechanisms is clearly visible here.

3.5.3. Particle location inside aggregates

The spatial position in the vertical direction (Z-position), where the primary particles ultimately end up in the aggregate structure, differs depending on their initial size (Figure S3). In $S_{0.3}$, the spheres settle rapidly and form aggregates with plates and rods that, according to their size, settle later. As a result of gravity, the mean spatial position of plates and rods inside late-stage aggregates is constrained to the location of settled spheres. As a result, a relatively flat conformation develops, as shown by the small height of the final aggregate (21 ± 2 cells). Spheres are involved in aggregation during downward sedimentation via rods in $S_{0.15}$ or start only to settle if they become aggregated in $S_{0.075}$. Such a size-specific behavior decides how and where the particles become located during aggregation. For scenarios with a decreasing impact of gravity, the mean Z-position of plates and rods inside late-state aggregates becomes less restricted to the bottom of the domain and, thus, these aggregates have a larger size in Z-direction ($S_{0.15}$: 46 ± 12 cells and $S_{0.075}$: 98 ± 7 cells). As the large spheres always settle faster or are involved in aggregates that settle quickly, their mean Z-position inside matured aggregates is deeper than the Z-position of rods and plates (Figure S3). Hence, the relative Z-position of the primary particles is controlled by the number and the size difference between initial primary particles. The resulting difference in settling velocity decides how they potentially form gradually layered sediments and anisotropic structures [31,61]. In contrast, the mean Z-position inside the no-gravity references is only driven by diffusion. Thus, the mean Z-position of plates, rods, and spheres remains at the center of the modeling domain.

In general, the resulting structures are constrained in Z-direction with increasing particle size and impact of gravity (Fig. 5). The spatial restrictions are also seen as an anisotropic distribution of particles inside late fractal states of aggregation.

4. Conclusion

Our model allows unraveling the effect of gravity on aggregation processes in a rigorous physical framework that brings together concepts and approaches of aggregate formation developed in soil science and colloidal sciences. We broaden the scope of established colloidal aggregation models in the framework of diffusion/reaction-limited aggregation [8,14,15] to natural aqueous and soil suspensions, where particles of various origin, shape, and properties are affected by gravity. In view of ongoing discussions about soil aggregate formation [33], we are convinced that mechanistic modeling of these processes including gravity can significantly promote our conceptual understanding of aggregation in natural systems. In particular, the explicit aggregate structure now accessible via computed tomography [62-64] calls for modeling approaches that reveal the relation between properties, processes, and the emerging three-dimensional structures.

For large particle sizes with a strong tendency to settle, we found an accelerated aggregation promoted by a bridging agent and spatial confinement due to sedimentation (mechanism I: indirect aggregation promoting effect of gravity). A direct impact of gravity on promoting aggregation (mechanism II) was caused by particles with a different settling velocity that collide during downward movement, as already identified in previous research [28,31,32,40]. If diffusion and settling velocity are not in balance, the partitioning of the system behavior into a diffusive- and a sedimentation-controlled domain slows down the aggregation (III: aggregation inhibiting effect of gravity).

The self-assembly of primary particles into aggregates has shown to be highly dynamic and results in hierarchic structures. The primary particle size decides how they are bound together and how more complex fractal structures form during aggregation. The establishment (pH = 9) or reduction of energy barriers (pH = 3) towards bridging agents forces a separation or results in the acceleration of aggregation processes. Thus, the properties and availability of the bridging agent have shown to govern aggregation even if the bridging agent is present only in small amounts [52]. This aggregation feedback on size and pH are essential for the fate of particles inside natural porous media like soils, sediments, or aquifers [2-4,48]. For example, gravity-driven aggregation and transport of clay-sized particles are crucial for soil-horizon formation during pedogenesis [4,65-67]. We demonstrated that the settling velocity, and thus the particle size, is decisive whether aggregation occurs with particles in suspension or after sedimentation. The resulting anisotropic structures and stratified sediments are typical for natural systems and frequently found in experimental aggregation studies [27,30]. As shown in our research, these structures result from the delicate balance between aggregation

and settling velocity, depending on the size, number, and type of particles. Throughout the scenarios, the three-dimensional visualization of particle self-assembly allowed us to explore the subtle dynamics, hierarchical aggregation mechanisms, and their dependence on gravity. In this way, our tool not only allows for to correctly reconstruct the physics of aggregation. As also described recently by Tateno & Tanaka (2019) [13] for congeneric colloids, process visualization strongly supports exploring phenomena in complex dynamic systems if not even being essential for their interpretation.

CRediT authorship contribution statement

Tom Guhra: Validation, Formal analysis, Investigation, Writing - original draft, Visualization. **Thomas Ritschel:** Methodology, Software, Validation, Writing - original draft. **Kai Uwe Totsche:** Conceptualization, Methodology, Writing - review & editing, Supervision, Project administration, Funding acquisition, Resources.

Declaration of Competing Interest

The authors declare that they have no known competing financial interests or personal relationships that could have appeared to influence the work reported in this paper.

Acknowledgment

We kindly acknowledge financial support by the Deutsche Forschungsgemeinschaft within the framework of the research unit 2179 “MAD Soil - Microaggregates: Formation and turnover of the structural building blocks of soils” (Project no.: 193380941; www.madsoil.uni-jena.de). We thank the reviewers for their valuable suggestions. The source code of the modeling software used in this paper and an application example is available under:

https://github.com/ThomasRitschel/gravity.

Appendix A. Supplementary data

Supplementary data to this article can be found online at https://doi.org/10.1016/j.jcis.2021.03.153.

References

[1] J. Buffle, G.G. Leppard, Characterization of aquatic colloids and macromolecules. 1. Structure and behaviour of colloidal material, Environ. Sci. Technol. 29 (1995) 2169–2175.
[2] J.N. Ryan, M. Elimelech, Colloid mobilization and transport in groundwater, Colloid Surf. A 107 (1996) 1–56.
[3] J. Gregory, Particles in water: properties and processes, CRC Press Taylor & Francis, 2006.
[4] E.M. Hotze, T. Phenrat, G.V. Lowry, Nanoparticle Aggregation: Challenges to understanding transport and reactivity in the environment, J. Environ. Qual. 39 (2010) 1909–1924.
[5] G. Trefalt, F.J.M. Ruiz-Cabello, M. Borkovec, Interaction forces, heteroaggregation, and deposition involving charged colloidal particles, J. Phys. Chem. B 118 (23) (2014) 6346–6355.
[6] A. Laganapan, M. Cerbelaud, R. Ferrando, C.T. Tran, B. Crespin, A. Videcoq, Computer simulations of heteroaggregation with large size asymmetric colloids, J. Colloid Interf. Sci. 514 (2018) 694–703.
[7] M.Y. Lin, H.M. Lindsay, D.A. Weitz, R.C. Ball, R. Klein, P. Meakin, Universality in colloid aggregation, Nature 339 (6223) (1989) 360–362.
[8] P. Meakin, Formation of fractal clusters and networks by irreversible diffusion-limited aggregation, Phys. Rev. Lett. 51 (13) (1983) 1119–1122.
[9] S. Sacanna, W.T.M. Irvine, L. Rossi, D.J. Pine, Lock and key colloids through polymerization-induced buckling of monodisperse silicon oil droplets, Soft Matter 7 (5) (2011) 1631–1634.
[10] M. Cerbelaud, A. Videcoq, P. Abélard, C. Pagnoux, F. Rossignol, R. Ferrando, Self-assembly of oppositely charged particles in dilute ceramic suspensions: predictive role of simulations, RSC Soft Matter 6 (2010) 370–382.
[11] A.H. Gröschel, A. Walther, T.I. Löbling, F.H. Schacher, H. Schmalz, A.H.E. Müller, Guided hierarchical co-assembly of soft patchy nanoparticles, Nature 503 (7475) (2013) 247–251.
[12] K. Miszta, J. de Graaf, G. Bertoni, D. Dorfs, R. Brescia, S. Marras, L. Ceseracciu, R. Cingolani, R. van Roij, M. Dijkstra, L. Manna, Hierarchical self-assembly of suspended branched colloidal nanocrystals into superlattice structures, Nature Mater. 10 (2011) 872–876.
[13] M. Tateno, H. Tanaka, Numerical prediction of colloidal phase separation by direct computation of Navier-Stokes equation, npj Comput, Mater. 5 (1) (2019), https://doi.org/10.1038/s41524-019-0178-z.
[14] T.A. Witten, L.M. Sander, Diffusion-limited aggregation, Phys. Rev. B 27 (9) (1983) 5686–5697.
[15] P. Meakin, Diffusion-limited aggregation in three dimensions: Results from a new cluster-cluster aggregation model, J. Colloid Interface Sci. 102 (1984) 491–504.
[16] M. Lattuada, H. Wu, M. Morbidelli, A simple model for the structure of fractal aggregates, J. Colloid Interface Sci. 268 (1) (2003) 106–120.
[17] P. Meakin, Fractal aggregates, Adv. Colloid Interface Sci. 28 (1987) 249–331.
[18] P. Meakin, A historical introduction to computer models for fractal aggregates, J. Sol-Gel Sci. Technol. 15 (1999) 7–117.
[19] K.H. Gardner, T.L. Theis, A unified kinetic model for particle aggregation, J. Colloid Interface Sci. 180 (1) (1996) 162–173.
[20] S.B. Grant, J.H. Kim, C. Poor, Kinetic theories for the coagulation and sedimentation of particles, J. Colloid Interface Sci. 238 (2) (2001) 238–250.
[21] P. Sandkühler, M. Lattuada, H. Wu, J. Sefcik, M. Morbidelli, Further insights into the universality of colloidal aggregation, Adv. Colloid Interface Sci. 113 (2-3) (2005) 65–83.
[22] S. Lazzari, L. Nicoud, B. Jaquet, M. Lattuada, M. Morbidelli, Fractal-like structures in colloid science, Adv. Colloid Interface Sci. 235 (2016) 1–13.
[23] S.G. Love, D.R. Pettit, S.R. Messenger, Particle aggregation in microgravity: Informal experiments on the International Space Station, Meteorit. Planet. Sci. 49 (2014) 732–739.
[24] C. Allain, M. Cloitre, F. Parisse, Settling by cluster deposition in aggregating colloidal suspensions, J. Colloid Interface Sci. 178 (2) (1996) 411–416.
[25] R. Folkersma, A.J.G. van Diemen, H.N. Stein, Understanding the influence of gravity on perikinetic coagulation on the basis of the DLVO theory, Adv. Colloid Interface Sci. 83 (1-3) (1999) 71–84.
[26] H.D. Newman, A. Yethiraj, Clusters in sedimentation equilibrium for an experimental hard-sphere-plus-dipolar Brownian colloidal system, Sci. Rep. 5 (1) (2015), https://doi.org/10.1038/srep13572.
[27] T. Guhra, T. Ritschel, K.U. Totsche, Formation of mineral–mineral and organo–mineral composite building units from microaggregate-forming materials including microbially produced extracellular polymeric substances, Eur. J. Soil Sci. 70 (3) (2019) 604–615.
[28] D.H. Melik, H.S. Fogler, Gravity-induced flocculation, J. Colloid Interface Sci. 101 (1) (1984) 72–83.
[29] R. Folkersma, H.N. Stein, Influence of gravity on perikinetic coagulation, Part II: Theoretical Analysis, J. Colloid Interface Sci. 206 (2) (1998) 494–504.
[30] J.K. Whitmer, E. Luijten, Sedimentation of aggregating colloids, J. Chem. Phys. 134 (3) (2011) 034510, https://doi.org/10.1063/1.3525923.
[31] A.S. Dukhin, S.S. Dukhin, P.J. Goetz, Gravity as a factor of aggregative stability and coagulation, Adv. Colloid Interface Sci. 134–135 (2007) 35–71.
[32] D.H. Melik, H.S. Fogler, Effect of gravity on Brownian flocculation, J. Colloid Interface Sci. 101 (1) (1984) 84–97.
[33] K.U. Totsche, W. Amelung, M.H. Gerzabek, G. Guggenberger, E. Klumpp, C. Knief, E. Lehndorff, R. Mikutta, S. Peth, A. Prechtel, N. Ray, I. Kögel-Knabner, Microaggregates in soils, J. Plant. Nutr. Soil Sci. 181 (1) (2018) 104–136.
[34] P. Meakin, Models for colloidal aggregation, Annu. Rev. Phys. Chem. 39 (1) (1988) 237–267.
[35] S. Stoll, J. Buffle, Computer simulations of colloids and macromolecules aggregate formation, Chimia 49 (1995) 300–307.
[36] N. Ray, A. Rupp, A. Prechtel, Discrete-continuum multiscale model for transport, biomass development and solid restructuring in porous media, Adv. Water Resour. 107 (2017) 393–404.
[37] A. Rupp, K.U. Totsche, A. Prechtel, N. Ray, Discrete-continuum multiphase model for structure formation in soils including electrostatic effects, Front. Environ. Sci. 6 (2018) 2018, https://doi.org/10.3389/fenvs.2018.00096.
[38] T. Ritschel, K.U. Totsche, Modeling the formation of soil microaggregates, Comput. and Geosci. 127 (2019) 36–43.
[39] W. Feller, An introduction to probability theory and its application, John Wiley & Sons Inc., 1957.
[40] M. Elimelech, J. Gregory, X. Jia, R.A. Williams, Particle deposition & aggregation - measurement, modelling and simulation, Butterworth-Heinemann, 1995.
[41] J. Israelachvili, Intermolecular and surface forces, Elsevier, 2011.
[42] K. Foroutan-pour, P. Dutilleul, D. Smith, Advances in the implementation of the box-counting method of fractal dimension estimation, Appl. Math. Comput. 105 (1999) 195–210.
[43] A. Marmur, W.N. Gill, E. Ruckenstein, Kinetics of cell deposition under the action of an external field, Bull. Math. Biol. 38 (6) (1976) 713–721.
[44] D.W. Marquardt, an algorithm for least-squares estimation of nonlinear parameters, J. Soc. Indust. Appl. Math. 11 (2) (1963) 431–441.
[45] B.E. Novich, T.A. Ring, Colloid stability of clays using photon correlation spectroscopy, Clay Clay Miner. 32 (1984) 400–406.
[46] L. Bergström, Hamaker constants of inorganic materials, Adv. Colloid Interface Sci. 70 (1997) 125–169.

[47] C.-Y. Xu, K.-Y. Deng, J.-y. Li, R.-K. Xu, Impact of environmental conditions on aggregation kinetics of hematite and goethite nanoparticles, J. Nanoparticle Res. 17 (10) (2015), https://doi.org/10.1007/s11051-015-3198-8.
[48] N.M. DeNovio, J.E. Saiers, J.N. Ryan, Colloid movement in unsaturated porous media: recent advances and future directions, Vadose Zone J. 3 (2) (2004) 338–351.
[49] M. Kosmulski, The pH dependent surface charging and points of zero charge. VIII. Update, Adv. Colloid Interface Sci. 275 (2020) 115–138.
[50] M. Kosmulski, P. Dahlsten, High ionic strength electrokinetics of clay minerals, Colloids Surf. A Physicochem. Eng. Asp. 291 (1-3) (2006) 212–218.
[51] A. E. González, in: Advances in Colloid Science, IntechOpen, 2016, https://doi.org/10.5772/65699.
[52] S. Goldberg, R.A. Glaubig, Effect of saturating cation, pH, and aluminium and iron oxide on the flocculation of kaolinite and montmorillonite, Clays Clay Miner. 3 (1987) 220–227.
[53] C. Allain, M. Cloitre, M. Wafra, Aggregation and sedimentation in colloidal suspensions, Phys. Rev. Letters 74 (8) (1995) 1478–1481.
[54] X. Li, B.E. Logan, Collision frequencies of fractal aggregates with small particles by differential sedimentation, Environ. Sci. Technol. 31 (4) (1997) 1229–1236.
[55] H.H. Wensink, H.N.W. Lekkerkerker, Sedimentation and multi-phase equilibria in mixtures of platelets and ideal polymer, Europhys. Lett. 66 (1) (2004) 125–131.
[56] G. Avvisati, T. Dasgupta, M. Dijkstra, Fabrication of colloidal laves phases via hard tetramers and hard spheres: Bulk phase diagram and sedimentation behavior, ACS Nano 11 (2017) 7702–11109.
[57] D.d.L. Heras, M. Schmidt, The phase stacking diagram of colloidal mixtures under gravity, Soft Matter 9 (36) (2013) 8636, https://doi.org/10.1039/c3sm51491a.
[58] I. Szilagyi, T. Szabo, A. Desert, G. Trefalt, T. Oncsik, M. Borkovec, Particle aggregation mechanisms in ionic liquids, Phys. Chem. Chem. Phys. 16 (20) (2014) 9515–9524.
[59] L.M. Sander, Fractal growth processes, Nature 322 (1986) 789–793.
[60] M. Hütter, Local structure evolution in particle network formation studied by brownian dynamics simulation, J. Colloid Interface Sci. 231 (2) (2000) 337–350.
[61] D. Heras, L.L. Treffenstädt, M. Schmidt, Reentrant network formation in patchy colloidal mixtures under gravity, Phys. Rev. E 93 (2016) 1–5.
[62] K. Ananyeva, W. Wang, A.J.M. Smucker, M.L. Rivers, A.N. Kravchenko, Can intra-aggregate pore structures affect the aggregate's effectiveness in protecting carbon?, Soil Biol. Biochem. 57 (2013) 868–875.
[63] A. Garbout, L.J. Munkholm, S.B. Hansen, Temporal dynamics for soil aggregates determined using X-ray CT scanning, Geoderma 204-205 (2013) 15–22.
[64] V.J.M.N.L. Felde, S.A. Schweizer, D. Biesgen, A. Ulbrich, D. Uteau, C. Knief, M. Graf-Rosenfellner, I. Kögel-Knabner, S. Peth, Wet sieving versus dry crushing: Soil microaggregates reveal different physical structure, bacterial diversity and organic matter composition in a clay gradient, Eur. J. Soil Sci. 72 (2) (2021) 810–828, https://doi.org/10.1111/ejss.v72.210.1111/ejss.13014.
[65] L.W. de Jonge, C. Kjaergaard, P. Moldrup, Colloids and colloid-facilitated transport of contaminants in soils, Vadose Zone J. 3 (2004) 321–325.
[66] C.J. Bronick, R. Lal, Soil structure and management: A review, Geoderma 124 (1-2) (2005) 3–22.
[67] K. Lehmann, R. Lehmann, K.U. Totsche, Event-driven dynamics of the total mobile inventory in undisturbed soil account for significant fluxes of particulate organic carbon, Sci. Total Environ. 756 (2021). org/10.1016/j.scitotenv.2020.143774.

The mechanisms of gravity-constrained aggregation in natural colloidal suspensions

Tom Guhra[a], Thomas Ritschel[a], and Kai Uwe Totsche[a*]

[a]*Department of Hydrogeology, Institute of Geosciences, Friedrich Schiller University Jena, 07749 Germany*

***Corresponding Author:** Kai Uwe Totsche

Email: kai.totsche@uni-jena.de

Keywords: pH, stochastic model, Derjaguin-Landau-Verwey-Overbeek (DLVO) theory, visualization tool, hierarchic structures, fractal dimension, graphical user interface (GUI)

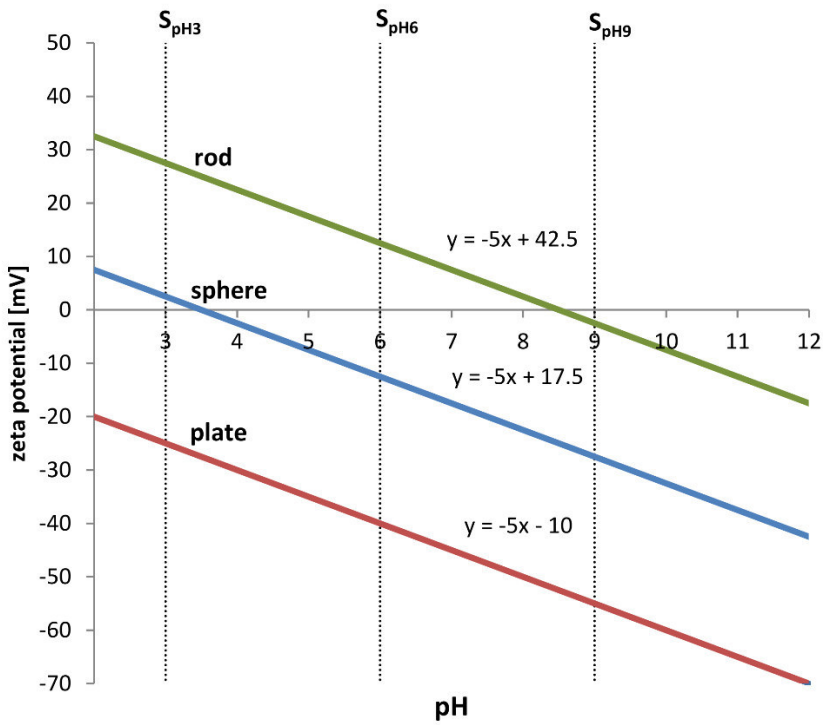

Figure S1: Assumed zeta potentials of the mineral prototypes rods (green), spheres (blue) and plates (red).

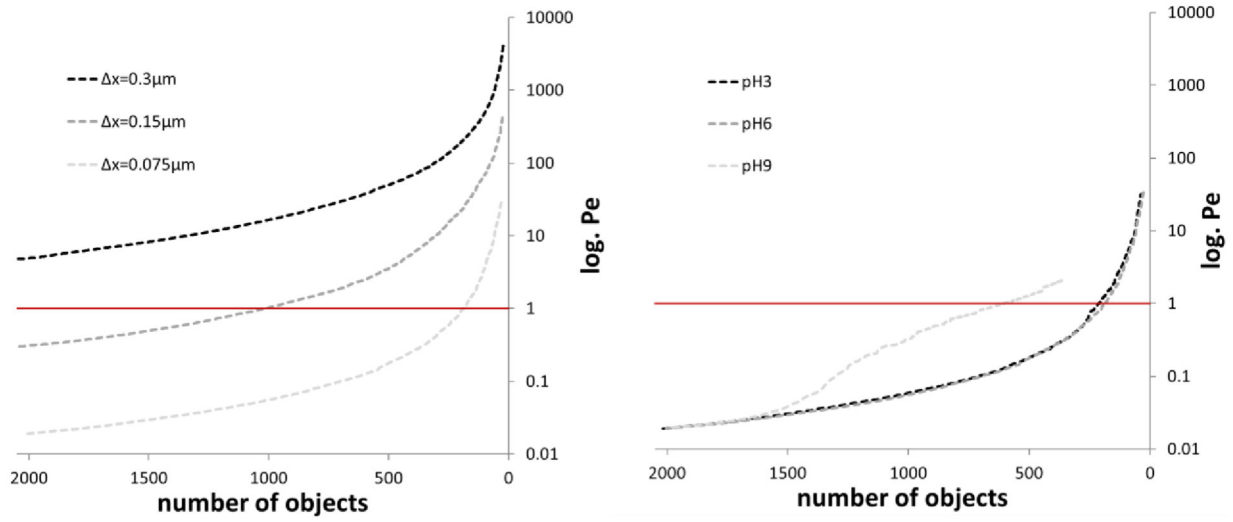

Figure S2: Péclet number (Pe) as function of the number of objects in gravity impacted systems for different sizes Δx=0.075 µm ($S_{0.075}$), 0.15 µm ($S_{0.1}$), 0.3 µm ($S_{0.3}$) and pH (pH=3, 6 and 9). The Péclet number of 1 represents the transition between diffusion-dominated and sedimentation-dominated conditions (red horizontal line).

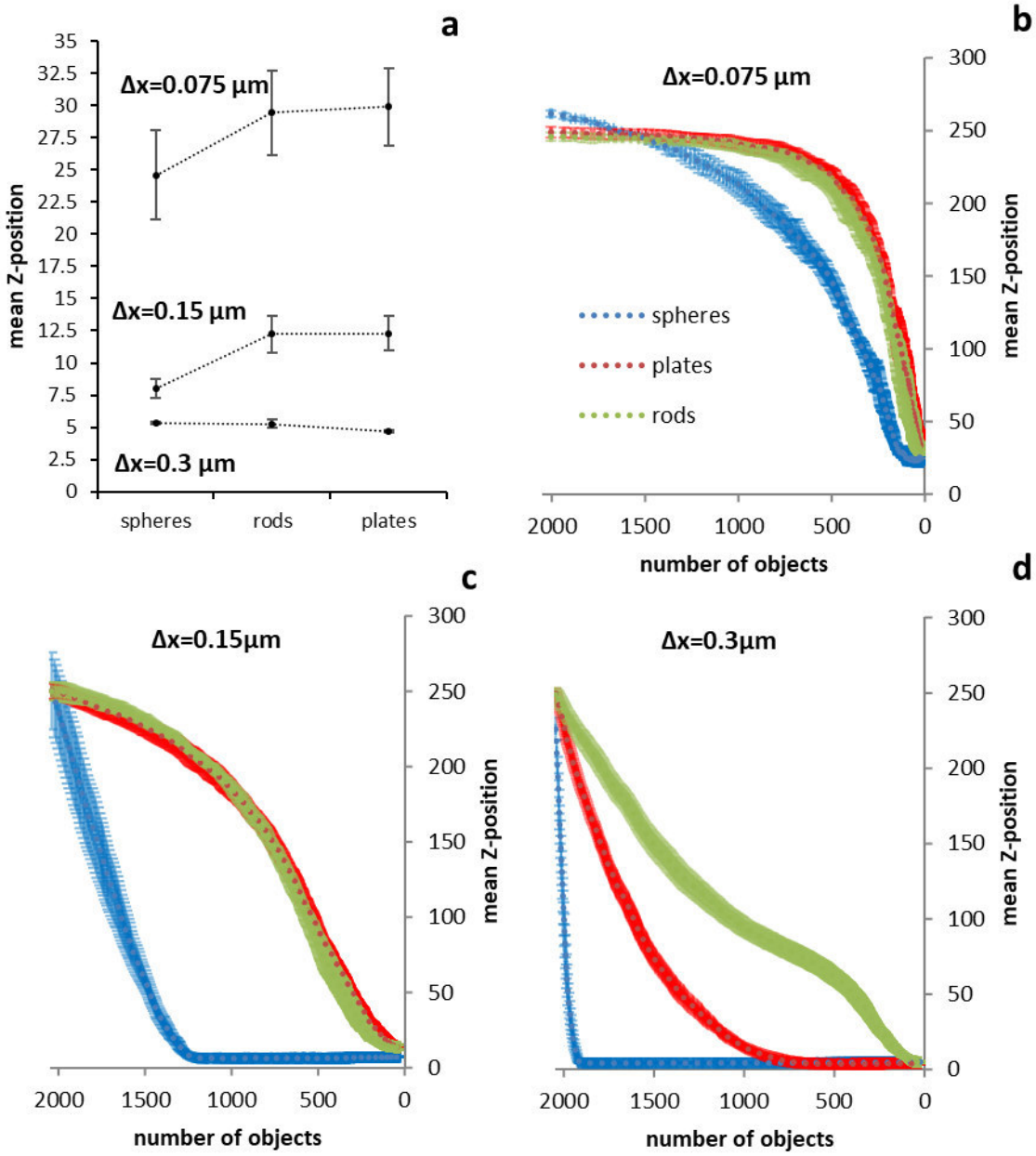

19

20 **Figure S3:** Mean Z-position of the mineral prototypes inside the final state aggregates (a) and the mean Z-position where the
21 unassociated mineral prototypes become bound into aggregates as function of number of objects for Δx=0.075 µm ($S_{0.075}$, b),
22 0.15 µm ($S_{0.15}$, c) and 0.3 µm ($S_{0.3}$, d). The standard deviation was calculated for n=3 (colored error bar).

23

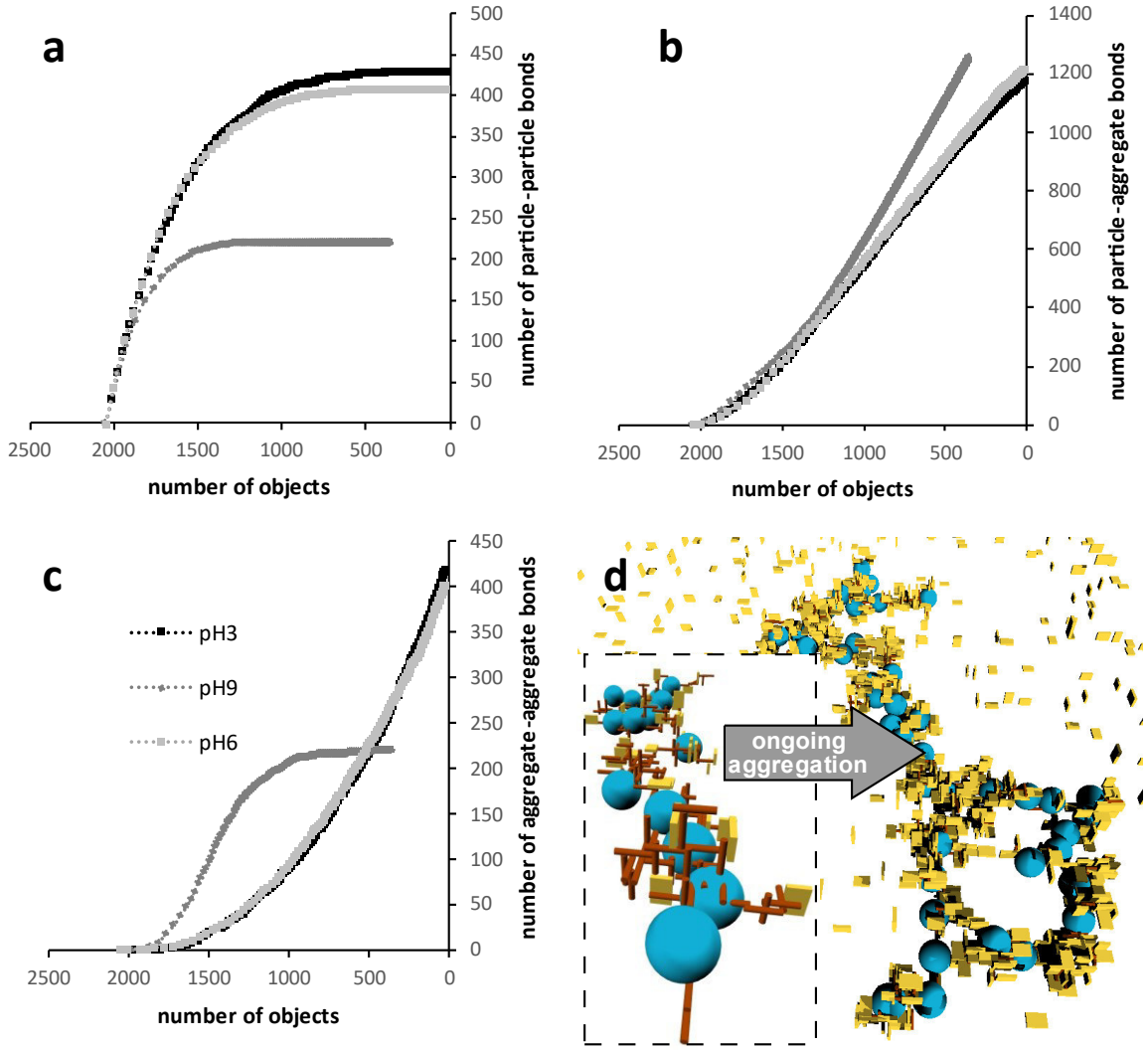

Figure S4: Number of particle-particle (a), particle-aggregate (b) and aggregate-aggregate bonds (c) at pH 3 (S_{pH3}), 6 ($S_{0.1}$; S_{pH6}) and 9 (S_{pH9}) under the impact of gravity (+G). Largest cluster (d) at pH 9 after the number of objects was reduced to 1400, predominantly consisting of spheres (blue) and rods (red) which become subsequently covered by plates (yellow) during aggregation (after the number of objects was reduced to 800).

Table S1: Size and pH specific energy barriers for all association combinations between the mineral prototypes (rod, plate, and sphere). Interactions for energy barrier > 30 k_BT are considered repulsive.

pH	dx (μm)	Energy barrier (k_BT)					
		sphere/sphere	sphere/rod	sphere/plate	rod/rod	rod/plate	plate/plate
6	0.075	24.05	0	>30	9.95	0	>30
6	0.15	>30	0	>30	28.15	0	>30
6	0.3	>30	0	>30	>30	0	>30
3	0.075	0	0.93	0	>30	0	>30
9	0.075	>30	0.93	>30	0	7.98	>30

3. Synoptic discussion

The presented *in vitro* and *in silico* studies provide detailed insights in important sub-processes and mechanisms of organo-mineral association and (micro-)aggregate formation from the aqueous phase. The mechanisms range from specific adsorption mechanisms of biogenic OM up to gravity-controlled phase separation which are critically discussed and put into context in the following sections.

3.1. Formation of organo-mineral associations

In $\mathbf{P_I}$ the way of biogenic OM into organo-mineral associations and soil aggregates was extensively discussed. In particular, the role of mineral type (e.g., Mikutta et al., 2012; Liu et al., 2013; Chen et al., 2021), environmental conditions (e.g., Omoike and Chorover, 2006; Cai et al., 2018), biogenic OM composition (Zhu et al., 2009) and molecular weight (Violante et al., 1995; Sheng et al., 2016) were indicated as controlling factors of organo-mineral association and aggregate formation. For example, in $\mathbf{P_{II}}$ and $\mathbf{P_{III}}$ we characterize the composition of two potential biogenic aggregation agents (cutaneous earthworm mucus and microbial EPS) as well as their adsorption behavior to goethite and illite (also for quartz for microbial EPS). In general, biogenic organic matter produced by microorganisms, plants and earthworms were found to be composed of a complex mixture of molecules including proteins, polysaccharides, carbohydrates and lipids (PI; Walker et al., 2003; Pan et al., 2010; Mahapatra and Banerjee, 2013; Frey, 2019). For microbial EPS the composition was reported as variable due to the impact of environmental conditions, purpose of excretion (e.g., communication, cell attachment or formation of biofilm matrix) or organism specific factors e.g., species and state of growth (Wingender et al., 1999; More et al., 2014; Flemming et al., 2016). The free microbial EPS of *Bacillus subtilis* ($\mathbf{P_{III}}$) harvested from the late stationary growth phase was found to be enriched in polysaccharides in comparison to proteins by Fourier-transform infrared spectroscopy (FTIR) and ^{13}C-nuclear magnetic resonance (NMR) spectroscopy ($\mathbf{P_{II}}$). Microbial EPS of *Bacillus subtilis* harvested at the early stationary growth phase (Liu et al., 2013) is differently composed and dominated by proteinious constituents ($\mathbf{P_{II}}$). In comparison, the composition of cutaneous mucus of two different earthworm species (*Lumbricus terrestris* L. and *Aporrectodea caliginosa* Sav.) was found as equivalent. Interestingly, mucus dominated by proteinious constituents shows similarities to microbial EPS of the early stationary growth phase. The comparison between $\mathbf{P_{II}}$ and $\mathbf{P_{III}}$ elucidates a different adsorption behavior of polysaccharide rich microbial EPS of the late stationary growth phase and protein rich mucus to goethite and illite. In general, we investigated mineral and biogenic OM composition specific adsorption behavior of mucus and bacterial EPS which led to a fractionation of biogenic OM between the solid (minerals) and the liquid phase (supernatants) during the batch experiments. In the case of goethite, exemplary phosphorus rich constituents absorb via the formation of Fe–O–P bonds (Omoike and Chorover, 2006) resulting in pH increase due to the release of surface hydroxyl groups. The treatments with illite were

unaffected in pH and we found only a slight adsorption of the polysaccharide rich EPS in comparison to protein rich mucus. In contrast, proteinious mucus constituents were found to adsorb under electrostatically unfavorable conditions where illite and mucus are negatively charged. Such hydrophobic interactions are typically reported for high molecular weight proteins (Yu et al., 2013) like bovine serum albumin (Kubiak-Ossowska et al., 2016; Kubiak-Ossowska et al., 2017). Consequently, an effective coating of mucus around illite and goethite was found, while the effect of a bacterial EPS coating was primary obtainable for goethite. As result we observe the formation of water-stable organo-mineral associations with screened surface charges in comparison to the bare mineral phase by the utilization of zeta potential measurements. For illite the surface charge of the mucus-illite association becomes less negative, whereas that of potential illite-EPS associations is barely influenced. For goethite, the bacterial EPS as well as mucus reduced the IEP of the associations in comparison to the bare goethite, but EPS seems to screen the surface of goethite more effectively. Thus, we found in accordance with $\mathbf{P_{II}}$ and $\mathbf{P_{III}}$, that approximately 5 to 6 mg mucus-C/g adsorb to goethite in comparison to more than 9 mg EPS-C/g. We attribute this to the previously mentioned important role of phosphorus containing constituents in the adsorption to goethite, if late stationary growth phase EPS was found to have a higher P/C-ratio than mucus (around 0.045 for EPS vs. approximatly 0.018 for mucus).

By comparing the polysaccharide rich microbial EPS ($\mathbf{P_{III}}$) with the protein rich mucus ($\mathbf{P_{II}}$) we get an impression how the composition of biogenic OM ($\mathbf{P_{I}}$) influences the formation of organo-mineral associations and their properties. Specifically, in terms of clay minerals as abundant secondary soil minerals the proteinious biogenic OM constituents are highlighted (Kleber et al., 2007) to form stable organo-mineral associations in soil (Le Mer et al., 2020). Moreover, Redmile-Gordon et al. (2020) attribute the stability of aggregates against wet sieving dominantly to proteins than polysaccharides. However, also polysaccharide rich biogenic OM like plant derived mucilage (containing more than 90 % polysaccharides: Carminati and Vetterlein, 2013) contribute massively to the alteration of soil properties (e.g., water retention: Ahmadi et al., 2017), organo-mineral association and aggregate formation (Morel et al., 1991; Grimal et al., 2001), especially in direct vicinity to the rhizosphere. According to our insights from $\mathbf{P_{II}}$ and $\mathbf{P_{III}}$, we avoid emphasizing one of the thematized organisms in its importance, since our literature research $\mathbf{P_{I}}$ clearly shows that these are interrelated via mutualistic relationships. For example, earthworms are dependent on the symbiotic bacteria in their gastrointestinal tract to improve the nutrient uptake from incorporated soil material (Lee, 1985; Lemtiri et al., 2014). In turn bacteria find stable environmental conditions inside earthworms (Brown et al., 2000). Furthermore, earthworm-formed structures like casts and burrow linings are enriched in carbon and nutrient elements and are frequently identified as spots of high microbial activity (Tiunov and Scheu, 1999; Aira et al., 2009; Stromberger et al., 2012). Recent studies like Le Mer et al. (2020)

contribute an enhanced availability of thermo-stable protein-enriched organo-mineral associations only to microbial EPS but consider the presence of earthworms predominantly as trigger for microbial activity due to (co-)decomposition. If we show that earthworm mucus is rich in proteinious constituents and is able to form water-stable mucus-mineral associations particularly with clay minerals, we would assume on the basis of $\mathbf{P_{II}}$ that a non-negligible proportion of the associations discussed in Le Mer et al. (2020) could be formed due to the direct influence of earthworms.

3.2. The role of biogenic OM in aggregate formation

The in $\mathbf{P_{II}}$ and $\mathbf{P_{III}}$ conducted batch experiments elucidate sometimes an unassociated fraction of organo-mineral associations, minerals and biogenic OM which is not involved in adsorption or the formation of aggregates and thus potentially available for transport, (im-)mobilization and decomposition (in the case of OM). In general, the alteration, release, and transport of potential MFMs and CBUs inside soil (Lehmann et al., 2021) is part of essential pedogenic processes like eluviation and illuviation leading to the formation of diagnostic soil horizons (Bronick and Lal, 2005; Ranville et al., 2005). If the soil is additionally impacted by bioturbation, soil biota activity and biogenic OM excretion, the fate of MFMs and CBUs can be additionally modified by the different roles of biogenic organic matter as gluing, separation, and bridging agent which we worked out in $\mathbf{P_{I}}$. Particularly, inside earthworm burrows as highly enlivened (Stromberger et al., 2012) preferential flow pathways (Lee and Foster, 1991; Edwards et al., 1993; Bastardie et al., 2005) mobilization and transport of organo-mineral associations has to be considered. For example, fresh earthworm casts are described as highly dispersible if no aging and drying leads to a strengthening of aggregate stability (Shipitalo and Protz, 1988, 1989) and are thus a potential source for mobile organo-mineral associations.

As mentioned above the surface charge of mucus- and EPS-mineral associations is altered in comparison to the bare minerals. Consequently, their interaction with each other or the immobile phase of soil differs in comparison to the bare mineral phases. For example, the batch reactor experiments of $\mathbf{P_{III}}$ clearly show the formation of mineral-mineral associations if no microbial EPS is available. At the experimental conditions (circumneutral pH), positively charged goethite serves as inorganic bridging agent and permits the aggregation between net negatively charged quartz and illite. Consequently, a fast formation of large gravitative sedimenting aggregates was observed. On the micro-scale, these aggregates show a homogeneous spatial arrangement of the single mineral constituents visualized with SEM-EDX mapping (scanning electron microscopy with energy-dispersive X-ray spectroscopy) and image analyses. The aggregation mediating effect of goethite as bridging aged is inhibited if this system was additionally treated with microbial EPS. Specifically, goethite becomes coated with EPS and the positive surface charges become screened which results in negative surface charges of the organo-mineral associations and electrostatic repulsion. As consequence, the EPS

enables a gravitative fractionation between small goethite, illite and greater quartz particles (Figure 7). Elemental mapping shows the separating effect also on the micro-scale where minerals are found to be distinct from each other in comparison to the EPS-free treatment. Generally, the stabilization of dispersions or the inhibition of aggregation due to OM surface screenings can be frequently found in literature as result of steric or electrostatic repulsion (e.g., PI; Tombácz et al., 2004; Flynn et al., 2012; Philippe and Schaumann, 2014; Pen et al., 2015). In contrast, during the batch experiments conducted for $\mathbf{P_{II}}$ an extensive aggregation of goethite-mucus associations can be found. Equally to $\mathbf{P_{III}}$ mucus was available in solution but additionally buffers the pH to the IEP of the newly formed organo-mineral associations and thus provoke a fast aggregation. Consequently, the energy barrier between the mucus-mineral associations was minimized and attractive Van der Waals forces take over. Under these conditions mucus serves as bridging agent and induces a fast aggregation in comparison to microbial EPS used in $\mathbf{P_{III}}$ which provokes a shielding by charge equalization under the applied experimental conditions (Figure 7). In addition, the formation of polymer bridges (Szilagyi et al., 2014b) is reported in literature for proteins and cannot be ruled out as additional aggregation supporting mechanism. However, the pH dependent surface properties of MFMs and CBUs were one aggregation controlling factor found in $\mathbf{P_{II}}$ and $\mathbf{P_{III}}$. In $\mathbf{P_{III}}$ also an enhanced electrolyte concentration was identified to contribute to an aggregation by reducing the range of electrostatic repulsion for EPS-free and containing treatments. With respect to the complex composition of biogenic OM from diverse species ($\mathbf{P_I}$) the opposing effects of low and high molecular weight OM with increasing electrolyte concentration have to be considered additionally, whereby for example bovine serum albumin (high molecular weight protein) permits aggregation at low electrolyte concentrations in comparison to cytochrome c (low molecular weight protein) (Sheng et al., 2016). Moreover, we only consider a biogenic OM availability in the same order of magnitude for $\mathbf{P_{II}}$ and $\mathbf{P_{III}}$ but the literature overview in $\mathbf{P_I}$ shows that aggregation is additionally affected by the amount and availability of OM. Narvekar et al. (2017) monitored a reduced homo-aggregation of colloidal hematite nanoparticles to a porous SiO_2 medium with increasing loadings of EPS (polysaccharide rich) on the hematite surfaces. In turn at low EPS loadings at hematite nanoparticles, the EPS-hematite associations start to homo-aggregate as the experimental pH approaches the IEP of the associations. Further studies report that also patchy distributed polymer coils were able to screen the charge of surfaces effective with increasing number (Duffadar et al., 2009). This is particularly relevant because Liu et al. (2013) report an inhomogeneous patchy distribution EPS on goethite surface in polysaccharide and proteins separated domains. A different behavior was reported by Flynn et al. (2012) for bovine serum albumin. Here the association of latex microspheres to a porous medium of iron-oxide coated sand was found as increased with increased protein availability.

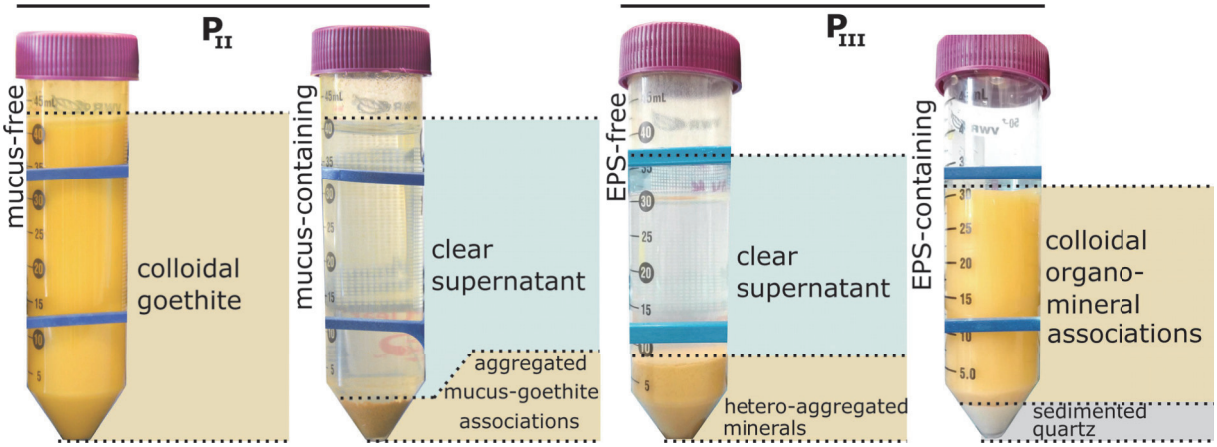

Figure 7: Completely mixed batch reactor experiments 30 min after stopping shaking. The mucus-free samples from P_{II} show a colloidal stable goethite in comparison to fast aggregating mucus-mineral association in mucus-containing samples. In comparison, EPS-free samples from P_{III} hetero-aggregate fast whereas EPS-containing samples separating in phases.

However, the function of biogenic OM as separation and bridging agent was shown as driven by many factors (e.g., pH, electric conductivity, soil biota activity and OM composition). Thus, to trace the fate of organo-mineral associations in natural porous media is quite challenging if the occurrence of alternating and dynamic environmental conditions is considered additionally. For example, the aging and drying of biogenically formed structures like earthworm casts is reported as increasing the water stability of aggregates (Shipitalo and Protz, 1989). For example, in **P_{III}** we conducted a drying step and found an increased aggregation stability in treatments containing microbial EPS in comparison to EPS-fee treatments. As mentioned in **P_I** during subsequent drying menisci evolves between particles and pull smaller particles and unassociated OM together. Thus, the contact area between greater particles increases (e.g., Horn and Dexter, 1989; Semmel et al., 1990; Horn et al., 1994; Denef et al., 2002). As result, in EPS-free attractive systems large quartz particles become totally covered and interlinked by illite and goethite. In contrast, the almost repulsive EPS-containing treatment represents mostly uncoated quartz particles which are merely interlinked at their contact points (Figure 8). Consequently, electrostatically unfavored organo-mineral associations and unassociated/loosely bound EPS become involved in this aggregation process, then external forces like menisci forces (Seiphoori et al., 2020) or an active compression of particles (Pen et al., 2015) are able to reduce the distance between otherwise electrostatically repulsive particles. Consequently, EPS and EPS coated minerals can potentially serve as gluing agent, in particular if they have a hydrophobic character after drying out, which leads to an enhanced water stability of resulting aggregates (Morel et al., 1991; Carminati et al., 2016). Such stabilizing effects are exemplary reported for bacteria cells and cell envelopes which serve as aggregation permitting after multiple wetting and drying cycles (Krause et al., 2019) and mucilage as well as EPS which are able to form filaments between soil particles after drying out (Benard et al.,

2019).

In summary we provide experimental evidence in $\mathbf{P_{II}}$ and $\mathbf{P_{III}}$ for the in $\mathbf{P_I}$ defined roles of biogenic OM in aggregate formation. The roles as separation and bridging agent were shown as affected by the pH and ionic strength of the solution and the type and availability of mineral and OM surface/functional groups. These factors become less relevant if an external force led to a close approach of particles and biogenic OM can take their role as gluing agent.

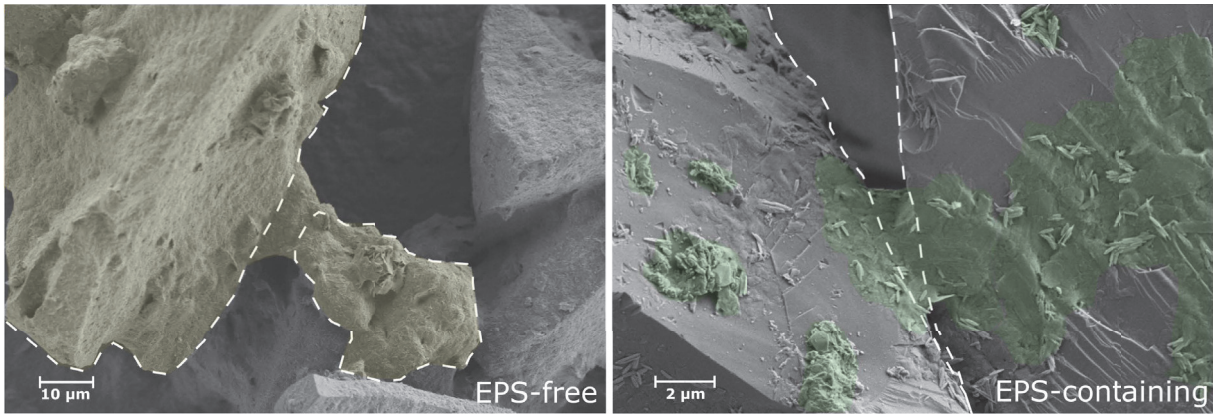

Figure 8: Scanning electron microscopy images of contact points between large quartz particles after conducting a drying step in PIII. The EPS-free sample is characterised by an extensive goethite/illite-coating and -bridges (highlighted in yellow) between greater particles (marked with white dashed line). In comparison, the sample from the EPS-containing treatment show particle enrichments primary at the narrowest point between larger particles (highlighted in green).

3.3. Comparison between *in vitro* and *in silico* studies

The shape, size, type of MFMs, type of additives in suspension and surface coatings/screenings are reported as important factors (Hotze et al., 2010) controlling the aggregation of MFMs in an aqueous system. Regarding the different boundary conditions which are relevant in soil and the multitude of potential scenarios, computational simulations are helpful tools to predict the self-assembly of oppositely charged particles/MFMs, validate conceptual assumptions and determine optima of aggregation (Cerbelaud et al., 2010). Furthermore, with the support of numerical studies can be shown that ongoing aggregation is a dynamic and hierarchical process (Tateno and Tanaka, 2019) which occurs as result of the stepwise formation of aggregates increasing in complexity (Szilagyi et al., 2014a). Thus, the successive formation of aggregates controlled by their initial boundary conditions was part of numeric experiments performed as in $\mathbf{P_{IV}}$ and $\mathbf{P_V}$.

3.3.1. Effect of boundary conditions on charge induced aggregation

As mentioned before the surface charge of particles is shaping the initial attachment of MFMs. Thus, we confirmed in $\mathbf{P_I}$, $\mathbf{P_{II}}$ and $\mathbf{P_{III}}$ that the adsorption and aggregation behavior of the most MFMs in soil (e.g., biogenic OM and soil minerals) is initially controlled by surface properties specific for the surrounding pH and electric conductivity (e.g., Hotze et al., 2010; Philippe and Schaumann, 2014;

Trefalt et al., 2014). But for more detailed insights in aggregation, further changes in the experimental boundary conditions like variable pH values, particle amounts, particle ratios and sizes rapidly lead to a massive increase of the experimental efforts.

For example, as part of $\mathbf{P_{IV}}$ we adjust the fractions of interacting mineral prototypes and can thus observe an optimum of aggregation if the net charge of the system tends to zero, which contributes to an equivalent amount of positively and negatively charged surface sites provided by the MFMs. A similar aggregation behavior was previously discussed for the aggregation of mucus-goethite associations ($\mathbf{P_{II}}$) near to their IEP/PZC. As result of such optimal charge circumstance, large fractal aggregates grow which are primarily limited in the availability of interaction partners. In natural systems further mechanisms limit the aggregate growth also under optimal conditions. Particularly, if transport and/or gravity is considered during aggregation the size/density specific translocations of growing aggregates and their increasing fragility against external stresses (González, 2002, 2016; Lazzari et al., 2016) affect aggregate growth and aggregation rates. For example, for scenarios modeled in $\mathbf{P_V}$ we found aggregation inhibiting effects if the charge specific energy barrier between the mineral prototypes becomes reduced (pH 3) and the aggregation is favored. Under such conditions a fast aggregate formation leads to fast gravitative separation between small particles/aggregates and large aggregates and thus to an increase in diffusion lengths between fast sedimenting/sedimented and still dispersed/slow sedimenting particles. An opposing behavior was found if the energy barriers were increased (pH 9), on the long-term the gravitative settlement led to reduction of the diffusion length and can enforce a close approach of MFMs.

If a charge difference between interacting MFMs occurs, we obtain an evolution of small and dense structures in $\mathbf{P_{III}}$ (mineral-mineral associations), for example if positively charged mineral prototypes are available in excess. The surface coating of oppositely charged surfaces lead to a shielding and an inhibition of further aggregate growth. For example, the inhibition of aggregation due to charge shielding of clay minerals by the addition of iron oxides is reported for experimental studies (Ohtsubo et al., 1991). Such shielding results in a similar phenomenology like that caused by a biogenic separation agent ($\mathbf{P_I}$) which we observe in the case of microbial EPS-screening investigated in $\mathbf{P_{III}}$. Here the microbial EPS-coatings as well as the availability of not associated EPS in solution force the charge equalization (surplus of negative surface charges) of interacting particles and enables subsequent gravitative particle separation according to the initial particle size.

Summarizing the observations from the *in vitro* and *in silico* studies it becomes clear that particle charge is an aggregation shaping factor, especially for the initial aggregation from the aqueous phase. However, for a comprehensive insight into the particle aggregation far more mechanisms like hydration pressure, Lewis acid base interactions, hydrogen bonding, steric and hydrophobic interactions have to be considered (e.g., Grasso et al., 2002; Min et al., 2008). Consequently, for systems containing organic

MFMs the classical DLVO theory was often found as insufficient. For example, for the adhesion of bacteria via EPS to mineral surfaces (Azeredo et al., 1999) or the deposition of nanoparticles on bacteria surface (Hwang et al., 2012) hydrophobic interaction are additionally considered. Thus, the application of the extended-DLVO was found as promising. Besides, the literature review of **P_I** discusses other aggregation control factors that are difficult to consider simultaneously and demonstrates why the use of simplified models and experiments is a useful tool for gaining insight into increasingly complex systems such as natural soils.

3.3.2. Effect of particle size

Beside the charge and number, the dimension of interplaying MFMs regulates aggregation (Min et al., 2008). For example, He et al. (2008) reports for the homo-aggregation of differently sized nano-hematite particles higher aggregation rates with decreasing particle sizes which is in line with the numerical results found for the three mineral prototypes investigated in **P_V**. However, for hetero-aggregation we observe in our numerical approach **P_{IV}** that especially the size ratio has massive implications for resulting aggregate size and compactness (Yates et al., 2008; Cerbelaud et al., 2017; Dultz et al., 2019). In particular, the particle size of small oppositely charged particles in relation to large particles decides how many small particles are needed for a charge neutralization of large particle surfaces as well as optimal aggregation (Yates et al., 2005). Thus, Dultz et al. (2019) refer an optimal aggregation for the hetero-aggregation of differently sized goethite and illite particles also to a balanced availability of positive and negative charges resulting in a measured net system charge near to zero. Furthermore, Katainen et al. (2006) shows by studying different particle sizes and surface roughness that the amount of the resulting contact areas between interacting surfaces is a leading factor for the strength of aggregation. A positive effect of a particle size mismatch for the improvement of aggregation was also reported during drying steps and the formation of menisci which are able to pull small particles between greater particles together and thus increase the contact area due to formation of solid bridges (Seiphoori et al., 2020). As mentioned above we attribute the formation of the largest aggregates found in **P_{III}** (Figure 8) to this mechanism which is more driven by particle size than particle charge.

The dynamics between differently sized particles become more complex if we consider the simultaneous impact of gravity which leads to a size/density specific sedimentation velocity (Dukhin et al., 2007) of interacting MFMs. As mentioned above, in **P_{III}** the differences in MFM size force the fractionation of equally charged (due to EPS coating) but differently sized MFMs which result in the formation of gradually layered sediments. Thus, gravitative controlled systems are characterized by phase separation in accordance with the physicochemical properties of the contained constituents which leads to the formation of distinct domains (e.g., Wensink and Lekkerkerker, 2004; de las Heras

and Schmidt, 2013; Avvisati et al., 2017). Equivalent to layered sediments, anisotropic formed aggregates are reported if gravity is considered in numerical und experimental studies (Dukhin et al., 2007; de las Heras et al., 2016; González, 2016). Here large aggregates and particles are able to sediment fast and thus can be predominantly found in the lower part of the finally formed aggregates. In comparison, small more diffusively controlled particles sediment later and can thus be found more often in the upper part of the final aggregates. Consequently, during the *in silico* experiments of $\mathbf{P_V}$ the distribution of the differently sized mineral prototypes inside aggregates formed under a gravity field are anisotropic on the Z-axis. Inside the gradual layered sediments found for EPS-containing treatments of $\mathbf{P_{III}}$ we also found a high degree of spatial self-organization controlled via the interplay of electrostatically repulsion and gravitative settlement. Considering the here found intensive effect of electrostatic repulsion on the spatial distribution of MFMs, one question remains: Why did we find an increase in particle size by laser light diffraction in a system which is obviously controlled by the separating effect of microbial EPS-coating (Figure 7)?

A possible explanation arises if we consider the functional roles of biogenically excreted OM from $\mathbf{P_I}$ together with the numerical simulations from $\mathbf{P_V}$. In $\mathbf{P_I}$ we extensively discussed the effect of a gluing agent which we defined as:

Gluing agents mediate aggregate stability and a close approach of particles and OM after an external force supply, e.g., compaction, gravitative sedimentation, and menisci forces/drying. Thereby, the aggregation inhibiting effect of the separation agents can be compensated after an external force provokes a close approach of soil particles until attractive short-range forces like Van Der Waals interactions take over and aging/drying leads to the agglutination of particles (e.g., due to hydrophobic particle interlinkages which increase their water stability). Here, the collision/attachment probability of particles is primarily controlled by the strength and duration of external force supply.

Hence beside the previously discussed meniscal forces (e.g., Denef et al., 2002; Seiphoori et al., 2020), gravity is also expected as aggregation supporting (Wilson et al., 2000) because it can potentially serve as external force which is able to provoke a close approach of electrostatic repulsive surfaces (Chen et al., 2010) and enhance the chance that further mechanisms lead to an aggregation e.g., hydrophobics or short-range Van Der Waals forces. Consequently, in $\mathbf{P_{III}}$ an aggregation could be provoked during the period of particle sedimentation which occurs successively after ending the batch experiments and before the particle size measurements were performed. In addition, in $\mathbf{P_V}$ gravity was identified as aggregation promoting for energy barrier limited systems because ongoing particle settlement resulted in a continuously decreasing mean distance between particles. In turn, this can also promote electrostatically controlled polymer bridging (Sheng et al., 2016), if gravitative sedimentation serve as external force supply during aggregation. In accordance, AFM studies of Szilagyi et al. (2014b) and Pen et al. (2015) clearly demonstrates also for electrostatically repulsive systems the bridging effect of

polymers if a compression of the polymer against the mineral surface was performed. Furthermore, after such a close approach energy is needed to remove the polymer functionalist AFM-tips from the mineral surfaces. The detected force distance curves exhibit a successive disruption of polymer chains. Combining these findings, EPS could serve as gluing agent after sedimentation and form more water stable aggregates then those resulting from the EPS-free treatment in $\mathbf{P_{III}}$.

However, based on the interrelated consideration of the *in silico* and *in vitro* studies, we confirm that the effect of biogenic OM on aggregation (in details discussed in $\mathbf{P_I}$) cannot be attributed to one specific functional role (bridging, gluing or separation) because these were identified as not mutually exclusive. Consequently, in natural three phase systems like soil, impacted by alternating boundary conditions and frequently disturbed and processed by soil biota, tracking the path of biogenically excreted OM is an ongoing challenge.

3.3.3. Dynamics of structure formation

In experimental studies the formation of aggregates was mostly measured by particle size increment via optical measurement techniques. The interactions between the individual MFMs, on the other hand, are invisible to most laboratory methods. In contrast, the *in silico* studies performed in $\mathbf{P_{IV}}$ and $\mathbf{P_V}$ allow an insight in the dynamic and hierarchical evolution of aggregates. For example, aggregation favouring scenarios of $\mathbf{P_{IV}}$ show the stepwise formation of aggregate structures which successively become increased in complexity. This aggregation process includes the initial formation of particle dimers and the formation of highly complex aggregates at later stages also reported in Szilagyi et al. (2014a). During subsequent aggregation, a stepwise self-organisation can be observed in accordance with the demixing of the colloidal suspension, whereby aggregates become formed and co-exist with free primary particles which become later involved in the aggregate structure (Tateno and Tanaka, 2019). In comparison, the aggregate growth was found as inhibited in $\mathbf{P_{IV}}$ if particle shielding occur and thus an aggregate growth was interrupted at an early stage of the numerical experiments. Here, an in excess available mineral prototype serves as separation agent and thus finally only small mineral-mineral associations are formed which are not able to further aggregate which each other. Furthermore, the dynamics of aggregate formation was found as function of the solid liquid ratio of the observed system. Thus, scenarios with high particle concentrations lead to the formation of large and coiled aggregates, in comparison to short chain-like aggregates at low concentrations. In attractive scenarios, high solid contents are characterised by fast aggregation due to short diffusion length. Furthermore, Hütter (2000) demonstrated for dense colloidal suspension and low energy barriers between the particles a fast aggregation since particles aggregate with their immediate neighbours and form voluminous aggregates. In comparison, an increase in the energy barrier led to a slow formation of denser aggregates since particles have to pass longer distances and enter also pre-existing structures

to find potential interaction partners.

However, in **P_V** the aggregation dynamics are expected to be increased in complexity if the third dimension and the impact of gravity was additionally considered in comparison to **P_{IV}**. In a gravitational field the aggregation becomes more complicated if aggregates grow until they become large enough to settle and form aggregates/sediments on the bottom of the observed domain (Allain et al., 1996). Furthermore, a spatial depletion of interacting particles/aggregates according to their size is able to provoke a coexistence of large and small particles/aggregates that are divided into separate domains (González, 2016). Consequently, for the gravity constrained scenarios the mean distance between particles is beside the effect of aggregation (depletion of potential interaction via aggregate formation) influenced by the gravitative movement of mineral prototypes and aggregates. For **P_V** we report three gravity-controlled aggregation mechanisms which operating simultaneously but in different degree according to the initial particles size and surface potentials. The first aggregation promoting mechanisms (I) is caused by the spatial confinement of particle during settlement which leads to ongoing reduction of the mean distance between particles and aggregates. The second aggregation mechanism (II) promotes aggregation due to differential settling whereby fast and slow particles/aggregates collide during settlement. The last described mechanism inhibits aggregation due to fractionation of particles/aggregates with different settling velocities (for details see **P_v**; Figure 9).

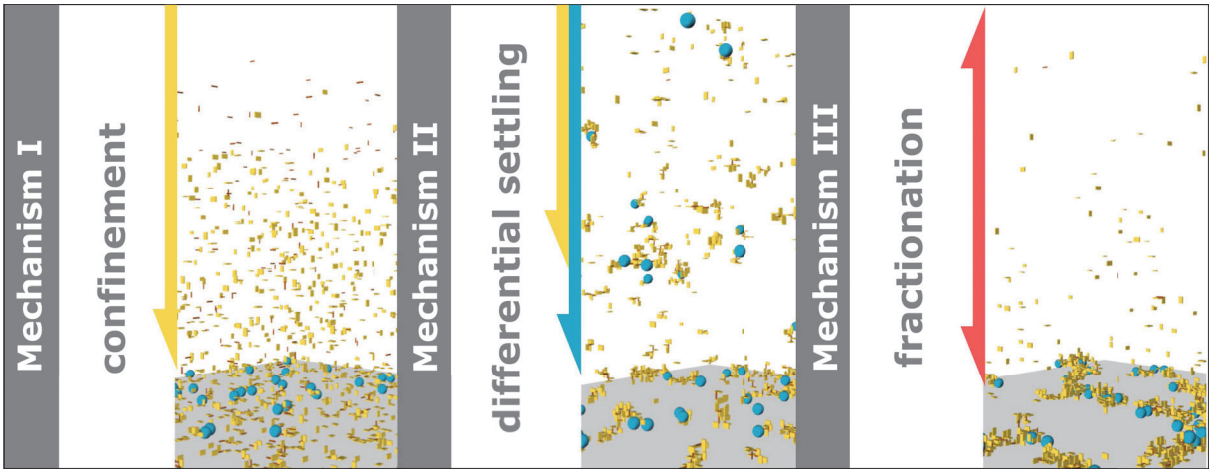

Figure 9: Simplified scheme of gravity-controlled aggregation mechanisms obtained in P_V which are able to indirectly promote (mechanism I: due to space confinement), directly promote (mechanism II: differential settling) and inhibiting (mechanism III: due to fractionation) the aggregation between three mineral prototypes (red rods, blue spheres and yellow plates).

We found that the dynamics of aggregation can be characterized by the successive bond formation between particles and aggregates which is a function of primary minerals size and the energy barriers in between. However, for the model applied in **P_V** these bonds are considered as irreversible but the strength of the bonds between particles decreases with increasing particle size as result of weaker Van der Waals forces (Sandkühler et al., 2005). In addition, with increasing aggregate size increasing shear stress act on the formed aggregates (Lazzari et al., 2016). Consequently, Allain et al. (1996) described

the collision rate in gravity driven systems as controlled by Brownian diffusion, settling motion (considered in $\mathbf{P_V}$) and the restructuring of aggregates after breakage (consider in $\mathbf{P_{IV}}$ as breakage rule). If the breakage of aggregates is considered simultaneously to gravity, higher fractal dimensions are reported as result of the occlusion of small aggregates and particles into the cavities of larger sedimenting clusters which lead to more compact structures (González, 2016). The relation between particle settlement and particles attraction is the deciding factor in whether a dense aggregating sediment is formed after particle settlement (settlement > attraction) or a loosely packed flocked sediments can be found (settlement < attraction) (Whitmer and Luijten, 2011). In the broadest sense, this observation can be applied to our example from $\mathbf{P_{III}}$ whereby the EPS-coatings hinders the aggregation in the liquid phase and enforces the formation of densely deposited sediments. Furthermore, for the EPS-free treatments and the mucus-mineral associations (pH near the IEP; obtained from $\mathbf{P_{II}}$) a fast aggregation of fluffy aggregates can be observed resulting also in voluminous sediments (Figure 7). Finally, in structured natural porous media the dynamics in aggregate formation underlay further aggregation shaping factors. Exemplary, the restrictions of the pore space as well as the interactions with the immobile phase were shown by Ritschel and Totsche (2020) as causing structural features during aggregation in response to particle transport, fluid flow, tortuosity, connectivity, and permeability of pores.

4. Conclusion

The initial aggregation from the aqueous phase is driven by electrostatic interaction between MFMs. Therefore, specifically the formation of homo-aggregates depends on the relation between positively and negatively charged surface sides and thus is controlled by the portions of oppositely charged MFMs and their size mismatch. Furthermore, the self-assembly of aggregates responds to the impact of perikinetic and orthokinetic aggregation processes. Specifically, directed particle movement or movement constrains (for example provoked via gravity) influence the aggregation dynamics and shape the spatial arrangement of MFMs inside aggregates. However, external forces are valid to overcome long range electrostatic barriers between MFMs and thus provoke an aggregation e.g., via short range attractive forces. Consequently, inside alternating natural systems like soil, characterized by shrinking and swelling, fluid and matter transport as well as periodic desiccation, electrostatics and external forces effect aggregate formation simultaneously. The dynamics in aggregation exponentiates with the activity of soil biota via bioturbation and biogenic OM secretion. For instance, earthworms, plant roots, bacteria, and fungi provide complex biopolymer mixtures containing organic macro-molecules like proteins, polysaccharides, and carbohydrates for different purposes like communication, nutrient release, or habitat optimization. Thus, these organisms alone, in mutualistic relationships or in food webs are able to shape soil structure and properties. Specifically, the transition zones between soil biota, detritus, and the mineral phase of soil (e.g., drilosphere and rhizosphere) is predestinated as hub for organo-mineral association and biogenic aggregate formation. Here soil mineral and still existing aggregates become permeated with biogenic OM, rearranged, compacted, or even disaggregated. In response to the biopolymer characteristics, soil mineral composition and the environmental properties, biogenic OM is found to take three prominent roles as bridging, separation, and gluing agent. As separation agent biogenic OM is able to screen the properties of pre-existing minerals, associations and aggregates and thus potentially provoke aggregation inhibiting conditions like charge equalization or steric repulsion. Vice versa, OM surface screenings as well as the presence of biogenic OM inside the soil solution harbors the potential to provoke aggregation inducing conditions. For example, solution pH and surface charge adaptations near to the IEP of interacting MFMs as well as the formation of polymer bridges are mechanisms which induce fast aggregation. In both these roles, the electrostatics (controlled by the pH and the expansion of the electric double layer around charged particles) are known as main mechanism of particle interaction or at least influencing further mechanisms via the modulation of collusion probability between MFMs in the aqueous phase. However, if an external force like gravity, compaction or menisci forces reduce the distance between MFMs, the meaning of electrostatics become massively reduced and partially compensated. Thus, alteration and drying out of aggregates can lead to the formation of water stable aggregates if hydrophobic biogenic OM is available as gluing agent. Finally, the feedback between reinforcing and

antagonistic mechanisms leads to a hierarchical and dynamic arrangement of particles, resulting in phase separation, formation of layered sediments and anisotropic structures, voluminous porous aggregates or even the formation of diagnostic soil horizons.

Future research efforts should address aggregation processes and structure formation from the perspective of different scientific subdivisions and scales, combining observations from *in situ* (field studies), *in vitro* (laboratory experiments), and *in silico* (computational methods) studies. In particular, the monocausal explanatory approaches repeatedly found in the literature, which overemphasize the importance of a single aspect of research, must be placed in a higher-level context. For example, laboratory-scale adsorption studies could help provide insight into nutrient storage/pollutant sequestration in soil, or experimental soil science reveals specific aggregation mechanisms underlying the formation of water-stable aggregates at the field scale. If we strive to implement the knowledge acquired, we will be able to develop sustainable soil management strategies and ensure the maintenance of soil quality and health under the influence of climate change.

5. References

Ahmadi, K., Zarebanadkouki, M., Ahmed, M.A., Ferrarini, A., Kuzyakov, Y., Kostka, S.J., Carminati, A., 2017. Rhizosphere engineering: Innovative improvement of root environment. Rhizosphere 3, 176-184.

Aira, M., McNamara, N.P., Piearce, T.G., Domínguez, J., 2009. Microbial communities of *Lumbricus terrestris* L. middens: structure, activity, and changes through time in relation to earthworm presence. Journal of Soils and Sediments 9, 54-61.

Ali, S., Bandyopadhyay, R., 2016. Aggregation and stability of anisotropic charged clay colloids in aqueous medium in the presence of salt. Faraday Discussions 186, 455-471.

Allain, C., Cloitre, M., Parisse, F., 1996. Settling by cluster deposition in aggregating colloidal suspensions. Journal of Colloid and Interface Science 178, 411-416.

Allain, C., Cloitre, M., Wafra, M., 1995. Aggregation and sedimentation in colloidal suspensions. Physical Review Letters 74, 1478.

Alvarez-Silva, M., Mirnezami, M., Uribe-Salas, A., Finch, J.A., 2010. Point of zero charge, isoelectric point and aggregation of phyllosilicate minerals. Canadian Metallurgical Quarterly 49, 405-410.

Assemi, S., Hartley, P.G., Scales, P.J., Beckett, R., 2004. Investigation of adsorbed humic substances using atomic force microscopy. Colloids and Surfaces A: Physicochemical and Engineering Aspects 248, 17-23.

Avvisati, G., Dasgupta, T., Dijkstra, M., 2017. Fabrication of colloidal laves phases via hard tetramers and hard spheres: Bulk phase diagram and sedimentation behavior. ACS Nano 11, 7702-7709.

Azeredo, J., Visser, J., Oliveira, R., 1999. Exopolymers in bacterial adhesion: interpretation in terms of DLVO and XDLVO theories. Colloids and Surfaces B: Biointerfaces 14, 141-148.

Baldock, J.A., 2002. Interactions of organic materials and microorganisms with minerals in the stabilization of structure, In: Huang, P.M., Bollag, J.M., Senesi, N. (Eds.), Interactions between Soil Particles and Microorganisms, pp. 85-131.

Bansal, P., Deshpande, A.P., Basavaraj, M.G., 2017. Hetero-aggregation of oppositely charged nanoparticles. Journal of Colloid and Interface Science 492, 92-100.

Barrios, E., 2007. Soil biota, ecosystem services and land productivity. Ecological Economics 64, 269-285.

Bastardie, F., Ruy, S., Cluzeau, D., 2005. Assessment of earthworm contribution to soil hydrology: A laboratory method to measure water diffusion through burrow walls. Biology and Fertility of Soils 41, 124-128.

Baveye, P.C., 2021. Bypass and hyperbole in soil research: Worrisome practices critically reviewed through examples. European Journal of Soil Science 72, 1-20.

Becker, T., Gorham, N., Shiers, D.W., Watling, H.R., 2011. In situ imaging of Sulfobacillus thermosulfidooxidans on pyrite under conditions of variable pH using tapping mode atomic force microscopy. Process Biochemistry 46, 966-976.

Benard, P., Zarebanadkouki, M., Brax, M., Kaltenbach, R., Jerjen, I., Marone, F., Couradeau, E., Felde, V.J., Kaestner, A., Carminati, A., 2019. Microhydrological niches in soils: How mucilage and EPS alter the

biophysical properties of the rhizosphere and other biological hotspots. Vadose Zone Journal 18, 180211.

Blume, H.-P., Brümmer, G.W., Horn, R., Kandeler, E., Kögel-Knabner, I., Kretzschmar, R., Stahr, K., Wilke, B.-M., Thiele-Bruhn, S., Welp, G., 2010. Scheffer/Schachtschabel: Lehrbuch der Bodenkunde. Spektrum Akademischer Verlag, Heidelberg.

Bottinelli, N., Jouquet, P., Capowiez, Y., Podwojewski, P., Grimaldi, M., Peng, X., 2015. Why is the influence of soil macrofauna on soil structure only considered by soil ecologists? Soil and Tillage Research 146, 118-124.

Bronick, C.J., Lal, R., 2005. Soil structure and management: A review. Geoderma 124, 3-22.

Brown, G.G., Barois, I., Lavelle, P., 2000. Regulation of soil organic matter dynamics and microbial activityin the drilosphere and the role of interactionswith other edaphic functional domains. European Journal of Soil Biology 36, 177-198.

Buettner, S.W., Kramer, M.G., Chadwick, O.A., Thompson, A., 2014. Mobilization of colloidal carbon during iron reduction in basaltic soils. Geoderma 221, 139-145.

Buffle, J., Leppard, G.G., 1995. Characterization of aquatic colloids and macromolecules. 1. Structure and behavior of colloidal material. Environmental Science & Technology 29, 2169-2175.

Burns, J.L., Yan, Y.-d., Jameson, G.J., Biggs, S., 1997. A light scattering study of the fractal aggregation behavior of a model colloidal system. Langmuir 13, 6413-6420.

Cai, P., Lin, D., Peacock, C.L., Peng, W., Huang, Q., 2018. EPS adsorption to goethite: molecular level adsorption mechanisms using 2D correlation spectroscopy. Chemical Geology 494, 127-135.

Campbell, E.E., Paustian, K., 2015. Current developments in soil organic matter modeling and the expansion of model applications: A review. Environmental Research Letters 10, 123004.

Cao, T., Borkovec, M., Trefalt, G., 2020. Heteroaggregation and homoaggregation of latex particles in the presence of alkyl sulfate surfactants. Colloids and Interfaces 4, 52.

Cao, Y., Wei, X., Cai, P., Huang, Q., Rong, X., Liang, W., 2011. Preferential adsorption of extracellular polymeric substances from bacteria on clay minerals and iron oxide. Colloids and Surfaces B: Biointerfaces 83, 122-127.

Carminati, A., Vetterlein, D., 2013. Plasticity of rhizosphere hydraulic properties as a key for efficient utilization of scarce resources. Annals of Botany 112, 277-290.

Carminati, A., Zarebanadkouki, M., Kroener, E., Ahmed, M.A., Holz, M., 2016. Biophysical rhizosphere processes affecting root water uptake. Annals of Botany 118, 561-571.

Cerbelaud, M., Videcoq, A., Abélard, P., Pagnoux, C., Rossignol, F., Ferrando, R., 2010. Self-assembly of oppositely charged particles in dilute ceramic suspensions: Predictive role of simulations. Soft Matter 6, 370-382.

Cerbelaud, M., Videcoq, A., Rossignol, F., Piechowiak, M.A., Bochicchio, D., Ferrando, R., 2017. Heteroaggregation of ceramic colloids in suspensions. Advances in Physics: X 2, 35-53.

Chartres, C.J., Kirby, J.M., Raupach, M., 1990. Poorly ordered silica and aluminosilicates as temporary cementing agents in hard-setting soils. Soil Science Society of America Journal 54, 1060-1067.

Chen, G., Hong, Y., Walker, S.L., 2010. Colloidal and bacterial deposition: Role of gravity. Langmuir 26, 314-319.

Chen, Y., Wang, M., Zhou, X., Fu, H., Qu, X., Zhu, D., 2021. Sorption fractionation of bacterial extracellular polymeric substances (EPS) on mineral surfaces and associated effects on phenanthrene sorption to EPS-mineral complexes. Chemosphere 263, 128264.

Chenu, C., Plante, A.F., 2006. Clay-sized organo-mineral complexes in a cultivation chronosequence: Revisiting the concept of the 'primary organo-mineral complex'. European Journal of Soil Science 57, 596-607.

Christensen, B.T., 2001. Physical fractionation of soil and structural and functional complexity in organic matter turnover. European Journal of Soil Science 52, 345-353.

Clavier, A., Praetorius, A., Stoll, S., 2019. Determination of nanoparticle heteroaggregation attachment efficiencies and rates in presence of natural organic matter monomers. Monte Carlo modelling. Science of the Total Environment 650, 530-540.

Cornell, R.M., Schwertmann, U., 2003. The iron oxides: Structure, properties, reactions, occurrences and uses. WILEY-VCH Verlag, Weinheim.

Costa, O.Y., Raaijmakers, J.M., Kuramae, E.E., 2018. Microbial extracellular polymeric substances: Ecological function and impact on soil aggregation. Frontiers in Microbiology 9, 1636.

Crawford, J.W., Deacon, L., Grinev, D., Harris, J.A., Ritz, K., Singh, B.K., Young, I., 2012. Microbial diversity affects self-organization of the soil–microbe system with consequences for function. Journal of the Royal Society Interface 9, 1302-1310.

Davis, N., Polhill, J.G., Aitkenhead, M.J., 2021. Measuring heterogeneity in soil networks: A network analysis and simulation-based approach. Ecological Modelling 439, 109308.

de las Heras, D., Schmidt, M., 2013. The phase stacking diagram of colloidal mixtures under gravity. Soft Matter 9, 8636-8641.

de las Heras, D., Treffenstädt, L.L., Schmidt, M., 2016. Reentrant network formation in patchy colloidal mixtures under gravity. Physical Review E 93, 030601.

Deckmyn, G., Flores, O., Mayer, M., Domene, X., Schnepf, A., Kuka, K., Van Looy, K., Rasse, D.P., Briones, M.J.I., Barot, S., 2020. KEYLINK: Towards a more integrative soil representation for inclusion in ecosystem scale models. I. Review and model concept. PeerJ 8, 1-69.

Denef, K., Six, J., Merckx, R., Paustian, K., 2002. Short-term effects of biological and physical forces on aggregate formation in soils with different clay mineralogy. Plant and Soil 246, 185-200.

Diao, Y., Espinosa-Marzal, R.M., 2016. Molecular insight into the nanoconfined calcite–solution interface. Proceedings of the National Academy of Sciences 113, 12047-12052.

Dogsa, I., Kriechbaum, M., Stopar, D., Laggner, P., 2005. Structure of bacterial extracellular polymeric substances at different pH values as determined by SAXS. Biophysical Journal 89, 2711-2720.

Dokou, E., Barteau, M.A., Wagner, N.J., Lenhoff, A.M., 2001. Effect of gravity on colloidal deposition studied by atomic force microscopy. Journal of Colloid and Interface Science 240, 9-16.

Duffadar, R., Kalasin, S., Davis, J.M., Santore, M.M., 2009. The impact of nanoscale chemical features

on micron-scale adhesion: Crossover from heterogeneity-dominated to mean-field behavior. Journal of Colloid and Interface Science 337, 396-407.

Dukhin, A.S., Dukhin, S.S., Goetz, P.J., 2007. Gravity as a factor of aggregative stability and coagulation. Advances in Colloid and Interface Science 134, 35-71.

Dultz, S., Woche, S.K., Mikutta, R., Schrapel, M., Guggenberger, G., 2019. Size and charge constraints in microaggregation: Model experiments with mineral particle size fractions. Applied Clay Science 170, 29-40.

Edwards, A.P., Bremner, J.M., 1967. Dispersion of soil particles by sonic vibration. Journal of Soil Science 18, 47-63.

Edwards, W.M., Shipitalo, M.J., Owens, L.B., Dick, W.A., 1993. Factors affecting preferential flow of water and atrazine through earthworm burrows under continuous no-till corn. Journal of Environmental Quality 22, 453-457.

Eusterhues, K., Neidhardt, J., Hädrich, A., Küsel, K., Totsche, K.U., 2014. Biodegradation of ferrihydrite-associated organic matter. Biogeochemistry 119, 45-50.

Evangelou, V.P., 1998. Environmental soil and water chemistry. John Wiley, New York, Chichester, Weinheim, Brisbane, Singapore, Toronto.

Fang, L., Cao, Y., Huang, Q., Walker, S.L., Cai, P., 2012. Reactions between bacterial exopolymers and goethite: A combined macroscopic and spectroscopic investigation. Water Research 46, 5613-5620.

Fang, L., Huang, Q., Wei, X., Liang, W., Rong, X., Chen, W., Cai, P., 2010. Microcalorimetric and potentiometric titration studies on the adsorption of copper by extracellular polymeric substances (EPS), minerals and their composites. Bioresource Technology 101, 5774-5779.

Felde, V.J.M.N.L., Schweizer, S.A., Biesgen, D., Ulbrich, A., Uteau, D., Knief, C., Graf-Rosenfellner, M., Kögel-Knabner, I., Peth, S., 2021. Wet sieving versus dry crushing: Soil microaggregates reveal different physical structure, bacterial diversity and organic matter composition in a clay gradient. European Journal of Soil Science 72, 810-828.

Flemming, H.-C., Wingender, J., Szewzyk, U., Steinberg, P., Rice, S.A., Kjelleberg, S., 2016. Biofilms: An emergent form of bacterial life. Nature Reviews Microbiology 14, 563-575.

Flores, O., Deckmyn, G., Yuste, J.C., Javaux, M., Uvarov, A., van der Linde, S., De Vos, B., Vereecken, H., Jiménez, J., Vinduskova, O., 2021. KEYLINK: Towards a more integrative soil representation for inclusion in ecosystem scale models—II: Model description, implementation and testing. PeerJ 9, 1-32.

Flynn, R.M., Yang, X., Hofmann, T., Von Der Kammer, F., 2012. Bovine serum albumin adsorption to iron-oxide coated sands can change microsphere deposition mechanisms. Environmental Science & Technology 46, 2583-2591.

Franco, A.L.C., Cherubin, M.R., Cerri, C.E.P., Six, J., Wall, D.H., Cerri, C.C., 2020. Linking soil engineers, structural stability, and organic matter allocation to unravel soil carbon responses to land-use change. Soil Biology and Biochemistry 150, 107998.

Freitas, T.K.F.S., Oliveira, V.M., De Souza, M.T.F., Geraldino, H.C.L., Almeida, V.C., Fávaro, S.L., Garcia, J.C., 2015. Optimization of coagulation-flocculation process for treatment of industrial textile wastewater using okra (*A. esculentus*) mucilage as natural coagulant. Industrial Crops and Products 76, 538-544.

Frey, S.D., 2019. Mycorrhizal fungi as mediators of soil organic matter dynamics. Annual Review of Ecology, Evolution, and Systematics 50, 237-259.

Fritzsche, A., Schröder, C., Wieczorek, A.K., Händel, M., Ritschel, T., Totsche, K.U., 2015. Structure and composition of Fe–OM co-precipitates that form in soil-derived solutions. Geochimica et Cosmochimica Acta 169, 167-183.

Golchin, A., Baldock, J.A., Oades, J.M., 1997. A model linking organic matter decomposition, chemistry, and aggregate dynamics, In: Lal, R., Kimble, J.M., Follett, R.F., Stewart, B.A. (Eds.), Soil processes and the carbon cycle. CRC Press, Boca Raton, Boston, New York, Washington, London, pp. 245-266.

Goldberg, S., Glaubig, R.A., 1987. Effect of saturating cation, pH, and aluminum and iron oxide on the flocculation of kaolinite and montmorillonite. Clays and Clay Minerals 35, 220-227.

González, A.E., 2002. Colloidal aggregation in the presence of a gravitational field. Journal of Physics: Condensed Matter 14, 2335.

González, A.E., 2016. Colloidal aggregation coupled with sedimentation: A comprehensive overview, In: Rahman, M.M., Asiri, A.M. (Eds.), Advances in colloid and interface science. IntechOpen, pp. 211-235.

Grasso, D., Subramaniam, K., Butkus, M., Strevett, K., Bergendahl, J., 2002. A review of non-DLVO interactions in environmental colloidal systems. Reviews in Environmental Science and Biotechnology 1, 17-38.

Grimal, J.Y., Frossard, E., Morel, J.L., 2001. Maize root mucilage decreases adsorption of phosphate on goethite. Biology and Fertility of Soils 33, 226-230.

Guhra, T., Ritschel, T., Totsche, K.U., 2019. Formation of mineral–mineral and organo–mineral composite building units from microaggregate-forming materials including microbially produced extracellular polymeric substances. European Journal of Soil Science 70, 604-615.

Guhra, T., Ritschel, T., Totsche, K.U., 2021. The mechanisms of gravity-constrained aggregation in natural colloidal suspensions. Journal of Colloid and Interface Science 597, 126-136.

Guhra, T., Stolze, K., Ritschel, T., Totsche, K.U., 2020a. The contribution of earthworms to soil aggregate formation, EGU General Assembly Conference Abstracts.

Guhra, T., Stolze, K., Schweizer, S., Totsche, K.U., 2020b. Earthworm mucus contributes to the formation of organo-mineral associations in soil. Soil Biology and Biochemistry 145, 107785.

Harrison, A.J., Corti, D.S., Beaudoin, S.P., 2015. Capillary forces in nanoparticle adhesion: A review of AFM methods. Particulate Science and Technology 33, 526-538.

He, Y.T., Wan, J., Tokunaga, T., 2008. Kinetic stability of hematite nanoparticles: The effect of particle sizes. Journal of Nanoparticle Research 10, 321-332.

Hong, Z., Chen, W., Rong, X., Cai, P., Dai, K., Huang, Q., 2013. The effect of extracellular polymeric substances on the adhesion of bacteria to clay minerals and goethite. Chemical Geology 360, 118-125.

Horn, R., Dexter, A.R., 1989. Dynamics of soil aggregation in an irrigated desert loess. Soil and Tillage Research 13, 253-266.

Horn, R., Taubner, H., Wuttke, M., Baumgartl, T., 1994. Soil physical properties related to soil structure.

Soil and Tillage Research 30, 187-216.

Hotze, E.M., Phenrat, T., Lowry, G.V., 2010. Nanoparticle aggregation: Challenges to understanding transport and reactivity in the environment. Journal of Environmental Quality 39, 1909-1924.

Hsu, J.-P., Liu, B.-T., 1998. Effect of particle size on critical coagulation concentration. Journal of Colloid and Interface Science 198, 186-189.

Hütter, M., 2000. Local structure evolution in particle network formation studied by brownian dynamics simulation. Journal of Colloid and Interface Science 231, 337-350.

Hwang, G., Ahn, I.-S., Mhin, B.J., Kim, J.-Y., 2012. Adhesion of nano-sized particles to the surface of bacteria: Mechanistic study with the extended DLVO theory. Colloids and Surfaces B: Biointerfaces 97, 138-144.

Ilina, S.M., Ollivier, P., Slomberg, D., Baran, N., Pariat, A., Devau, N., Sani-Kast, N., Scheringer, M., Labille, J., 2017. Investigations into titanium dioxide nanoparticle and pesticide interactions in aqueous environments. Environmental Science: Nano 4, 2055-2065.

Jastrow, J.D., Miller, R.M., 1998. Soil aggregate stabilization and carbon sequestration: Feedbacks through organomineral associations, In: Lal, R., Kim, J.-Y., Follett, R.F., Stewart, B.A. (Eds.), Soil Processes and the Carbon Cycle. CRC Press, Boca Raton, Boston, New York, Washington, London, pp. 245–266.

Jeldres, R.I., Fawell, P.D., Florio, B.J., 2018. Population balance modelling to describe the particle aggregation process: A review. Powder Technology 326, 190-207.

Jiang, C.-L., Séquaris, J.-M., Vereecken, H., Klumpp, E., 2012. Effects of inorganic and organic anions on the stability of illite and quartz soil colloids in Na-, Ca-and mixed Na–Ca systems. Colloids and Surfaces A: Physicochemical and Engineering Aspects 415, 134-141.

Jiang, H., Zhen, X., Liu, G.-r., Yu, Y.-w., Zhang, D., 2013. Interaction forces between muscovite and silica surfaces in electrolyte solutions measured with AFM. Transactions of Nonferrous Metals Society of China 23, 1783-1788.

Katainen, J., Paajanen, M., Ahtola, E., Pore, V., Lahtinen, J., 2006. Adhesion as an interplay between particle size and surface roughness. Journal of Colloid and Interface Science 304, 524-529.

Kleber, M., Eusterhues, K., Keiluweit, M., Mikutta, C., Mikutta, R., Nico, P.S., 2015. Mineral–organic associations: Formation, properties, and relevance in soil environments. Advances in Agronomy 130, 1-140.

Kleber, M., Sollins, P., Sutton, R., 2007. A conceptual model of organo-mineral interactions in soils: Self-assembly of organic molecular fragments into zonal structures on mineral surfaces. Biogeochemistry 85, 9-24.

Kögel-Knabner, I., Amelung, W., 2021. Soil organic matter in major pedogenic soil groups. Geoderma 384, 114785.

Kögel-Knabner, I., Guggenberger, G., Kleber, M., Kandeler, E., Kalbitz, K., Scheu, S., Eusterhues, K., Leinweber, P., 2008. Organo-mineral associations in temperate soils: Integrating biology, mineralogy, and organic matter chemistry. Journal of Plant Nutrition and Soil Science 171, 61-82.

Kosmulski, M., 2011. The pH-dependent surface charging and points of zero charge: V. Update. Journal of Colloid and Interface Science 353, 1-15.

Kosmulski, M., 2016. Isoelectric points and points of zero charge of metal (hydr)oxides: 50 years after Parks' review. Advances in Colloid and Interface Science 238, 1-61.

Kosmulski, M., 2020. The pH dependent surface charging and points of zero charge. VIII. Update. Advances in Colloid and Interface Science 275, 102064.

Kosmulski, M., Dahlsten, P., 2006. High ionic strength electrokinetics of clay minerals. Colloids and Surfaces A: Physicochemical and Engineering Aspects 291, 212-218.

Krause, L., Biesgen, D., Treder, A., Schweizer, S.A., Klumpp, E., Knief, C., Siebers, N., 2019. Initial microaggregate formation: Association of microorganisms to montmorillonite-goethite aggregates under wetting and drying cycles. Geoderma 351, 250-260.

Kubiak-Ossowska, K., Jachimska, B., Mulheran, P.A., 2016. How negatively charged proteins adsorb to negatively charged surfaces: a molecular dynamics study of BSA adsorption on silica. The Journal of Physical Chemistry B 120, 10463-10468.

Kubiak-Ossowska, K., Tokarczyk, K., Jachimska, B., Mulheran, P.A., 2017. Bovine serum albumin adsorption at a silica surface explored by simulation and experiment. The Journal of Physical Chemistry B 121, 3975-3986.

Kwon, K.D., Vadillo-Rodriguez, V., Logan, B.E., Kubicki, J.D., 2006. Interactions of biopolymers with silica surfaces: Force measurements and electronic structure calculation studies. Geochimica et Cosmochimica Acta 70, 3803-3819.

Labille, J., Thomas, F., Milas, M., Vanhaverbeke, C., 2005. Flocculation of colloidal clay by bacterial polysaccharides: effect of macromolecule charge and structure. Journal of Colloid and Interface Science 284, 149-156.

Lagaly, G., Schulz, O., Zimehl, R., 1997. Dispersionen und Emulsionen: Eine Einführung in die Kolloidik feinverteilter Stoffe einschließlich der Tonminerale. Springer-Verlag, Berlin, Heidelberg.

Laganapan, A., Cerbelaud, M., Ferrando, R., Tran, C.T., Crespin, B., Videcoq, A., 2018. Computer simulations of heteroaggregation with large size asymmetric colloids. Journal of Colloid and Interface Science 514, 694-703.

Landeweert, R., Hoffland, E., Finlay, R.D., Kuyper, T.W., van Breemen, N., 2001. Linking plants to rocks: ectomycorrhizal fungi mobilize nutrients from minerals. Trends in Ecology & Evolution 16, 248-254.

Larrahondo, J.M., Choo, H., Burns, S.E., 2011. Laboratory-prepared iron oxide coatings on sands: Submicron-scale small-strain stiffness. Engineering Geology 121, 7-17.

Lauth, G.J., Kowalczyk, J., 2016. Einführung in die Physik und Chemie der Grenzflächen und Kolloide. Springer Spektrum, Heidelberg.

Lavelle, P., 2002. Functional domains in soils. Ecological Research 17, 441-450.

Lavelle, P., Decaëns, T., Aubert, M., Barot, S.b., Blouin, M., Bureau, F., Margerie, P., Mora, P., Rossi, J.-P., 2006. Soil invertebrates and ecosystem services. European Journal of Soil Biology 42, S3-S15.

Lavelle, P., Spain, A., Blouin, M., Brown, G., Decaëns, T., Grimaldi, M., Jiménez, J.J., McKey, D., Mathieu, J., Velasquez, E., 2016. Ecosystem engineers in a self-organized soil: A review of concepts and future research questions. Soil Science 181, 91-109.

Lavelle, P., Spain, A., Fonte, S., Bedano, J.C., Blanchart, E., Galindo, V., Grimaldi, M., Jimenez, J.J., Velasquez, E., Zangerlé, A., 2020. Soil aggregation, ecosystem engineers and the C cycle. Acta Oecologica 105, 103561.

Lazzari, S., Nicoud, L., Jaquet, B., Lattuada, M., Morbidelli, M., 2016. Fractal-like structures in colloid science. Advances in Colloid and Interface Science 235, 1-13.

Le Mer, G., Barthod, J., Dignac, M.-F., Barré, P., Baudin, F., Rumpel, C., 2020. Inferring the impact of earthworms on the stability of organo-mineral associations, by Rock-Eval thermal analysis and ^{13}C NMR spectroscopy. Organic Geochemistry 144, 104016.

Lee, K.E., 1985. Earthworms: Their ecology and relationships with soils and land use. Academic Press Inc., London.

Lee, K.E., Foster, R.C., 1991. Soil fauna and soil structure. Soil Research 29, 745-775.

Lehmann, A., Zheng, W., Rillig, M.C., 2017. Soil biota contributions to soil aggregation. Nature Ecology & Evolution 1, 1828-1835.

Lehmann, K., Lehmann, R., Totsche, K.U., 2021. Event-driven dynamics of the total mobile inventory in undisturbed soil account for significant fluxes of particulate organic carbon. Science of the Total Environment 756, 143774.

Lehmann, K., Schaefer, S., Babin, D., Köhne, J.M., Schlüter, S., Smalla, K., Vogel, H.-J., Totsche, K.U., 2018. Selective transport and retention of organic matter and bacteria shapes initial pedogenesis in artificial soil-A two-layer column study. Geoderma 325, 37-48.

Lemtiri, A., Colinet, G., Alabi, T., Cluzeau, D., Zirbes, L., Haubruge, É., Francis, F., 2014. Impacts of earthworms on soil components and dynamics. A review. Biotechnologie, Agronomie, Société et Environnement 18, 121-133.

Liang, L., Wang, L., Nguyen, A.V., Xie, G., 2017. Heterocoagulation of alumina and quartz studied by zeta potential distribution and particle size distribution measurements. Powder Technology 309, 1-12.

Lin, D., Ma, W., Jin, Z., Wang, Y., Huang, Q., Cai, P., 2016. Interactions of EPS with soil minerals: a combination study by ITC and CLSM. Colloids and Surfaces B: Biointerfaces 138, 10-16.

Liu, W., Sun, Z., Forsling, W., Du, Q., Tang, H., 1999. A comparative study of surface acid–base characteristics of natural illites from different origins. Journal of Colloid and Interface Science 219, 48-61.

Liu, X., Eusterhues, K., Thieme, J.r., Ciobota, V., Höschen, C., Mueller, C.W., Küsel, K., Kögel-Knabner, I., Rösch, P., Popp, J.r., 2013. STXM and NanoSIMS investigations on EPS fractions before and after adsorption to goethite. Environmental Science & Technology 47, 3158-3166.

Long, J., Xu, Z., Masliyah, J.H., 2006. Role of illite–illite interactions in oil sands processing. Colloids and Surfaces A: Physicochemical and Engineering Aspects 281, 202-214.

Mahapatra, S., Banerjee, D., 2013. Fungal exopolysaccharide: Production, composition and applications. Microbiology Insights 6, 1-16.

McBride, M.B., Baveye, P., 2002. Diffuse double-layer models, long-range forces, and ordering in clay colloids. Soil Science Society of America Journal 66, 1207-1217.

McMaster, T.J., 2012. Atomic Force Microscopy of the fungi–mineral interface: Applications in mineral dissolution, weathering and biogeochemistry. Current Opinion in Biotechnology 23, 562-569.

Menon, M., Mawodza, T., Rabbani, A., Blaud, A., Lair, G.J., Babaei, M., Kercheva, M., Rousseva, S., Banwart, S., 2020. Pore system characteristics of soil aggregates and their relevance to aggregate stability. Geoderma 366, 114259.

Metin, C.O., Bonnecaze, R.T., Lake, L.W., Miranda, C.R., Nguyen, Q.P., 2014. Aggregation kinetics and shear rheology of aqueous silica suspensions. Applied Nanoscience 4, 169-178.

Meurer, K.H.E., Chenu, C., Coucheney, E., Herrmann, A.M., Keller, T., Kätterer, T., Nimblad Svensson, D., Jarvis, N., 2020. Modelling dynamic interactions between soil structure and the storage and turnover of soil organic matter. Biogeosciences 17, 5025-5042.

Mikutta, R., Baumgärtner, A., Schippers, A., Haumaier, L., Guggenberger, G., 2012. Extracellular polymeric substances from *Bacillus subtilis* associated with minerals modify the extent and rate of heavy metal sorption. Environmental Science & Technology 46, 3866-3873.

Mikutta, R., Zang, U., Chorover, J., Haumaier, L., Kalbitz, K., 2011. Stabilization of extracellular polymeric substances (*Bacillus subtilis*) by adsorption to and coprecipitation with Al forms. Geochimica et Cosmochimica Acta 75, 3135-3154.

Min, Y., Akbulut, M., Kristiansen, K., Golan, Y., Israelachvili, J., 2008. The role of interparticle and external forces in nanoparticle assembly. Nature Materials 7, 527-538.

More, T.T., Yadav, J.S.S., Yan, S., Tyagi, R.D., Surampalli, R.Y., 2014. Extracellular polymeric substances of bacteria and their potential environmental applications. Journal of Environmental Management 144, 1-25.

Morel, J.L., Habib, L., Plantureux, S., Guckert, A., 1991. Influence of maize root mucilage on soil aggregate stability. Plant and Soil 136, 111-119.

Mosley, L.M., Hunter, K.A., Ducker, W.A., 2003. Forces between colloid particles in natural waters. Environmental Science & Technology 37, 3303-3308.

Narvekar, S.P., Ritschel, T., Totsche, K.U., 2017. Colloidal stability and mobility of extracellular polymeric substance amended hematite nanoparticles. Vadose Zone Journal 16, 1-10.

Nichols, K.A., Halvorson, J.J., 2013. Roles of biology, chemistry, and physics in soil macroaggregate formation and stabilization. The Open Agriculture Journal 7, 107-117.

Nwadialo, B.E., Mbagwu, J.S.C., 1991. An analysis of soil components active in microaggregate stability. Soil Technology 4, 343-350.

Oades, J.M., 1984. Soil organic matter and structural stability: Mechanisms and implications for management. Plant and Soil 76, 319-337.

Ohtsubo, M., 1989. Interaction of iron oxides with clays. Clay Science 7, 227-242.

Ohtsubo, M., Yoshimura, A., Wada, S.-I., Yong, R.N., 1991. Particle interaction and rheology of illite-iron oxide complexes. Clays and Clay Minerals 39, 347-354.

Olsen, A., Franks, G., Biggs, S., Jameson, G.J., 2005. Bi-modal hetero-aggregation rate response to particle dosage. The Journal of Chemical Physics 123, 204904.

Omoike, A., Chorover, J., 2004. Spectroscopic study of extracellular polymeric substances from *Bacillus subtilis*: Aqueous chemistry and adsorption effects. Biomacromolecules 5, 1219-1230.

Omoike, A., Chorover, J., 2006. Adsorption to goethite of extracellular polymeric substances from *Bacillus subtilis*. Geochimica et Cosmochimica Acta 70, 827-838.

Pan, X., Song, W., Zhang, D., 2010. Earthworms (*Eisenia foetida*, Savigny) mucus as complexing ligand for imidacloprid. Biology and Fertility of Soils 46, 845-850.

Pen, Y., Zhang, Z.J., Morales-García, A.L., Mears, M., Tarmey, D.S., Edyvean, R.G., Banwart, S.A., Geoghegan, M., 2015. Effect of extracellular polymeric substances on the mechanical properties of *Rhodococcus*. Biochimica et Biophysica Acta 1848, 518-526.

Philippe, A., Schaumann, G.E., 2014. Interactions of dissolved organic matter with natural and engineered inorganic colloids: A review. Environmental Science & Technology 48, 8946-8962.

Pot, V., Portell, X., Otten, W., Garnier, P., Monga, O., Baveye, P.C., 2021. Accounting for soil architecture and microbial dynamics in microscale models: Current practices in soil science and the path ahead. European Journal of Soil Science, 1-23.

Praetorius, A., Labille, J., Scheringer, M., Thill, A., Hungerbühler, K., Bottero, J.-Y., 2014. Heteroaggregation of titanium dioxide nanoparticles with model natural colloids under environmentally relevant conditions. Environmental Science & Technology 48, 10690-10698.

Ramakrishna, S.N., Clasohm, L.Y., Rao, A., Spencer, N.D., 2011. Controlling adhesion force by means of nanoscale surface roughness. Langmuir 27, 9972-9978.

Ramos, A.C.H., McBride, M.B., 1996. Goethite dispersibility in solutions of variable ionic strength and soluble organic matter content. Clays and Clay Minerals 44, 286-296.

Ranville, J.F., Chittleborough, D.J., Beckett, R., 2005. Particle-size and element distributions of soil colloids: Implications for colloid transport. Soil Science Society of America Journal 69, 1173-1184.

Ray, N., Rupp, A., Prechtel, A., 2017. Discrete-continuum multiscale model for transport, biomass development and solid restructuring in porous media. Advances in Water Resources 107, 393-404.

Redmile-Gordon, M., Gregory, A.S., White, R.P., Watts, C.W., 2020. Soil organic carbon, extracellular polymeric substances (EPS), and soil structural stability as affected by previous and current land-use. Geoderma 363, 114143.

Ritschel, T., Lehmann, K., Brunzel, M., Vitz, J., Nischang, I., Schubert, U.S., Totsche, K.U., 2021. Well-defined poly (ethylene glycol) polymers as non-conventional reactive tracers of colloidal transport in porous media. Journal of Colloid and Interface Science 584, 592-601.

Ritschel, T., Totsche, K., 2020. Aggregate formation dynamics driven by 3D fluid flow in natural porous media, EGU General Assembly Conference Abstracts.

Ritschel, T., Totsche, K.U., 2019. Modeling the formation of soil microaggregates. Computers & Geosciences 127, 36-43.

Robertson, A.D., Paustian, K., Ogle, S., Wallenstein, M.D., Lugato, E., Cotrufo, M.F., 2019. Unifying soil organic matter formation and persistence frameworks: the MEMS model. Biogeosciences 16, 1225-1248.

Ruckenstein, E., Prieve, D.C., 1976. Adsorption and desorption of particles and their chromatographic separation. AIChE Journal 22, 276-283.

Rupp, A., Guhra, T., Meier, A., Prechtel, A., Ritschel, T., Ray, N., Totsche, K.U., 2019. Application of a cellular automaton method to model the structure formation in soils under saturated conditions: A mechanistic approach. Frontiers in Environmental Science 7, 170.

Rupp, A., Totsche, K.U., Prechtel, A., Ray, N., 2018. Discrete-continuum multiphase model for structure formation in soils including electrostatic effects. Frontiers in Environmental Science 6, 96.

Sandkühler, P., Lattuada, M., Wu, H., Sefcik, J., Morbidelli, M., 2005. Further insights into the universality of colloidal aggregation. Advances in Colloid and Interface Science 113, 65-83.

Scheidegger, A., Borkovec, M., Sticher, H., 1993. Coating of silica sand with goethite: Preparation and analytical identification. Geoderma 58, 43-65.

Scheu, S., 1991. Mucus excretion and carbon turnover of endogeic earthworms. Biology and Fertility of Soils 12, 217-220.

Schrader, S., 1994. Influence of earthworms on the pH conditions of their environment by cutaneous mucus secretion. Zoologischer Anzeiger 233.

Seiphoori, A., Ma, X.-g., Arratia, P.E., Jerolmack, D.J., 2020. Formation of stable aggregates by fluid-assembled solid bridges. Proceedings of the National Academy of Sciences 117, 3375-3381.

Semenov, V.M., Lebedeva, T.N., Pautova, N.B., Khromychkina, D.P., Kovalev, I.V., Kovaleva, N.O., 2020. Relationships between the size of aggregates, particulate organic matter content, and decomposition of plant residues in soil. Eurasian Soil Science 53, 454–466.

Semmel, H., Horn, R., Hell, U., Dexter, A.R., Schulze, E.D., 1990. The dynamics of soil aggregate formation and the effect on soil physical properties. Soil Technology 3, 113-129.

Sheng, A., Liu, F., Xie, N., Liu, J., 2016. Impact of proteins on aggregation kinetics and adsorption ability of hematite nanoparticles in aqueous dispersions. Environmental Science & Technology 50, 2228-2235.

Shih, Y., Zhuang, C., Tso, C., Lin, C., 2012. The effect of electrolytes on the aggregation kinetics of titanium dioxide nanoparticle aggregates. Journal of Nanoparticle Research 14, 1-11.

Shipitalo, M.J., Protz, R., 1988. Factors influencing the dispersibility of clay in worm casts. Soil Science Society of America Journal 52, 764-769.

Shipitalo, M.J., Protz, R., 1989. Chemistry and micromorphology of aggregation in earthworm casts. Geoderma 45, 357-374.

Six, J., Bossuyt, H., Degryze, S., Denef, K., 2004. A history of research on the link between (micro) aggregates, soil biota, and soil organic matter dynamics. Soil and Tillage Research 79, 7-31.

Sollins, P., Gregg, J.W., 2017. Soil organic matter accumulation in relation to changing soil volume, mass, and structure: Concepts and calculations. Geoderma 301, 60-71.

Sondi, I., Bišćan, J., Pravdić, V., 1996. Electrokinetics of pure clay minerals revisited. Journal of Colloid and Interface Science 178, 514-522.

Stromberger, M.E., Keith, A.M., Schmidt, O., 2012. Distinct microbial and faunal communities and

translocated carbon in *Lumbricus terrestris* drilospheres. Soil Biology and Biochemistry 46, 155-162.

Strubbe, F., Beunis, F., Marescaux, M., Neyts, K., 2007. Charging mechanism in colloidal particles leading to a linear relation between charge and size. Physical Review E 75, 031405.

Syngouna, V.I., Chrysikopoulos, C.V., 2016. Cotransport of clay colloids and viruses through water-saturated vertically oriented columns packed with glass beads: Gravity effects. Science of the Total Environment 545, 210-218.

Szilagyi, I., Szabo, T., Desert, A., Trefalt, G., Oncsik, T., Borkovec, M., 2014a. Particle aggregation mechanisms in ionic liquids. Physical Chemistry Chemical Physics 16, 9515-9524.

Szilagyi, I., Trefalt, G., Tiraferri, A., Maroni, P., Borkovec, M., 2014b. Polyelectrolyte adsorption, interparticle forces, and colloidal aggregation. Soft Matter 10, 2479-2502.

Tateno, M., Tanaka, H., 2019. Numerical prediction of colloidal phase separation by direct computation of Navier–Stokes equation. npj Computational Materials 5, 1-9.

Tawari, S.L., Koch, D.L., Cohen, C., 2001. Electrical double-layer effects on the Brownian diffusivity and aggregation rate of Laponite clay particles. Journal of Colloid and Interface Science 240, 54-66.

Tiraferri, A., Hernandez, L.A.S., Bianco, C., Tosco, T., Sethi, R., 2017. Colloidal behavior of goethite nanoparticles modified with humic acid and implications for aquifer reclamation. Journal of Nanoparticle Research 19, 107.

Tisdall, J.M., Oades, J.M., 1982. Organic matter and water-stable aggregates in soils. Journal of Soil Science 33, 141-163.

Tiunov, A.V., Scheu, S., 1999. Microbial respiration, biomass, biovolume and nutrient status in burrow walls of *Lumbricus terrestris* L.(Lumbricidae). Soil Biology and Biochemistry 31, 2039-2048.

Tombácz, E., Csanaky, C., Illés, E., 2001. Polydisperse fractal aggregate formation in clay mineral and iron oxide suspensions, pH and ionic strength dependence. Colloid and Polymer Science 279, 484-492.

Tombácz, E., Libor, Z., Illés, E., Majzik, A., Klumpp, E., 2004. The role of reactive surface sites and complexation by humic acids in the interaction of clay mineral and iron oxide particles. Organic Geochemistry 35, 257-267.

Tombácz, E., Szekeres, M., 2004. Colloidal behavior of aqueous montmorillonite suspensions: The specific role of pH in the presence of indifferent electrolytes. Applied Clay Science 27, 75-94.

Tombácz, E., Szekeres, M., 2006. Surface charge heterogeneity of kaolinite in aqueous suspension in comparison with montmorillonite. Applied Clay Science 34, 105-124.

Totsche, K.U., Amelung, W., Gerzabek, M.H., Guggenberger, G., Klumpp, E., Knief, C., Lehndorff, E., Mikutta, R., Peth, S., Prechtel, A., 2018. Microaggregates in soils. Journal of Plant Nutrition and Soil Science 181, 104-136.

Totsche, K.U., Rennert, T., Gerzabek, M.H., Kögel-Knabner, I., Smalla, K., Spiteller, M., Vogel, H.J., 2010. Biogeochemical interfaces in soil: The interdisciplinary challenge for soil science. Journal of Plant Nutrition and Soil Science 173, 88-99.

Trefalt, G., Ruiz-Cabello, F.J.M., Borkovec, M., 2014. Interaction forces, heteroaggregation, and deposition involving charged colloidal particles. The Journal of Physical Chemistry B 118, 6346-6355.

Trefalt, G., Szilágyi, I., Borkovec, M., 2020. Schulze-Hardy rule revisited. Colloid and Polymer Science 298, 961-967.

Tunega, D., Gerzabek, M.H., Haberhauer, G., Totsche, K.U., Lischka, H., 2009. Model study on sorption of polycyclic aromatic hydrocarbons to goethite. Journal of Colloid and Interface Science 330, 244-249.

Upendar, S., Mani, E., Basavaraj, M.G., 2018. Aggregation and stabilization of colloidal spheroids by oppositely charged spherical nanoparticles. Langmuir 34, 6511-6521.

Violante, A., De Cristofaro, A., Rao, M.A., Gianfreda, L., 1995. Physicochemical properties of protein-smectite and protein-Al (OH) x-smectite complexes. Clay Minerals 30, 325-336.

Wagai, R., Mayer, L.M., Kitayama, K., 2009. Extent and nature of organic coverage of soil mineral surfaces assessed by a gas sorption approach. Geoderma 149, 152-160.

Walker, T.S., Bais, H.P., Grotewold, E., Vivanco, J.M., 2003. Root exudation and rhizosphere biology. Plant Physiology 132, 44-51.

Wang, H., Dong, Y., Zhu, M., Li, X., Keller, A.A., Wang, T., Li, F., 2015. Heteroaggregation of engineered nanoparticles and kaolin clays in aqueous environments. Water Research 80, 130-138.

Wang, L.-L., Wang, L.-F., Ren, X.-M., Ye, X.-D., Li, W.-W., Yuan, S.-J., Sun, M., Sheng, G.-P., Yu, H.-Q., Wang, X.-K., 2012. pH dependence of structure and surface properties of microbial EPS. Environmental Science & Technology 46, 737-744.

Wensink, H.H., Lekkerkerker, H.N.W., 2004. Sedimentation and multi-phase equilibria in mixtures of platelets and ideal polymer. Europhysics Letters 66, 125-131.

Whitmer, J.K., Luijten, E., 2011. Sedimentation of aggregating colloids. The Journal of Chemical Physics 134, 034510.

Wilson, H.J., Pietraszewski, L.A., Davis, R.H., 2000. Aggregation of charged particles under electrophoresis or gravity at arbitrary Peclet numbers. Journal of Colloid and Interface Science 221, 87-103.

Wingender, J., Neu, T.R., Flemming, H.-C., 1999. What are bacterial extracellular polymeric substances?, In: Wingender, J., Neu, T.R., Flemming, H.-C. (Eds.), Microbial Extracellular Polymeric Substances. Springer, Berlin, Heidelberg, New York, Barcelona, Hong Kong, London, Milan, Paris, Singapore, Tokyo, pp. 1-19.

Wu, H., Lattuada, M., Sandkühler, P., Sefcik, J., Morbidelli, M., 2003. Role of sedimentation and buoyancy on the kinetics of diffusion limited colloidal aggregation. Langmuir 19, 10710-10718.

Xu, Y., Axe, L., 2005. Synthesis and characterization of iron oxide-coated silica and its effect on metal adsorption. Journal of Colloid and Interface Science 282, 11-19.

Yang, Y.-J., Kelkar, A.V., Corti, D.S., Franses, E.I., 2016. Effect of interparticle interactions on agglomeration and sedimentation rates of colloidal silica microspheres. Langmuir 32, 5111-5123.

Yates, P.D., Franks, G.V., Biggs, S., Jameson, G.J., 2005. Heteroaggregation with nanoparticles: Effect of particle size ratio on optimum particle dose. Colloids and Surfaces A: Physicochemical and Engineering Aspects 255, 85-90.

Yates, P.D., Franks, G.V., Jameson, G.J., 2008. Orthokinetic heteroaggregation with nanoparticles: Effect

of particle size ratio on aggregate properties. Colloids and Surfaces A: Physicochemical and Engineering Aspects 326, 83-91.

Yu, W.H., Li, N., Tong, D.S., Zhou, C.H., Lin, C.X.C., Xu, C.Y., 2013. Adsorption of proteins and nucleic acids on clay minerals and their interactions: A review. Applied Clay Science 80, 443-452.

Yudina, A., Kuzyakov, Y., 2019. Saving the face of soil aggregates. Global Change Biology 25, 3574-3577.

Zech, S., Dultz, S., Guggenberger, G., Prechtel, A., Ray, N., 2020. Microaggregation of goethite and illite evaluated by mechanistic modeling. Applied Clay Science 198, 105845.

Zhao, W., Yang, S., Huang, Q., Cai, P., 2015. Bacterial cell surface properties: role of loosely bound extracellular polymeric substances (LB-EPS). Colloids and Surfaces B: Biointerfaces 128, 600-607.

Zhou, D., Keller, A.A., 2010. Role of morphology in the aggregation kinetics of ZnO nanoparticles. Water Research 44, 2948-2956.

Zhu, P., Long, G., Ni, J., Tong, M., 2009. Deposition kinetics of extracellular polymeric substances (EPS) on silica in monovalent and divalent salts. Environmental Science & Technology 43, 5699-5704.

Zhu, X., Chen, H., Li, W., He, Y., Brookes, P.C., Xu, J., 2014. Aggregation kinetics of natural soil nanoparticles in different electrolytes. European Journal of Soil Science 65, 206-217.

Zhuang, J., Yu, G.-R., 2002. Effects of surface coatings on electrochemical properties and contaminant sorption of clay minerals. Chemosphere 49, 619-628.

Zou, Y., Jayasuriya, S., Manke, C.W., Mao, G., 2015. Influence of nanoscale surface roughness on colloidal force measurements. Langmuir 31, 10341-10350.